



UNIVERSIDADE ESTADUAL DE CAMPINAS - UNICAMP  
FACULDADE DE ENGENHARIA QUÍMICA - FEQ

RUTH NÓBREGA QUEIROZ

**APLICAÇÃO DE ADSORVENTE COMPÓSITO DE ÓXIDO DE GRAFENO-  
QUITOSANA PARA ADSORÇÃO DE HIDROCARBONETOS POLICÍCLICOS  
AROMÁTICOS (HPA) DE EFLUENTE DE ÁGUA PRODUZIDA**

***APPLICATION OF GRAPHENE OXIDE-CHITOSAN ADSORBENT COMPOSITE FOR  
ADSORPTION OF POLYCYCLIC AROMATIC HYDROCARBON (PAH) FROM  
PRODUCED WATER EFFLUENT***

CAMPINAS – SP

2022

RUTH NÓBREGA QUEIROZ

**APLICAÇÃO DE ADSORVENTE COMPÓSITO DE ÓXIDO DE GRAFENO-  
QUITOSANA PARA ADSORÇÃO DE HIDROCARBONETOS POLICÍCLICOS  
AROMÁTICOS (HPA) DE EFLUENTE DE ÁGUA PRODUZIDA**

***APPLICATION OF GRAPHENE OXIDE-CHITOSAN ADSORBENT COMPOSITE FOR  
ADSORPTION OF POLYCYCLIC AROMATIC HYDROCARBON (PAH) FROM  
PRODUCED WATER EFFLUENT***

Dissertação apresentada à Faculdade de Engenharia Química da Universidade Estadual de Campinas como parte dos requisitos necessários para a obtenção do título de Mestra em Engenharia Química.

Dissertation presented to the Faculty of Chemical Engineering of the University of Campinas as part of the requirements for the degree of Master in Chemical Engineering.

**Orientadora:** Prof.<sup>a</sup> Dr.<sup>a</sup>. Melissa Gurgel Adeodato Vieira

**Coorientadora:** Prof.<sup>a</sup>. Dr.<sup>a</sup>. Patrícia Prediger

ESTE TRABALHO CORRESPONDE À  
VERSÃO FINAL DA DISSERTAÇÃO  
DEFENDIDA PELA ALUNA RUTH  
NÓBREGA QUEIROZ, ORIENTADA PELA  
PROF.<sup>a</sup>. DR.<sup>a</sup>. MELISSA GURGEL  
ADEODATO VIEIRA.

CAMPINAS – SP

2022

Ficha catalográfica  
Universidade Estadual de Campinas  
Biblioteca da Área de Engenharia e Arquitetura  
Rose Meire da Silva - CRB 8/5974

Q32a Queiroz, Ruth Nóbrega, 1996-  
Aplicação de adsorvente compósito de óxido de grafeno-quitosana para adsorção de hidrocarbonetos policíclicos aromáticos (HPA) de efluente de água produzida / Ruth Nóbrega Queiroz. – Campinas, SP : [s.n.], 2022.

Orientador: Melissa Gurgel Adeodato Vieira.  
Coorientador: Patrícia Prediger.  
Dissertação (mestrado) – Universidade Estadual de Campinas, Faculdade de Engenharia Química.

1. Adsorção. 2. Óxido de grafeno. 3. Quitosana. 4. Hidrocarbonetos policíclicos aromáticos. 5. Simulação molecular. I. Vieira, Melissa Gurgel Adeodato, 1979-. II. Prediger, Patrícia, 1984-. III. Universidade Estadual de Campinas. Faculdade de Engenharia Química. IV. Título.

Informações para Biblioteca Digital

**Título em outro idioma:** Application of graphene oxide-chitosan adsorbent composite for adsorption of polycyclic aromatic hydrocarbon (PAH) from produced water effluent

**Palavras-chave em inglês:**

Adsorption

Graphene oxide

Chitosan

Polycyclic aromatic hydrocarbon

Molecular simulation

**Área de concentração:** Engenharia Química

**Titulação:** Mestra em Engenharia Química

**Banca examinadora:**

Melissa Gurgel Adeodato Vieira [Orientador]

Maria Regina Wolf Maciel

Adriano Luiz Tonetti

**Data de defesa:** 11-07-2022

**Programa de Pós-Graduação:** Engenharia Química

**Identificação e informações acadêmicas do(a) aluno(a)**

- ORCID do autor: <https://orcid.org/0000-0003-2110-8080>

- Currículo Lattes do autor: <http://lattes.cnpq.br/7620753065433500>

## **FOLHA DE APROVAÇÃO**

Folha de Aprovação da Defesa de Dissertação de Mestrado defendida por Ruth Nóbrega Queiroz – RA 265836 e aprovada em 11 de julho de 2022 pela banca examinadora constituída pelos seguintes doutores:

Prof.<sup>a</sup> Dr.<sup>a</sup> Melissa Gurgel Adeodato Vieira  
Presidente e Orientadora  
Faculdade de Engenharia Química – FEQ/UNICAMP

Prof.<sup>a</sup> Dr.<sup>a</sup> Maria Regina Wolf Maciel  
Banca examinadora  
Faculdade de Engenharia Química – FEQ/UNICAMP

Prof. Dr. Adriano Luiz Tonetti  
Banca examinadora  
Faculdade de Engenharia Civil, Arquitetura e Urbanismo – FECFAU/UNICAMP

*A ATA da Defesa com as respectivas assinaturas dos membros encontra-se no SIGA/Sistema de Fluxo de Dissertação/Tese e na Secretaria do Programa da Unidade.*

## AGRADECIMENTOS

Agradeço, em primeiro lugar, a Deus, que é minha fortaleza e meu refúgio, sempre estando ao meu lado todos os dias.

A toda a minha família, em especial a meus pais, Maria José e Aefferson, por todo amor, carinho e incentivo. A meu irmão Samuel por todo incentivo.

A Kezarque por todo amor, apoio, incentivo e companheirismo ao longo de todos esses anos. Você me motiva a seguir em frente e alcançar meus objetivos todos os dias.

A todos os meus amigos e colegas de trabalho por todo o apoio, boas vibrações, momentos risadas e aconselhamentos.

A minha orientadora professora Dr<sup>a</sup> Melissa Gurgel Adeodato Vieira e minha coorientadora professora Dr<sup>a</sup> Patrícia Prediger, por toda confiança, ensinamentos, sugestões, críticas construtivas e apoio.

Aos professores Dr<sup>a</sup> Meuris Gurgel Carlos da Silva e Dr. Valmor Roberto Mastelaro (IFSC/USP) pela colaboração no desenvolvimento da pesquisa.

Ao programa de pós-graduação em Engenharia Química da Unicamp pela infraestrutura e equipe excepcionais.

Agradeço aos colegas e amigos do LEA/LEPA pela troca de conhecimentos e de experiências, e por todos os momentos de companheirismo no dia-a-dia. A Tauany Neves (FT/UNICAMP) pela parceria.

Aos professores Dr<sup>a</sup> Maria Regina Wolf Maciel, Dr. Adriano Luiz Tonetti, Dr. Leonardo Vasconcelos Fregolente e Dr. Lucas Meili (membro suplente), por terem aceitado participar da banca examinadora deste exame de qualificação.

Ao Programa de Recursos Humanos da Agência Nacional do Petróleo (PRH-ANP), programa nº 29 (Processo 043919/2020), Tecnologias de Produção e Processos para Refino de Petróleo, pelo financiamento deste projeto de pesquisa, tornando possível a produção desta dissertação. Agradecimento também ao auxílio do CENAPAD SP pela concessão da licença de *softwares* para a simulação molecular.

Agradeço a todos que de forma direta ou indireta contribuíram para a realização deste trabalho, os meus sinceros agradecimentos!

## RESUMO

Os hidrocarbonetos policíclicos aromáticos (PAHs) são poluentes orgânicos formados principalmente pela combustão incompleta de matéria orgânica, como petróleo, gás e carvão. A presença de PAHs pode causar danos irreparáveis ao meio ambiente e aos seres vivos, o que tem gerado uma preocupação global com os riscos de curto e longo prazo que a emissão desses poluentes pode causar. Neste contexto, muitas tecnologias têm sido desenvolvidas nas últimas décadas visando à identificação e ao tratamento desses compostos, principalmente, os PAHs presentes nas águas residuais da indústria petrolífera. Diante disto, esta dissertação de mestrado teve como objetivo geral avaliar o potencial de remoção de três PAHs típicos (naftaleno, antraceno e fluoranteno), presentes em efluentes sintéticos e reais, por meio da aplicação de compósitos adsorventes de óxido de grafeno e quitosana magnética, sintetizados por rotas convencional e verde. O óxido de grafeno (GO) foi sintetizado através do método de Hummer modificado. As nanopartículas magnéticas de ferro ( $\text{Fe}_3\text{O}_4$ ) foram sintetizadas por rotas convencional e química verde, posteriormente, as mesmas foram incorporadas ao GO e à quitosana, para formar os compósitos magnéticos de GO-quitosana, usando o glurataldeído e proantocianidina como agentes reticulantes, respectivamente. Diferentes técnicas de caracterização foram aplicadas para determinar as propriedades térmicas (TG/DTG), estruturais (BET, XPS e FTIR), cristalográficas (DRX) e texturais (MEV) antes e após o processo de adsorção. Os resultados dos testes de afinidade indicaram que o sistema PAH/adsorvente mais promissor foi o naftaleno/G-mCS/GO, com um percentual remoção de 93,55%. Os resultados obtidos a partir da simulação molecular indicaram que as moléculas de naftaleno apresentam maior estabilidade que o antraceno e o fluoranteno, o que contribui para aumentar as interações hidrofóbicas e  $\pi$ - $\pi$  entre as moléculas de PAH e a superfície adsorvente. Os resultados obtidos por meio do experimento de planejamento experimental DCCR indicaram que a concentração inicial de naftaleno e a dosagem do adsorvente têm influência significativa sobre a capacidade de adsorção ( $\text{mmol.g}^{-1}$ ). Os ensaios de adsorção e o estudo termodinâmico apontaram ambas a fisissorção e a quimissorção como os mecanismos, principal e secundário, respectivamente, envolvidos no processo de adsorção do naftaleno, por meio da influência das interações  $\pi$ - $\pi$ , hidrofóbicas e eletrostáticas. Além disso, o estudo termodinâmico indicou que o adsorvente verde possui alta afinidade pelo naftaleno e o processo é espontâneo e endotérmico. A capacidade máxima de adsorção ( $q_{\text{max}}$ ) de naphthaleno por G-mCS/GO foi de  $334,37 \text{ mg.g}^{-1}$  a  $20^\circ\text{C}$ . O adsorvente verde foi efetivamente regenerado com metanol e utilizado por cinco ciclos consecutivos, com percentual de recuperação de naftaleno após os ciclos de aproximadamente 75%, e perda de massa total de cerca de 6,8%. O compósito verde também foi aplicado na adsorção de naftaleno em amostras de água de rio, visando avaliar a viabilidade do método em aplicações reais, com eficiência de adsorção de aproximadamente 70%. Portanto, os resultados obtidos nesta dissertação apontaram o G-mCS/GO como um material promissor e sustentável para a remediação de hidrocarbonetos aromáticos policíclicos de efluentes industriais.

**Palavras-chave:** Adsorção; Nanoadsorventes Verdes; Óxido de grafeno, Quitosana; Hidrocarbonetos Policíclicos Aromáticos; Simulação molecular; Regeneração.

## ABSTRACT

Polycyclic aromatic hydrocarbons (PAHs) are organic pollutants mainly formed by the incomplete combustion of organic matter such as oil, gas and coal. The presence of PAHs can cause irreparable damage to the environment and to living beings, which has generated a global concern with the short and long-term risks that the emission of these pollutants can cause. In this context, many technologies have been developed in the latest decades aiming the identification of these compounds, especially the PAHs present in wastewater from the oil industry. Therefore, this master's thesis has as main objective to evaluate the potential of removal of three typical PAHs (naphthalene, anthracene and fluoranthene), present in synthetic and real effluents, through the application of adsorbent composites of graphene oxide and magnetic chitosan, synthesized by conventional and green routes. Graphene oxide (GO) was synthesized by the modified Hummer's method. The magnetic iron nanoparticles ( $\text{Fe}_3\text{O}_4$ ) were synthesized by conventional and green chemical routes, later, they were incorporated into GO and chitosan, to form the GO-chitosan magnetic composites, using glutaraldehyde and proanthocyanidin as crosslinking agents, respectively. Different characterization techniques were applied to determine the thermal (TG/DTG), structural (BET, XPS and FTIR), crystallographic (XRD) and textural (SEM) properties before and after the adsorption process. The results of the affinity tests indicated that the most promising PAH/adsorbent system was naphthalene/G-mCS/GO, with a removal percentage of 93.55%. The results obtained through molecular simulation indicated that naphthalene molecules present greater stability than anthracene and fluoranthene, which contributes to increase hydrophobic and  $\pi$ - $\pi$  interactions between PAH molecules and the adsorbent surface. The results obtained through the CCD experimental design experiment indicated that the initial concentration of naphthalene and the adsorbent dosage have a significant influence on the adsorption capacity ( $\text{mmol.g}^{-1}$ ). The adsorption assays and the thermodynamic study showed both physisorption and chemisorption as the main and secondary mechanisms, respectively, involved in the process of adsorption of naphthalene, through the influence of  $\pi$ - $\pi$ , hydrophobic and electrostatic interactions. In addition, the thermodynamic study indicated that the green adsorbent has a high affinity for naphthalene and the process is spontaneous and endothermic. The maximum adsorption capacity ( $q_{\text{max}}$ ) of naphthalene by G-mCS/GO was  $334.37 \text{ mg.g}^{-1}$  at  $20^\circ\text{C}$ . The green adsorbent was effectively regenerated with methanol and used for five consecutive cycles, with a percentage of naphthalene recovery after cycles of approximately 75%, and a total mass loss of approximately 6.8%. The green composite was also applied in the adsorption of naphthalene in river water samples, aiming to evaluate the viability of the method in real applications, with adsorption efficiency of approximately 70%. Therefore, the results obtained in this dissertation pointed to G-mCS/GO as a promising and sustainable material for the remediation of polycyclic aromatic hydrocarbons from industrial effluents.

**Keywords:** Adsorption; Green Nanoadsorbents; Graphene Oxide, Chitosan; Polycyclic Aromatic Hydrocarbons; Molecular simulation; Regeneration.

## LISTA DE ILUSTRAÇÕES

Figura 1.1. Esquema das principais etapas de execução da dissertação de mestrado. ....	19
Figure 2.1. Number of documents published per year, which address technologies for the removal of PAHs from wastewater, from 2008 to 2021, based on searches in the ScienceDirect, RSC and ACS databases. ....	24
Figure 2.2. Schematic representation of the types of adsorbents used for PAHs adsorption from wastewater. ....	27
Figure 2.3. Classification of nanomaterials, based on shape and dimension, in zero-dimensional (0D), one-dimensional (1D), two-dimensional (2D) and three-dimensional (3D). ....	42
Figure 2.4. Synthesis of graphene from graphite and chemical reduction of GO. ....	49
Figure 2.5. Schematic diagram of the main types of green reducing agents for the synthesis of rGO. ....	51
Figure 3.1. Schematic diagram of the synthesis of: a) C-mCS/GO and b) G-mCS/GO. ....	78
Figure 3.2. a) XRD diffractograms and b) FT-IR spectrum of G-mCS/GO (blue line); C-mCS/GO (black line); G-Fe <sub>3</sub> O <sub>4</sub> (green line) and C-Fe <sub>3</sub> O <sub>4</sub> (pink line). ....	86
Figure 3.3. High-resolution of C (1s) (a-b); O (1s) (c-d); N (1s) (e-f) and Fe (2p) (g-h). ....	88
Figure 3.4. Magnetization curves of the C-mCS/GO and G-mCS/GO. ....	90
Figure 3.5. SEM micrographs of: C-mCS/GO a) 2000x, b) 5000 x magnification; G-mCS/GO c) 2000x, d) 4500 x magnification; e) C-Fe <sub>3</sub> O <sub>4</sub> , and f) G-Fe <sub>3</sub> O <sub>4</sub> . ....	91
Figure 3.6. TG/DTG curves and Zeta potential for: (a-c) C-mCS/GO; (b-c) G-mCS/GO and the Zeta potential in suspension with (d) naphthalene; (e) anthracene; (f) and fluoranthene solutions. ....	94
Figure 3.7. Chemical structures, optimized geometry and the electrostatic potential of PAHs molecules: a) naphthalene; b) anthracene; c) fluoranthene. ....	96
Figure 3.8. 3-D contours of HOMO and LUMO: a) naphthalene; b) anthracene; c) fluoranthene (Positive Phase: Blue Color; Negative Phase: Red Color). ....	97
Figure 3.9. Removal efficiency (%Rem) of PAHs (naphthalene, anthracene and fluoranthene). Conditions: C <sub>0</sub> =0.01 mmol.L <sup>-1</sup> , dosage of adsorbent of 0.1 mg.mL <sup>-1</sup> , 25 °C for 30 min. ....	99
Figure 3.10. Adsorption mechanisms of PAHs into the G-mCS/GO. ....	101
Figure 4.1. Methodological representation of the preparation steps for the green mCS/GO. ....	113
Figure 4.2. BET isotherms (a) and pore size distribution (b) of green mCS/GO and green mCS/GO+NAP. ....	121
Figure 4.3. Thermogravimetric curves (a) and Raman spectrum (b) of green mCS/GO and green mCS/GO + NAP. ....	123
Figure 4.4. High-resolution of C(1s) (a); O(1s) (b); N(1s) (c) and Fe(2p) (d). ....	124
Figure 4.5. XRD patterns of green mCS/GO + NAP (a) and FT-IR spectra of green mCS/GO + NAP (black line) and regenerated green mCS/GO + NAP (red line). ....	125
Figure 4.6. SEM images of green mCS/GO + NAP (a-b) and green mCS/GO + NAP regenerated (c-d). ....	126
Figure 4.7. Pareto Chart (a) and Response surface for Y (mmol.g <sup>-1</sup> ) as a function of NAP concentration (mmol.L <sup>-1</sup> ) and mCS/GO dosage (mg.mL <sup>-1</sup> ). ....	129
Figure 4.8. Adsorption kinetics curves of NAP onto the green adsorbent (a); Fitting of the experimental data to the PFO and PSO (b); EMTR (c) and IP models (d). ....	131
Figure 4.9. Adsorption isotherms at 20 °C, 30 °C and 40 °C (a); Langmuir, Freundlich and Dubinin-Radushkevich adsorption isotherm models at 20 °C (b); 30 °C (c) and 40 °C. ....	132

Figure 4.10. Plot of $\ln K_c$ versus $1/T$ (a); Plot of $\ln C_e$ versus $1/T$ obtained for the adsorption of NAP onto green mCS/GO (b). .....	135
Figure 4.11. Efficiency of different elution solvents in NAP recovery (a); Regeneration cycles of NAP onto green mCS/GO using methanol as eluent (b); NAP removal (%) in ultrapure water and river water (c). .....	139

## LISTA DE TABELAS

Table 2.1. Search Outline Strategies used on the review. ....	23
Table 2.2. Kinetic models: Pseudo-First Order's (PFO) and Pseudo-Second Order's (PSO). 29	
Table 2.3. Parameters of the pseudo-first order and pseudo-second order models adjusted to the adsorption kinetic data obtained under experimental conditions of initial PAH concentration, temperature, pH, stirring speed, contact time and dosage of different nanoadsorbent materials. ....	30
Table 2.4. Models for fixed-bed adsorption columns. ....	34
Table 2.5. Main adsorption equilibrium models. ....	36
Table 2.6. Models of adsorption isotherms for the removal of PAHs by different nanoadsorbent materials. ....	37
Table 2.7. Thermodynamic parameters for the removal of PAHs by different nanoadsorbent materials. ....	41
Table 2.8. Summary of sources and methodologies used on the green synthesis of graphene-based nanomaterials. ....	53
Table 2.9. Evaluation of the efficiency of different PAH removal techniques. ....	60
Table 3.1. Characterization analysis of C-mCS/GO and G-mCS/GO composites. ....	81
Table 3.2. Elemental mass composition (%) of C-mCS/GO and G-mCS/GO and C-Fe <sub>3</sub> O <sub>4</sub> and G-Fe <sub>3</sub> O <sub>4</sub> particles. ....	87
Table 3.3. Elemental mass composition (%) of C-mCS/GO and G-mCS/GO and C-Fe <sub>3</sub> O <sub>4</sub> and G-Fe <sub>3</sub> O <sub>4</sub> particles. ....	92
Table 3.4. Physicochemical properties of naphthalene, anthracene and fluoranthene molecules. ....	95
Table 3.5. Quantum chemical parameters of naphthalene, anthracene and fluoranthene using the B3LYP/6-31G (d,p) model. ....	97
Table 3.6. Adsorption capacity of PAHs by the adsorbents (C-mCS/GO and G-mCS/GO). ..	99
Table 3.7. Comparison of the adsorption capacity and removal efficiency of C-mCS/GO and G-mCS/GO with other adsorbents studied in the literature. ....	100
Table 4.1. Green mCS/GO characterization techniques before and after the adsorptive process. ....	114
Table 4.2. Experimental conditions investigated in the central composite design. ....	115
Table 4.3. Central composite design (CCD) matrix of experiments. ....	116
Table 4.4. Kinetics and equilibrium models. ....	118
Table 4.5. SS <sub>BET</sub> , pore volume and diameter of green mCS/GO before and after NAP adsorption. ....	121
Table 4.6. Results of ANOVA for quadratic model. ....	127
Table 4.7. Fit parameters of kinetic models PFO, PSO, EMTR and IP. ....	130
Table 4.8. Fit parameters of equilibrium isotherm models Langmuir, Freundlich and Dubinin-Radushkevich. ....	133
Table 4.9. Thermodynamic parameters for NAP adsorption at 20 °C, 30 °C and 40 °C. ....	134
Table 4.10. Isothermic heat values ( $\Delta H_{st}$ ) obtained through the adsorption of NAP onto green mCS/GO. ....	136
Table 4.11. Comparison of the $q_{max}$ for the green mCS/GO with other adsorbents. ....	138
Tabela 5.1. Resultados de eficiência de remoção (%) dos PAHs para os materiais adsorventes. ....	150

Tabela 5.2. Parâmetros de ajuste dos modelos cinéticos, de equilíbrio e termodinâmicos.... 152

## LISTA DE SIGLAS E ABREVIACOES

ANOVA – Anlise de varincia;  
ANP – Agncia Nacional do Petrleo;  
ANT – Antraceno;  
BET – Brunauer, Emmett and Teller method;  
CCD – Central Composite Design;  
EDS – Energy Dispersive X-ray Spectroscopy;  
EMTR – External Mass Transfer Resistance;  
FTIR – Fourier transform infrared spectroscopy;  
FLT – Floranteno;  
IP – Intraparticle diffusion;  
NAP – Naftaleno;  
PAHs – Polycyclic Aromatic Hydrocarbons;  
 $q_{\max}$  – maximum adsorption capacity;  
rpm – rotao por minuto;  
PFO – Pseudo-First Order;  
PSO - Pseudo-Second Order;  
SEM – Scanning Electron Microscopy (SEM);  
 $SSA_{\text{BET}}$  – Specific Surface Area;  
TG/DTG – Thermogravimetric analysis;  
XPS – X-ray photoelectron spectroscopy;  
XRD – X-ray diffraction;  
 $\Delta H^\circ$  – Variao de Entalpia;  
 $\Delta G^\circ$  – Variao da Energia Livre de Gibbs;  
 $\Delta S^\circ$  – Variao de Entropia.

## SUMÁRIO

<b>Capítulo 1. Introdução e objetivos</b> .....	16
<b>1.1. Motivação à pesquisa e Relevância</b> .....	16
<b>1.2. Objetivos</b> .....	17
1.2.1. Objetivo geral.....	17
1.2.2. Objetivos específicos .....	18
<b>1.3. Apresentação da dissertação em capítulos</b> .....	18
<b>Capítulo 2. Revisão Bibliográfica</b> .....	21
<b>2.1. Introduction</b> .....	22
<b>2.2. Research strategy</b> .....	23
<b>2.3. Sources of Polycyclic aromatic hydrocarbons (PAHs)</b> .....	24
<b>2.4. Adsorption processes for PAHs removal</b> .....	26
2.4.1 General concepts .....	26
2.4.2 Adsorption kinetics.....	27
2.4.3 Adsorption modelling for packed beds.....	33
2.4.4 Adsorption isotherms.....	35
2.4.5 Adsorption thermodynamics.....	39
<b>2.5. Nanomaterial-based adsorbents</b> .....	42
2.5.1 Graphene-based nanomaterials: Conventional chemistry .....	45
2.5.2 Adsorption by green graphene-based nanomaterials.....	50
2.5.3 Application of green synthesized nanomaterials for PAHs removal .....	55
2.5.4. Comparison with other PAHs removal technologies .....	58
<b>2.6. Challenges, future prospects and conclusions</b> .....	62
<b>Acknowledgements</b> .....	63
<b>References</b> .....	63
<b>Capítulo 3. Síntese dos materiais adsorventes e teste de afinidade</b> .....	74
<b>3.1. Introduction</b> .....	75
<b>3.2. Materials and methods</b> .....	76
3.2.1. Materials and reagents .....	76
3.2.2. Preparation of conventional and green mCS/GO.....	77
3.2.3. Preparation of graphene oxide (GO).....	78
3.2.4. Conventional synthesis of Fe <sub>3</sub> O <sub>4</sub> magnetic particles .....	79
3.2.5. Conventional synthesis of magnetic chitosan (mCS) .....	79
3.2.6. Conventional synthesis of mCS/GO .....	80
3.2.7. Green synthesis of Fe <sub>3</sub> O <sub>4</sub> magnetic particles .....	80

3.2.8. Green synthesis of mCS/GO .....	80
3.2.9. Characterization analyses.....	81
3.2.10. Molecular modeling .....	82
3.2.11. Adsorptive affinity assays .....	83
<b>3.3. Results and discussion .....</b>	<b>84</b>
3.3.1. Conventional and green mCS/GO characterizations .....	84
3.3.1.1. Evaluation of the crystal structure of synthesized materials.....	84
3.3.1.2. Functional group identification.....	85
3.3.1.3. Evaluation of chemical composition and functional groups.....	86
3.3.1.4. Magnetization curves .....	89
3.3.1.5. Evaluation of morphological properties of synthesized materials.....	90
3.3.1.6. Evaluation of the thermal properties of adsorbents .....	92
3.3.1.7. pH evaluation .....	93
3.3.2. Molecular simulation .....	95
3.3.3. Adsorptive affinity assays.....	98
3.3.4. Mechanisms of PAH adsorption .....	101
<b>3.4. Challenges, limitations and future prospects .....</b>	<b>102</b>
<b>3.5. Conclusions.....</b>	<b>103</b>
<b>Declaration of Interest.....</b>	<b>103</b>
<b>CRedit authorship contribution statement .....</b>	<b>103</b>
<b>Acknowledgment .....</b>	<b>104</b>
<b>References.....</b>	<b>104</b>
<b>Capítulo 4. Estudo de adsorção do naftaleno em green mCS/GO .....</b>	<b>110</b>
<b>4.1. Introduction .....</b>	<b>111</b>
<b>4.2. Methodology .....</b>	<b>112</b>
4.2.1. Green mCS/GO synthesis .....	113
4.2.2. Characterization analysis .....	113
4.2.3. CCD experiment .....	114
4.2.4. Adsorption assays .....	116
4.2.4.1. Kinetic study .....	117
4.2.4.2. Equilibrium study.....	118
4.2.4.3. Regeneration study.....	119
4.2.5. HPLC quantification analysis .....	119
<b>4.3. Results and discussion .....</b>	<b>120</b>
4.3.1. Adsorbent characterizations before and after NAP adsorption.....	120

4.3.2. Statistical analysis .....	127
4.3.3. Adsorption kinetics .....	129
4.3.4. Adsorption isotherms .....	132
4.3.5. Thermodynamic study .....	134
4.3.6. Adsorption Mechanisms .....	136
4.3.8. Adsorption of PAHs from river water samples .....	139
<b>4.4. Conclusions.....</b>	<b>140</b>
<b>Declaration of Interest.....</b>	<b>141</b>
<b>CRedit authorship contribution statement .....</b>	<b>141</b>
<b>Acknowledgment .....</b>	<b>141</b>
<b>References.....</b>	<b>141</b>
<b>Capítulo 5. Discussão Geral.....</b>	<b>148</b>
<b>Capítulo 6. Conclusão Geral e Sugestões .....</b>	<b>154</b>
<b>REFERÊNCIAS .....</b>	<b>157</b>
<b>ANEXO I. Licenças de publicação de artigos na dissertação .....</b>	<b>160</b>
<b>ANEXO II. Materiais Suplementares.....</b>	<b>163</b>

## Capítulo 1. Introdução e objetivos

### 1.1. Motivação à pesquisa e Relevância

Os efluentes gerados pelo setor de petróleo e gás apresentam elevado potencial poluidor, devido à presença de compostos orgânicos poluentes, como os Hidrocarbonetos Policíclicos Aromáticos (PAHs<sup>1</sup>). Diante disto, a indústria do petróleo tem buscado o desenvolvimento de tecnologias cada vez mais eficientes para o tratamento de efluentes, visando assim atender as demandas sociais, econômicas e ambientais (Abdel-Shafy and Mansour, 2016).

A água produzida (AP) caracteriza-se como um subproduto da indústria de petróleo e gás, podendo ser utilizada para reinjeção em poços petrolíferos, visando aumentar a produção do mesmo, ou também pode ser descartada após o seu tratamento. A presença de PAHs na água produzida representa uma grande fonte de preocupação para o setor, devido ao seu elevado potencial tóxico e poluidor, podendo causar danos irreparáveis aos ecossistemas, principalmente ao meio aquático (Beyer et al., 2020).

Muitos estudos têm sido desenvolvidos visando à otimização dos processos de tratamento de águas residuais, dentre os quais se destacam a degradação microbiana (Sun et al., 2019), que é um método de biorremediação, que consiste na utilização de microrganismos para a remoção de compostos poluentes (Qi et al., 2017). Outros métodos de tratamento podem ser utilizados, como os processos de oxidação avançados (POAs) (Haneef et al., 2020), a separação por membranas (Li et al., 2019) e os processos adsorptivos (Song et al., 2021). Neste contexto, os processos adsorptivos têm sido muito utilizados por apresentarem baixo custo de investimento, alta seletividade, aplicabilidade em baixas concentrações, podendo ainda ser aplicados em processos em batelada e contínuos, além da possibilidade de regeneração e de reutilização do adsorvente (Nasuhoglu et al., 2012).

Os materiais à base de grafeno têm chamado a atenção de pesquisadores quanto a sua aplicação como adsorventes para a remediação de PAHs em águas residuais. Os materiais à base de grafeno possuem algumas características, como elevada área superficial, resistência mecânica e baixo custo potencial de produção, o que facilita sua aplicação em processos de tratamento de efluentes industriais (Chen e Huang, 2020).

A quitosana é um biopolímero obtido através da reação de desacetilação da quitina, apresentando alta biocompatibilidade e biodegradabilidade, o que a torna biológica e

---

<sup>1</sup> A sigla PAHs foi padronizada em inglês ao longo desta dissertação.

quimicamente aceitável para aplicações diversas. Ela pode ser aplicada como floculante, coagulante e adsorvente para a remoção de contaminantes como metais tóxicos, tinturas, pesticidas, antibióticos e contaminantes orgânicos de águas residuais (Pal et al., 2020). Diante disso, a combinação do óxido de grafeno (GO) com a quitosana pode contribuir para a modificação das características do GO, melhorando consideravelmente o seu desempenho na remoção de poluentes orgânicos, aumentando assim a eficiência do processo adsorativo (Neves et al., 2020).

A aplicação de nanoadsorventes verdes, produzidos a partir de agentes naturais (como extratos de plantas, frutas e microrganismos), que atuam como redutores na geração de adsorventes para a remoção de poluentes orgânicos do meio ambiente, tem despertado a atenção de pesquisadores (Queiroz et al., 2022b). Extratos vegetais, microrganismos e resíduos agrícolas possuem uma variedade de compostos ativos e metabólitos que podem atuar como agentes estabilizadores, reticulantes ou capeadores nos processos de síntese, possibilitando assim o desenvolvimento de novos compósitos com alta eficiência, ecologia e baixo custo (Shi et al., 2020; Zhang et al., 2021). Assim, o preparo, a caracterização e a aplicação destes materiais sustentáveis têm sido o foco principal de alguns estudos, devido à sua capacidade de minimizar os efeitos tóxicos causados pelo uso de reagentes químicos nos processos convencionais de síntese de adsorventes (Bolade et al., 2020).

Neste contexto, fica clara a relevância desta pesquisa, a qual traz contribuições originais acerca da adsorção de PAHs em efluentes da indústria do petróleo e gás, visando preencher lacunas na literatura, no que diz respeito à aplicação de materiais ecologicamente corretos para a remoção de poluentes em águas residuais. Diante disso, os estudos apresentados ao longo dos capítulos desta dissertação buscam propor uma metodologia alternativa e sustentável para a síntese de materiais à base de grafeno, visto que este tema tem grande relevância para o contexto atual.

## **1.2. Objetivos**

### **1.2.1. Objetivo geral**

O desenvolvimento desta pesquisa de mestrado teve como objetivo principal avaliar o potencial de remoção de Hidrocarbonetos Policíclicos Aromáticos (PAHs), presentes em efluentes sintéticos e reais, por meio da aplicação de compósitos adsorventes de óxido de grafeno e quitosana magnética, sintetizados por rotas convencional e verde.

### 1.2.2. Objetivos específicos

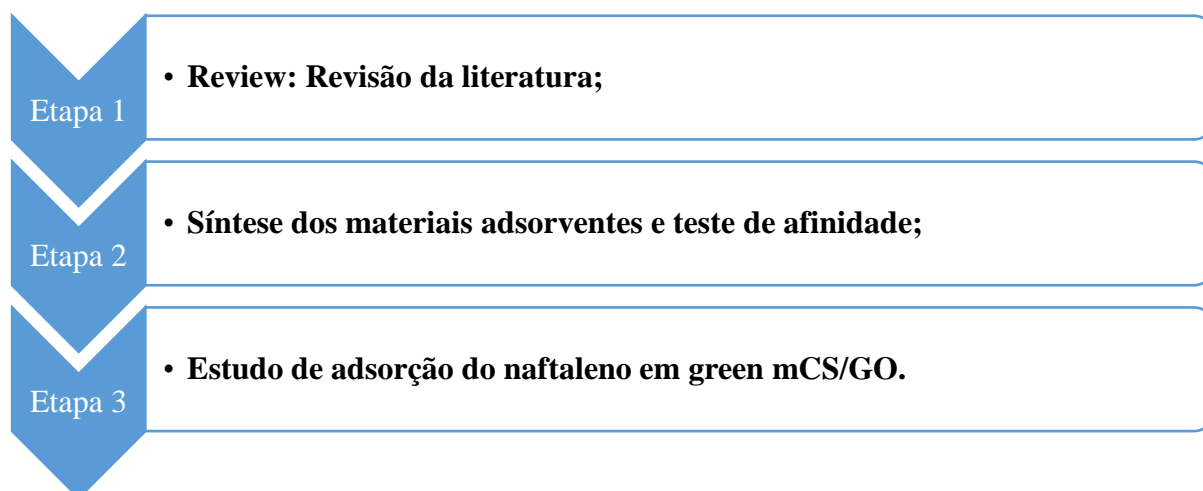
Para atender o objetivo geral, foram propostos os seguintes objetivos específicos:

- Sintetizar nanopartículas de ferro magnéticas por rotas convencional e química verde e incorporá-las à quitosana e ao óxido de grafeno (GO);
- Caracterizar os materiais sintetizados;
- Avaliar a afinidade adsortiva entre diferentes PAHs e os nanocompósitos magnéticos de óxido de grafeno-quitosana para seleção do sistema com maior potencial de remoção;
- Avaliar a influência do pH na adsorção do PAH selecionado pelos nanocompósitos magnéticos de óxido de grafeno-quitosana, por meio da análise de potencial zeta;
- Analisar o efeito dos fatores experimentais por meio de um planejamento experimental do tipo delineamento composto central rotacional (DCCR);
- Investigar a cinética e o equilíbrio de adsorção do PAH selecionado em um sistema de banho finito;
- Determinar as grandezas termodinâmicas do processo de adsorção do PAH selecionado em um sistema de banho finito;
- Realizar a simulação molecular dos adsorbatos investigados;
- Caracterizar as partículas adsorventes pós-processo adsortivo e investigar o(s) mecanismo(s) de adsorção.

### 1.3. Apresentação da dissertação em capítulos

Esta dissertação de mestrado foi estruturada em capítulos, de forma que os resultados obtidos foram apresentados em um conjunto de três etapas, conforme apresentado na Figura 1.1. Cada etapa da pesquisa foi discutida por meio de artigos científicos publicados ao longo do desenvolvimento desta pesquisa. Estes artigos estão apresentados no formato de manuscritos os quais foram publicados/submetidos em periódicos internacionais, conforme dispostos nos Capítulos 2 a 4. Além disso, o Capítulo 5 apresenta uma discussão geral dos resultados obtidos na pesquisa, trazendo um resumo contextualizado das etapas envolvidas no desenvolvimento desta pesquisa.

**Figura 1.1.** Esquema das principais etapas de execução da dissertação de mestrado.



O **Capítulo 2** apresenta o artigo de revisão publicado no periódico *Journal of Hazardous Materials* e intitulado “*Adsorption of Polycyclic Aromatic Hydrocarbons from wastewater using graphene-based nanomaterials synthesized by conventional chemistry and green synthesis: A critical review*”, o qual traz discussões sobre a síntese e aplicações de diferentes adsorventes à base de grafeno para a remoção de PAHs. Além disso, este artigo aborda o tema sobre o desenvolvimento de nanoadsorventes verdes, visando a sua aplicação em processos adsorptivos de contaminantes orgânicos da indústria do petróleo.

O **Capítulo 3** apresenta o artigo publicado no periódico *Journal of Cleaner Production* e intitulado “*Comparative efficiency of polycyclic aromatic hydrocarbon removal by novel graphene oxide composites prepared from conventional and green synthesis*”, o qual compara o desempenho adsorptivo dos adsorventes C-mCS/GO e G-mCS/GO para a remoção de PAHs. Também foi realizada a simulação molecular dos PAHs (naftaleno, antraceno e fluoranteno), visando determinar os possíveis mecanismos envolvidos no processo de adsorção.

O **Capítulo 4** apresenta o artigo submetido ao periódico *Environmental Science and Pollution Research* e intitulado “*Adsorption of naphthalene polycyclic aromatic hydrocarbon from wastewater by a green magnetic composite based on chitosan and graphene oxide*”, o qual apresenta um estudo cinético, de equilíbrio e termodinâmico sobre a adsorção de naftaleno no adsorvente verde mCS/GO. Também foi realizado um planejamento experimental do tipo DCCR, um estudo de regeneração do adsorvente e uma aplicação do mesmo em uma amostra de efluente real.

No **Capítulo 5** tem-se uma discussão geral sobre os principais resultados obtidos nesta dissertação de mestrado. Finalmente, no **Capítulo 6**, são reportadas as conclusões gerais desta

pesquisa, bem como as sugestões para trabalhos futuros usando a tecnologia de adsorção de PAHs em nanomateriais adsorventes verdes.

## Capítulo 2. Revisão Bibliográfica

### **Adsorption of Polycyclic Aromatic Hydrocarbons from wastewater using graphene-based nanomaterials synthesized by conventional chemistry and green synthesis: A critical review<sup>2</sup>**

Ruth Nóbrega Queiroz<sup>a</sup>, Patrícia Prediger<sup>b</sup>, Melissa Gurgel Adeodato Vieira<sup>a\*</sup>

<sup>a</sup>Process and Product Development Department, School of Chemical Engineering, University of Campinas – UNICAMP, Albert Einstein Avenue, 500, 13083-852 Campinas, São Paulo, Brazil.

<sup>b</sup>School of Technology, University of Campinas – UNICAMP, 13484-332 Limeira, São Paulo, Brazil.

\*melissag@unicamp.br

#### **ABSTRACT**

Polycyclic aromatic hydrocarbons (PAHs) are organic pollutants formed mainly by the incomplete combustion of organic matter, such as oil, gas and coal. The presence of PAHs can cause irreparable damage to the environment and living beings, which has generated a global concern with the short- and long-term risks that the emission of these pollutants can cause. Many technologies have been developed in the last decades aiming at the identification and treatment of these compounds, mainly, the PAHs from wastewater. This review features an overview of studies on the main methods of PAHs remediation from wastewater, highlighting the adsorption processes, through the application of different adsorbent nanomaterials, with a main focus on graphene-based nanomaterials, synthesized by conventional and green routes. Batch and fixed-bed adsorptive processes were evaluated, as well as, the mechanisms associated with such processes, based on kinetic, equilibrium and thermodynamic studies. Based on the studies analyzed in this review, green nanomaterials showed higher efficiency in removing PAHs than the conventional nanomaterials. As perspectives for future research, the use of green nanomaterials has shown to be sustainable and promising for PAHs remediation, so that further

---

<sup>2</sup> Manuscript published in *Journal of Hazardous Materials* 422 (2022) 126904. DOI: 10.1016/j.jhazmat.2021.126904. Reprinted with permission from *Journal of Hazardous Materials*. Copyright 2021 Elsevier (Anexo I).

studies are needed to overcome the possible challenges and limitations of green synthesis methodologies.

**Keywords:** PAHs; Remediation; Green nanomaterials; Carbon-based nanomaterials; Graphene.

## 2.1. Introduction

Industrial wastewater, including oil from the oil sector, has a high pollutant potential, due to the presence of aromatic pollutants, such as Polycyclic Aromatic Hydrocarbons (PAHs). Based on this, some methodologies for treating industrial effluents have been applied to remove such contaminants from ecosystems, thus seeking to meet socio-environmental and economic demands. The presence of PAHs in wastewater represents a major source of concern for the industrial sector, since they can cause irreparable damage to the environment and to humans, due to their high toxic and polluting potential (Beyer et al., 2020).

Many studies have been developed aiming to optimize the wastewater treatment processes, such as bioremediation methods, which are based on the application of microorganisms that perform the biodegradation of polluting compounds through their microbial activity (Qi et al., 2017). Other treatment methods can be applied, such as chemical oxidation, coagulation-flocculation, membrane separation and adsorption (Scurtu, 2009). Among these technologies, the adsorptive processes have been widely used, as they present low production cost, high selectivity, applicability in low concentrations, they can be applied in continuous and batch processes. In addition to this, adsorbent materials can be regenerated and reused in other adsorptive cycles (Nasuhoglu et al., 2012).

Some graphene-based materials have attracted the attention of researchers regarding their use for the PAHs adsorption from wastewater. Graphene-based materials have some characteristics, such as high surface area, mechanical resistance and low-cost production, which facilitate their use for the treatment of effluents by adsorption processes (Chen and Huang, 2020).

The application of green nanoadsorbents, produced by means of natural agents (plants extracts, fruits and microorganisms), for the removal of organic pollutants, like PAHs, from the environment, has been the main focus of some studies, due to their capacity to minimize the toxic effects caused by the use of chemical reagents in the conventional synthesis processes of adsorbents (Bolade et al., 2020).

In this context, this review aims to critically address researches about PAHs removal from wastewater, using different remediation technologies, but with a main focus on the adsorption of PAHs by means of graphene-based materials, synthesized by conventional and green methods. Therefore, the main topics that will be covered in this review are: (i) Overview of Polycyclic Aromatic Hydrocarbons, sources and removal techniques; (ii) General concepts of adsorption, kinetics, isotherms, thermodynamics and fixed-bed applications; (iii) Nanomaterial-based adsorbents; (iv) Adsorption of PAHs by graphene-based nanomaterials; (v) Green synthesized nanomaterials for PAHs removal.

## 2.2. Research strategy

As a research strategy for the development of this review, initially, a wide bibliographic search was carried out through the scientific document bases Royal Society of Chemistry (RSC), ScienceDirect and American Chemical Society (ACS). The search was carried out using as keywords, "PAHs removal from wastewater", "PAHs adsorption", "graphene-based nanomaterials", "green nanomaterials", "green nanomaterials for PAHs removal" and other similar terms. As exclusion criteria, the articles were selected between the years 2008 to 2021, and considering only indexed articles written in English. To identify the articles of interest, a combination of terms was used, which were called 'Search Outline Strategies', as shown in Table 2.1, in which the 'base terms' on the left were combined with the 'complementary terms' on the right.

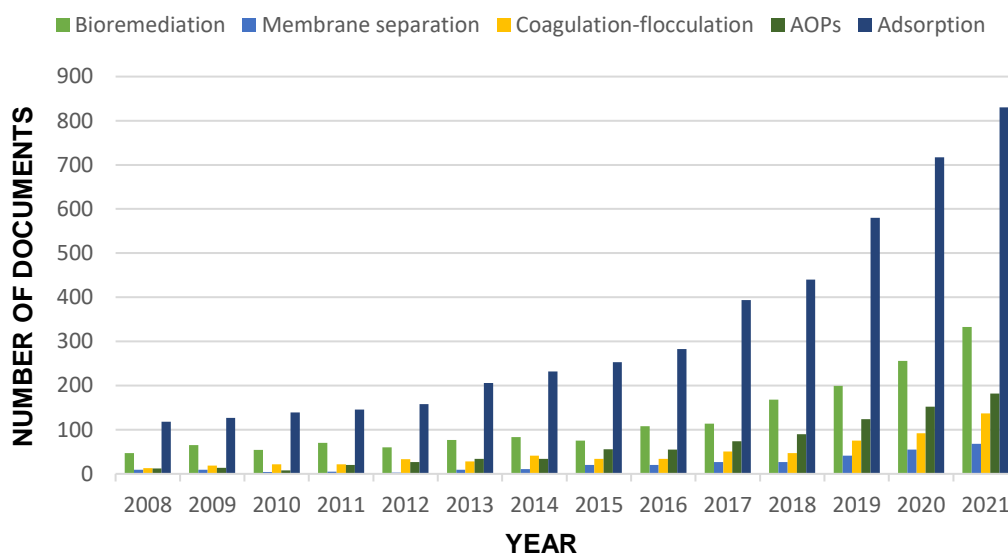
**Table 2.1.** Search Outline Strategies used on the review.

Base terms	Complementary terms
PAHs	Wastewater
	Remediation technologies
Adsorption	Adsorbents
	Kinetics, isotherms and thermodynamics
Graphene	Fixed-bed
	Green
Nanomaterials	Synthesis

Applying the established search strategy, an average of 8170 articles were found, adding up all the databases used. After analyzing the titles, 200 articles were selected for reading the abstracts. After analyzing the abstracts, the literature was selected to be discussed in the review

based on its relevance to the subject and its references. At the end, a total of 65 articles were chosen, covering experimental and observational studies, which met the initially proposed criteria. It is important to highlight that this review emphasizes, mainly, the adsorption of PAHs by graphene-based nanomaterials (synthesized by conventional and green route) from wastewater. However, other PAHs remediation technologies have also been addressed. Figure 2.1 graphically shows the number of documents published per year and the most applied methods for removing PAHs from wastewater, based on searches in the ScienceDirect, RSC and ACS databases.

**Figure 2.1.** Number of documents published per year, which address technologies for the removal of PAHs from wastewater, from 2008 to 2021, based on searches in the ScienceDirect, RSC and ACS databases.



### 2.3. Sources of Polycyclic aromatic hydrocarbons (PAHs)

Polycyclic aromatic hydrocarbons (PAHs) can be defined as nonpolar organic substances formed basically by carbon and hydrogen atoms. In general, PAHs are formed through incomplete combustion of organic matter and fossil fuels, such as gas, oil, coal, wood, smoked foods, among others (Abdel-Shafy and Mansour, 2016; Ghosal et al., 2016).

PAHs can be divided into two classifications: (LMW) low molecular weight PAHs and (HMW) high molecular weight PAHs. LMW PAHs have a central structure composed of two or three aromatic rings, for example, naphthalene, acenaphthene, fluorene, anthracene and phenanthrene. HMW PAHs have molecular structures composed of four or more aromatic

rings, for example, fluoranthene, pyrene and benzofluoranthenes. LMW PAHs have greater volatility and solubility than HMW PAHs, which makes them break more easily than HMW PAHs. (Adeniji et al., 2018) (see Fig. S1 and Table S1).

The main sources of PAHs for the environment can be of natural (biological) or anthropogenic (pyrogenic and petrogenic) origins (see Fig. S2). Biological PAHs are those produced through the enzymatic activity of some types of plants and bacteria or formed through the degradation of organic matter. Some biological sources of PAHs are: volcanoes, enzymatic activity of bacteria and algae, degradation of plant matter and rocky sediments containing oil and gas (Abdel-Shafy and Mansour, 2016).

Pyrogenic PAHs are formed through a pyrolysis process, in which organic substances are exposed to high temperatures (350° to 1200°C) in the absence of oxygen. They are usually formed through incomplete combustion of biomass and fossil fuels, and are found in greater concentrations in urban areas (Abdel-Shafy and Mansour, 2016; Masood et al., 2016).

PAHs can also be found in crude oil, which can form during the maturation process, or even in petroleum products, which can be called petrogenic PAHs. These PAHs can be found during the stages of transportation, storage and consumption of oil and its derivatives. Oil spills in oceans and rivers, leaks in storage tanks and emission of gases during transport, are among the main factors responsible for the increase in the concentration of petrogenic PAHs in the environment (Abdel-Shafy and Mansour, 2016; Nikitha et al., 2017).

Produced water (PW) is characterized as a by-product of the petrochemical industry, which can be used for reinjection in oil wells, to increase its production, or it can also be discarded after its treatment (Abdullahi et al., 2021). The concentration of PAHs in wastewater from petrogenic origin represents a major source of concern for the sector. Despite representing a small fraction (about 0.306%) of the composition of the PW, PAHs are considered risky components, due to their high toxic and polluting potential, which can last for many years in the ecosystems, and can cause irremediable damage to human health, due to their carcinogenic, genotoxic and mutagenic potential (Beyer et al., 2020; Mukhopadhyay et al., 2020).

## 2.4. Adsorption processes for PAHs removal

### 2.4.1 General concepts

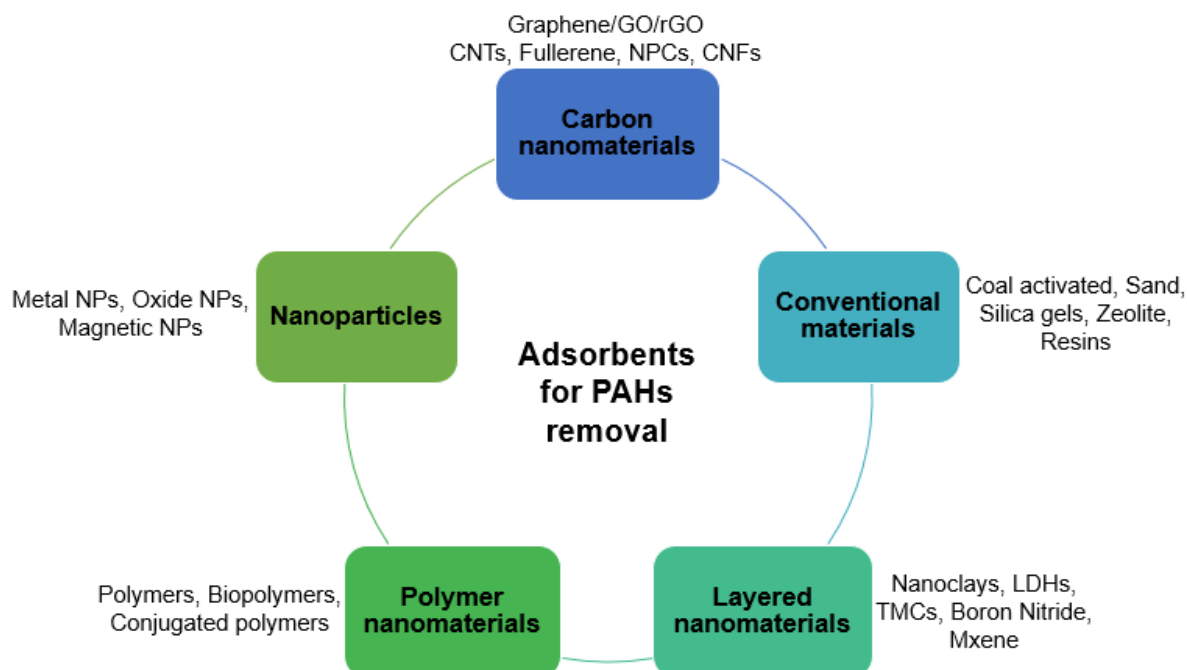
Adsorption is characterized as a surface phenomenon, which is associated with factors such as the porous structure and the chemical properties of the adsorbent solid. Differences in molar mass, shape or polarity are the main factors that contribute to the separation of adsorbate from the fluid phase, as they allow the attachment of some molecules to the surface of the adsorbent material. The nature of the interactions between adsorbate and adsorbent influences the classification of adsorbent processes, which can be classified into two mechanisms, physical adsorption (physisorption) and chemical adsorption (chemisorption) (Marczewska and Marczewski, 2002).

The physisorption processes are reversible and occur at low temperatures, so that the bonds between the adsorbate and the adsorbent surface occur through relatively weak electrostatic interactions, being attributed to dipole-dipole, Van der Waals and  $\pi$ - $\pi$  interactions, dispersion interactions and hydrogen bonding (Ruthven, 1984). The chemisorption processes are irreversible and, generally, occur at high temperatures, allowing chemical interactions to be established through the electronic transfer between the adsorbent surface and the adsorbate, generating changes in the chemical nature of the adsorbate (Lander, 1964; Muscat and Newns, 1978).

The adsorptive processes are operated in two main modes: batch flow and continuous flow systems. Batch adsorption is widely used to treat small volumes, often used on a pilot scale in laboratories. These systems are composed of a batch reactor containing a colloidal suspension of an adsorbent in the presence of an adsorbate that is mixed in a certain time. The effect of parameters such as temperature, adsorbate concentration, amount of adsorbent, agitation speed and particle size of the adsorbent are also evaluated, until the equilibrium condition is reached (Schweich and Sardin, 1981). Continuous adsorption systems are applied, generally, for industrial scale processes. Of all techniques used for the contact between adsorbate and the adsorbent in these processes, the fixed bed column of continuous flow is the most applied. In studies of continuous adsorption systems, parameters such as initial concentration of adsorbate, flow of adsorbate, column bed height, pH, particle size of the adsorbent, system temperature, breaking points and exhaustion, have their effect evaluated in column adsorptive processes (Gupta et al., 1998).

The schematic representation of the main types of adsorbents used for PAHs adsorption from wastewater is shown in Figure 2.2. It is important to emphasize that, in this review, only carbon-based adsorbents will be addressed.

**Figure 2.2.** Schematic representation of the types of adsorbents used for PAHs adsorption from wastewater.



#### 2.4.2 Adsorption kinetics

Adsorption kinetics studies are very important for the understanding of the mechanisms that control the adsorptive processes, as well as their limiting steps and the determination of the ideal process conditions. Factors such as pH, adsorbate concentration, temperature, size and specific surface area of the adsorbent, directly influence the adsorption kinetics (Ho and McKay, 1999). The main kinetic models applied to the study of the behavior of adsorbents, as well as, the mechanisms that control the adsorption, are the Pseudo-First Order (PFO), proposed by Lagergren (1898), and Pseudo-Second Order (PSO), proposed by Ho and McKay (1999), models. Table 2.2 displays the equations of the PFO and PSO models, as well as their linearized forms.

Ruiz et al. (2020) proposed the synthesis of an ecologically correct and low-cost production of material, aiming at the remediation of PAHs from water sources. In this study, chitosan granules were modified by means of FeO and TiO<sub>2</sub> through ionic cross-linking (Ch-

FeO/TiO<sub>2</sub>), in which FeO was synthesized by the coprecipitation method and TiO<sub>2</sub> by the green chemistry method. SEM, XRD, FTIR and BET techniques were used to characterize the obtained nanomaterial, then it was applied for NAP removal from seawater samples. Through the adsorption studies, an equilibrium time of 240 min and an adsorption capacity of 33 mg.g<sup>-1</sup> were obtained. The experimental kinetic data showed a better adjustment to the PSO's model, indicating that chemisorption is the mechanism that governs NAP adsorption. The experimental equilibrium data had a better adjustment to Freundlich's model, which suggests the formation of a heterogeneous multilayered surface.

In the study developed by Eeshwarasinghe et al. (2018), PAHs (naphthalene, acenaphene, fluorene and phenanthrene) were removed from wastewater using granular activated carbon (GAC). Batch adsorption and fixed-bed column experiments were conducted to evaluate the efficiency of GAC in the PAHs removal. For the batch adsorption experiments, the kinetic data were better adjusted to the PFO's model, which points out that the main mechanism associated with this process is the physisorption. The experimental data of batch equilibrium adsorption were better described by the Freundlich's model, which suggests heterogeneous adsorption. In dynamic adsorption by fixed-bed column, the curves had a better adjustment to the Thomas's model. The results showed that the batch adsorption and the fixed bed column were able to effectively remove PAHs from wastewater.

Table 2.3 displays the results obtained for several studies by adjusting the PFO and PSO models to the experimental kinetic data for the adsorption of PAHs from wastewater by different nano-adsorbent materials. In the studies evaluated, the PSO model had a better adjustment to the kinetic experimental data of PAHs adsorption from wastewater, inferring that chemisorption is the main mechanism involved in this process. This model is derived from the Langmuir's kinetic model equation, which states that the adsorptive process is governed by chemical reactions that occur on a homogeneous surface. Generally, the PSO model best represents the kinetic data for most adsorptive systems, as it has the ability to "smooth out" the experimental data, in addition to providing the best correlation for the systems studied, over the entire process time, however, this model is better suited to experimental data in the initial stages of the adsorptive process (Ho and McKay, 1999; Plazinski et al., 2009).

**Table 2.2.** Kinetic models: Pseudo-First Order's (PFO) and Pseudo-Second Order's (PSO).

Kinetic model	Equation	Linearized form
PFO: Related with the adsorbent's adsorption capacity (Lagergren, 1898).	$q(t) = q_e(1 - e^{-k_1 t}) \quad (1)$	$\ln(q_e - q(t)) = \ln q_e - k_1 t \quad (2)$
PSO: Related with the chemisorption of adsorbate in the adsorbent (Ho and McKay, 1999).	$q(t) = \frac{k_2 q_e^2 t}{1 + k_2 q_e t} \quad (3)$	$\frac{t}{q(t)} = \frac{1}{k_2 q_e^2} + \frac{t}{q_e} \quad (4)$

$q(t)$ : adsorbate concentration on the adsorbent surface at time  $t$  (min) ( $\text{mg}\cdot\text{g}^{-1}$ ),  $q_e$ : adsorbate concentration in equilibrium on the adsorbent surface ( $\text{mg}\cdot\text{g}^{-1}$ ),  $k_1$ : PFO's rate constant ( $\text{min}^{-1}$ ) and  $k_2$ : PSO's rate constant ( $\text{g}\cdot\text{mg}^{-1}\cdot\text{min}^{-1}$ ).

**Table 2.3.** Parameters of the pseudo-first order and pseudo-second order models adjusted to the adsorption kinetic data obtained under experimental conditions of initial PAH concentration, temperature, pH, stirring speed, contact time and dosage of different nanoadsorbent materials.

PAHs	Nanoadsorbent	Experimental conditions	Pseudo-first-order (PFO)			Pseudo-second-Order (PSO)			References
			$q_e(\text{mg.g}^{-1})$	$k_1(\text{min}^{-1})$	$R^2$	$q_e(\text{mg.g}^{-1})$	$k_2(\text{g.mg}^{-1}.\text{min}^{-1})$	$R^2$	
NAP	Functionalized MCM-41	$C_0$ : 30 $\text{mg.L}^{-1}$ , 298K, pH 4, 200 rpm, 20 min, D: 0.02 $\text{g.L}^{-1}$	41	0.049	0.949	67	0.00124	0.9957	Albayati and Kalash (2020)
ANT	N-Doped Graphene (NRGO)	$C_0$ : 1 $\text{mg.L}^{-1}$ , 298K, pH 7, 150 rpm, 48 h, D: 10 $\text{g.L}^{-1}$	6.416	0.001	0.956	8.771	$6.66 \times 10^{-5}$	0.876	Song et al. (2021)
NAP	Reduced Oxide Chitosan beads modified with iron oxide (FeO) and titanium dioxide (TiO <sub>2</sub> ) (Ch-FeO/TiO <sub>2</sub> )	$C_0$ : 100 ppm, 298K, pH: 8, 175 rpm, 48 h, D: 3 $\text{g.L}^{-1}$	19.9	0.0169	0.8885	36.4	0.0011	0.9952	Ruiz et al. (2020)
NAP ACN PHEN	Silica-based organic-inorganic nanohybrid material (NH <sub>2</sub> -SBA-15)	$C_0$ (NAP): 6 $\text{mg.L}^{-1}$ , $C_0$ (ACN): 6 $\text{mg.L}^{-1}$ , $C_0$ (PHN): 4 $\text{mg.L}^{-1}$ , 298K, pH 5, 150 rpm, 24 h, D: 3 $\text{g.L}^{-1}$	NAP: 1.20 ANC: 1.02 PHEN: 0.403	NAP: 0.78 ANC: 2.06 PHEN: 0.361	NAP: 0.942 ANC: 0.837 PHEN: 0.975	NAP: 1.26 ANC: 1.10 PHEN: 0.43	NAP: 1.19 ANC: 2.81 PHEN: 0.46	NAP: 0.975 ANC: 0.914 PHEN: 0.988	Balati et al. (2015)
NAP	ZnO/Ag/GO nanocomposite	$C_0$ : 50 $\text{mg.L}^{-1}$ , 298K, 20 min, D: 0.25 $\text{g.L}^{-1}$	-	-	-	162.6	0.0278	0.98	Mukwevho et al. (2020)
NAP FLU	Hydroxyl functionalized multiwall carbon nanotubes (MWCNT-OH)	$C_0$ (NAP): 5 $\mu\text{g.L}^{-1}$ , $C_0$ (FLU): 5 $\mu\text{g.L}^{-1}$ , 293K, 5 to 30 min, D: 10 $\text{mg.L}^{-1}$	NAP: 1.081 FLU: 0.731	NAP: 0.021 FLU:- 0.079	NAP: 0.069 FLU: 0.276	NAP: 57.471 FLU: 59.880	NAP: 0.058 FLU: 0.444	NAP: 1.000 FLU: 0.997	Akinpelu et al. (2019)
NAP ACE	Graphene oxide (GO) on the surface of amino-functionalized sand particles	$C_0$ (NAP): 400 $\mu\text{g.L}^{-1}$ , $C_0$ (ACE): 400 $\mu\text{g.L}^{-1}$ , 2 h, D: 8 $\text{g.L}^{-1}$	NAP: 1.7038 ACE: 2.332	NAP: 0.0275 ACE: 0.0275	NAP: 0.9188 ACE: 0.9188	NAP: 2.963 ACE: 3.418	NAP: 0.0204 ACE: 0.0132	NAP: 0.9970 ACE: 0.9953	Mortazavi et al. (2019)

ACE	Modified silicagel	$C_{0(ACE)}$ : 3.31 $\mu\text{g.L}^{-1}$ , 298K, 350 rpm, 1-5 h, D: 1 $\text{mg.L}^{-1}$	0.227	0.167	0.983	0.258	0.817	0.959	Hall et al. (2009)
NAP	Granular Activated Carbon (GAC)	$C_{0(NAP)}$ : 6 $\text{mg.L}^{-1}$ , $C_{0(ACE)}$ : 6 $\text{mg.L}^{-1}$ , $C_{0(ACN)}$ : 6 $\text{mg.L}^{-1}$ , $C_{0(FLU)}$ : 6 $\text{mg.L}^{-1}$ , $C_{0(PHE)}$ : 6 $\text{mg.L}^{-1}$ , 297K, 120 rpm, 24 h, D: 2-50 $\text{mg.L}^{-1}$	NAP: 13.8	NAP: 0.0113	NAP: 0.993	NAP: 17.3	NAP: 0.00061	NAP: 0.983	Eeshwarasinghe et al. (2018)
ACE			ACE: 14.7	ACE: 0.01	ACE: 0.995	ACE: 18.5	ACE: 0.00053	ACE: 0.997	
ACN			ACN: 15.7	ACN: 0.0116	ACN: 0.997	ACN: 20.5	ACN: 0.0005	ACN: 0.991	
FLU			FLU: 13.0	FLU: 0.0085	FLU: 0.993	FLU: 16.5	FLU: 0.00051	FLU: 0.996	
PHEN			PHEN: 11.8	PHEN: 0.0086	PHEN: 0.994	PHEN: 14.8	PHEN: 0.0006	PHEN: 0.999	
PYR			Green synthesized iron oxide nanoparticles (IONPs)	$C_{0(PYR)}$ : 100 $\mu\text{g.L}^{-1}$ , $C_{0(BAP)}$ : 1 $\mu\text{g.L}^{-1}$ , pH 7, 150 min, D: 90 $\text{mg.L}^{-1}$	PYR: 0.992	PYR: 18.9	PYR: 0.96	PYR: 0.96	
BAP			BAP: 0.0094	BAP: 15.7	BAP: 0.887	BAP: 0.0099	BAP: 0.0023	BAP: 0.996	
NAP	Granular activated carbon (GAC)	$C_{0(NAP)}$ : 5 $\text{mg.L}^{-1}$ , $C_{0(ACE)}$ : 20 $\text{mg.L}^{-1}$ , $C_{0(FLU)}$ : 5 $\text{mg.L}^{-1}$ , $C_{0(ANT)}$ : 20 $\text{mg.L}^{-1}$ , $C_{0(PYR)}$ : 5 $\text{mg.L}^{-1}$ , $C_{0(FLT)}$ : 10 $\text{mg.L}^{-1}$ , 294K, pH 7, 400 min, D: 0.6 $\text{g.L}^{-1}$	NAP: 12.12	NAP: 0.012AC	NAP: 0.87	NAP: 15.19	NAP: $1.7 \times 10^{-5}$	NAP: 0.95	Valderrama et al. (2008)
ACE			ACE: 15.22	ACE: 0.0099	ACE: 0.97	ACE: 20.81	ACE: $3.2 \times 10^{-4}$	ACE: 0.97	
FLU			FLU: 0.021	FLU: 0.021	FLU: 0.92	FLU: 12.90	FLU: $5.7 \times 10^{-4}$	FLU: 0.99	
ANT			ANT: 10.59	ANT: 0.015	ANT: 0.93	ANT: 15.50	ANT: $5.9 \times 10^{-4}$	ANT: 0.99	
PYR			PYR: 14.60	PYR: 0.014	PYR: 0.91	PYR: 12.89	PYR: $3.1 \times 10^{-4}$	PYR: 0.98	
FLT			FLT: 7.11	FLT: 9.88	FLT: 0.011	FLT: 0.90	FLT: 18.76	FLT: $1.4 \times 10^{-4}$	
PHEN	Graphene wool (GW)	$C_{0(PHEN)}$ : 50 $\text{ng.L}^{-1}$ , $C_{0(PYR)}$ : 50 $\text{ng.L}^{-1}$ , 298K, pH <sub>(PHEN)</sub> 6.8, pH <sub>(PHEN)</sub> 6.7, 200 rpm, 24 h, D: 0.5 $\text{mg.mL}^{-1}$	PHEN: 6.02	PHEN: $1.028 \times 10^{-3}$	PHEN: 0.4227	PHEN: 28.33	PHEN: $1.43 \times 10^{-3}$	PHEN: 0.9998	Adeola and Forbes (2019)
PYR			PYR: 28.33	PYR: $1.29 \times 10^{-3}$	PYR: 0.5772	PYR: 41.84	PYR: $6.83 \times 10^{-4}$	PYR: 0.9995	

PHEN ANT	Nanoscale valent nanoparticles (NZVIs) (Fe@SiO <sub>2</sub> @PDA)	zero- iron	C <sub>0</sub> (PHEN): 0.5 mg.L <sup>-1</sup> , C <sub>0</sub> (ANP): 0.4 mg.L <sup>-1</sup> , 298K, pH 7, 200 rpm, 5 min to 12 h, D: 2 g.L <sup>-1</sup>	PHEN: 0.089 ANT: 0.035	PHEN: 0.003 ANT: 0.003	PHEN: 0.795 ANT: 0.772	PHEN: 0.194 ANT: 0.367	PHEN: 0.15 ANT: 2.22	PHEN: 0.998 ANT: 0.999	Li et al. (2017)
-------------	---	---------------	--	---------------------------------	---------------------------------	---------------------------------	---------------------------------	----------------------------	---------------------------------	------------------

C<sub>0</sub>: Initial concentration of PAHs; D: Adsorbent dosage; q<sub>e</sub>: Adsorbate concentration in equilibrium on the adsorbent surface (mg.g<sup>-1</sup>); k<sub>1</sub>: Pseudo-first-order rate constant (min<sup>-1</sup>); k<sub>2</sub>: Pseudo-second-order rate constant (g.mg<sup>-1</sup>.min<sup>-1</sup>).

### 2.4.3 Adsorption modelling for packed beds

The dynamic modeling of adsorption is very important because it allows the development of models that can help in predicting the mechanisms involved in the adsorptive processes. The most applied mathematical models for fixed-bed adsorption columns are based on the hypotheses of axial dispersion, external mass transfer, intraparticle diffusion and non-linear isotherms (Ruthven, 1984). The main models for studying column adsorption are: Thomas, Bohart-Adams and Yoon-Nelson. Thomas's model is the most used for the study of adsorption columns. However, other alternative models have been developed, aiming at modeling fixed-bed adsorption columns, including the Dual Site Diffusion's model (DualSD), which starts from the principles of the mass conservation law. The main models for fixed-bed adsorption columns are displayed in Table 2.4.

Mortazavi et al. (2019) performed the thermal reduction of graphene oxide (GO), followed by chemical bonding to amino-functionalized sand particles (AFSPs) to obtain a nanoadsorbent. The nanoadsorbent obtained was applied to the adsorption of PAHs (NAP and ACE) from wastewater. For batch experiments, a CCD type of experimental design was applied to evaluate the effects of the factors: initial PAH concentration, total dissolved solids (TDS), contact time and adsorbent dosage. The experimental kinetic data had a better adjustment to the PSO and intraparticle diffusion models, while the experimental equilibrium data had a better adjustment to the Langmuir's, Redlich-Peterson's and Dubinin-Radushkevich's models for NAP and for ACE the experimental data had a better adjustment to the Redlich-Peterson's and Freundlich's models. A continuous flow adsorption was also carried out to evaluate the performance of the adsorbent in a fixed-bed, using a mini-column. The experimental data had a better adjustment to the Thomas's model.

Batch systems are important for determining the kinetic and thermodynamic parameters of the process and are generally applied to small volumes of effluents. On the other hand, continuous flow systems are a simple and economical method that can be applied to the processing of large amounts of wastewater.

**Table 2.4.** Models for fixed-bed adsorption columns.

Models	Equation
Thomas (1944)	$\ln\left(\frac{C_0}{C_t} - 1\right) = \frac{K_T q_0 m}{Q} - K_T C_0 t \quad (5)$
Bohart-Adams (1920)	$\ln\left(\frac{C_t}{C_0}\right) = K_{BA} C_0 t - \frac{K_{BA} N_0 Z}{V} \quad (6)$
Yoon-Nelson (1984)	$\ln\left(\frac{C_t}{C_0 - C_t}\right) = K_{YN} t - \tau K_{YN} \quad (7)$
Dual Site Diffusion (DualSD) Andrade et al. (2020)	$\frac{\partial C}{\partial t} = Da \frac{\partial^2 C}{\partial z^2} - u_0 \frac{\partial C}{\partial z} - \frac{\rho_B}{\varepsilon} \frac{\partial q}{\partial t} \quad (8)$

$C_0$ : initial concentration of contaminant ( $\text{mg.L}^{-1}$ ),  $K_T$ : constant of Thomas's model ( $\text{L.min}^{-1}.\text{mg}^{-1}$ ),  $C_t$  is the concentration of effluent obtained at time ( $\text{mg.L}^{-1}$ ),  $m$ : mass of the adsorbent in the column (g),  $Q$ : flow rate ( $\text{mL.min}^{-1}$ ),  $q_0$ : capacity of adsorption obtained from Thomas's model ( $\text{mg.g}^{-1}$ ),  $K_{BA}$ : Bohart- Adams kinetic rate constant ( $\text{L.min}^{-1}.\text{mg}^{-1}$ ),  $N_0$ : capacity of adsorption of the adsorbent obtained from Bohart- Adams's model ( $\text{mg.g}^{-1}$ ),  $Z$ : height (or length) of the bed (cm),  $V$ : linear speed (velocity) ( $\text{cm.min}^{-1}$ ),  $K_{YN}$ : Yoon-Nelson proportional constant ( $\text{min}^{-1}$ ) and  $\tau$  is the time when  $C_t=0.5 C_0$ ,  $C$ : concentration of pollutant in the liquid phase ( $\text{mmol.L}^{-1}$ ),  $q$ : amount of pollutant at the adsorbent ( $\text{mmol.g}^{-1}$ ),  $D_a$ : axial dispersion coefficient ( $\text{cm}^2.\text{min}^{-1}$ ),  $u_0$ : interstitial velocity ( $\text{cm.min}^{-1}$ ),  $\rho_B$ : fixed-bed density ( $\text{g.L}^{-1}$ ) and  $\varepsilon$ : void fraction.

#### 2.4.4 Adsorption isotherms

Through the study of the adsorption isotherms, it is possible to determine the equilibrium concentration of the adsorbate ( $C_e$ ) and the concentration of the adsorbate in the adsorbent phase ( $q_e$ ). The evaluation of the process occurs at constant temperature, and the amount adsorbed by the adsorbent mass depends on the pressure and the final temperature. Other factors, such as the volume of distribution of the pores and the magnitude of the adsorption enthalpy, are obtained through the adsorption isotherms. Favorable isotherms approach a maximum for high concentrations and tend to be linear for low concentrations (Kinniburgh, 1986). The most used adsorption equilibrium models are displayed in Table 2.5.

Adeola and Forbes (2019) applied in their study graphene wool (GW) for the adsorption of PHEN and PYR from synthetic wastewater. The variables that influenced the adsorptive processes of PAHs are: pH, temperature, TDS of the solution and initial concentration of PAHs. The kinetic experimental adsorption data had a better fit to the PSO model, which suggests that the chemisorption is the predominant mechanism in the adsorption process. The Sips's model (Freundlich - Langmuir) showed a better adjustment to the experimental data for PHEN and PYR. The value of  $q_{\max}$  by the Langmuir's model for PHEN and PYR was 5 and 20  $\text{mg}\cdot\text{g}^{-1}$ , respectively, and a 99% of reduction was obtained, for all PAHs from wastewater. Thermodynamic studies have shown that the adsorptive processes have an endothermic and spontaneous nature.

Table 2.6 displays the values of the maximum adsorption capacity ( $q_{\max}$ ) and the values obtained by adjusting the models to the equilibrium experimental data of PAHs adsorption by different nanoadsorbent materials. The Langmuir's and Freundlich's models are the most used to describe the adsorption equilibrium. In most of the studies evaluated, the Freundlich's model showed a better adjustment to the equilibrium data, which indicates that the PAHs adsorption occurs in multilayers with interaction between the adsorbed molecules.

**Table 2.5.** Main adsorption equilibrium models.

Models	Equation
Langmuir (1918)	$q_e = \frac{q_{max}K_L C_e}{1 + K_L C_e} \quad (9)$
Freundlich (1906)	$q_e = K_F C_e^{\frac{1}{n}} \quad (10)$

$q_e$ : adsorption equilibrium capacity ( $\text{mg.g}^{-1}$ ),  $C_e$ : equilibrium concentration of adsorbate ( $\text{mg.L}^{-1}$ ),  $q_{max}$ : maximum adsorption capacity ( $\text{mg.g}^{-1}$ ),  $K_L$ : Langmuir's equilibrium constant associated with the affinity of the sites ( $\text{L.mg}^{-1}$ ),  $K_F$ : Freundlich's constant [ $(\text{mg.g}^{-1}).(\text{L.mg}^{-1})^{1/n}$ ] and  $n$  is the empirical constant associated with the adsorption intensity.

**Table 2.6.** Models of adsorption isotherms for the removal of PAHs by different nanoadsorbent materials.

PAHs	Nanoadsorbent	Experimental conditions	Isotherm models	$q_{\max}$ (mg.g <sup>-1</sup> )	Additional information	References
NAP ANT PYR	Reduced graphene oxides (rGOs)	$C_0$ (NAP): 0.1 mmol.L <sup>-1</sup> , $C_0$ (ANT): 0.1 mmol.L <sup>-1</sup> , $C_0$ (PYR): 0.1 mmol.L <sup>-1</sup> , 298K, pH: 6.5	L F	NAP: 766.59 ANT: 80.92 PYR: 198.003	L (NAP): $K_L = 0.0223$ , $R^2 = 0.966$ L (ANT): $K_L = 0.411$ , $R^2 = 0.963$ L (PYR): $K_L = 0.343$ , $R^2 = 0.976$ F (NAP): $K_F = 15.92$ , $1/n=0.928$ , $R^2 = 0.998$ F (ANT): $K_F = 247.17$ , $1/n=0.312$ , $R^2 = 0.978$ F (PYR): $K_F = 369.06$ , $1/n=0.298$ , $R^2 = 0.998$	Sun et al. (2013)
NAP	ZnO/Ag/GO nanocomposite	$C_0$ : 50 mg.L <sup>-1</sup> , 298K, 20 min, D: 0.25 g.L <sup>-1</sup>	L F	500	L: $K_L = 0.0247$ , $R^2 = 0.67$ F: $K_F = 8.166$ , $1/n = 0.13$ , $R^2 = 0.95$	Mukwevho et al. (2020)
NAP FLU	Hydroxyl functionalized multiwall carbon nanotubes (MWCNT-OH)	$C_0$ (NAP): 5 µg.L <sup>-1</sup> , $C_0$ (FLU): 5 µg.L <sup>-1</sup> , 293K, 5 to 30 min, D: 10 mg.L <sup>-1</sup>	L F	NAP: 57.401 FLU: 61.235	L (NAP): $K_L = 277.78$ , $R^2 = 0.9703$ L (FLU): $K_L = 1428.6$ , $R^2 = 0.9517$ F (NAP): $K_F = 177.73$ , $1/n=0.585$ , $R^2 = 0.9614$ F (FLU): $K_F = 330.04$ , $1/n=0.373$ , $R^2 = 0.7767$	Akinpelu et al. (2019)
NAP	Graphene (G) and Graphene oxide (GO)	$C_0$ (NAP): 5 mg.L <sup>-1</sup> , 296K, pH 5, 24h	F	-	F (G): $K_F = 14.17$ , $n = 0.47$ , $R^2 = 0.97$ F (GO): $K_F = 0.93$ , $n = 0.40$ , $R^2 = 0.99$	Pei et al. (2013)
NAP	Reduced graphene oxide/iron oxide (GO/FeO•Fe <sub>2</sub> O <sub>3</sub> )	$C_0$ (NAP): 0.156 mmol.L <sup>-1</sup> , 283.15K, pH 7, 48h, D: 0.1 g.L <sup>-1</sup>	L F	337.088	L: $K_L = 2.42 \times 10^{-3}$ , $R^2 = 0.981$ F: $K_F = 0.0223$ , $n = 0.65$ , $R^2 = 0.981$	Yang et al. (2013)
PYR BAP	Green synthesized iron oxide nanoparticles (IONPs)	$C_0$ (PYR): 100 µg.L <sup>-1</sup> , $C_0$ (BAP): 1 µg.L <sup>-1</sup> , pH 7, 150 min, D: 90 mg.L <sup>-1</sup>	L F	0.895	L (PYR): $K_L = 1.62 \times 10^{-4}$ , $R^2 = 0.905$ L (BAP): $K_L = 3.37 \times 10^{-4}$ , $R^2 = 0.981$ F (PYR): $K_F = 6.3 \times 10^{-4}$ , $n = 3.14$ , $R^2 = 0.895$ F (BAP): $K_F = 0.31 \times 10^{-4}$ , $n = 3.56$ , $R^2 = 0.97$	Hassan et al. (2018)
NAP ACE	Graphene oxide (GO) on the surface of amino-functionalized sand particles	$C_0$ (NAP): 400 µg.L <sup>-1</sup> , $C_0$ (ACE): 800 µg.L <sup>-1</sup> , 2 h, D: 10 g.L <sup>-1</sup>	L F	NAP: $6.555 \times 10^{-3}$ ACE: 0.0178	L (NAP): $K_L = 1.776$ , $R^2 = 0.999$ L (ACE): $K_L = 1.7899$ , $R^2 = 0.965$ F (NAP): $K_F = 5.616$ , $n = 1.541$ , $R^2 = 0.9963$ F (ACE): $K_F = 16.373$ , $n = 1.3031$ , $R^2 = 0.999$	Mortazavi et al. (2019)

PHEN PYR	Graphene wool (GW)	C <sub>0</sub> : 1-5 mg.L <sup>-1</sup> , 298K, pH <sub>(PHEN)</sub> 6.8, pH <sub>(PYR)</sub> 6.7, 200 rpm, 24 h, D: 0.667 g.L <sup>-1</sup>	L F	PHEN: 5.0 PYR: 20.0	L (PHEN): K <sub>L</sub> = 181.8, R <sup>2</sup> = 0.9793 L (PYR): K <sub>L</sub> = 6.85, R <sup>2</sup> = 0.9635 F (PHEN): K <sub>F</sub> = 16.2, n = 0.6218, R <sup>2</sup> = 0.9906 F (PYR): K <sub>F</sub> = 114.4, n = 0.9665, R <sup>2</sup> = 0.9685	Adeola and Forbes (2019)
NAP	Chitosan beads modified with iron oxide (FeO) and titanium dioxide (TiO <sub>2</sub> ) (Ch-FeO/ TiO <sub>2</sub> )	C <sub>0</sub> : 80 ppm, 298K, pH: 8, 175 rpm, 48 h, D: 3 g.L <sup>-1</sup>	L F	149.3	L: K <sub>L</sub> = 0.47, R <sup>2</sup> = 0.9303 F: K <sub>F</sub> = 52.57, n = 1.12, R <sup>2</sup> = 0.9979	Ruiz et al. (2020)
ANT	N-Doped Reduced Graphene Oxide (NRGO)	C <sub>0</sub> : 1 mg.L <sup>-1</sup> , 298K, pH 7, 150 rpm, 48 h, D: 10 g.L <sup>-1</sup>	L F	2.811	L: K <sub>L</sub> = 46.195, R <sup>2</sup> = 0.772 F: K <sub>F</sub> = 380.277, n = 0.873, R <sup>2</sup> = 0.983	Song et al. (2021)

C<sub>0</sub>: Initial concentration of PAHs; D: Adsorbent dosage; L: Langmuir model; F: Freundlich model; K<sub>L</sub>: Langmuir equilibrium constant related to the affinity of the binding sites (L.mg<sup>-1</sup>); K<sub>F</sub>: Freundlich constant related to the adsorption capacity [(mg.g<sup>-1</sup>).(L.mg<sup>-1</sup>)<sup>1/n</sup>]; n: Empirical constant related to the intensity of adsorption (dimensionless); q<sub>max</sub>: Maximum adsorption capacity (mg.g<sup>-1</sup>).

#### 2.4.5 Adsorption thermodynamics

The values of the Gibbs free energy variation ( $\Delta G^\circ$ ), entropy variation ( $\Delta S^\circ$ ) and enthalpy variation ( $\Delta H^\circ$ ) are calculated through thermodynamic studies, so that, it is possible to understand the characteristics of the adsorptive processes. The processes are considered exothermic when ( $\Delta H^\circ < 0$ ), otherwise the processes are endothermic ( $\Delta H^\circ > 0$ ). It is also possible to determine the spontaneity of the system, so that the adsorptive process has a spontaneous nature when ( $\Delta G^\circ < 0$ ), or not spontaneous nature ( $\Delta G^\circ > 0$ ). The adsorbent has high affinity with adsorbate when ( $\Delta S^\circ > 0$ ) or low affinity when ( $\Delta S^\circ < 0$ ). From the magnitude of these parameters, it is also possible to determine whether the adsorption mechanism is governed by chemisorption or physisorption.

Sharma et al. (2017) performed the synthesis of superparamagnetic nanocomposites carbon/ZnFe<sub>2</sub>O<sub>4</sub> (C/ZnFe<sub>2</sub>O<sub>4</sub>) using the reflux method. The nanomaterial obtained was characterized by the techniques of FTIR, XRD, VSM, BET, FESEM, HRTEM and EDX. C/ZnFe<sub>2</sub>O<sub>4</sub> was used in the adsorption of NAP and 2-naphthol from wastewater, in a batch adsorption process. The kinetic and equilibrium experimental data had a better adjustment to the PFO and Langmuir's models, respectively. Through the thermodynamic adsorption, the parameters  $\Delta H^\circ$ ,  $\Delta S^\circ$  and  $\Delta G^\circ$  were determined, which influences the nature of the adsorption. The results indicated that the adsorptive process had a spontaneous nature ( $\Delta G^\circ < 0$ ), in addition to presenting high affinity for adsorbate ( $\Delta S^\circ > 0$ ). The  $\Delta H^\circ$  value was positive ( $\Delta H^\circ > 0$ ), so the process is endothermic, which indicates that the adsorption was governed, mainly, by the physisorption mechanism, which was also confirmed by the adjustment of the equilibrium data to the Langmuir's model.

Yang et al. (2013) synthesized rGO/FeO•Fe<sub>2</sub>O<sub>3</sub> nanocomposites, in which rGO stands for the reduced form of GO, aiming at their application in the adsorption of contaminants 1-naphthylamine, 1-naphthol and NAP, from synthetic wastewater. The experimental equilibrium data had a better adjustment to Freundlich's model, for all pollutants, indicating the presence of heterogeneous adsorption sites. The thermodynamic studies of NAP adsorption showed that the calculation of the parameters  $\Delta H^\circ$ ,  $\Delta S^\circ$  and  $\Delta G^\circ$ , indicated that the adsorptive process has a spontaneous nature ( $\Delta G^\circ < 0$ ), endothermic nature ( $\Delta H^\circ > 0$ ) and a high affinity of adsorbate (NAP) for the adsorbent (rGO/FeO•Fe<sub>2</sub>O<sub>3</sub>) ( $\Delta S^\circ > 0$ ).

Table 2.7 displays the thermodynamic parameters and experimental data from several PAHs adsorption studies using different nano-adsorbent materials. The results showed that most PAHs adsorption processes are endothermic, as they present positive values of enthalpy

variation ( $\Delta H^\circ$ ), which vary from -51.2 to 40.98 kJ.mol<sup>-1</sup>, depending on the system. The results also showed that most of the processes are spontaneous, as they present negative values of variation of Gibbs Free Energy ( $\Delta G^\circ$ ). Table 7 also shows that in most studies the values of entropy variation ( $\Delta S^\circ$ ) are positive, ranging from -164 to 161.21 J.mol<sup>-1</sup>.K<sup>-1</sup>, according to the system. The PAHs evaluated have a high affinity for the adsorbents, according to the results presented in the evaluated articles.

**Table 2.7.** Thermodynamic parameters for the removal of PAHs by different nanoadsorbent materials.

PAHs	Nanoadsorbent materials	T (K)	$\Delta G^\circ$ (kJ.mol <sup>-1</sup> )		$\Delta H^\circ$ (kJ.mol <sup>-1</sup> )		$\Delta S^\circ$ (J.mol <sup>-1</sup> .K <sup>-1</sup> )		References			
PYR BAP	Green synthesized iron oxide nanoparticles (IONPs)	293	PYR	BAP					Hassan et al. (2018)			
		303	-1.7x10 <sup>-3</sup>	-2.17x10 <sup>-3</sup>	PYR	BAP						
		313	-1.4x10 <sup>-3</sup>	-1.78x10 <sup>-3</sup>	-17.2x10 <sup>-3</sup>	-22.13x10 <sup>-3</sup>	PYR	BAP				
		323	-0.95x10 <sup>-3</sup>	-1.10x10 <sup>-3</sup>			-52.68	-67.07				
			-0.34x10 <sup>-3</sup>	-0.50x10 <sup>-3</sup>								
NAP	Functionalized MCM-41	298	-7.831						Albayati and Kalash (2020)			
		308	-7.393		-23.004		-50.273					
		318	-6.8456									
NAP	Reduced graphene oxide/iron oxide (GO/FeO•Fe <sub>2</sub> O <sub>3</sub> )	283	-4.31						Yang et al. (2013)			
		303	-8.26		40.98		161.21					
		323	-10.70									
		303	-2.16									
NAP	Carbon/ZnFe <sub>2</sub> O <sub>4</sub>	313	-2.61						Sharma et al. (2017)			
		323	-3.07		11.51		45.12					
		333	-3.32									
		343	-3.97									
PHEN	Orange Rind Activated Carbon (ORAC)	293	10.40						Gupta and Singh (2018)			
		303	12.14		20.47		0.1138					
		313	12.61									
		323	14.04									
PHEN ANT	Nanoscale zero-valent iron nanoparticles (NZVIs) (Fe@SiO <sub>2</sub> @PDA)	298	PHEN	ANT					Li et al. (2017)			
		303	-2.40	-5.15	PHEN	ANT	PHEN	ANT				
		308	-1.55	-4.94	-51.2	-17.1	-164.0	40.0				
			-0.735	-4.74								
NAP ANT PYR	Rice straw (RS) and Sugarcane bagasse (SB)	288		RS	SB		RS	SB		Younis et al. (2014)		
			NAP:	6.08	5.50	NAP:	20.10	21.32	NAP:		48.9	54.9
			ANT:	7.36	6.22	ANT:	14.66	16.94	ANT:		25.6	37.1
			PYR:	7.39	6.52	PYR:	10.48	19.07	PYR:	10.9	43.2	

Thermodynamic parameters can be expressed by equations:  $\Delta G^\circ = -RT \ln K_C$  and  $\Delta G^\circ = \Delta H^\circ - T\Delta S^\circ$ , where  $K_C$ : constant of chemical equilibrium, R: ideal gas constant (8.314 J. mol<sup>-1</sup>. K<sup>-1</sup>) and T: temperature (K).

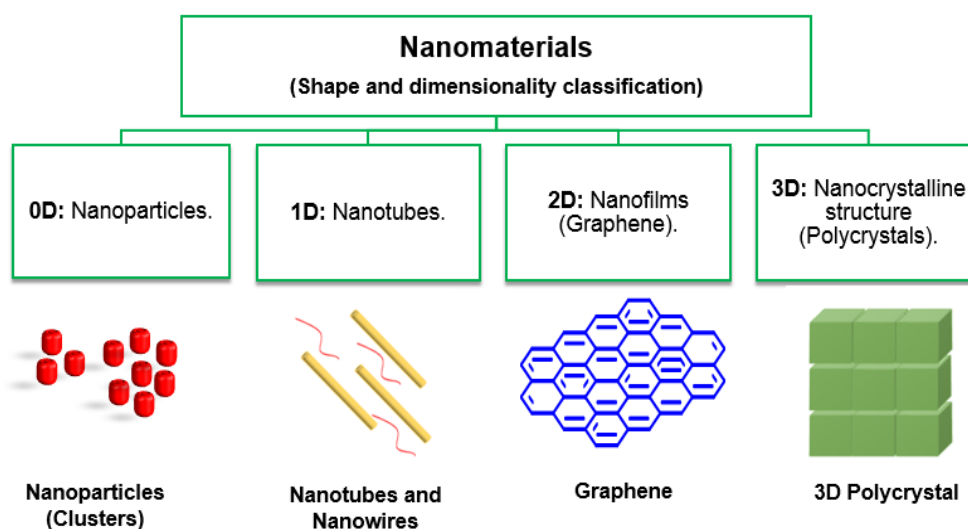
## 2.5. Nanomaterial-based adsorbents

According to the recommendations of IUPAC (2012), nanomaterials can be defined as materials whose particles in any form have dimensions that vary in a nanoscale of 1-100nm (Vert et al., 2012). The most common types of nanomaterials are: nanofilaments, nanopowders, nanotubes, nanowires, nanocables, nanofilms and nanoblocks. Different physical, chemical or mechanical mechanisms can be applied for the preparation of nanomaterials, according to the desired characteristics (Zhang, 2018).

The relationship between surface area and volume is one of the factors responsible for the characteristics of a given nanomaterial. The main physical properties are melting point and optical adsorption vary depending on the size and shape of the nanomaterials (Asha and Narain, 2020). Nanomaterials can be characterized in terms of shape and dimensionality, so that they can be classified into four categories (Pokropivny and Skorokhod, 2007), as illustrated in Figure 2.3:

- Zero-dimensional (0D): Nanoparticles, molecules, clusters, fullerenes, rings, particles, grains, powders, schwartzons, metcarbs and thoroids;
- One-dimensional (1D): Nanotubes (CNT), nanowires, nanofibers, springs, needles and pillars;
- Two-dimensional (2D): Nanofilms (Graphene), nanolayers;
- Three-dimensional (3D): Nanocrystalline structure, powder skeletons and skeletons of fiber.

**Figure 2.3.** Classification of nanomaterials, based on shape and dimension, in zero-dimensional (0D), one-dimensional (1D), two-dimensional (2D) and three-dimensional (3D).



Particle size is a very important parameter, as its decrease can directly affect the particle's interaction in the chemical reactions, since the decrease of the particle size can increase the number of pending (or exposed) bonds in the reaction environment. On the other hand, the decrease in particle size can generate an exponential increase in the reaction speed, as well as a decrease in the reaction temperature. Nanomaterials have some important enhanced chemical properties, such as a greater number of reactive sites, high hydrophilicity and the possibility of functionalization (Mercier et al., 2002).

The mechanical properties of nanomaterials vary according to the type of base material, environment and external loads. To carry out an in-depth analysis of the mechanical properties, some factors must be taken into account, such as, the surface structure, porosity, functionalization, preparation methods and chemical treatments. Metallic nanomaterials have as main mechanical properties: resistance, plasticity, hardness, tenacity, fragility, elasticity, ductility, stiffness and yield stress. Inorganic non-metallic materials, on the other hand, are mostly fragile, and organic materials do not have properties such as, rigidity and fragility, most of which are flexible (Reghunadhan et al., 2018; Wu et al., 2020).

The surface reactivity of nanomaterials is attributed to their chemical, physical and mechanical properties. Their high surface reactivity enables the nanometric crystals to aggregate into micrometric particles. Some nanomaterials have unique adsorptive properties that are attributed to the differences in reactive surface sites and also to regions of disorder on the surface (Chakravarty and Dash, 2013).

Carbon-based nanomaterials can be applied in wastewater treatment processes to remove polluting compounds. Factors such as the presence of functional groups, pore size and volume, degree of polarity, among others, directly influences the remediation processes. The analysis of the physical-chemical characteristics of adsorbents based on nanomaterials influences the performance of the adsorbent in the adsorption and desorption processes. The evaluation of the performance of the adsorbents is carried out by means of adsorption tests under stationary and dynamic conditions (Chakravarty and Dash, 2013; Saleh et al., 2019).

Mukwevho et al. (2020) performed the synthesis of the ZnO/Ag/GO nanocomposite. The nanomaterial was applied for the adsorption and photodegradation of NAP from synthetic wastewater by visible light. The adsorbent obtained was characterized by the techniques of XRD, UV-vis, FTIR, XPS, SEM and TEM, through which it was possible to determine the chemical, structural and morphological characteristics of the nanomaterial. The XRD analysis confirmed the hexagonal structure of the nanoparticles, indicating that the introduction of Ag and GO did not alter the hexagonal structure of ZnO. Then, the nanomaterial was applied in

adsorption and later in the photodegradation of NAP. The kinetic and equilibrium experimental data had a better adjustment to the PSO and Freundlich's model, respectively. An adsorption capacity of  $500 \text{ mg}\cdot\text{g}^{-1}$  was obtained and 80% of NAP reduction was achieved in a contact time of 20 min. The efficiency of removal of NAP improved after the application of the photodegradation process, obtaining 92% of reduction in 50 min.

Zhang et al. (2019) reported the synthesis of three carbon-based magnetic nanomaterials (CNMs), MMWCNTs, MSWCNT and MGNS, which were applied for PHEN removal from wastewater. The results obtained through the characterizations by TEM, FTIR and XRD, indicated that the CNMs were coated with iron oxide nanoparticles. The determination of magnetism showed that there was the formation of magnetic nanoparticles. The PSO model had a better adjustment to the adsorption kinetic data, while the Dubinin-Astakhov's model had a better adjustment to the adsorption equilibrium data. The thermodynamic parameters ( $\Delta G^\circ$ ,  $\Delta H^\circ$  and  $\Delta S^\circ$ ) are negative, which indicates that the adsorptive process of PHEN by the synthesized CNMs is spontaneous, exothermic and with reduced entropy.

Graphene-based materials have gained prominence in the remediation processes of organic, inorganic and gaseous contaminants, due to their high surface area and relatively low production cost. Given these advantages, graphene-based adsorbents can be applied in the PAHs adsorption processes from wastewater. Huang et al. (2019) reported the PHEN adsorption by magnetic graphene oxide (MGO), chemically reduced magnetic graphene (MCRG) and reduced graphene by magnetic annealing (MARG), from synthetic wastewater. The factors pH, heavy metal ions and natural organic matter concentrations, had their effect evaluated. MCRG showed a greater adsorption capacity for PHEN, due to the higher surface area and pore volume, obtained for MCRG adsorbent. The  $\pi$ - $\pi$  interaction was the dominant mechanism in the MCRG adsorption process. Dubinin-Astakhov's model had a better adjustment to the experimental equilibrium data.

Huang et al. (2018) prepared rGO/polyHIPEs emulsions by using 2-ethylhexyl acrylate and ethylene glycol dimethacrylate. The adsorbent materials obtained were applied for PAHs adsorption from wastewater. SEM analysis showed a superficial open cell morphology, which contributes to good permeability and rapid mass transfer. The surface area of the materials was determined by the BET method, which indicated that the specific surface area increased when the amount of rGO increased. The adsorption isotherms indicated that the adsorbents showed a higher adsorption capacity and good cycle stability for PAHs. The predominant mechanism of adsorption was the  $\pi$ - $\pi$  and hydrophobic interaction. After the adsorption process with

rGO/polyHIPEs, the levels of PAHs present in the water decreased, falling below the standard value established by the European Food Safety Authority (EFSA).

### 2.5.1 Graphene-based nanomaterials: Conventional chemistry

The application of graphene-based materials as adsorbents to remove contaminants from the environment has gained prominence in the current context. Graphene-based materials have unique physicochemical properties, such as high specific area, thermal conductivity, electron mobility and mechanical strength, which makes graphene an ideal material for applications in adsorption processes of organic components in the oil industry (Perreault et al., 2015).

Graphene-based materials present a 2D layer of  $sp^2$ -hybridized carbon atoms, forming a hexagonal structure, similar to an ordered honeycomb. It often exhibits excellent thermal and electrical conductivity, and mechanical strength (Stankovich et al., 2006). Graphene has gained notoriety since 2004, when it was first isolated from graphite by the mechanical exfoliation method, whose methodology was described by Novoselov et al. (2004). Since then, its properties have been explored aiming its application in different processes, such as adsorption, separation and photocatalysis. Therefore, some studies have been developed with a main focus on the properties of graphene for its application in the separation of toxic compounds present in oily waters of the petroleum industry.

Alghunaimi et al. (2019) synthesized a material based on graphene grafted with 9-octadecenoic acid, the material obtained was applied for the remediation of organic pollutants from oily water. Graphene was synthesized from graphite through a chemical treatment process, then it was grafted with 9-octadecenoic acid, which is used as a linker agent, forming the 9-octadecenoic acid grafted graphene (OG). Then, an emulsion polymerization of styrene was carried out, in order to obtain a hydrophobic material, POG. FTIR and SEM analyzes confirmed the presence of graphene in the structure of the synthesized materials. The performance of POG composites in the separation of organic pollutants (hexane, heptane, nonane, decane and hexadecane) from water was evaluated. The results indicated that the greater the proportion of graphene grafted with 9-octadecenoic acid, the greater the absorption efficiency of the composite and the faster the adsorption rate of the organic components. A regeneration study of the composite was also carried out, which indicated that the adsorption rate remained constant. The study pointed out that the POG has potential application for the remediation of organic pollutants from effluents of the oil industry, among which PAHs can be included.

Graphene oxide (GO) has a monolayer, which is obtained by treating graphene with strong oxidants, containing in its structure functional groups, such as hydroxyl, carboxyl, carbonyl and epoxy (Zhang et al., 2016). The preparation of graphene oxide (GO) was carried out for the first time by Brodie (1859), who subjected Ceylon graphite to a treatment with an oxidation mixture composed of potassium chlorate and fuming nitric acid. After the Brodie's report in 1859, other procedures were proposed for the formulation of graphene oxide, in which, for the most part, they use mixtures with strong oxidizers (Hummer and Offeman, 1958).

Hummer's method is one of the most used methods by researchers for the production of GO, being introduced by Hummer and Offeman (1958). According to this method, the following reagents are used for the oxidation of graphene: 100g of graphite powder, 50g of  $\text{NaNO}_3$ , 2.3L of  $\text{H}_2\text{SO}_4$  and 300g of  $\text{KMnO}_4$ . One of the advantages of the Hummer's method is that the oxidative process takes a few hours to produce a high amount of GO, in addition to producing a greater amount of oxygen when compared to the Brodie's method. However, one of the main limitations of the Hummer's method is related to the emission of toxic gases, such as  $\text{NO}_2$ ,  $\text{N}_2\text{O}_4$  and explosive gases, such as  $\text{ClO}_2$ . In addition, the presence of residual ions,  $\text{Na}^+$  and  $\text{NO}_3^-$ , generated due to the use of  $\text{NaNO}_3$  as a reagent, can be difficult to remove from the effluents (Chen et al., 2013; Chua and Pumera, 2014).

Some studies have been developed aiming to propose modifications to the Hummer's method in order to minimize the toxic effects attributed to the conventional method. Alkhouzaam et al. (2020) performed the synthesis of GO nanoparticles by the modified Hummer's method, varying operational conditions, such as temperature, reagent stoichiometry and oxidation time. The synthesis of the GO was carried out in two stages: in the first stage, the oxidation of graphite in the GO was carried out; in the second stage, the material was washed, aiming at the elimination of impurities, such as acids, manganese salts, among others. The Hummer's method was modified by varying the reaction temperature, time and reagent stoichiometry, in a  $\text{NaNO}_3$  free reaction medium. The obtained materials were characterized by the techniques of SEM, TEM, XPS, FTIR, Raman spectroscopy and TGA. The results of the FTIR spectra indicated the presence of oxygen related bands (ORB), which confirmed the oxidation of graphite. The results of the TGA indicated that the thermal decomposition of the GO depended on the elementary compositions, so that the GO with low oxygen content had high thermal stability and vice versa.

In a study developed by Fadillah et al. (2019), modifications to the Hummer's method for the GO synthesis were proposed. Fadillah et al. (2019) performed the synthesis of a graphene oxide/alginate (GO/Alg) composite aiming at its potential application for the

remediation of dyes from wastewater, through the combination of electrochemical and adsorption techniques. GO was synthesized by the modified Hummer's method using powdered graphite, then the alginate was incorporated into the GO, using  $\text{CaCl}_2$  as a crosslinking agent, thus forming the GO/Alg beads. The results of the XRD and FTIR characterizations indicated that GO was successfully synthesized by the modified Hummer's method. The XRD and FTIR analyses, respectively, indicated the characteristic peak of GO and the presence of functional groups C-OH, which indicates that the graphite was effectively oxidized, forming the graphite oxide. The results also indicated that the combination of electrochemical and adsorption techniques were efficient for the remediation of methylene blue (MB) from wastewater.

The methodologies proposed by Alkhouzaam et al. (2020) and Fadillah et al. (2019) for the synthesis of GO, through the modified Hummer's method, are promising methods for the efficient synthesis of GO, contributing to minimize the generation of toxic effluents due to the use of chemical reagents, such as  $\text{NaNO}_3$ . The results indicated that the synthesized materials are promising for the remediation of organic pollutants, such as PAHs, from wastewater.

The presence of petrogenic PAHs in the aquatic environment can cause harmful damage to marine biota, due to its toxic and polluting potential, the application of graphene-based adsorbents can decrease the concentration of these contaminants in the marine environment, due to the excellent adsorptive properties of graphene. Álvarez et al. (2021) carried out a study to evaluate the adsorption of petrogenic PAHs from the aquatic environment by applying GO, synthesized by conventional Hummer's method. The materials obtained were characterized by TEM and AFM techniques. Through TEM analysis, it was observed that the maximum platelet length was approximately 13  $\mu\text{m}$ , while through AFM analysis showed a thickness of  $0.612 \pm 0.176$  nm for the GO platelets. The adsorption results indicated a high GO adsorption capacity for BaP, so that, for a initial concentration of  $100 \mu\text{g}\cdot\text{L}^{-1}$ , a 98% of reduction was obtained after 40 hours. For the other fractions of PAHs, there was a 95.7% of reduction for PHEN, 84.4% for FLU and 51.5% for ACE, after 40 hours.

A new type of functionalized graphene oxide, produced by mixing GO with brilliant blue (BB) was proposed by Zhang et al. (2013). GO was synthesized by the modified Hummer's method, and then BB was incorporated into GO, forming a new functional composite BBGO. SEM, AFM and FTIR analyzes indicated that the BBGO composite was successfully obtained, indicating the presence of GO in its structure. BBGO was applied as an adsorbent for the removal of two types of PAHs (anthracenemethanol (AC) and FLT) from a synthetic effluent. The adsorptive experiments were carried out in batch, after the adsorptive process, the AC/BBGO and FLT/BBGO complexes were removed from the system through a coagulation-

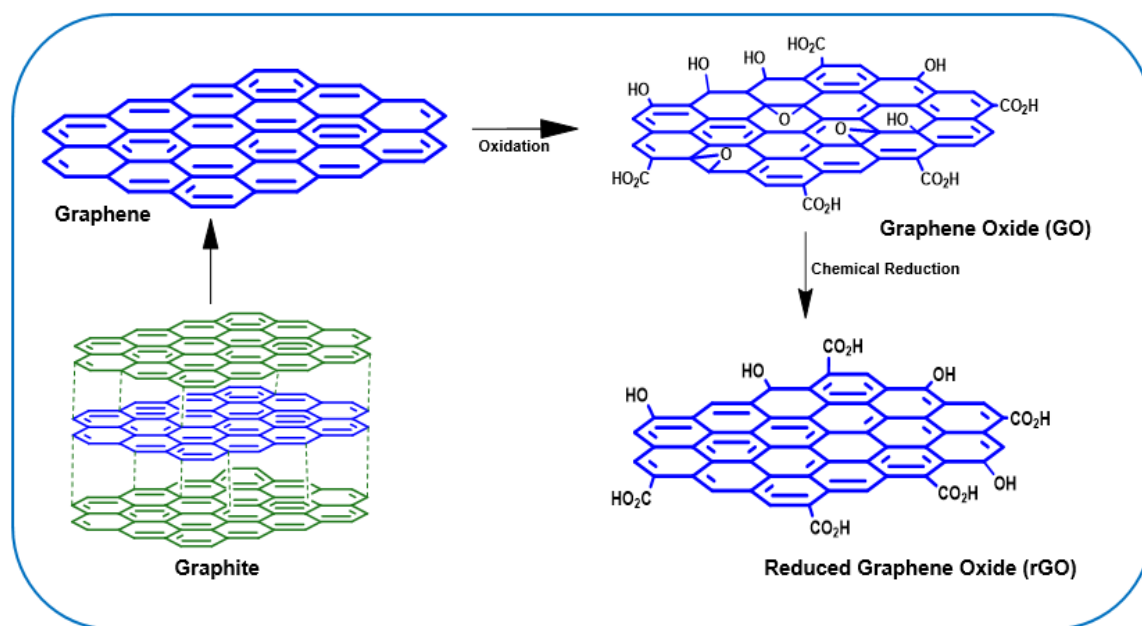
flocculation process at 60 °C and pH 3.0. The adsorption results indicated high adsorption capacity for AC and FLT, a 72% of reduction for AC was obtained after 11 days and a 93.2% of reduction for FLT was obtained after 1.4 hours (100 min).

The adsorptive studies carried out by Álvarez et al. (2021) and Zhang et al. (2013) indicated that graphene-based adsorbents are efficient for the removal of PAHs from wastewater, which can be proven by the high adsorption capacities obtained by the studies. The BBGO nanocomposite synthesized by Zhang et al. (2013) demonstrated to be quite promising for the remediation of FLT from effluents.

One of the most important characteristics of GO is that it can be reduced by the reaction of GO with a reducing agent, thus generating GO in its reduced form (rGO). rGO has attracted the attention for its large-scale applications, due to its low production cost. For the reduction of graphene oxide, some methods have been studied, such as thermal reduction, chemical reduction through reducing agents and photoreduction (Pei and Cheng, 2012; Chen and Huang, 2020).

By reducing the GO, the structure and properties of pure graphene are partially restored, but the carbon plane structure remains altered, due to the incomplete removal of the functional groups with oxygen. The GO reduction aims to eliminate the epoxy and hydroxyl groups, however, the carboxyl, carbonyl and ester groups are still present at the edges and in some defective areas. The rGO, due to modifications of its structure and properties, has an ability to interact with the analyte through  $\pi$ - $\pi$  or by hydrophobic interactions, which gives it a high affinity for aromatic compounds, such as PAHs (Pei and Cheng, 2012; Gomis et al., 2020). Figure 2.4 illustrates the synthesis of graphene from graphite and chemical reduction of GO.

**Figure 2.4.** Synthesis of graphene from graphite and chemical reduction of GO.



The reduction of graphene oxide can cause changes in its chemical structure, thus generating carbon vacancies, besides that, the presence of residual functional groups in the rGO structure can also cause changes in the mechanical and electronic properties. The process of chemical reduction of the GO can contribute to the reduction of the surface area and electrical conductivity of the material, while the process of thermal reduction can change the structure and the mechanical resistance of the rGO, thus generating a substantial decrease in the mass of the GO (Bagri et al., 2010; Chen and Huang, 2020).

Song et al. (2021) performed the synthesis of rGO doped with nitrogen (NRGO) using the hydrothermal method. The material obtained was used as an adsorbent for the removal of ANT and 2-MAQ, from synthetic wastewater. Through the FTIR analysis, the presence of the functional groups of GO, rGO and NRGO was observed. SEM analysis showed that the degree of aggregation of the NRGO layers is lower than the degree of aggregation of the rGO, which indicates that the introduction of nitrogen into the structure of the rGO reduced the folding of the crushed leaves after the process of thermal reduction, however, it did not destroy the structure of graphene. The equilibrium experimental data were better adjusted to Freundlich's model and the kinetics experimental data were better adjusted to PFO model for ANT and PSO for 2-MAQ. The adsorption capacity of NRGO was 5.77 and 9.29 mg.g<sup>-1</sup> for ANT and 2-MAQ, respectively. The adsorbent remained efficient after the third cycle of use, according to the regeneration study.

Therefore, the study by Song et al. (2020) showed that the reduction of GO, followed by the introduction of nitrogen in its structure, can contribute to improve the properties of GO and increase the adsorption capacity of hydrophobic substances, such as PAHs.

### 2.5.2 Adsorption by green graphene-based nanomaterials

Adsorption is one of the most widely used methods for the remediation of pollutants, due to the low cost and high efficiency of contaminant recovery, such as PAHs. The term 'green adsorption' has been widely used to refer to adsorptive processes that use environmentally friendly methods to produce adsorbents from natural, biodegradable and non-toxic sources. Green adsorbents are produced, in general, using agricultural residues or materials that can work at room temperature or in sunlight, thus reducing the process costs (Rani and Shanker, 2018).

Green nanotechnology is used for the production of green adsorbents, aiming to minimize the toxic effects caused by the use of chemical reagents, thus optimizing the synthesis processes of nanomaterials, for the production of adsorbents with pore size and morphology of interest for its application in adsorptive processes. For the synthesis of green nanomaterials, natural agents are used, such as plant extracts, biodegradable materials and microorganisms. Some factors, such as concentration of the extracts, reaction time, precursor agents and pH, influence the synthesis processes of these green materials, as they directly influence the final features of the product (Mahmoud, 2020).

The synthesis processes of nanomaterials, whether by conventional or green chemistry, involve three factors: capping agent, reducing agent and solvent. In processes involving green chemistry, capping agents and reducing agents, in general, are non-toxic and less polluting, whereas the solvents are of natural origin. Capping agents are used to stabilize the nanoparticles, control the morphology and protect the aggregation surface, some capping agents used in green synthesis are polysaccharides and biomolecules, due to their high biocompatibilities and low toxicity. Reducing agents are used in chemical reduction processes, polysaccharides, such as  $\beta$ -D-glucose, peptides and proteins can also be used as green reducing agents. Solvents are widely used for the dissolution of precursors, assisting in heat transfer and dispersion of nanoparticles, water is one of the most used solvents because it is environmentally friendly, non-toxicity and non-flammability. Other alternative solvents that have been applied in green synthesis

processes are supercritical fluids, supercritical carbon dioxide and deep eutectic solvents<sup>3</sup> (Duan et al., 2015).

The conventional synthesis of graphene-based nanomaterials by the Hummer's method involves the use of chemical reagents harmful to the environment, in this context, some studies have reported the development of green methodologies for the synthesis of these nanomaterials through the use of natural agents, such as plants extracts and biodegradable waste. Table 2.8 summarizes the sources and methodologies used for the green synthesis of graphene-based nanomaterials. Figure 2.5 shows a schematic diagram of the main types of green reducing agents used for the synthesis of reduced GO.

**Figure 2.5.** Schematic diagram of the main types of green reducing agents for the synthesis of rGO.



Tewatia et al. (2020) reported the reduction of GO through the use of a green reducing agent, ascorbic acid, also known as vitamin C. The GO was synthesized by modified Hummer's method, in which  $\text{NaNO}_3$  were removed with an increase in the amount of  $\text{KMnO}_4$ . To reduce the GO, 5 g of ascorbic acid were added to the aqueous solution with a concentration of  $5 \text{ g.L}^{-1}$  of GO, the solution was stirred at 600 rpm at a constant temperature of  $60 \text{ }^\circ\text{C}$ . The results of the FTIR analyzes showed that the functional groups were removed after the chemical reduction process. The XRD analysis showed the presence of a wider peak after the reduction of the GO,

<sup>3</sup> Correção de ionic liquids para deep eutectic solvents.

which indicates that there was the removal of the functional oxygen group and the restoration of the C=C bonds. However, due to the peak width, it was concluded that removal of functional groups containing oxygen was incomplete, in addition, the presence of intercalated H<sub>2</sub>O molecules was detected.

Hou et al. (2017) performed the reduction of GO through the use of *Lycium barbarum* extract as a green and natural reducing agent. GO was synthesized by the Hummer's method, followed by its reduction through the use of *Lycium barbarum*, as a reducing agent. The material obtained was characterized by XRD, TEM, SEM, FTIR, XPS, RAMAN spectroscopy and TGA analyses. SEM analysis indicated a nanosheet-like morphology, which is characteristic of rGO. FTIR analysis indicated a decrease in peak intensity for functional groups containing oxygen, which confirmed the reduction of GO. The study pointed out that the mechanism of GO reduction was possible due to the active components present in *Lycium barbarum* fruits, as they have a high affinity of binding to groups containing oxygen to form their corresponding oxides and other by-products. The rGO reduced by *Lycium barbarum* had a C/O ratio of 6.5, while the rGO reduced by hydrazine hydrate had a C/O ratio of 6.6.

**Table 2.8.** Summary of sources and methodologies used on the green synthesis of graphene-based nanomaterials.

Nanomaterials	Methodology	Morphology	Characterizations	Other informations	References
GO and rGO	Modified Hummer's method and reduction by Ascorbic acid (vitamin C).	-	XRD, UV-visible spectroscopy, FTIR and RAMAN spectroscopy	Functional groups of GO: O-OH, C=O, C-OH and C-O.	Tewatia et al. (2020)
rGO	Improved Hummer's method and reduction by fresh ginger and garlic extracts.	Nanosheets	XRD, FTIR, TEM, RAMAN spectroscopy and UV-visible spectroscopy	Functional groups of GO: O-OH, C=O and C-O.	Rattan et al. (2020)
Ag NPs-F-rGO	Hummer's method and reduction by <i>Capparis spinosa</i> fruit extract.	Sheets morphology	FTIR, XRD, VSM, TEM and SEM	Functional groups of GO: O-OH, C=O, C-O, C=C and C-O-C.	Zarei et al. (2021)
L-rGO	Hummer's method and reduction by <i>Lycium barbarum</i> extract.	Nanosheets	XRD, TEM, SEM, FTIR, XPS, RAMAN spectroscopy and TGA	C/O ratio (GO): 1.35 C/O ratio (L-rGO): 6.5 C/O ratio (H-rGO): 6.6	Hou et al. (2017)
rGO	Hummer's method and reduction by green tea extract	Multi-layered sheets	SEM, FTIR, UV - visible spectroscopy and electrochemical sensing of SY	Functional groups of GO: O-OH, C=O and C-O.	Vatandost et al. (2020)
rGO	Modified Hummer's method and reduction by <i>Esfand</i> seed (ES) extract (ESE).	Nanosheets	XRD, FE-SEM, TGA, FTIR, RAMAN spectroscopy and EDS	C/O ratio (GO): 0.33 C/O ratio (rGO): 0.18	Ramezanzadeh et al. (2020)
rGO-Ag/ZnO	L-Methionine (L-Met) as green reductants and stabilizing agent.	Mixed morphologies of spherical, rose flower-petal, and hexagonal shape	SEM/EDS, TEM, XRD and UV - DRS	85% of degradation of MB after 210 min of irradiation.	Belachew et al. (2020)

The C/O ratio obtained by Hou et al. (2017) for the rGO reduced by the natural agent *Lycium barbarum* (6.5) is very close to the C/O ratio obtained by the use of hydrazine hydrate, which indicates that the natural agent has a reduction capacity comparable to the hydrazine hydrate. Through this study, it can be concluded that GO was effectively reduced by *Lycium barbarum*.

Zarei et al. (2021) accomplished the synthesis of the green nanocomposite Ag NPs-F-rGO using the fruit extract of *Capparis spinosa* as a reducing agent. GO was synthesized by the Hummer's method. The Ag<sup>+</sup> ions were coordinated with GO and then reduced by the fruit extract *Capparis spinosa* forming the AgNPs, which was converted to form rGO. The nanomaterial obtained was characterized by the analyzes of FTIR, TEM, SEM, and XRD. The FTIR analysis showed the existence of functional groups with oxygen, thus confirming the formation of the GO structure. The XRD analysis confirmed the presence of the characteristic peaks of rGO, and through SEM analysis sheets morphology was observed. The results indicated that *Capparis spinosa* is a promising reducing agent for the GO reduction.

Vatandost et al. (2020) performed the green synthesis of rGO by using green tea extract as a reducing and stabilizing agent. GO was synthesized by the Hummer's method, followed by its reduction using green tea extract. The nanomaterial obtained was characterized by SEM, FTIR, UV-visible spectroscopy and electrochemical sensing of SY techniques. SEM analysis showed a morphology with multi-layered sheets on top of each other, rough surface and wavy structures, complying with the UV-visible spectroscopy analysis, which confirmed the formation of rGO. The FTIR analysis showed a decrease in the intensity of the peaks belonging to the hydroxyl groups of the GO, which indicates a successful reduction of the GO. The results revealed that the green tea extract acted not only as a reducing agent, but also as a functionalizing agent for the rGO structure.

Ramezanzadeh et al. (2020) obtained rGO by using *Esfand* seed extract (ESE) as green reducing agents. GO was synthesized by the modified Hummer's method, followed by its reduction using ESE. The rGO-ESE sheets were modified by metallic zinc ions, thus obtaining the rGO-ESE-Zn(II) sheets. The nanomaterial obtained was characterized by XRD, FE-SEM, TGA, FTIR, RAMAN spectroscopy and EDS analyses. The results of Raman, FE-SEM, EDS and FTIR analyzes indicated the disappearance of the carbonyl absorption peak, which confirmed the GO reduction. The XDR analysis revealed a significant increase in the D-spacing of the GO leaves after interaction with ESE-Zn(II). The calculated C/O ratio for GO was 0.33 and the C/O ratio for rGO was 0.18. This result indicates that the GO was reduced by the ESE

molecules, in addition, the ESE was absorbed by the GO sheets, which resulted in an increase in the oxygen content.

The studies reported in this subsection pointed out that GO syntheses, as well as their reductions through the use of green reducing agents, were performed successfully. The results of the characterization analyzes indicated that reduced graphene oxide (rGO) was obtained, without any loss of its properties. The green reducing agents used in the studies present themselves as ecologically correct and low-cost methodologies for green GO reduction, thus replacing the use of traditional reducing agents, such as hydrazine and sodium borohydride, which are potentially toxic. Based on the results and discussions presented, it can be concluded that the use of natural reducers are a simple and economical method for the preparation of rGO, thus contributing to minimize the generation of toxic effluents during the synthesis processes.

### 2.5.3 Application of green synthesized nanomaterials for PAHs removal

Some green and low-cost methodologies have been developed over the years to remove petrogenic PAHs from wastewater. Crisafulli et al. (2008) conducted a study to investigate the removal efficiency of PAHs using low-cost natural adsorbents, such as sugar cane bagasse, green coconut shells, chitin, and chitosan. The adsorptive process of PAHs (PRY, ANT, ACE, NAP) occurred under the following operational conditions: initial concentration of PAHs 5.0 – 15.0 mg.L<sup>-1</sup>, room temperature (28 ± 2°C) and pH 7.5. The equilibrium experimental data had a better adjustment to Freundlich's model. Green coconut shells showed the best efficiency in removing PAHs from wastewater. A comparative performance analysis was also carried out with conventional adsorbents, such as activated carbon, cellulose, silica, and Amberlite T. The results indicated that green coconut shells and sugar cane bagasse were more efficient for the removal of PAHs from wastewater, than silica and Amberlite T.

Younis et al. (2014) accomplished the adsorption of PAHs from the oil industry wastewater using residual biomass from rice straw (RS) and sugar cane bagasse (SB), as low cost bioadsorbents. The bioadsorbents were applied to remove NAP, ANT and PYR, so that the adsorption experiments were conducted by batch adsorption, taking into account factors such as PAH concentration, temperature and contact time. The experimental kinetic data, for NAP, followed the PFO model, while for ANT and PYR, the kinetic data followed the PSO model, indicating that the physisorption and chemisorption were the determining mechanisms in the adsorptive process. The adsorption isotherms had a better fit and greater accuracy to the Langmuir's model, for all PAHs analyzed. By calculating the thermodynamic parameters, the

nature of the adsorptive processes was determined. The results indicated that the bioadsorptive process had a non-spontaneous nature ( $\Delta G^\circ > 0$ ), good affinity for the adsorbate ( $\Delta S^\circ > 0$ ) and endothermic nature ( $\Delta H^\circ > 0$ ), indicating a strong interaction between bioadsorbents and PAHs. The adsorption results confirmed that the SB showed higher PAH adsorption efficiency than the RS.

The results obtained through the studies developed by Crisafully et al. (2008) and Younis et al. (2014) pointed out sugar cane bagasse as a simple and low-cost bioadsorbent for the remediation of PAHs from effluents from the petroleum industry.

The synthesis of green magnetic nanomaterials has been in the spotlight in the current context, due to their potential application in the removal of inorganic and organic compounds, such as PAHs, from domestic and industrial effluents (Nasrollahzadeh et al., 2020). Inbaraj et al. (2021) carried out the green synthesis of a magnetic activated carbon by using green tea leaves (MNPs-GTAC), aiming at its application for the remediation of BaA, BbF, CHR and BaP, from wastewater. The material obtained was characterized by the BET-N<sub>2</sub> method, XRD, FTIR, SEM/TEM, TGA and SQUID-VSM analyses. The kinetics experimental data was better adjusted to the PSO model, reaching 80% removal in 5 min. The equilibrium experimental data had a better adjustment to the Langmuir's model and had the following maximum adsorption capacities: 28.08 mg.g<sup>-1</sup> for BbF, 22.75 mg.g<sup>-1</sup> for CHR, 19.14 mg.g<sup>-1</sup> for BaP and 15.86 mg.g<sup>-1</sup> for BaA. Through the thermodynamic studies it was found that the nature of the adsorptive process was endothermic and spontaneous.

Shanker et al. (2017) presented in their studies a green synthesis method of an iron hexacyanoferrate nanostructure (FeHCF) using *Sapindus-mukorossi* as a natural surfactant. The TEM analysis showed that the nanoparticles have a hexagonal, rod and spherical shape. The XRD analysis showed a high crystallinity of the synthesized material. The nanomaterials were applied to the photocatalytic degradation and adsorption of PAHs from wastewater (ANT, PHEN, CHR, FLU and BaP), under the following operational conditions: 50 mg.L<sup>-1</sup> of initial concentration of PAHs, dosage of adsorbent 25 mg, neutral pH and solar radiation. FeHCFs generated a significant reduction in PAHs (70 - 90% of reduction).

Hassan et al. (2018) effected the green synthesis of iron oxide nanoparticles (IONPs) by using extract from pomegranate peel. The nanomaterial obtained was applied in the adsorption of BaP and PYR from synthetic wastewater. Through the XRD analysis, the characteristic peaks of the iron oxide nanoparticles were observed, indicating that the amorphous structure of Fe<sub>2</sub>O<sub>3</sub> was obtained. The factors that were evaluated in the adsorption of PAHs are: concentration of PAHs, dosage of adsorbent, pH and temperature. The maximum adsorption capacities of IONPs

obtained was 0.029 and 2.8 mg.g<sup>-1</sup> for BaP and PYR, respectively. Through the thermodynamic study, it was determined that the adsorptive process was spontaneous and exothermic, the kinetic data obtained had a better adjustment to the PSO model and the equilibrium data had a better adjustment to Langmuir's model. IONPs showed 98.5% of reduction for PRY and 99% for BaP.

The studies developed by Inbaraj et al. (2021), Shanker et al. (2017) and Hassan et al. (2018) successfully performed the green synthesis of magnetic nanoparticles using natural extracts. The green magnetic nanoparticles synthesized in the studies were applied in the adsorption of PAHs from wastewater and the results indicated high removal efficiency of PAHs in all studies. In the study developed by Li et al (2017), the conventional synthesis of magnetic nanoparticles was carried out aiming its application in the adsorption of PAHs from wastewater. The results revealed an efficiency of removal of PAHs superior to 80%, for ANT and PHEN. Comparing the removal efficiencies of green magnetic nanoparticles with conventional ones, it can be concluded that the use of green nanomaterials presents itself as a simple, sustainable, promising and low-cost methodology for the adsorption of organic contaminants.

Due to the polluting and toxic effects of PAHs to the environment, some studies have been developed aiming at the application of green graphene-based nanomaterials for the remediation of these contaminants from wastewater. Xiao et al. (2017) synthesized a graphene-like material through the carbonization and activation of sugar cane, which was applied for the removal of NAP, PHEN and 1-naphthol from wastewater. The morphological analysis indicated the obtaining of a turbostratic monolayer of graphene nanosheets and the results of FTIR and XPS showed the presence of the functional groups characteristic of GO. The adsorptive experiments were conducted in batch and the results showed an adsorption capacity of 615.8, 431.2 and 2040 mg.g<sup>-1</sup> for NAP, PHEN and 1-naphthol, respectively. The equilibrium experimental data had a better adjustment to Freundlich's model.

Cheng et al. (2019) proposed an innovative and green route to synthesis of a material through hydrothermal treatment, followed by an activation by KHCO<sub>3</sub>, to transform crop residues, rape straw and corn cob into an adsorbent called porous carbons (PCs). The material characterizations using SEM, XRD, RAMAN spectroscopy and FTIR techniques indicated the presence of graphene in its structure, through the abundant presence of C=C, in addition, the material presented the morphology of graphene sheets, which is characteristic of graphene. The XRD analysis showed the presence of the hexagonal structure characteristic of graphite, confirming its existence in the structure, which made it possible to increase the adsorption capacity through  $\pi$ - $\pi$  interactions with PAHs. The materials obtained were applied to the

adsorption of NAP, ACE and PHEN from wastewater. The adsorption experiments were performed in batch and the kinetic and equilibrium experimental data had a better fit to the PSO and Freundlich's models, respectively. The maximum adsorption capacities for PAHs were 592.97, 480.27, and 692.27 mg.g<sup>-1</sup> for NAP, ACE and PHEN, respectively.

The experimental data of PAHs adsorption obtained in the study by Xiao et al. (2017) indicated that a graphene-like material, synthesized from sugar cane biomass, may have a high capacity for adsorption of PAHs from effluents. Comparing the adsorptive performance of the green GO, synthesized by Xiao et al. (2017), with the GO obtained in the study developed by Wang et al. (2014), using the conventional Hummer's method, in which an adsorption capacity of 68.66 and 69.86 mg.g<sup>-1</sup> was obtained for NAP and PHEN, respectively, the superiority of the material obtained by the green route is evidenced. The results obtained by Cheng et al. (2019) also showed that GO synthesized by the green route is an ecological and promising adsorbent for the remediation of PAHs from wastewater.

#### 2.5.4. Comparison with other PAHs removal technologies

Besides the adsorptive processes, many technologies, such as bioremediation, membrane separation, coagulation-flocculation and chemical oxidation processes (see Fig. S3), have been developed aiming at the remediation of petrogenic PAHs wastewater. Table 2.9 summarizes PAHs treatment technologies, as well the efficiency of removal.

The bioremediation processes consist of using microorganisms to remove pollutants, through its metabolic activity. Bioremediation has presented itself as a promising, sustainable, efficient and low-cost solution for the remediation of petrogenic PAHs from wastewater (Behera et al., 2018). Despite the advantages of bioremediation, the main limitations to be overcome are related to the low bioavailability of pollutants, low microbial adaptability, the need for a long residence time and large area (Shahsavari et al., 2019). Sun et al. (2019) reported, in their study, the PAHs removal from coke wastewater using the strain *Pseudomonas aeruginosa* S5 to produce the biosurfactant. The effect of the biosurfactant on the solubility of three HMW PAHs (PHEN, FLU, BaP) was evaluated. The results indicated that when the biosurfactant concentration exceeded the established critical micellar concentration (CMC), there was a linear increase in the solubility of the evaluated PAHs. The results also showed that the addition of *P. aeruginosa* S5 to the coke wastewater led to a 55% of reduction in the concentration of PAHs in 15 days, from 9141.02 to 5117.16 µg.L<sup>-1</sup>.

PAHs can also be removed from wastewater through the application of different membrane separation technologies. The pressure-driven membrane processes are divided into three types: microfiltration (Goswami et al., 2019), ultrafiltration (Smol and Makuła, 2012) and reverse osmosis (Smol et al., 2015). Membrane separation processes main advantages are lower energy consumption, less risk of pollution and low cost of reprocessing. However, the use of a single separation technique may not be a good efficient solution for removing contaminants, so they are usually used in combination with other methods. Some processes apply, for example, ultrafiltration in conjunction with reverse osmosis or even ultrafiltration combined with microfiltration, among other methods (Yu et al., 2017). Márquez et al. (2015) evaluated the viability of a multi-barrier treatment (MBT) for the remediation of PHEN, orange II, phenol and 4-chlorophenol from synthetic industrial wastewater. Following the MBT methodology, a pre-treatment of the effluent was carried out by microfiltration membrane (MF), and then, hydrogen peroxide ( $H_2O_2$ /UVC) photolysis using a medium pressure Hg Lamp (MP) and granulated activated carbon (GAC). The results showed a degradation of 85% of the contaminants after the MBT treatment, thus generating a reduction in the toxicity of the effluents after the MF treatment.

Coagulation-flocculation is a physical-chemical process that can be used to remove colloidal suspensions and to eliminate organic compounds, such as PAHs, from water and wastewater (Smol and Makuła, 2017). This technique has as main advantages: easy operation, low operating cost and simple equipment. The main limitations of these methods concern the treatment of oily wastewater due to the characteristics of the components dissolved in the oil mixture, which increases the complexity of the treatment, requiring the combination of this treatment with other methods. In addition, the treatment of oily wastewater can result in secondary pollution of water bodies, which can hinder treatment by the coagulation-flocculation technique (Zhao et al., 2021). Shabeer et al. (2014) conducted a study aimed at removing PAHs (NAP, ACE, PHEN, FLT, ANT and PYR) from wastewater. The effluent treatment process involved the PAHs adsorption by organo-modified nano-clays, then a coagulation-flocculation treatment was performed with alum and poly aluminum chloride (PAC). The application of the combined adsorption and coagulation-flocculation methods resulted in an effective and relatively simple methodology for the remediation of PAHs, obtaining a reduction between 37-100%.

**Table 2.9.** Evaluation of the efficiency of different PAH removal techniques.

PAHs	Sources	Treatment techniques	PAHs Removal	References
PHEN, FLT and BAP	Coking Water	Bioremediation	Reduction from 9141.02 to 5117.16 $\mu\text{g.L}^{-1}$ (55% of reduction)	Sun et al. (2019)
PHEN	Synthetic industrial wastewater	Microfiltration- $\text{H}_2\text{O}_2$ /UV-Catalytic wet peroxide oxidation	85% of reduction	Márquez et al. (2015)
ACE, PHEN, CHR and PYR	Municipal wastewater	Bioremediation-Microfiltration + UV disinfection	$43 \pm 14\%$ of reduction	Qiao et al. (2019)
NAP, ACE, PHEN, FLT, ANT and PYR	Synthetic wastewater	Adsorption + Coagulation-flocculation	37.4 to 100% of reduction	Shabeer et al. (2014)
NAP and PYR	Synthetic wastewater	Chemical oxidation – Using Electrochemical oxidation and Fenton oxidation	Electrochemical oxidation: 80 – 81% of reduction; Fenton oxidation: 46 % of reduction	Tran et al. (2010)
ANT and PYR	Synthetic wastewater	Activated carbon	Maximum removal of >99% (after 4h of contact)	Rasheed et al. (2015)
ANT	Synthetic wastewater	Adsorption by nitrogen-doped reduced graphene oxide (NRGO)	Adsorption capacities: $5.77 \text{ mg.g}^{-1}$ ; Adsorption efficiency: 58%	Song et al. (2021)
NAP, PHEN and PYR	Synthetic wastewater	Adsorption by graphene oxide/ $\text{Ag}_3\text{PO}_4$ (GO/ $\text{Ag}_3\text{PO}_4$ )	82,1% to 100% of reduction (in 7.5h)	Yang et al. (2018)

PAHs concentration in wastewater can also be reduced through the application of advanced oxidation processes (AOPs). AOPs involve the application of different chemical reagents in order to increase the formation of radicals, generating the degradation of the compound of interest, allowing its remediation of the environment. These processes are presented as a viable technique for the removal of contaminants, as they enable high efficiency, relatively short remediation time and can be applied to different concentrations of pollutants. However, it is an expensive process, in addition, they can form intermediate compounds resistant to their complete chemical degradation, which can prolong the treatment time (Ferrarese et al., 2008; Smol and Makuła, 2017). Haneef et al. (2020), in their studies, evaluated the use of nanoscale zero valiant iron (nZVI) and  $\text{H}_2\text{O}_2$  to remove PAHs from produced water collected in an oil and gas exploration field in the South East Asian. The process was carried out in batch and the concentration of nZVI and  $\text{H}_2\text{O}_2$ , pH and reaction time, had their effect evaluated. Central Composite Design (CCD) planning was applied through the response surface methodology (RSM), aiming at obtaining the optimum operating conditions of the remediation process. The experimental results showed a maximum removal of 89.5% for PAHs and 75.3% for chemical oxygen demand (COD). The ideal conditions obtained by the CCD were:  $4.35 \text{ g.L}^{-1}$  and  $1.60 \text{ g.L}^{-1}$  concentrations of nZVI and  $\text{H}_2\text{O}_2$  respectively, 2.94 pH and 199.9 min reaction time.

Compared to other remediation technologies, adsorptive processes are presented as a simple, fast and efficient technology for the remediation of PAHs. Various types of adsorbents can be used for PAHs removal, such as activated carbon (Rasheed et al., 2015), organobentonite (Wu and Zhu 2012), zeolites (Wołowiec et al., 2017), silica-based mesoporous materials (SBMM) (Yuan et al., 2018), graphene-based nanomaterials (Song et al., 2021). It is important to highlight that during the process of developing an adsorbent material it is necessary to study the kinetics, equilibrium and thermodynamics of adsorption.

The main challenges to be overcome by the adsorptive processes concern the development of ecologically correct and efficient methodologies for the synthesis of adsorbent materials, thus aiming to minimize the toxic effects caused by the excessive use of chemical reagents. The articles discussed in this review pointed out adsorption as an efficient and promising technique for PAH removal, when compared to other remediation technologies.

## 2.6. Challenges, future prospects and conclusions

This review addressed the main sources and harmful effects caused by the presence of PAHs in the environment, as well as the different technologies applied to remove them from wastewater in recent decades (2008-2021). Although they are generally found in lower concentrations, PAHs can cause irreversible damage to the environment and to humans, due to their high potential for genotoxicity, mutagenicity and carcinogenicity. This review covered the main studies on the adsorption of PAHs from wastewater by graphene-based nanomaterials, synthesized by conventional and green routes. Different methodologies for the synthesis of graphene-based adsorbents were discussed. The adsorptive processes were compared with other conventional remediation technologies, and presented themselves as more economical and efficient for the removal of petrogenic PAHs from wastewater.

The adsorption of different types of PAHs by different adsorbents was discussed, considering the efficiency of kinetic, equilibrium, thermodynamic and breakthrough curve parameters. The studies approached indicated, by means of the maximum adsorption capacities, that the removal efficiency for each type of PAHs depends on the effect of pH, contact time, temperature, concentration and affinity for adsorbate. Most of the adsorptive processes evaluated were spontaneous in nature and chemisorption was the main mechanism associated with the processes, since most kinetic data had a better adjustment to the PSO's model. Batch and fixed-bed adsorptive processes were also evaluated.

Different methodologies for the green synthesis of nanomaterials were addressed, due to the great relevance of this topic for the present time. The studies discussed showed the reduction of GO through the use of green reducing agents, such as plant extracts, microorganisms and biomass residues, as a sustainable, simple and low-cost method for the synthesis of rGO. The adsorption of PAHs through the use of green nanomaterials had an adsorption capacity comparable to the conventional nanomaterials. However, it is also important to highlight that there are still many challenges to be overcome by green synthesis processes, especially with regard to the process efficiency and the structural and thermal properties of green materials. Despite the growing number of studies that address the application of green nanomaterials to remove PAHs, there are still gaps in the literature about the application of green reduced GO for the removal of petrogenic PAHs from wastewater. In this context, some perspectives for future studies can be addressed, such as: (i) Study of the adsorptive properties of green rGO for the remediation of wastewater PAHs; (ii) Studies on the reuse/regeneration of green nanoadsorbents; (iii) Application of green adsorbents in dynamic

fixed-bed systems; (iv) Economic analysis of costs for application in large-scale adsorptive systems aiming industrial use; (v) Life cycle analysis for the synthesis of the adsorbent and the adsorptive process in order to assess the environmental impact.

### Acknowledgements

The authors of this paper are grateful for the financial support of the Human Resources Training Program for the Oil, Natural Gas and Biofuels Sector (PRH-ANP) (Number 29), Brazilian National Research Council (CNPq) (Grant #308046/2019-6 and Grant #141469/2018-8), São Paulo Research Foundation (FAPESP) (Grant #2019/11353-8; #2019/07822-2) and Coordination for the Improvement of Higher Education Personnel (CAPES) (Finance Code 001).

### References

- Abdel-Shafy, H. I., Mansour, M. S. M., 2016. A review on polycyclic aromatic hydrocarbons: Source, environmental impact, effect on human health and remediation. *Egyptian Journal of Petroleum*. 25, 107-123. <http://dx.doi.org/10.1016/j.ejpe.2015.03.011>.
- Abdullahi, B. O., Ahmed, E., Abdulgader, H. A., Alghunaimi, F., Saleh, T. A., 2021. Facile fabrication of hydrophobic alkylamine intercalated graphene oxide as absorbent for highly effective oil-water separation. *Journal of Molecular Liquids*. 325, 115057. <https://doi.org/10.1016/j.molliq.2020.115057>.
- Adeniji, A. O., Okoh, O. O., Okoh, A. I., 2018. Analytical Methods for Polycyclic Aromatic Hydrocarbons and their Global Trend of Distribution in Water and Sediment: A Review, in: Zoveidavianpoor, M. (Eds.), *Recent Insights in Petroleum Science and Engineering*. IntechOpen, pp. 393-428.
- Adeola, A. O., Forbes, P. B. C., 2019. Optimization of the sorption of selected polycyclic aromatic hydrocarbons by regenerable graphene wool. *Water Science & Technology*. 80, 1931–1943. <https://doi.org/10.2166/wst.2020.011>.
- Albayati, T. M., Kalash, K. R., 2020. Polycyclic aromatic hydrocarbons adsorption from wastewater using different types of prepared mesoporous materials MCM-41 in batch and fixed bed column. *Process Safety and Environmental Protection*. 133, 124-136. <https://doi.org/10.1016/j.psep.2019.11.007>.
- Alghunaimi, F. I., Alsaeed, D. J., Harith, A. M., Saleh, T. A., 2019. Synthesis of 9-octadecenoic acid grafted graphene modified with polystyrene for efficient light oil removal from water. *Journal of Cleaner Production*. 233, 946-953. <https://doi.org/10.1016/j.jclepro.2019.05.239>.

Alkhouzaama, A., Qiblaweya, H., Khraisheha, M., Atiehb, M., Al-Ghouti, M., 2019. Synthesis of graphene oxides particle of high oxidation degree using a modified Hummers method. *Ceramics International*. 46, 23997-24007. <https://doi.org/10.1016/j.ceramint.2020.06.177>.

Álvarez, I. M., Menach, K. L., Devier, M. H., Barbarin, I., Tomovska, R., Cajaraville, M. P., Budzinski, H., Orbea, A., 2021. Uptake and effects of graphene oxide nanomaterials alone and in combination with polycyclic aromatic hydrocarbons in zebrafish. *Science of The Total Environment*. 775, 145669. <https://doi.org/10.1016/j.scitotenv.2021.145669>.

Akinpelu, A. A., Ali, M. E., Johan, M. R., Saidur, R., Chowdhury, Z. Z., Shemsi, A. M., Saleh, T. A., 2019. Effect of the oxidation process on the molecular interaction of polyaromatic hydrocarbons (PAH) with carbon nanotubes: Adsorption kinetic and isotherm study. *Journal of Molecular Liquids*. 289, 111107. <https://doi.org/10.1016/j.molliq.2019.111107>.

Alkhadher, S. A. A., Al-Odaini, N. A., 2016. Anthropogenic waste indicators (AWIs), particularly PAHs and LABs, in Malaysian sediments: Application of aquatic environment for identifying anthropogenic pollution. *Marine Pollution Bulletin*. 102, 160-175. <https://doi.org/10.1016/j.marpolbul.2015.11.032>.

Andrade, J. R., Oliveira, M. F., Canevesi, R. L. S., Landers, R., Silva, M. G. C., Vieira, M. G. A., 2020. Comparative adsorption of diclofenac sodium and losartan potassium in organophilic clay-packed fixed-bed: X-ray photoelectron spectroscopy characterization, experimental tests and theoretical study on DFT-based chemical descriptors. *Journal of Molecular Liquids*. 312, 113427. <https://doi.org/10.1016/j.molliq.2020.113427>.

Asha, A. B., Narain, R., 2020. Nanomaterials properties, in: Narain, R. (Eds.), *Polymer Science and Nanotechnology*. Elsevier Inc., Canada, pp. 343-359.

Bagri, A., Mattevi, C., Acik, M., Chabal, Y. J., Chhowalla, M., Shenoy, V. B., 2010. Structural evolution during the reduction of chemically derived graphene oxide. *Nature Chemistry*. 2, 581-587. <https://doi.org/10.1038/nchem.686>.

Behera, B. K., Das, A., Sarkar, D. J., Weerathunge, P., Parida, P. K., Das, B. K., Thavamani, P., Ramanathan, R., Bansal, V., 2018. Polycyclic Aromatic Hydrocarbons (PAHs) in inland aquatic ecosystems: Perils and remedies through biosensors and bioremediation. *Environmental Pollution*. 241, 212-233. <https://doi.org/10.1016/j.envpol.2018.05.016>.

Belachew, N., Kahsay, M. H. K., Tadesse, A., Basavaiah, K., 2020. Green synthesis of reduced graphene oxide grafted Ag/ZnO for photocatalytic abatement of methylene blue and antibacterial activities. *Journal of Environmental Chemical Engineering*. 8, 104106. <https://doi.org/10.1016/j.jece.2020.104106>.

Beyer, J., Goksøyr, A., Hjermmann, D. O., Klungsøyr, J., 2020. Environmental effects of offshore produced water discharges: A review focused on the Norwegian continental shelf. *Marine Environmental Research*. 162, 105-155. <https://doi.org/10.1016/j.marenvres.2020.105155>.

Bolade, O. P., Williams, A. B., Benson, N. U., 2020. Green synthesis of iron-based nanomaterials for environmental remediation: A review. *Environmental Nanotechnology, Monitoring & Management*. 13, 100279. <https://doi.org/10.1016/j.enmm.2019.100279>.

Bohart, G. S., Adams, E. Q., 1920. Some aspects of the behavior of charcoal with respect to chlorine. *J. Am. Chem. Soc.* 42, 523-544. <https://doi.org/10.1021/ja01448a018>.

Brodie, B. C., 1859. On the Atomic Weight of Graphite. *Philosophical Transactions of the Royal Society of London.* 149, 249-259. <https://doi.org/10.1098/rstl.1859.0013>.

Chakravarty, R., Dash, A., 2013. Role of Nanoporous Materials in Radiochemical Separations for Biomedical Applications. *Journal of Nanoscience and Nanotechnology.* 13, 2431-2450. DOI:10.1166/jnn.2013.7349.

Chen, J., Yao, B., Li, C., Shi, G., 2013. An improved Hummers method for eco-friendly synthesis of graphene oxide. *Carbon.* 64, 225-229. <http://dx.doi.org/10.1016/j.carbon.2013.07.055>.

Chen, W. H., Huang, J. R., 2020. Adsorption of organic including pharmaceutical and inorganic contaminants in water toward graphene-based materials, in: Maldonado, A. J. H., Blaney, L. (Eds.), *Contaminants of Emerging Concern in Water and Wastewater.* Elsevier Inc., pp. 93-113.

Cheng, H., Bian, Y., Wang, F., Jiang, X., Ji, R., Gu, C., Yang, X., Song, Y., 2019. Green conversion of crop residues into porous carbons and their application to efficiently remove polycyclic aromatic hydrocarbons from water: Sorption kinetics, isotherms and mechanism. *Bioresource Technology.* 284, 1-8. <https://doi.org/10.1016/j.biortech.2019.03.104>.

Chua, C. K., Pumera, M., 2014. Chemical reduction of graphene oxide: a synthetic chemistry viewpoint. *Chem. Soc. Rev.* 43: 291 - 312. <https://doi.org/10.1039/c3cs60303b>.

Crisafully, R., Milhome, M. A. L., Cavalcante, R. M., Silveira, E. R., Keukeleire, D. D., Nascimento, R. F., 2008. Removal of some polycyclic aromatic hydrocarbons from petrochemical wastewater using low-cost adsorbents of natural origin. *Bioresource Technology.* 99, 4515-4519. <https://doi.org/10.1016/j.biortech.2007.08.041>.

Duan, H., Wang, D., Li, Y., 2015. Green chemistry for nanoparticle synthesis. *Chem. Soc. Rev.* 44, 5778-5792. <https://doi.org/10.1039/c4cs00363b>.

Fadillah, G., Saleh, T. A., Wahyuningsih, S., Putri, E. N. K., Febrianastuti, S., 2019. Electrochemical removal of methylene blue using alginate-modified graphene adsorbents. *Chemical Engineering Journal.* 378, 122140. <https://doi.org/10.1016/j.cej.2019.122140>.

Ferrarese, E., Andreottola, G., Oprea, I. A., 2008. Remediation of PAH-contaminated sediments by chemical oxidation. *Journal of Hazardous Materials.* 152, 128-139. <https://doi.org/10.1016/j.jhazmat.2007.06.080>.

Freundlich, H. M. F., 1906. Over the adsorption in solution. *Urnal Phys Chem.* 57,385-471.

Gan, L., Lu, Z., Cao, D., Chen, Z., 2018. Effects of cetyltrimethylammonium bromide on the morphology of green synthesized Fe<sub>3</sub>O<sub>4</sub> nanoparticles used to remove phosphate. *Materials Science & Engineering C.* 82, 41-45. <https://doi.org/10.1016/j.msec.2017.08.073>.

Ghosal, D., Ghosh, S., Dutta, T. K., Ahn, Y., 2016. Current State of Knowledge in Microbial Degradation of Polycyclic Aromatic Hydrocarbons (PAHs): A Review. *Frontiers in Microbiology*. 7, 1369. <https://doi.org/10.3389/fmicb.2016.01369>.

Gomis, V. V., Grau, J., Benedé, J. L., Chisvert, A., Salvador, A., 2020. Reduced graphene oxide-based magnetic composite for trace determination of polycyclic aromatic hydrocarbons in cosmetics by stir bar sorptive dispersive microextraction. *Journal of Chromatography A*. 1624, 461229. <https://doi.org/10.1016/j.chroma.2020.461229>.

Goswami, L., Kumar, R. V., Pakshirajan, K., Pugazhenth, G., 2019. A novel integrated biodegradation—Microfiltration system for sustainable wastewater treatment and energy recovery. *Journal of Hazardous Materials*. 365, 707-715. <https://doi.org/10.1016/j.jhazmat.2018.11.029>.

Gupta, H., Singh, S., 2018. Kinetics and thermodynamics of phenanthrene adsorption from water on orange rind activated carbon. *Environmental Technology & Innovation*. 10, 208-214. <https://doi.org/10.1016/j.eti.2018.03.001>.

Gupta, V. K., Srivastava, S. K., Mohan, D., Sharma, S., 1998. Design parameters for fixed bed reactors of activated carbon developed from fertilizer waste for the removal of some heavy metal ions. *Waste Management*. 17, 517-522. [https://doi.org/10.1016/S0956-053X\(97\)10062-9](https://doi.org/10.1016/S0956-053X(97)10062-9).

Hall, S., Tang, R., Baeyens, J., Dewil, R., 2009. Removing polycyclic aromatic hydrocarbons from water by adsorption on silicagel. *Polycyclic Aromatic Compounds*. 29, 160–183. DOI: 10.1080/10406630903017534.

Haneef, T., Mustafa, M. R. U., Rasool, K., Ho, Y. C., Kutty, S. R. M., 2020. Removal of Polycyclic Aromatic Hydrocarbons in a Heterogeneous Fenton Like Oxidation System Using Nanoscale Zero-Valent Iron as a Catalyst. *Water*. 12, 2430. <https://doi.org/10.3390/w12092430>.

Hassan, S. S. M., Shafy, H. I. A., Mansour, M. S. M., 2018. Removal of pyrene and benzo(a)pyrene micropollutant from water via adsorption by green synthesized iron oxide nanoparticles. *Advances in Natural Sciences: Nanoscience and Nanotechnology*. 9, 015006. <https://doi.org/10.1088/2043-6254/aaa6f0>.

Hou, D., Liu, Q., Cheng, H., Zhang, H., Wang, S., 2017. Green reduction of graphene oxide via *Lycium barbarum* extract. *Journal of Solid State Chemistry*. 246, 351-356. <http://dx.doi.org/10.1016/j.jssc.2016.12.008>.

Huang, D., Xu, B., Wu, J., Brookes, P. C., Xu, J., 2019. Adsorption and desorption of phenanthrene by magnetic graphene nanomaterials from water: Roles of pH, heavy metal ions and natural organic matter. *Chemical Engineering Journal*. 368, 390-399. <https://doi.org/10.1016/j.cej.2019.02.152>.

Huang, Y., Zhang, W., Ruan, G., Li, X., Cong, Y., Du, F., Li, J., 2018. Reduced Graphene Oxide-Hybridized Polymeric High-Internal Phase Emulsions for Highly Efficient Removal of Polycyclic Aromatic Hydrocarbons from Water Matrix. *Langmuir*. 34, 3661–3668. <https://doi.org/10.1021/acs.langmuir.8b00005>.

Hummers, W. S.; Offeman, R. E., 1958. Preparation of Graphitic Oxide. *Journal of the American Chemical Society*. 80, 1339.

Ho, Y.S., McKay, G., 1999. Pseudo-second order model for sorption processes. *Process Biochemistry*. 34, 451–465. [https://doi.org/10.1016/S0032-9592\(98\)00112-5](https://doi.org/10.1016/S0032-9592(98)00112-5).

Inbaraj, B. S., Sridhar, K., Chen, B. H., 2021. Removal of polycyclic aromatic hydrocarbons from water by magnetic activated carbon nanocomposite from green tea waste. *Journal of Hazardous Materials*. 415, 125701. <https://doi.org/10.1016/j.jhazmat.2021.125701>.

Kinniburgh, D. G., 1986. General Purpose Adsorption Isotherms. *Environmental Science and Technology*. 20, 895-904. <https://doi.org/10.1021/es00151a008>.

Lagergren, S., 1898. About the theory of so-called adsorption of soluble substances. *Kungliga Svenska Vetenskapsakademiens. Handlingar*. 24, 1-39.

Lander, J. J., 1964. Chemisorption and ordered surface structure. *Surface Science*. 1, 125-164. [https://doi.org/10.1016/0039-6028\(64\)90024-X](https://doi.org/10.1016/0039-6028(64)90024-X).

Langmuir, I., 1918. The adsorption of gases on plane surfaces of glass, mica and platinum. *J Am Chem Soc*. 40, 1361.

Li, J., Zhou, Q., Liu, Y., Lei, M., 2017. Recyclable nanoscale zero-valent iron-based magnetic polydopamine coated nanomaterials for the adsorption and removal of phenanthrene and anthracene. *Science and Technology of Advanced Materials*. 18, 3-16. <https://doi.org/10.1080/14686996.2016.1246941>.

Li, S., Luo, J., Hang, X., Zhao, S., Wan, Y., 2019. Removal of polycyclic aromatic hydrocarbons by nanofiltration membranes: Rejection and fouling mechanisms. *Journal of Membrane Science*. 582, 264-273. <https://doi.org/10.1016/j.memsci.2019.04.008>.

Mahmoud, A. E. D., 2020. Nanomaterials: Green Synthesis for Water Applications, in: Kharissova, O. V., Martínez, L. M. T., Kharisov, B. I. (Eds.), *Handbook of Nanomaterials and Nanocomposites for Energy and Environmental Applications*. Springer Nature, Switzerland, pp. 1 – 21. [https://doi.org/10.1007/978-3-030-11155-7\\_67-1](https://doi.org/10.1007/978-3-030-11155-7_67-1).

Márquez, J. J. R., Herrera, M. G. P., Díaz, M. L. M., Merino, A. A., Manzano, M.A., 2015. Combined AOPs for potential wastewater reuse or safe discharge based on multi-barrier treatment (microfiltration-H<sub>2</sub>O<sub>2</sub>/UV-catalytic wet peroxide oxidation). *Chemical Engineering Journal*. 270, 80-90. <http://dx.doi.org/10.1016/j.cej.2015.02.011>.

Marczewska, A. D., Marczewski, A. W., 2002. Effect of adsorbate structure on adsorption from solutions. *Applied Surface Science*. 196, 264-272. [https://doi.org/10.1016/S0169-4332\(02\)00064-8](https://doi.org/10.1016/S0169-4332(02)00064-8).

Masood, N., Zakaria, M. P., Halimoon, N., Aris, A. Z., Magam, S. M., Kannan, N., Mustafa, S., Ali, M. M., Keshavarzifard, M., Vaezzadeh, V., Alkhadher, S. A. A., Al-Odaini, N. A., 2016. Anthropogenic waste indicators (AWIs), particularly PAHs and LABs, in Malaysian sediments: Application of aquatic environment for identifying anthropogenic pollution. *Marine Pollution Bulletin*. 102, 160-175. <https://doi.org/10.1016/j.marpolbul.2015.11.032>.

Mercier, J. P., Zambelli, G., Kurz, W., 2002. Nanomaterials and nanostructured materials, in: Mercier, J. P., Zambelli, G., Kurz, W. (Eds.), *Introduction to Materials Science*. Elsevier Ltd., pp. 421-438. <https://doi.org/10.1016/B978-2-84299-286-6.50023-8>.

Mortazavi, M., Baghdadi, M., Javadi, N. H. S., Torabian, A., 2019. The black beads produced by simultaneous thermal reducing and chemical bonding of graphene oxide on the surface of amino-functionalized sand particles: Application for PAHs removal from contaminated waters. *Journal of Water Process Engineering*. 31, 100798. <https://doi.org/10.1016/j.jwpe.2019.100798>.

Mukhopadhyay, S.; Dutta, R.; Das, P., 2020. A critical review on plant biomonitors for determination of polycyclic aromatic hydrocarbons (PAHs) in air through solvent extraction techniques. *Chemosphere*. 251, 126441. <https://doi.org/10.1016/j.chemosphere.2020.126441>.

Mukwevho, N., Gusain, R., Kankeu, E. F., Kumar, N., Waanders, F., Ray, S. S., 2020. Removal of naphthalene from simulated wastewater through adsorption-photodegradation by ZnO/Ag/GO nanocomposite. *Journal of Industrial and Engineering Chemistry*. 81, 393-404. <https://doi.org/10.1016/j.jiec.2019.09.030>.

Muscat, J. P., Newns, D. M., 1978. Chemisorption on metals. *Progress in Surface Science*. 9, 1-43. [https://doi.org/10.1016/0079-6816\(78\)90005-9](https://doi.org/10.1016/0079-6816(78)90005-9).

Nasuhoglu, D.; Rodayan, A.; Berk, D.; Yargeau, V., 2012. Removal of the antibiotic levofloxacin (LEVO) in water by ozonation and TiO<sub>2</sub> photocatalysis. *Chemical Engineering Journal*. 189-190, 41-48. <https://doi.org/10.1016/j.cej.2012.02.016>.

Nasrollahzadeh, M., Sajjadi, M., Irvani, S., Varma, R. S., 2020. Green-synthesized nanocatalysts and nanomaterials for water treatment: Current challenges and future perspectives. *Journal of Hazardous Materials*. 401, 123401. <https://doi.org/10.1016/j.jhazmat.2020.123401>.

Nikitha, T., Satyaprakash, M., Vani, S., Sadhana, B., Padal, S. B., 2017. A Review on Polycyclic Aromatic Hydrocarbons: Their Transport, Fate and Biodegradation in the Environment. *Int. J. Curr. Microbiol. App. Sci*. 6, 1627-1639. <https://doi.org/10.20546/ijcmas.2017.604.199>.

Novoselov, K. S., Geim, A. K., Morozov, S. V., Jiang, D., Zhang, Y., Dubonos, S. V., Grigorieva, I. V., Firsov, A. A., 2004. Electric Field Effect in Atomically Thin Carbon Films. *Science*. 306, 666-669. <https://doi.org/10.1126/science.1102896>.

Pei, S., Cheng, H. M., 2012. The reduction of graphene oxide. *Carbon*. 50, 3210-3228. <https://doi.org/10.1016/j.carbon.2011.11.010>.

Pei, Z., Li, L., Sun, L., Zhang, S., Shan, X., Yang, S., Wen, B., 2013. Adsorption characteristics of 1,2,4-trichlorobenzene, 2,4,6-trichlorophenol, 2-naphthol and naphthalene on graphene and graphene oxide. *Carbon*. 51, 156-163. <http://dx.doi.org/10.1016/j.carbon.2012.08.024>.

Perreault, F.; Faria, A. F.; Elimelech, M., 2015. Environmental applications of graphene-based nanomaterials. *Chem. Soc. Rev*. 44, 5861-5896. <https://doi.org/10.1039/c5cs00021a>.

Plazinski, W., Rudzinski, W., Plazinska, A., 2009. Theoretical models of sorption kinetics including a surface reaction mechanism: A review. *Advances in Colloid and Interface Science*. 152, 2–13. <https://doi.org/10.1016/j.cis.2009.07.009>.

Pokropivny, V.V., Skorokhod, V.V., 2007. Classification of nanostructures by dimensionality and concept of surface forms engineering in nanomaterial Science. *Materials Science and Engineering*. 27, 990-993. <https://doi.org/10.1016/j.msec.2006.09.023>.

Qi, Y.; Wang, C.; Lv, C.; Lun, Z.; Zheng, C., 2017. Removal Capacities of Polycyclic Aromatic Hydrocarbons (PHAs) by a Newly Isolated Strain from Oilfield Produced Water. *International Journal of Environmental Research and Public Health*. 14, 215. <https://doi.org/10.3390/ijerph14020215>.

Qiao, M., Fu, L., Cao, W., Bai, Y., Huang, Q., Zhao, X., 2019. Occurrence and removal of polycyclic aromatic hydrocarbons and their derivatives in an ecological wastewater treatment plant in South China and effluent impact to the receiving river. *Environmental Science and Pollution Research*. 26, 5638-5644. <https://doi.org/10.1007/s11356-018-3839-4>.

Ramezanzadeh, M., Bahlakeh, G., Ramezanzadeh, B., 2020. Green synthesis of reduced graphene oxide nanosheets decorated with zinc-centered metal-organic film for epoxy-ester composite coating reinforcement: DFT-D modeling and experimental explorations. *Journal of the Taiwan Institute of Chemical Engineers*. 114, 311-330. <https://doi.org/10.1016/j.jtice.2020.09.003>.

Rasheed, A., Farooq, F., Rafique, U., Nasreen, S., Ashraf, M. A., 2015. Analysis of sorption efficiency of activated carbon for removal of anthracene and pyrene for wastewater treatment. *Desalination and Water Treatment*. 57, 145-150. <https://doi.org/10.1080/19443994.2015.1015304>.

Rani, M., Shanker, U., 2018. Remediation of Polycyclic Aromatic Hydrocarbons Using Nanomaterials. In: Crini, G., Lichtfouse, E. (Eds.), *Green Adsorbents for Pollutant Removal*. Springer, Cham, pp. 343-387.

Rattan, S., Kumar, S., Goswamy, J. K., 2020. Graphene oxide reduction using green chemistry. *Materials today: Proceedings*. 26, 3327–3331. <https://doi.org/10.1016/j.matpr.2019.09.168>.

Reghunadhan, A., Kalarikkal, N., Thomas, S., 2018. Mechanical Property Analysis of Nanomaterials, in: Bhagyaraj, S. M., Oluwafemi, O. S., Kalarikkal, N., Thomas, S. (Eds), *Characterization of Nanomaterials*. Elsevier Ltd., pp. 191-212.

Ruiz, D. A. P., Ávila, G. D., Suesca, C. A., Delgado, A. D. G., Herrera, A., 2020. Ionic Cross-Linking Fabrication of Chitosan-Based Beads Modified with FeO and TiO<sub>2</sub> Nanoparticles: Adsorption Mechanism toward Naphthalene Removal in Seawater from Cartagena Bay Area. *ACS Omega*. 5, 26463–26475. <https://dx.doi.org/10.1021/acsomega.0c02984>.

Ruthven, D. M., 1984. *Principles of adsorption and adsorption processes*. New York, NY: John Wiley & Sons.

Saikia, I., Hazarika, M., Hussian, N., Das, M. R., Tamuly, C., 2017. Biogenic synthesis of Fe<sub>2</sub>O<sub>3</sub>@SiO<sub>2</sub> nanoparticles for ipso-hydroxylation of boronic acid in water. *Tetrahedron Letters*. 58, 4255-4259. <https://doi.org/10.1016/j.tetlet.2017.09.075>.

Saleh, T. A., Parthasarathy, P., Irfan, M., 2019. Advanced functional polymer nanocomposites and their use in water ultra-purification. *Trends in Environmental Analytical Chemistry*. 24, e00067. <https://doi.org/10.1016/j.teac.2019.e00067>.

Schweich, D., Sardin, M., 1981. Adsorption, partition, ion exchange and chemical reaction in batch reactors or in columns - A review. *Journal of Hydrology*. 50, 1-33. [https://doi.org/10.1016/0022-1694\(81\)90059-7](https://doi.org/10.1016/0022-1694(81)90059-7).

Scurtu, C. T., 2009. Treatment of produced water: targeting dissolved compounds to meet a zero harmful discharge in oil and gas production. Thesis (Degree of Philosophiae Doctor) - Norwegian University of Science and Technology.

Shabeer, T. P. A., Saha, A., Gajbhiye, V. T., Gupta, S., Manjaiah, K. M., Varghese, E., 2014. Removal of Poly Aromatic Hydrocarbons (PAHs) from Water: Effect of Nano and Modified Nano-clays as a Flocculation Aid and Adsorbent in Coagulation-flocculation Process. *Polycyclic Aromatic Compounds*. 34, 452-467. <http://dx.doi.org/10.1080/10406638.2014.895949>.

Shahsavari, E., Schwarz, A., Medina, A. A., Ball, A. S., 2019. Biological Degradation of Polycyclic Aromatic Compounds (PAHs) in Soil: a Current Perspective. *Current Pollution Reports*. 5, 84-92. <https://doi.org/10.1007/s40726-019-00113-8>.

Shanker, U., Jassal, V., Rani, M., 2017. Green synthesis of iron hexacyanoferrate nanoparticles: Potential candidate for the degradation of toxic PAHs. *Journal of Environmental Chemical Engineering*. 5, 4108-4120. <https://doi.org/10.1016/j.jece.2017.07.042>.

Sharma, A., Siddiqi, Z. M., Pathania, D., 2017. Adsorption of polyaromatic pollutants from water system using carbon/ZnFe<sub>2</sub>O<sub>4</sub> nanocomposite: Equilibrium, kinetic and thermodynamic mechanism. *Journal of Molecular Liquids*. 240, 361-371. <https://doi.org/10.1016/j.molliq.2017.05.083>.

Smol, M., Makuła, M. W. 2012. Effectiveness in the removal of polycyclic aromatic hydrocarbons from industrial wastewater by ultrafiltration technique. *Archives of Environmental Protection*. 38, 49-58. DOI: 10.2478/v10265-012-0040-6.

Smol, M., Makuła, M. W., Mielczarek, K., Bohdziewicz, J., Włóka, D., 2015. The Use of Reverse Osmosis in the Removal of PAHs from Municipal Landfill Leachate. *Polycyclic Aromatic Compounds*. 36, 20-39. <http://dx.doi.org/10.1080/10406638.2014.957403>.

Smol, M., Makuła, M. W., 2017. The Effectiveness in the Removal of PAHs from Aqueous Solutions in Physical and Chemical Processes: A Review. *Polycyclic Aromatic Compounds*. 37, 292-313. <https://doi.org/10.1080/10406638.2015.1105828>.

Song, T., Tian, W., Qiao, K., Zhao, J., Chu, M., Du, Z., Wang, L., Xie, W., 2021. Adsorption Behaviors of Polycyclic Aromatic Hydrocarbons and Oxygen Derivatives in Wastewater on N-Doped Reduced Graphene Oxide. *Separation and Purification Technology*. 254, 117565. <https://doi.org/10.1016/j.seppur.2020.117565>.

Stankovich, S., Dikin, D. A., Dommett, G. H. B., Kohlhaas, K. M., Zimney, E. J., Stach, E. A., Piner, R. D., Nguyen, S. T., Ruoff, R. S., 2006. Graphene-based composite materials. *Nature*. 442, 282 – 286. DOI:10.1038/nature04969.

Subramaniam, V., Subashchandrabose, S. R., Thavamani, P., Megharaj, M., Chen, Z., Naidu, R., 2015. *Chlorococcum* sp. MM11—a novel phyco-nanofactory for the synthesis of iron nanoparticles. *J. Appl. Phycol.* 27, 1861–1869. DOI 10.1007/s10811-014-0492-2.

Sun, S., Wang, Y., Zang, T., Weib, J., Wua, H., Weib, C., Qiu, G., Lib, F., 2019. A biosurfactant-producing *Pseudomonas aeruginos* S5 isolated from coking wastewater and its application for bioremediation of polycyclic aromatic hydrocarbons. *Bioresource Technology*. 281, 421-428. <https://doi.org/10.1016/j.biortech.2019.02.087>.

Sun, Y., Yang, S., Zhao, G., Wang, Q., Wang, X., 2013. Adsorption of polycyclic aromatic hydrocarbons on graphene oxides and reduced graphene oxides. *Chem. Asian J.* 8, 2755-61. DOI: 10.1002/asia.201300496.

Tewatia, K., Sharma, A., Sharma, M., Kumar, A., 2020. Synthesis of graphene oxide and its reduction by green reducing agente. *Materials Today: Proceedings*. 44, 3933-3938. <https://doi.org/10.1016/j.matpr.2020.09.294>

Thomas, H. C., 1944. Heterogeneous Ion Exchange in a Flowing System. *J. Am. Chem. Soc.* 66, 1664–1666. <https://doi.org/10.1021/ja01238a017>.

Tran, L. H., Drogui, P., Mercier, G., Blais, J. F., 2010. Comparison between Fenton oxidation process and electrochemical oxidation for PAH removal from an amphoteric surfactant solution. *J. Appl. Electrochem.* 40, 1493–1510. DOI 10.1007/s10800-010-0128-4.

Unuabonah, E. I., Omorogie, M. O., Oladoja, N. A., 2019. Modeling in Adsorption: Fundamentals and Applications, in: Kyzas, G. Z., Mitropoulos, A. C. (Eds), *Composite Nanoadsorbents: Micro and Nano Technologies*. Elsevier Inc., pp. 85-118.

Valderrama, C., Gamisans, X., Heras, X., Farran, A., Cortina, J. L., 2008. Sorption kinetics of polycyclic aromatic hydrocarbons removal using granular activated carbon: Intraparticle diffusion coefficients. *Journal of Hazardous Materials*. 157, 386–396. <https://doi.org/10.1016/j.jhazmat.2007.12.119>.

Vatandost, E., Saraei, A. G. H., Chekin, F., Raeisi, S. N., SHAHIDI, S. A., 2020. Green tea extract assisted green synthesis of reduced graphene oxide: Application for highly sensitive electrochemical detection of sunset yellow in food products. *Food Chemistry: X*. 6, 100085. <https://doi.org/10.1016/j.fochx.2020.100085>.

Vert, M.; Doi, Y.; Hellwich, K. H.; Hess, M.; Hodge, P.; Kubisa, P.; Rinaudo, M.; Schué, F., 2012. Terminology for biorelated polymers and applications (IUPAC Recommendations 2012). *Pure and Applied Chemistry*. 84, 377-410. <http://dx.doi.org/10.1351/PAC-REC-10-12-04>.

Wołowiec, M., Muir, B., Zięba, K., Bajda, T., Kowalik, M., Franus, W., 2017. Experimental Study on the Removal of VOCs and PAHs by Zeolites and Surfactant-Modified Zeolites. *Energy Fuels*. 31, 8803–8812. <https://doi.org/10.1021/acs.energyfuels.7b01124>.

Wang, J., Chen, Z., Chen, B., 2014. Adsorption of Polycyclic Aromatic Hydrocarbons by Graphene and Graphene Oxide Nanosheets. *Environmental Science and Technology*. 48, 4817-4825. <https://doi.org/10.1021/es405227u>.

Wu, Z., Zhu, L., 2012. Removal of polycyclic aromatic hydrocarbons and phenols from coking wastewater by simultaneously synthesized organobentonite in a one-step process. *Journal of Environmental Sciences*. 24, 248-253. [https://doi.org/10.1016/S1001-0742\(11\)60780-8](https://doi.org/10.1016/S1001-0742(11)60780-8).

Xiao, X., Chen, B., Zhu, L., Schnoor, J. L., 2017. Sugar Cane-Converted Graphene-like Material for the Superhigh Adsorption of Organic Pollutants from Water via Coassembly Mechanisms. *Environmental Science & Technology*. 51, 12644–12652. <https://doi.org/10.1021/acs.est.7b03639>.

Yang, X., Li, J., Wen, T., Ren, X., Huang, Y., Wang, X., 2013. Adsorption of naphthalene and its derivatives on magnetic graphene composites and the mechanism investigation. *Colloids and Surfaces A: Physicochemical and Engineering Aspects*. 422, 118–125. <http://dx.doi.org/10.1016/j.colsurfa.2012.11.063>.

Yang, X., Cai, H., Bao, M., Yu, J., Lu, J., Li, Y., 2018. Insight into the highly efficient degradation of PAHs in water over graphene oxide/Ag<sub>3</sub>PO<sub>4</sub> composites under visible light irradiation. *Chemical Engineering Journal*. 334, 355-376. <https://doi.org/10.1016/j.cej.2017.09.104>.

Yoon, Y. H., Nelson, J. H., 1984. Application of Gas Adsorption Kinetics I. A Theoretical Model for Respirator Cartridge Service Life. *American Industrial Hygiene Association Journal*. 45, 509–516. <https://doi.org/10.1080/15298668491400197>.

Younis, S. A., El-Gendy, N. S., El-Azab, W. I., Moustafa, Y. M., 2014. Kinetic, isotherm, and thermodynamic studies of polycyclic aromatic hydrocarbons biosorption from petroleum refinery wastewater using spent waste biomass. *Desalination and Water Treatment*. 56, 3013-3023. <https://doi.org/10.1080/19443994.2014.964331>.

Yu, L., Han, M., He, F., 2017. A review of treating oily wastewater. *Arabian Journal of Chemistry*. 10, 1913-1922. <https://doi.org/10.1016/j.arabjc.2013.07.020>.

Yuan, P., Li, X., Wang, W., Liu, H., Yan, Y., Yang, H., Yue, Y., Bao, X., 2018. Tailored design of differently modified mesoporous materials to deeply understand the adsorption mechanism for PAHs. *Langmuir*. 34, 15708–15718. <https://doi.org/10.1021/acs.langmuir.8b03299>.

Zarei, M., Seyedi, N., Maghsoudi, S., Nejad, M. S., Sheibani, H., 2021. Green synthesis of Ag nanoparticles on the modified graphene oxide using Capparis spinosa fruit extract for catalytic reduction of organic dyes. *Inorganic Chemistry Communications*. 123, 108327. <https://doi.org/10.1016/j.inoche.2020.108327>.

Zhang, B., 2018. Introduction, in: Zhang, B. (Eds), *Physical Fundamentals of Nanomaterials*. Elsevier Inc., China, pp. 1-18.

Zhang, C., Wu, L., Cai, D., Zhang, C., Wang, N., Zhang, J., Wu, Z., 2013. Adsorption of Polycyclic Aromatic Hydrocarbons (Fluoranthene and Anthracenemethanol) by Functional

Graphene Oxide and Removal by pH and Temperature-Sensitive Coagulation. *Applied Materials and Interfaces*. 5, 4783-4790. <https://doi.org/10.1021/am4002666>.

Zhang, J., Li, R., Ding, G., Wang, Y., Wang, C., 2019. Sorptive removal of phenanthrene from water by magnetic carbon nanomaterials. *Journal of Molecular Liquids*. 293, 111540. <https://doi.org/10.1016/j.molliq.2019.111540>.

Zhang, Y., Wu, B., Xu, H., Liu, H., Wang, M., He, Y., Pan, B., 2016. Nanomaterials-enabled water and wastewater treatment. *NanoImpact*. 3–4, 22–39. <http://dx.doi.org/10.1016/j.impact.2016.09.004>.

Zhao, C., Zhou, J., Yan, Y., Yang, L., Xing, G., Li, H., Wu, P., Wang, M., Zheng, H., 2021. Application of coagulation/flocculation in oily wastewater treatment: A review. *Science of The Total Environment*. 765, 142795. <https://doi.org/10.1016/j.scitotenv.2020.142795>.

### Capítulo 3. Síntese dos materiais adsorventes e teste de afinidade

#### Comparative efficiency of polycyclic aromatic hydrocarbon removal by novel graphene oxide composites prepared from conventional and green synthesis<sup>4</sup>

Ruth Nóbrega Queiroz<sup>a</sup>, Tauany de Figueiredo Neves,<sup>b</sup> Meuris Gurgel Carlos da Silva<sup>a</sup>, Valmor Roberto Mastelaro<sup>c</sup>, Melissa Gurgel Adeodato Vieira<sup>a</sup> and Patrícia Prediger<sup>b\*</sup>

<sup>a</sup>Process and Product Development Department, School of Chemical Engineering, University of Campinas – UNICAMP, Albert Einstein Avenue, 500, 13083-852 Campinas, São Paulo, Brazil.

<sup>b</sup>School of Technology, University of Campinas – UNICAMP, 13484-332 Limeira, São Paulo, Brazil.

<sup>c</sup>São Carlos Institute of Physics, University of São Paulo, Av. Trabalhador São Carlense, 400, São Carlos, SP, 13566-590, Brazil.

\*prediger@unicamp.br

#### Abstract

New materials have been developed based on the pillars of green chemistry; however, few studies compare the potential of these materials with that of conventional materials. In this study, two composites based on graphene oxide and magnetic chitosan were synthesized, one by the green route (G-mCS/GO) and the other by the conventional route (C-mCS/GO), using proanthocyanidin (PAS) and glutaraldehyde as crosslinking agents, respectively. Then, they were applied as adsorbents in the removal of polycyclic aromatic hydrocarbons (PAHs) from synthetic wastewater to compare their performance. Through XRD analysis, the crystallographic properties were obtained, FT-IR analyses indicated the presence of functional groups associated with graphene oxide, chitosan and Fe<sub>3</sub>O<sub>4</sub> particles, and the magnetization curves indicated greater saturation magnetization for G-mCS/GO. Adsorption assays were performed at 298 K for 30 min at pH 6.5, an adsorbent dosage of 0.1 mg.mL<sup>-1</sup> and an initial PAH concentration of 0.01 mmol. L<sup>-1</sup> showed a greater adsorptive capacity of G-mCS/GO for

---

<sup>4</sup> Manuscript published in *Journal of Cleaner Production* 361 (2022) 132244. DOI: 10.1016/j.jclepro.2022.132244. Reprinted with permission from *Journal of Cleaner Production*. Copyright 2022 Elsevier (Anexo I).

naphthalene ( $0.093 \text{ mmol.g}^{-1}$ ) and anthracene ( $0.089 \text{ mmol.g}^{-1}$ ), with removal efficiencies of 93.55% and 89.25%, respectively. On the other hand, C-mCS/GO showed a better removal efficiency for fluoranthene ( $0.076 \text{ mmol.g}^{-1}$ ), 76.07%. The results obtained through the molecular simulation indicated that naphthalene molecules have greater stability than anthracene and fluoranthene, which contributes to increasing the hydrophobic and  $\pi$ - $\pi$  interactions between the PAH molecules and the adsorbent surface, thus inducing an increase in the adsorptive capacity. The results of this study indicate that G-mCS/GO is a potential and sustainable adsorbent for PAH removal from wastewater.

**Keywords:** Green Synthesis; Graphene oxide; Chitosan; Adsorption; PAHs; Molecular simulation.

### 3.1. Introduction

Polycyclic aromatic hydrocarbons (PAHs) are organic compounds formed mainly through anthropogenic activities, which involve pyrolysis and petrogenic processes (exploration and production of oil and gas). Despite being found in relatively low concentrations, these pollutants are highly toxic and carcinogenic contaminants that can cause damage to human health and the environment when present in industrial effluents, especially those from the petroleum industry. 16 PAHs were listed by the United States Environmental Protection Agency (US EPA) as emerging pollutants, including naphthalene, anthracene and fluoranthene (Queiroz et al., 2022).

Different technologies, such as bioremediation (Song et al., 2021), membrane separation (Li et al., 2019), advanced oxidation processes (AOPs) (Haneef et al., 2020), coagulation-flocculation (Wang et al., 2020) and adsorptive processes (Li et al., 2020), have been studied to efficiently remove PAHs from industrial effluents. Among these technologies, adsorption processes are being increasingly studied due to their high selectivity, low production cost, easy adsorbent recovery and high efficiency (Brião et al., 2018). Graphene-based materials, especially graphene oxide (GO), have been applied as adsorbents for the removal of contaminants due to their characteristics, such as high surface area, chemical stability, presence of oxygenated functional groups, mechanical resistance and low production cost (Song et al., 2021). These characteristics are responsible for the excellent adsorptive properties for the removal of organic compounds from wastewater, which have attracted the attention of researchers to its application in PAH adsorption: fluoranthene (Hsu et al., 2019); naphthalene

and anthracene (Adeola and Forbes, 2022); naphthalene (Maswanganyi et al. 2021); phenanthrene (Huang et al., 2019); and anthracene (Song et al., 2021).

Chitosan is a biodegradable polymer obtained through the deacetylation of chitin, which allows its application in different processes. It can be applied as a flocculant, coagulant and adsorbent for the removal of contaminants such as toxic metals, dyes, pesticides, antibiotics and organic contaminants (Pal et al., 2020). Therefore, the combination of GO with chitosan can contribute to modifying the characteristics of GO, considerably improving its performance in removing organic pollutants and thus increasing the efficiency of the adsorption process (Neves et al., 2020).

The application of natural agents in the synthesis of adsorbent materials has been highlighted in recent years as an alternative methodology to minimize the use of toxic chemical reagents (Queiroz et al., 2022). Plant extracts, microorganisms and agricultural waste have a variety of active compounds and metabolites that can act as stabilizing, crosslinking or capping agents in the synthesis processes, thus enabling the development of new composites with high efficiency, eco-friendliness and low cost (Shi et al., 2020; Zhang et al., 2021).

Therefore, in this study, the synthesis of two composites based on graphene oxide (GO) and magnetic chitosan (mCS) was performed, one by the green route using the extract of water hyacinth (*Eichhornia crassipes*) and proanthocyanidin (PAS) as a stabilizing agent and crosslinking, respectively, and another by the conventional route using glutaraldehyde as a crosslinking agent. The adsorbents were applied for the removal of PAHs from synthetic wastewater to compare the adsorptive performance of both materials. Naphthalene, anthracene and fluoranthene were selected as PAHs in the study, and their physicochemical and structural properties were evaluated through a molecular simulation. The adsorptive affinity assay results were evaluated along with the molecular simulation results to determine the possible mechanisms that govern the adsorptive processes.

## **3.2. Materials and methods**

### **3.2.1. Materials and reagents**

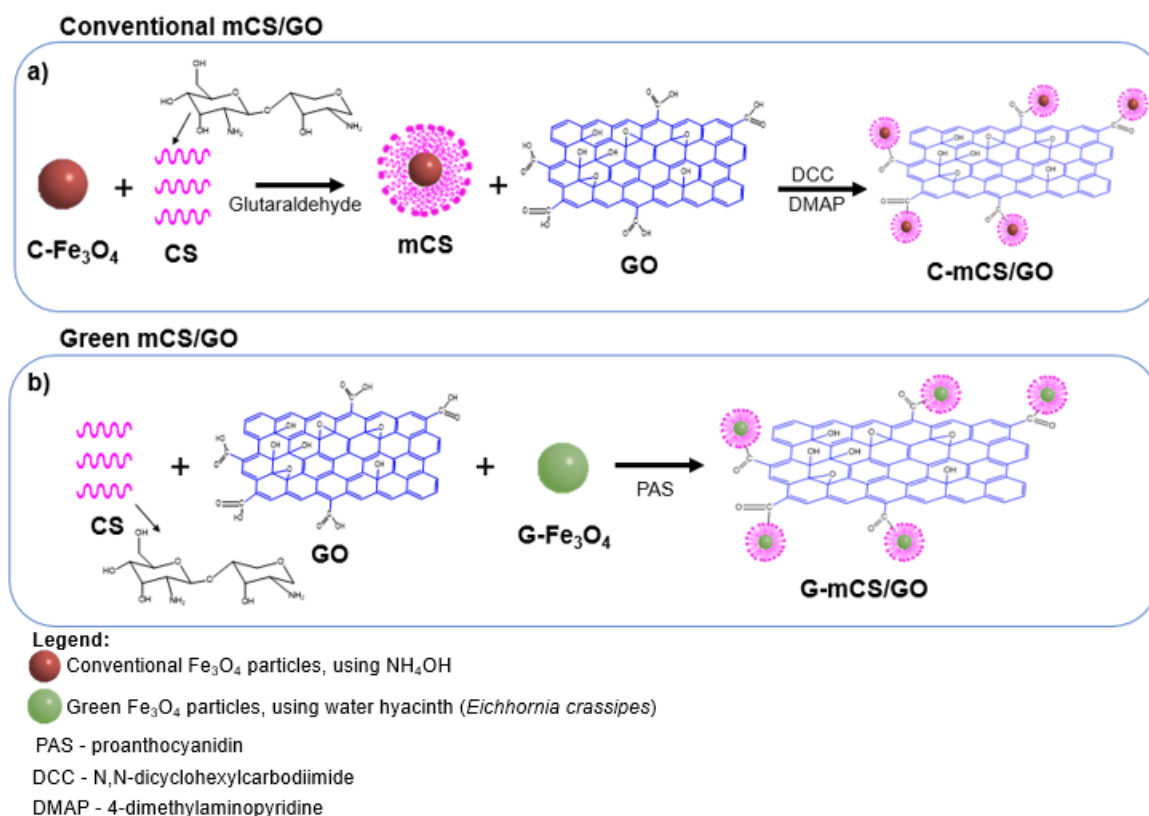
Mineral graphite micrograf 99507 UJ - (Nacional Grafite Ltda., Limeira, SP, Brasil); Concentrated sulfuric acid ( $H_2SO_4$ ) - (ACS); Potassium persulfate ( $K_2S_2O_8$ ) - (ACS); Phosphorus pentoxide ( $P_2O_5$ ) (high purity, 99%) - (Sigma Aldrich); Sodium nitrate ( $NaNO_3$ ) - (ACS); Potassium permanganate ( $KMnO_4$ ) (high purity, 99%) - (CRQ Eireli Chemical Products); Hydrogen peroxide ( $H_2O_2$ ) (Grade II, 30% w/w) - (Sigma Aldrich); Hydrochloric

acid (HCl) (37%) - (ACS); Iron (II) chloride ( $\text{FeCl}_2 \cdot 4\text{H}_2\text{O}$ ) - (Dynamics); Iron (III) chloride ( $\text{FeCl}_3 \cdot 6\text{H}_2\text{O}$ ) - (Sigma Aldrich); Ammonium hydroxide ( $\text{NH}_4\text{OH}$ ) (28%) - (CRQ Eireli Chemical Products); Chitosan (CS) - (low molecular weight, 75-85% deacetylated, Sigma Aldrich, Code: 448869); Liquid Vaseline (mineral oil) - (Dynamics); Oleic acid - (Synth); Acetic acid ( $\text{CH}_3\text{COOH}$ ) (60%) - (Synth); Glutaraldehyde (Grade II, 25% w/w) - (Sigma Aldrich); Pure petroleum ether (30 -60 °C) - (Sigma Aldrich); Sodium hydroxide (NaOH) (high purity, 99.99%) - (Synth); Dry N,N-dimethylformamide (DMF) (anhydrous, 99.8%) - (Sigma Aldrich); N,N-dicyclohexylcarbodiimide (DCC) (high purity, 99%) - (Sigma Aldrich); 4-dimethylaminopyridine (DMAP) (high purity, 99%) - (Sigma Aldrich); Methanol ( $\text{CH}_3\text{OH}$ ) (P.A.) - (ACS); ethanol ( $\text{C}_2\text{H}_5\text{OH}$ ) (technical grade, 99%) - (Sigma Aldrich); acetone ( $\text{C}_3\text{H}_6\text{O}$ ) (P.A.) - (ACS); water hyacinth extract (*Eichhornia crassipes*) - (UNICAMP, Limeira, SP, Brazil); proanthocyanidin (PAS) - (Galena); naphthalene (NAP) (purity, 99%) - (Sigma Aldrich); anthracene (ANT) (purity, 99%) - (Sigma Aldrich); fluoranthene (FLT) (purity, 99%) - (Sigma Aldrich); methanol ( $\text{CH}_3\text{OH}$ ) (HPLC Grade) – (ACS); acetonitrile ( $\text{C}_2\text{H}_3\text{N}$ ) (HPLC Grade) – (ACS); ultrapure water (OS20LXE, Gehaka).

### 3.2.2. Preparation of conventional and green mCS/GO

A schematic diagram of the steps involved in the conventional and green mCS/GO synthesis processes is shown in Fig. 3.1. Fig. 3.1 (a) presents the steps of the synthesis of C-mCS/GO, in which, initially, magnetic chitosan (mCS) is prepared using glutaraldehyde as a crosslinking agent, followed by the preparation of the composite C-mCS/GO using DCC and DMAP. Fig. 3.1 (b) shows the synthesis of G-mCS/GO, in which CS, GO and G- $\text{Fe}_3\text{O}_4$  are crosslinked using proanthocyanidin. The synthesis methodology of C-mCS/GO and G-mCS/GO is described in detail in sections 2.2.1. to 2.2.6.

**Figure 3.1.** Schematic diagram of the synthesis of: a) C-mCS/GO and b) G-mCS/GO.



### 3.2.3. Preparation of graphene oxide (GO)

The synthesis of GO was performed by the modified Hummers method (1958) using preoxidized graphite according to the methodology reported by Prediger et al. (2018). Initially, the preparation of preoxidized graphite was carried out by adding 20 g of mineral graphite, 120 mL of  $\text{H}_2\text{SO}_4$ , 10 g of  $\text{K}_2\text{SO}_4$  and 10 g of  $\text{P}_2\text{O}_5$  in a beaker in an ice bath with magnetic stirring. When the system reached room temperature, it was heated at 80 °C for 6 h. When it reached room temperature, the solution was added dropwise to a beaker containing 1 L of ultrapure water, and the system was placed in an ice bath with magnetic stirring. The obtained mixture was washed with ultrapure water to reach pH 6.

For the synthesis of GO, by the modified Hummers method (1958), the preoxidized graphite was added to an Erlenmeyer flask containing 500 mL of concentrated  $\text{H}_2\text{SO}_4$  under magnetic stirring and an ice bath. Then, 10 g of  $\text{NaNO}_3$  was slowly added to the system, and after 2 h, 60 g of  $\text{KMnO}_4$  was added to the medium. The system was kept reacting at 0 °C for 1 h and then kept reacting at 25 °C for 7 days. After that, the system was cooled in an ice bath, and then 2 L of ultrapure water and 100 mL of aqueous  $\text{H}_2\text{O}_2$  (3% v/v) were added. The system was heated at 100 °C for 30 min and then cooled and placed in a conical tube, which was

subjected to centrifugation at 8000 rpm for 5 min. In a centrifuge system, the precipitate obtained was washed with 10 L of a 3% H<sub>2</sub>SO<sub>4</sub> and 0.5% H<sub>2</sub>O<sub>2</sub> solution. Then, the material was washed with a 10% HCl solution and, finally, washed with ultrapure water to reach pH 5. After the washing steps, the material obtained was stored in dialysis bags, which were immersed in ultrapure water to remove the salts present in the material. The immersion water was changed and monitored over time until the conductivity value was equal to the characteristic conductivity of ultrapure water. The material obtained was diluted in ultrapure water and submitted to an ultrasound bath for 1 h to form GO.

#### 3.2.4. Conventional synthesis of Fe<sub>3</sub>O<sub>4</sub> magnetic particles

The conventional synthesis of magnetic iron particles (C-Fe<sub>3</sub>O<sub>4</sub>) was performed based on the methodology reported by Silva et al. (2013). Initially, 600 mL of water, 60 mL of iron(II) chloride solution (0.6 M), 60 mL of iron(III) chloride solution (1.1 M) and 3 mL of oleic acid were added to a volumetric flask under magnetic stirring and ambient atmosphere. Then, NH<sub>4</sub>OH was added dropwise to the system until it reached pH 11. When the mixture reached pH 11, it was heated at 85 °C for 30 min, washed with ultrapure water and filtered in a Büchner funnel until reaching pH 7. The material was dried in an oven at 100 °C for 48 h.

#### 3.2.5. Conventional synthesis of magnetic chitosan (mCS)

The conventional synthesis of magnetic chitosan (mCS) was performed based on the methodology reported by Wang et al. (2016). Initially, 3 g of chitosan (CS) was dissolved in a 2% CH<sub>3</sub>COOH solution in a 1 L volumetric flask. The system was kept under strong agitation for 2 h, followed by an ultrasound bath for 10 min. After that, 6.5 g of Fe<sub>3</sub>O<sub>4</sub> magnetic particles were added under mechanical agitation. The system obtained was subjected to an ultrasonic bath for 10 min and then subjected to mechanical agitation for 1 h. After that, 200 mL of mineral oil was slowly added to the mixture, and the system was kept under mechanical agitation for 30 min. Then, 30 mL of glutaraldehyde was added to the system, which was subjected to mechanical agitation for 1 h. The mixture obtained was placed in a beaker containing a solution of NaOH (1 M) and stirred for 1 h. The material obtained was filtered with petroleum ether, subjected to a 5 min ultrasound bath, washed with ethanol and subjected to a 5 min ultrasound bath. After the ultrasound bath, the material was washed with ultrapure water to reach pH 7. Finally, it was dried at 100 °C for 48 h in an oven.

### 3.2.6. Conventional synthesis of mCS/GO

The conventional synthesis of mCS/GO (C-mCS/GO) was performed according to the adapted methodology reported by Maleki and Paydar (2015). In a volumetric flask, flamed, 2.3 g of GO and 300 mL of DMF were added under a nitrogen atmosphere and magnetic stirring. The mixture was subjected to magnetic stirring for 2 h, followed by an ultrasound bath for 1 h. After that, 20.7 g of DCC and 13.8 g of DMAP were placed into the mixture under a nitrogen atmosphere at 25 °C. The system was subjected to magnetic stirring for 48 h. The material obtained was submitted to a filtering step in a Büchner funnel with an aqueous solution of CH<sub>3</sub>COOH (2%) to remove the extra CS. Then, the filtrate was subjected to an ultrasonic bath for 10 min. Subsequently, the material obtained was subjected to a sequential washing step with ultrapure water, methanol, acetone and ultrapure water. Finally, the product obtained was dispersed in water, placed in an amber glass bottle, and kept in the refrigerator.

### 3.2.7. Green synthesis of Fe<sub>3</sub>O<sub>4</sub> magnetic particles

The green synthesis of magnetic iron particles (G-Fe<sub>3</sub>O<sub>4</sub>) was performed based on the adapted methodology reported by Zhang et al. (2021). Initially, the water hyacinth (*Eichhornia crassipes*) leaves were washed, dried at room temperature and ground to prepare the leaf extract. Then, a solution of FeCl<sub>2</sub>.4H<sub>2</sub>O and FeCl<sub>3</sub>.6H<sub>2</sub>O (2 M) with a molar ratio of 2 Fe<sup>3+</sup>:1 Fe<sup>2+</sup> was prepared. Subsequently, 100 mL of water hyacinth extract and 3 mL of oleic acid were added to the solution. The mixture was subjected to magnetic stirring for 2 h, and then an aqueous solution of NaOH (1 M) was added dropwise until it reached pH 7. The mixture was stirred for 1 h at 55 °C, and then an aqueous solution of NaOH (2 M) was added dropwise until it reached pH 11. It was subjected to strong magnetic stirring for 30 min. The material obtained was washed with ethanol and then with ultrapure water to reach pH 7. The material obtained was dried for 48 h in an oven.

### 3.2.8. Green synthesis of mCS/GO

The green synthesis of mCS/GO (G-mCS/GO) followed the adapted methodology reported by Santos et al. (2020). In a volumetric flask, 3 g of CS was dissolved in 625 mL of ultrapure water under ambient atmosphere and strong magnetic stirring for 1 h. Subsequently, the system was placed in an ultrasound bath for 1 h and again kept under strong magnetic

agitation for 1 h. Then, 2.5 g of dried GO was added to the homogeneous mixture. It was kept under magnetic stirring for 1 h, followed by an ultrasound bath for 1 h and again subjected to strong magnetic stirring for 8 h. After that, 6 g of green Fe<sub>3</sub>O<sub>4</sub> magnetic particles were added to the system under strong magnetic stirring for 6 h. After that, the content of the volumetric flask was transferred to a beaker, and the system was subjected to mechanical agitation (150 rpm). Then, 6 g of PAS was added to the system under ambient atmosphere and mechanical agitation for 2 h. Subsequently, the material obtained was submitted to a washing step with ultrapure water and then dispersed in water, placed in an amber glass bottle, and kept in the refrigerator.

### 3.2.9. Characterization analyses

Table 3.1 presents the analytical techniques applied for the characterization of the composites C-mCS/GO and G-mCS/GO.

**Table 3.1.** Characterization analysis of C-mCS/GO and G-mCS/GO composites.

Technique	Equipment	Procedure
X-ray diffraction (XRD)	Shimadzu XRD7000, Japan	Vacuum dried at 130 °C for 12 h. Cu K $\alpha$ radiation with $\lambda = 0.154$ nm, operating at 40 kV and 30 mA, at 25 °C.
X-ray photoelectron spectroscopy (XPS)	XPS spectrometer (ScientaOmicron ESCA+) with a high-performance hemispheric analyzer (EAC2000). The analysis of the XPS spectra was realized by using the CASA XPS software.	Al K $\alpha$ ( $h\nu = 1486.6$ eV) radiation as the excitation source, $10^{-9}$ Pa. The XPS high-resolution spectra were recorded at constant pass energy of 20 eV with a 0.05 eV per step.
Fourier transform infrared spectroscopy (FTIR)	Thermo Scientific equipment (Nicolet 6700, Madison/USA).	KBr method, range 4000–400 cm $^{-1}$ , resolution 4 cm $^{-1}$ , and scan 32.
Magnetization curves	Vibrating sample magnetometer (VSM)	Function of a magnetic field (Oe), at room temperature.

Scanning Electron Microscopy (SEM) and Energy Dispersive X-ray Spectroscopy (EDS)	Jeol model J6360 LV	A drop of the suspension containing the composites was placed on a silicon wafer and vacuum dried. N <sub>2</sub> atmosphere and flow of 50 mL.min <sup>-1</sup> , from 25 °C to 1000 °C with heating rate of 10 °C.min <sup>-1</sup> .
Thermogravimetric analysis (TG/DTG)	DTG-60, Shimadzu, Japan	C <sub>0</sub> =0.001 mg.mL <sup>-1</sup> , at 25 °C.
Zeta potential (mV)	Zetasizer Nano ZS ZEN3600 (Malvern)	The pH of the suspensions (4, 6, 8, 10) were adjusted by adding HCl and NaOH solutions.

---

### 3.2.10. Molecular modeling

Molecular modeling was applied to describe the chemical structures and establish quantitative relationships between the physicochemical properties of PAH molecules (naphthalene, anthracene and fluoranthene). Through molecular modeling, it is possible to perform theoretical functional density (DFT) calculations, thus aiming to detail the geometric properties, as well as calculate the quantum chemical molecular descriptors of the PAHs, which include the HOMO - highly occupied molecular orbital energy ( $E_H$ ), LUMO - lowest unoccupied molecular orbital energy ( $E_L$ ) and chemical energy change ( $\Delta_{HL}$ ).

The electronic chemical potential ( $\mu$ ), global chemical hardness ( $\eta$ ) and the general electrophilicity index ( $\omega$ ) values can be calculated from the values of  $E_H$  and  $E_L$ , according to Equations (3.1), (3.2) and (3.3):

$$\mu = \frac{-(E_H + E_L)}{2} \quad (3.1)$$

$$\eta = \frac{(-E_H + E_L)}{2} \quad (3.2)$$

$$\omega = \frac{\mu^2}{2\eta} \quad (3.3)$$

The chemical structures of the PAHs were designed by using ChemDraw® software (version 16), and then the 3D molecular structures were designed by using Avogadro® software (version 1.2.0). The quantum chemical descriptors and the minimum energy geometry of the

PAHs were analyzed by using DFT calculations implemented in the Gaussian® software (version 09). DFT calculations were performed by Beck's theoretical model, 3-parameter, Lee-Yang-Parr correlation (B3LYP) and as base set 6-31G (d) and 6-31G (d,p), which are used to optimize the molecular geometry of organic molecules, such as PAHs, to obtain a stable molecular structure, as well as to minimize the system energy.

From the optimized geometry of the molecules obtained through Avogadro®, calculations were performed in Gaussian® by using the B3LYP model and the 6-31G (d) and 6-31G (d,p) polarization functions, aiming to determine if the obtained geometry is stable. For calculation purposes, the effect of water as a solvent was taken into account for the simulations. The HOMO ( $E_H$ ) and LUMO ( $E_L$ ) molecular orbitals were also obtained through Avogadro® by using the Test file from the Gaussian® directory. The electrostatic potential map of the PAHs was obtained through Avogadro®, applying the van der Waals model as the 'Surface type'.

### 3.2.11. Adsorptive affinity assays

The adsorptive assays were carried out in triplicate to evaluate the affinity of the PAHs (naphthalene, anthracene and fluoranthene) for the adsorbents (conventional and green mCS/GO). Initially, synthetic stock solutions were prepared at 10 mg. L<sup>-1</sup> by dissolving naphthalene in methanol (4% CH<sub>3</sub>OH/96% H<sub>2</sub>O), anthracene in acetonitrile (30% C<sub>2</sub>H<sub>3</sub>N/70% H<sub>2</sub>O) and fluoranthene in acetonitrile (15% C<sub>2</sub>H<sub>3</sub>N/85% H<sub>2</sub>O), which were stored in an amber glass bottle and kept in the refrigerator. The working solutions of naphthalene, anthracene and fluoranthene used in the affinity assays were prepared from dilutions of the PAH stock solutions at 0.01 mmol. L<sup>-1</sup> (1.28, 1.78 and 2.02 mg. L<sup>-1</sup>, respectively).

The adsorption experiments were performed in a batch system in a shaker (Jeio Tech, SI-600R, South Korea) in triplicate with stirring at 200 rpm at 25 °C ± 1 °C for 30 min to reach adsorption equilibrium. To evaluate the affinity of PAHs for the adsorbents over the time of the experiment, a dosage of adsorbent of 0.1 mg.mL<sup>-1</sup> was used. After the adsorption processes, the adsorbents were removed by magnetic separation, and then the materials were centrifuged under stirring at 6000 rpm for 15 min.

The residual concentration of naphthalene in synthetic wastewater was measured using a high-performance liquid chromatography system (HPLC) (Shimadzu), which consists of a CTO-10ASVP heating oven, SPD-10AV UV-Vis detector, LC-10AD gradient pump and CBM-10A connection module. The HPLC system was equipped with a C18 column (5 μ, 150 mm x 4.6 mm) (Phenomenex, Torrance, USA) with a 25 μL manual sample injector, and the

chromatographic data obtained were processed using LC Solution software. The mobile phase consisted of 85% methanol and 15% deionized water at a flow rate of 1 mL.min<sup>-1</sup>, wavelength set at 254 nm and column temperature of 25 °C. Before injecting the samples into the HPLC system, they were filtered with a PTFE syringe filter (0.45 μm) to completely remove the adsorbent particles from the system. The residual concentrations of anthracene and fluoranthene in synthetic wastewater were measured by a UV–vis spectrophotometer (Shimadzu/UV-1900) using the absorption peaks set at 251 nm and 236 nm for anthracene and fluoranthene, respectively. More information regarding the PAH calibration curves is described in the Supplementary Material (see Table S1).

The removal efficiency (%Rem) and adsorption capacity (q(t)), in mmol.g<sup>-1</sup>, were calculated using equations (3.4) and (3.5), respectively:

$$\%Rem = \frac{(C_0 - C_f)}{C_0} \cdot 100 \quad (3.4)$$

$$q(t) = \frac{(C_0 - C_f)}{m} \cdot V \quad (3.5)$$

where  $C_0$  is the initial PAH concentration (mmol. L<sup>-1</sup>),  $C_f$  is the concentration of PAHs after the adsorption process (mmol. L<sup>-1</sup>),  $V$  is the volume of the solution (L) and  $m$  is the adsorbent mass (g).

### 3.3. Results and discussion

#### 3.3.1. Conventional and green mCS/GO characterizations

##### 3.3.1.1. Evaluation of the crystal structure of synthesized materials

The diffractograms of the composites are shown in Fig. 3.2 (a). Conventional and green Fe<sub>3</sub>O<sub>4</sub> (C-Fe<sub>3</sub>O<sub>4</sub> and G- Fe<sub>3</sub>O<sub>4</sub>, respectively) particles showed diffraction peaks at 30.3°, 35.5°, 43.4°, 57.3°, and 62.9°, corresponding to the crystallographic planes (2 2 0), (3 1 1), (4 0 0), (5 1 1) and (4 4 0), respectively. The results confirm the obtainment of Fe<sub>3</sub>O<sub>4</sub> particles in cubic form, as reported in the literature (Neves et al., 2020; Shi et al., 2020). Through the diffraction patterns, it was not possible to observe the presence of the peaks at 21° and 33°, corresponding to the planes (1 1 0) and (1 0 4), respectively, which indicates that the Fe<sub>3</sub>O<sub>4</sub> particles are not present in their composition goethite [ $\alpha$ -Fe<sup>3+</sup>O(OH)] and hematite (Fe<sub>2</sub>O<sub>3</sub>) (Solano et al., 2021). The average crystal sizes were determined by Debye-Scherrer's equation ( $D = K\lambda \cdot (\beta \cos\theta)^{-1}$ ), where  $D$  is the crystal size (nm),  $K$  is the Debye-Scherrer's constant (0.94),  $\lambda$  is the wavelength

(0.15406 nm),  $\beta$  is the maximum width of the highest intensity peaks at half height and  $\theta$  is the diffraction angle. The average crystal sizes of the C-Fe<sub>3</sub>O<sub>4</sub> and G-Fe<sub>3</sub>O<sub>4</sub> particles, taking into account the highest intensity peaks, were 7.2 and 13.2 nm, respectively.

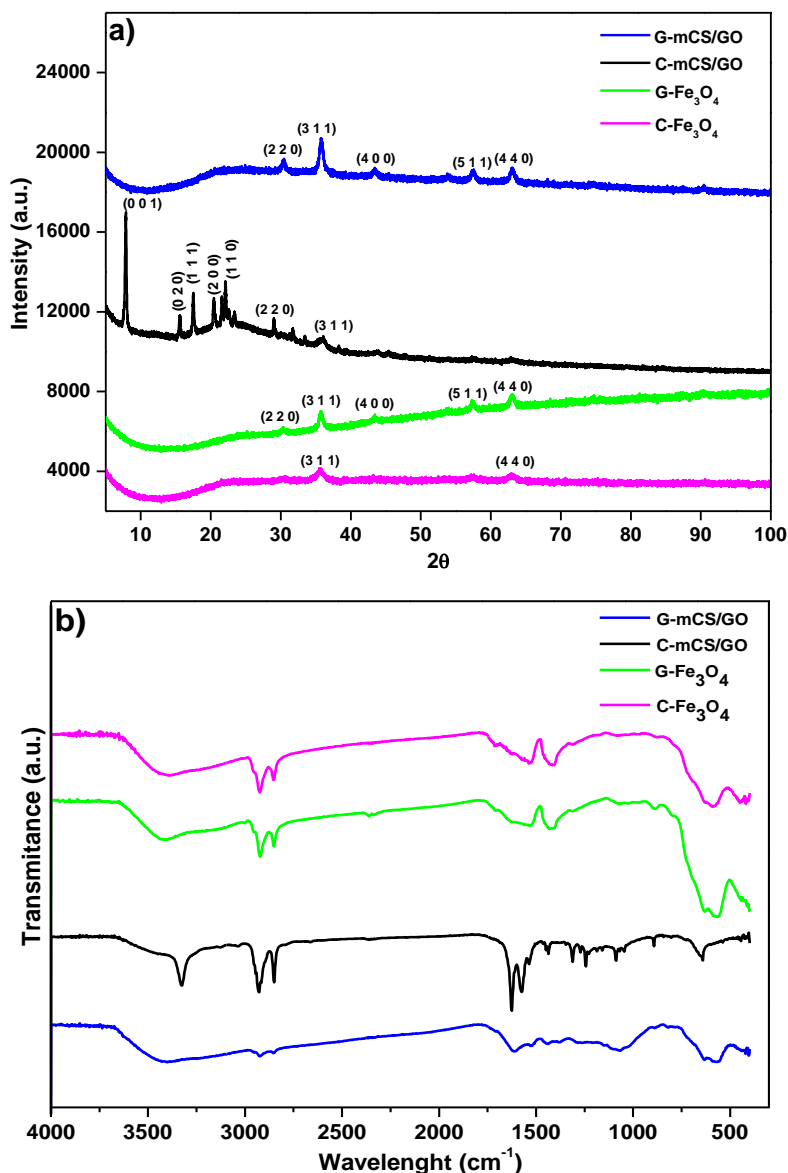
The XRD diffractogram of C-mCS/GO indicated the presence of a greater intensity peak at 7.9°, referring to the crystallographic plane (0 0 1) of GO, with an interplanar distance of 1.28 nm, calculated according to Bragg's equation. In the literature, GO shows a peak at approximately 10°, and this shift may be associated with the incorporation of mCS, thus increasing the repulsion between the GO nanosheets. It is also possible to observe the presence of a peak at 22.3°, referring to the crystallographic plane (1 1 0), which is associated with the presence of mCS (Neves et al., 2020). Furthermore, characteristic peaks of Fe<sub>3</sub>O<sub>4</sub> particles in their dominant cubic form were observed in the XRD pattern of both composites (Prediger et al., 2018; Neves et al., 2020).

### 3.3.1.2. Functional group identification

The FT-IR spectra of the composites are shown in Fig. 3.2 (b). The C-Fe<sub>3</sub>O<sub>4</sub> and G-Fe<sub>3</sub>O<sub>4</sub> spectra showed the presence of two bands at 2920 and 2850 cm<sup>-1</sup>, which are associated with the stretching vibrations of the -CH<sub>2</sub>- groups, attributed to the presence of oleic acid and water hyacinth extract in the synthesis of Fe<sub>3</sub>O<sub>4</sub> particles (Silva et al., 2013). The bands at 1470 and 570 cm<sup>-1</sup> can be associated with the stretching vibration of the Fe-O bond, thus indicating the presence of magnetite (Zhang et al., 2021).

The spectrum of C-mCS/GO showed a peak at 3330 cm<sup>-1</sup>, which corresponds to the stretching vibrations of the N-H and O-H groups (Gul et al., 2016). Furthermore, it is possible to verify that C-mCS/GO and G-mCS/GO showed peaks at 2920, 2850 and 645 cm<sup>-1</sup>, which are attributed to the presence of Fe<sub>3</sub>O<sub>4</sub> magnetic particles (Wang et al., 2015). The peak at 1620 cm<sup>-1</sup> is associated with stretching vibrations of the C=O groups, which can be attributed to the presence of -COOH groups and can also be associated with the presence of residual amide groups attributed to CS (Travlou et al., 2013; Tang et al., 2021). Finally, the peaks at 1070 and 1230 cm<sup>-1</sup> correspond to the stretching vibrations of the C-O and -COOH groups, respectively (Neves et al., 2020).

**Figure 3.2.** a) XRD diffractograms and b) FT-IR spectrum of G-mCS/GO (blue line); C-mCS/GO (black line); G-Fe<sub>3</sub>O<sub>4</sub> (green line) and C-Fe<sub>3</sub>O<sub>4</sub> (pink line).



### 3.3.1.3. Evaluation of chemical composition and functional groups

Through XPS analysis, the chemical composition of the composites, the nature of their functional groups, and the  $sp^3$  and  $sp^2$  components of the carbon atoms were determined (Prediger et al., 2018). Fig. S1 (a) and (b) present the survey spectra of the C-mCS/GO and G-mCS/GO samples, respectively. Both survey spectra show characteristic peaks of GO, such as C (1 s) at 285.7 eV and O (1 s) at 531.3/530.2 eV. The survey also shows peaks related to N(1 s) at 400.2/400.8 eV and Fe (2p) peaks at 711.2/711.3 eV and 723.6/725.4 eV, associated with the incorporation of CS and the presence of Fe<sub>3</sub>O<sub>4</sub>, respectively, in the structures of C-mCS/GO and G-mCS/GO (Li et al., 2017; Neves et al., 2020). The elemental composition (%) of C, O,

N and Fe for both materials calculated from XPS analysis is shown in Table 3.2. The Fe content in G-mCS/GO is higher (3.5%), as well as its oxygen content (26.3%) when compared to C-mCS/GO, which is associated with a better incorporation of Fe<sub>3</sub>O<sub>4</sub> particles, thus indicating a greater magnetic potential of this material when compared to the conventional one.

**Table 3.2.** Elemental mass composition (%) of C-mCS/GO and G-mCS/GO and C-Fe<sub>3</sub>O<sub>4</sub> and G-Fe<sub>3</sub>O<sub>4</sub> particles.

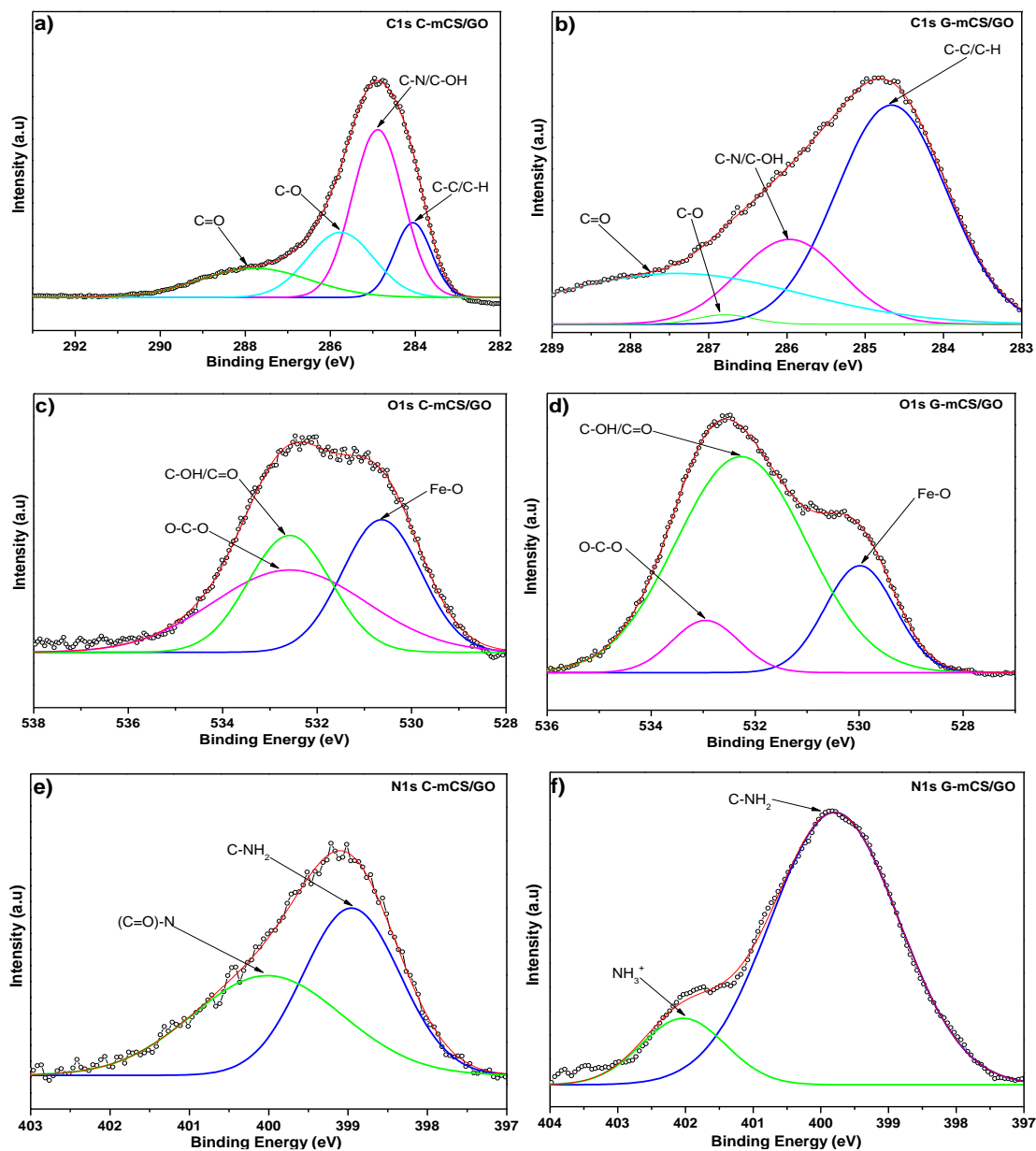
Elements	C-mCS/GO	G-mCS/GO
C (1s)	79.3	69.3
O (1s)	14.1	26.3
N (1s)	4.9	0.9
Fe (2p)	1.7	3.5

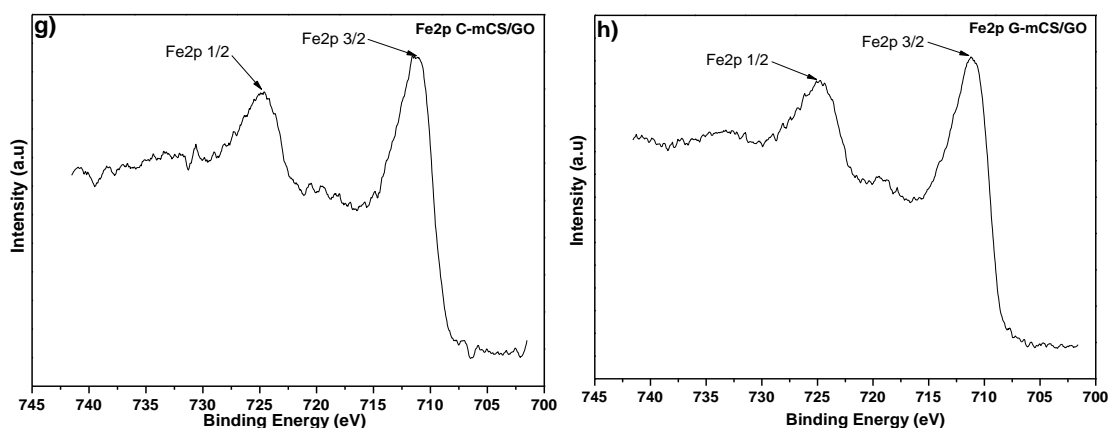
The high-resolution XPS spectrum of C-mCS/GO for C (1s) (Fig. 3.3a) revealed the presence of five peaks centered at 284.5, 285.3, 286.8, and 288.3 eV, which correspond to C-C/C-H (50.3%), C-N/C-OH (29.5%), C-O (13.3%, hydroxyl and epoxy) and (C=O) (6.9%), respectively (Neves et al., 2020). The high-resolution XPS for O (1s) (Fig. 3.3c) indicated the presence of three peaks at 530.6, 532.1, and 533.2 eV, attributed to the functional groups containing oxygen Fe-O (38.8%), C-OH/C=O (33.6%) and O-C-O (27.6%) (Tang et al., 2021). Regarding nitrogen, the high-resolution N (1s) spectrum (Fig. 3.3e) showed the presence of peaks at 399.1 and 400.5 eV, which are associated with the nitrogenous functional groups C-NH<sub>2</sub> (75.7%) and (C=O)-N (24.3%), thus indicating the presence of chitosan in the structure (Zuo et al., 2013; Francisco et al., 2015). In the high-resolution Fe (2p) spectrum (Fig. 3g), the peaks at 711.4 and 724.6 eV, associated with Fe 2p<sub>3/2</sub> and Fe 2p<sub>1/2</sub>, respectively, indicate the formation of Fe<sub>3</sub>O<sub>4</sub> (Wang et al., 2015).

The high-resolution XPS spectrum of G-mCS/GO for C (1s) (Fig. 3.3b) confirmed the presence of four peaks centered at 284.6, 285.8, 286.9, and 288.5 eV, which correspond to C-C/C-H (54.1%), C-N/C-OH (28.8%), C-O (8.7%) and C=O (9.0%), respectively [24]. The high-resolution XPS for O (1s) (Fig. 3.3d) indicated the presence of three peaks at 530.2, 532.1, 533.1 eV, attributed to the functional groups containing oxygen Fe-O (32.1%), C-OH/C=O (35.6%) and O-C-O (32.2%) (Neves et al., 2020). Regarding nitrogen, the high-resolution N (1s) spectrum (Fig. 3.3f) showed the presence of peaks at 399.5 and 401.9 eV, which are associated with the nitrogenous functional groups C-NH<sub>2</sub> (78.9%) and NH<sub>3</sub><sup>+</sup> (21.1%, protonated amine groups), thus indicating the presence of chitosan in the structure of the material

(Francisco et al., 2015; Zhang et al., 2019). In the Fe (2p) high-resolution spectrum (Fig. 3h), the peaks at 711.1 and 724.9 eV, associated with Fe 2p<sub>3/2</sub> and Fe 2p<sub>1/2</sub>, respectively, indicate the formation of Fe<sub>3</sub>O<sub>4</sub> (Tang et al., 2021).

**Figure 3.3.** High-resolution of C (1s) (a-b); O (1s) (c-d); N (1s) (e-f) and Fe (2p) (g-h).



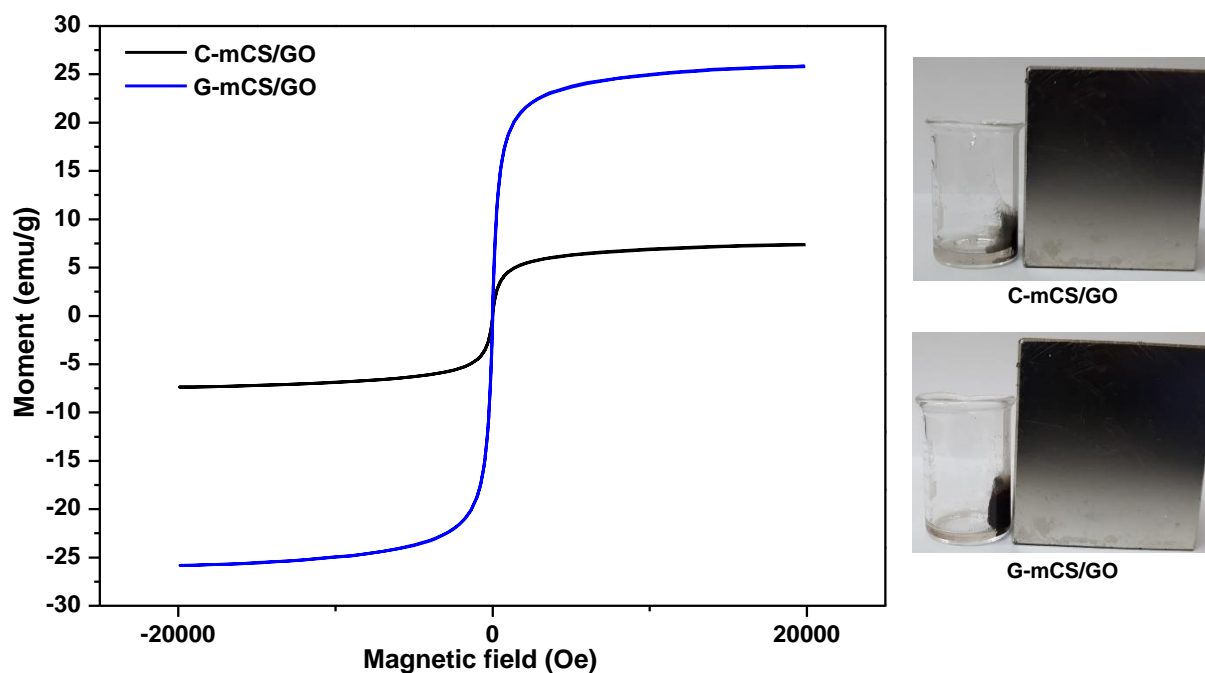


### 3.3.1.4. Magnetization curves

Fig. 3.4 shows the C-mCS/GO and G-mCS/GO magnetization curves. The results indicated that C-mCS/GO and G-mCS/GO show superparamagnetic properties at room temperature, as the magnetization curves obtained do not exhibit coercivity, which indicates that they can be removed from a suspension with a permanent magnet (Zhang et al., 2021).

The calculated saturation magnetization values were 26 emu/g and 7.5 emu/g for G-mCS/GO and C-mCS/GO, respectively. This decrease may be related to the methodology applied for the synthesis of  $\text{Fe}_3\text{O}_4$  magnetic particles, since in the green protocol, water hyacinth extract was used, which is rich in polyphenols, acting as a stabilizing agent for the iron particles (Shi et al., 2020). This decrease can also be associated with the type of crosslinking agent applied in the synthesis of mCS/GO, glutaraldehyde for the conventional synthesis and PAS for the green synthesis. Comparing the results of C-mCS/GO and G-mCS/GO, it is observed that PAS had a better action as a crosslinking agent, which allowed a greater incorporation of G- $\text{Fe}_3\text{O}_4$  particles into the material, thus generating an increase in the value of saturation magnetization of G-mCS/GO (Neves et al., 2020; Shahraki et al., 2020).

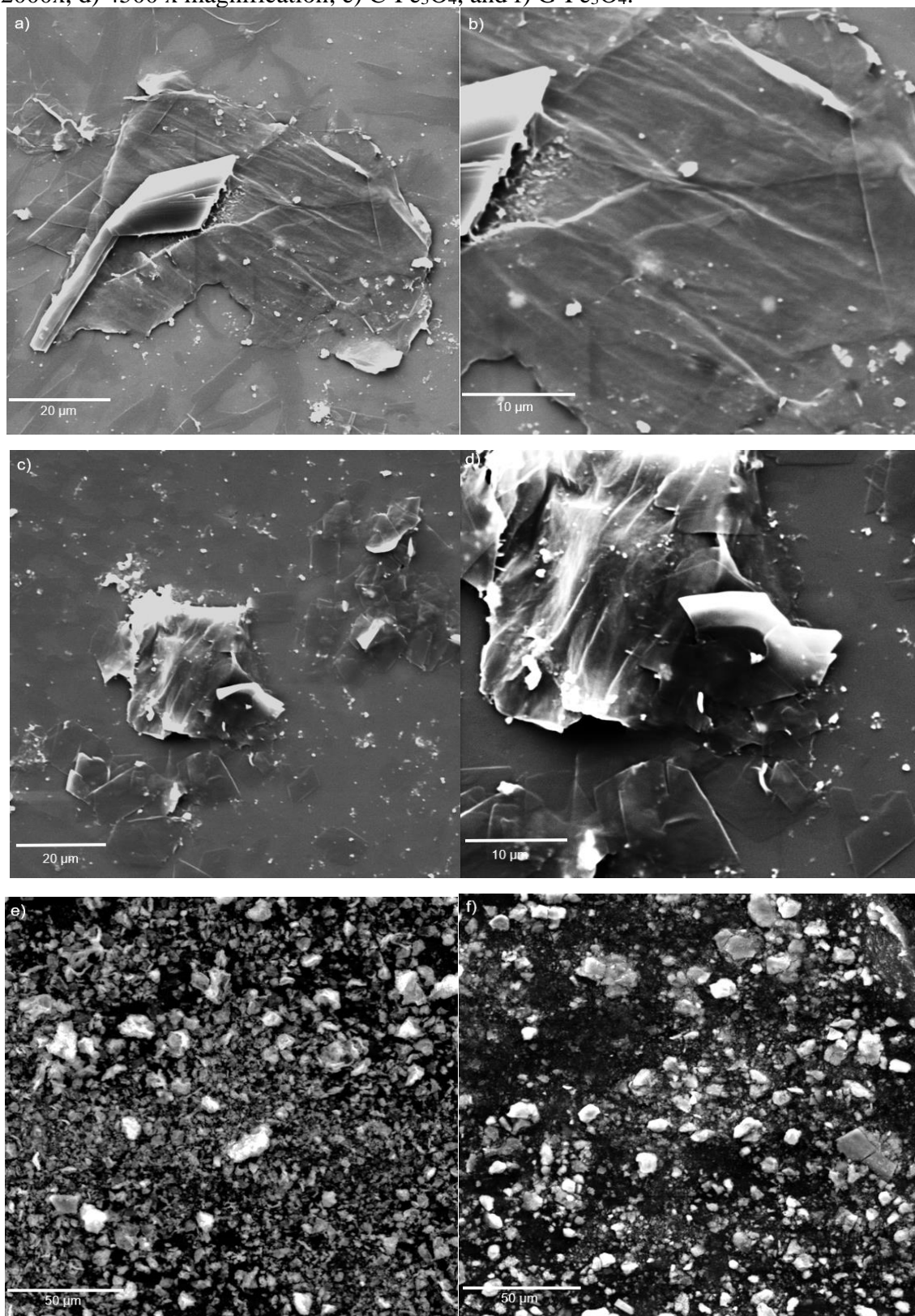
**Figure 3.4.** Magnetization curves of the C-mCS/GO and G-mCS/GO.



### 3.3.1.5. Evaluation of morphological properties of synthesized materials

The micrographs of the composites were determined by SEM and are shown in Fig. 3.5 (a-f). Fig. 3.5 (a-d) shows the micrographs of C-mCS/GO and G-mCS/GO, in which the morphologies were verified in the form of two-dimensional layers with a wrinkled surface, similar to crushed sheets, which are typical of materials containing GO (Jiang et al., 2016; Song et al., 2021). Furthermore, it is possible to observe spherical  $\text{Fe}_3\text{O}_4$  particles well distributed on the surface of the composites, which can be associated with the presence of hydrogen bonds between the  $\text{Fe}_3\text{O}_4$  particles and the functional groups present on the surface of GO (Sheshmani et al., 2014). Fig. 3.5 (e-f) shows micrographs of the aggregated  $\text{Fe}_3\text{O}_4$  magnetic particles, which are associated with the van der Waals interactions between  $\text{Fe}_3\text{O}_4$  (Neves et al., 2020).

**Figure 3.5.** SEM micrographs of: C-mCS/GO a) 2000x, b) 5000 x magnification; G-mCS/GO c) 2000x, d) 4500 x magnification; e) C-Fe<sub>3</sub>O<sub>4</sub>, and f) G-Fe<sub>3</sub>O<sub>4</sub>.



The chemical elements identified through EDS and SEM analyses, as well their mass compositions (%), are shown in Table 3.3. The difference in N composition values between the XPS and EDS analyses can be attributed to differences in the analytical techniques, since EDS analysis is a semiquantitative technique and, therefore, has its limitations. By EDS analysis, the Fe<sub>3</sub>O<sub>4</sub> magnetic particles have chemical elements C, O and Fe. The presence of C in the Fe<sub>3</sub>O<sub>4</sub> magnetic particles is associated with the presence of oleic acid, which is used as a stabilizing agent in the conventional protocol to prevent particle aggregation. For the G-Fe<sub>3</sub>O<sub>4</sub> particles, the presence of C is associated with the polyphenols present in the water hyacinth extract, used as a stabilizing agent in the green protocol (Shi et al., 2020).

The C-mCS/GO and G-mCS/GO composites contained the chemical elements C, N, O and Fe. In both composites, the nitrogen detected in the EDS analysis is associated with the amine functional groups present in CS (Subedi et al., 2019). The mass composition of Fe in G-mCS/GO is greater than that in C-mCS/GO, in accordance with the results obtained through XPS analyses, which is associated with its higher saturation magnetization when compared to that of the conventional composite. This increase can be associated with the crosslinking agent PAS used in the green synthesis process, which enables greater crosslinking of the Fe<sub>3</sub>O<sub>4</sub> particles, preventing their leaching into the medium during the washing step and providing excellent magnetic properties to G-mCS/GO (Shi et al., 2020).

**Table 3.3.** Elemental mass composition (%) of C-mCS/GO and G-mCS/GO and C-Fe<sub>3</sub>O<sub>4</sub> and G-Fe<sub>3</sub>O<sub>4</sub> particles.

Mass composition (%)				
Elements	C-mCS/GO	G-mCS/GO	C-Fe <sub>3</sub> O <sub>4</sub>	G-Fe <sub>3</sub> O <sub>4</sub>
C	53.17	45.32	14.22	12.55
N	26.45	19.88	-	-
O	18.91	25.95	27.47	21.30
Fe	1.47	8.84	57.60	66.15

### 3.3.1.6. Evaluation of the thermal properties of adsorbents

The thermogravimetric curves of C-mCS/GO and G-mCS/GO obtained through TG/DTG analysis are shown in Fig. 3.6 (a, b). Through the thermogravimetric curve of C-mCS/GO (Fig. 3.6(a)), it is observed that the mass loss occurs through three stages. In the first stage, the temperature ranged from 26 to 139 °C, with a mass loss of 1.56%, referring to the evaporation of water adsorbed on the surface of the material. The second stage, which occurs

between 139 and 262 °C, has a mass loss of 52.92%, which is attributed to the decomposition of oxygenated functional groups such as carbonyls, hydroxyls, epoxides, carboxylic acids and nitrogen oxides. Between 262 and 645 °C, the third stage was observed with a mass loss of 24.99%, which is associated with mCS decomposition (Ganguly et al., 2011; Gul et al., 2016). Through DTG analysis, a major mass loss was observed with an exothermic signal at approximately 200 °C, which is associated with the decomposition of oxygenated species, thus generating the formation of byproducts such as CO, CO<sub>2</sub> and steam (Guo et al., 2012).

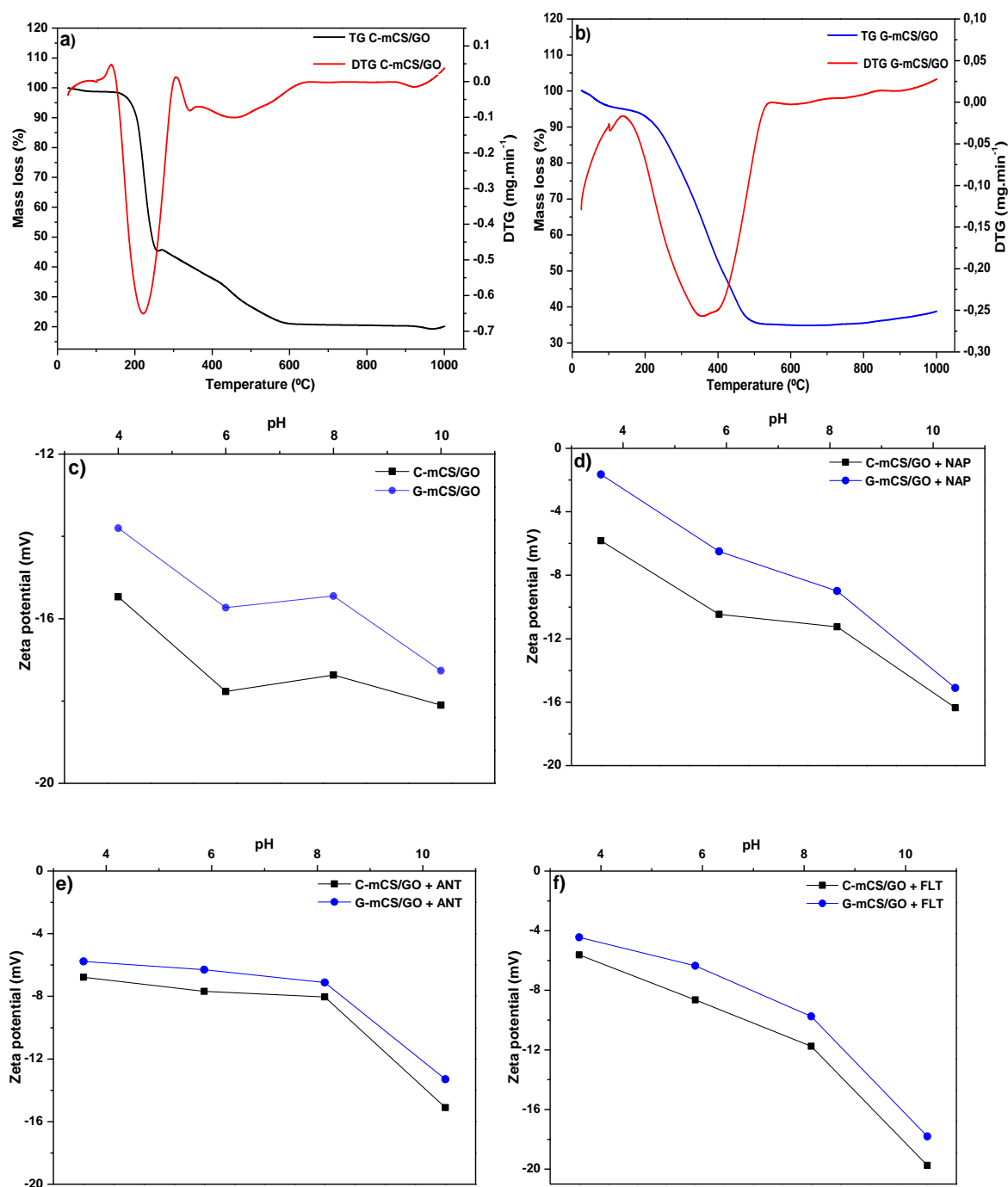
Through the thermogravimetric curve of G-mCS/GO (Fig. 3.6(b)), it can be observed that the mass loss occurs through two distinct stages. The first stage is verified between 26 and 131 °C, showing a mass loss of 4.68%, referring to the evaporation of water adsorbed on the surface of the material. The second stage, which occurs in the temperature range from 131 to 642 °C, with a mass loss of 60.24%, is associated with the decomposition of functional groups containing oxygen, as well as the decomposition of mCS. Through DTG analysis, it is observed that the major mass loss occurs at approximately 300-400 °C, which is associated with the pyrolysis processes of the oxygenated functional groups, thus generating CO, CO<sub>2</sub> and steam. Through this analysis, it can also be observed that the thermal decomposition of mCS/GO produces the release of gases, thus generating a thermal expansion of the material, which can be confirmed by the major mass loss at this stage. The results indicate that the green composite presents greater stability to thermal degradation than the conventional composite since its decomposition occurs at higher temperatures (Stankovich et al, 2007; Gul et al., 2016).

#### 3.3.1.7. pH evaluation

Zeta potential (mV) is a very important factor for determining the magnitude and sign of the surface charge of a colloidal suspension, thus aiming to evaluate its stability and electrostatic interactions between nanomaterials in this suspension (Yang et al., 2010). Fig. 3.6(c) shows the zeta potential (mV) for C-mCS/GO and G-mCS/GO at different pH values (4, 6, 8, 10). Zeta potential measurements indicated that, for the evaluated pH range, both nanomaterials had negative values. C-mCS/GO presented more negative zeta potential values for all pH ranges, indicating that the suspension of nanomaterials is more stable, even under acidic conditions (Gurunathan et al., 2014). The G-mCS/GO zeta potential values also indicate the presence of a less negatively charged nanomaterial, which may be associated with the presence of protonated functional groups from the G-Fe<sub>3</sub>O<sub>4</sub> particles (Fe<sup>2+</sup> and Fe<sup>3+</sup>), since XPS results indicated a higher content of iron in G-mCS/GO. This increase may be attributed to the

performance of the crosslinking agent (PAS) used in the synthesis process of the green adsorbent (Han et al., 2012; Kalliola et al., 2017).

**Figure 3.6.** TG/DTG curves and Zeta potential for: (a-c) C-mCS/GO; (b-c) G-mCS/GO and the Zeta potential in suspension with (d) naphthalene; (e) anthracene; (f) and fluoranthene solutions.



### 3.3.2. Molecular simulation

Through the molecular simulations performed by using ChemDraw® and Avogadro® software, information on the physicochemical and geometric properties of PAHs was obtained. Table 3.4 shows the physicochemical properties of the naphthalene, anthracene and fluoranthene molecules calculated by ChemDraw® and Avogadro® software.

**Table 3.4.** Physicochemical properties of naphthalene, anthracene and fluoranthene molecules.

Properties	Naphthalene	Anthracene	Fluoranthene
Molecular formula	C <sub>10</sub> H <sub>8</sub>	C <sub>14</sub> H <sub>10</sub>	C <sub>16</sub> H <sub>10</sub>
Molecular weight	128.171 g.mol <sup>-1</sup>	178.229 g.mol <sup>-1</sup>	202.251 g.mol <sup>-1</sup>
Melting point	261.08 K	351.38 K	425.42 K
Boiling point	474.06 K	589.54 K	651.56 K
Critical temperature	757.95 K	859.11 K	898.65 K
log K <sub>ow</sub> <sup>a</sup>	3.37	4.54	5.22
Dipole Moment <sup>b</sup>	0 Debye	0 Debye	0.3291 Debye

<sup>a</sup>Mackay *et al.*, 1992.

<sup>b</sup>Estimated through chemical modeling software Gaussian®.

Fig. 3.7 shows the chemical structures, optimized geometry and electrostatic potential of PAH molecules (naphthalene, anthracene and fluoranthene) obtained by using ChemDraw®, Avogadro® and GaussView® software. The optimization of the isolated PAHs was performed through the B3LYP method, with 6-31G (d) and 6-31G (d,p) as the basis set. Fig. S2 shows the lowest molecular energies of the optimized PAH geometries, so that the most stable conformers, that is, the lowest energies, were obtained by the 6-31G (d,p) base set. Additional stability and vibrational frequency calculations were performed to ensure that the structures are stable and that they correspond to the minimum energy settings (Salter and Foresman, 1998). Tables S2-S4 show the optimized bond lengths of the PAH molecules, where the bond lengths represent the distance between the center of the two bonded atoms.

The naphthalene, anthracene and fluoranthene molecules have their largest dimensions of 7.201 Å, 9.546 Å and 9.045 Å, respectively, as shown in Fig. 3.7. The electrostatic potential map of the PAH molecules, calculated by GaussView 5® software, is also shown in Fig. 3.7, which provides information about the distribution of electron density. The electrostatic potential map indicates the electron distribution in each region of the PAH molecules, where

the blue color represents the electron-poor regions and the red color represents the electron-rich regions (Mishra and Yadav, 2012; Santos et al., 2014).

**Figure 3.7.** Chemical structures, optimized geometry and the electrostatic potential of PAHs molecules: a) naphthalene; b) anthracene; c) fluoranthene.

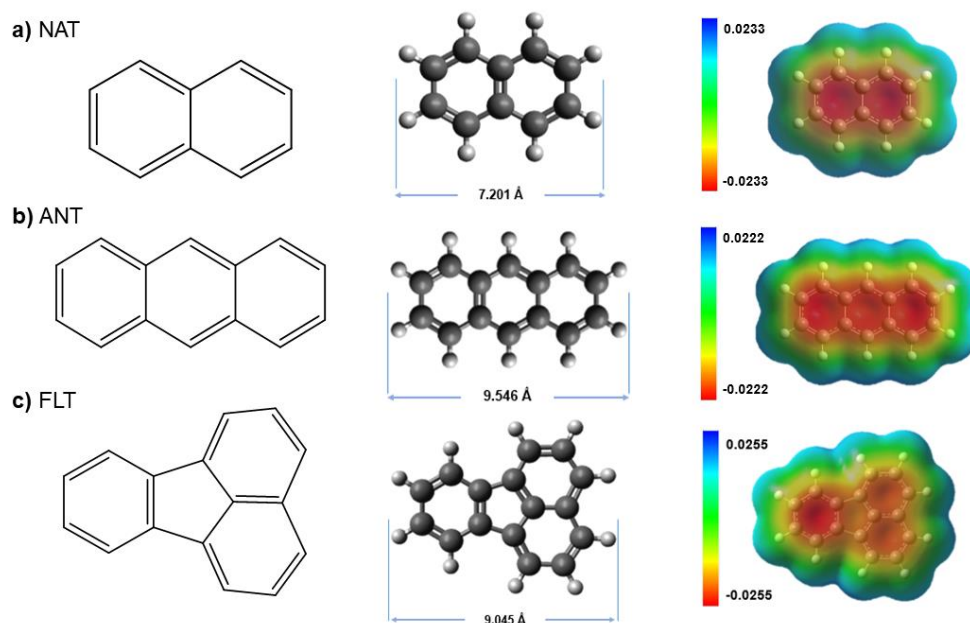
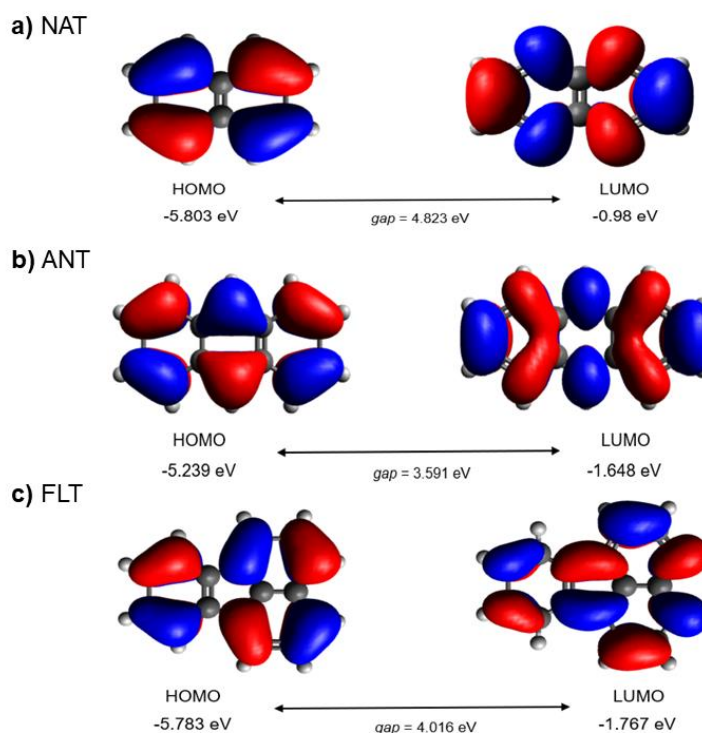


Fig. 3.8 shows the HOMO and LUMO 3-D contours of naphthalene, anthracene and fluoranthene molecules. Table 3.4 presents the quantum chemical parameters obtained for the PAHs through the B3LYP/6-31G(d,p) model. The energy of the boundary orbitals (HOMO and LUMO) assessment is very important to understand the mechanisms involved in the adsorptive processes because through these quantum chemical descriptors, it is possible to delimit the regions in which molecules can donate (HOMO) or accept electrons (LUMO). The higher the HOMO is, the greater the electron donating capacity, and the lower the LUMO is, the easier it is to accept electrons. Through the HOMO and LUMO energy values presented in Fig. 3.8 and Table 3.5, it is possible to observe that ANT has a greater capacity to donate electrons than the other PAHs evaluated, while naphthalene has greater acceptance of electrons (Mishra and Yadav, 2012; Santos et al., 2014).

**Figure 3.8.** 3-D contours of HOMO and LUMO: a) naphthalene; b) anthracene; c) fluoranthene (Positive Phase: Blue Color; Negative Phase: Red Color).



**Table 3.5.** Quantum chemical parameters of naphthalene, anthracene and fluoranthene using the B3LYP/6-31G (d,p) model.

Quantum chemical parameters	Naphthalene	Anthracene	Fluoranthene
HOMO energy ( $E_H$ , eV)	-5.803	-5.239	-5.783
LUMO energy ( $E_L$ , eV)	-0.980	-1.648	-1.767
Energy gap ( $\Delta_{HL}$ , eV)	4.823	3.591	4.016
Chemical potential ( $\mu$ , eV)	3.391	3.443	3.775
Chemical hardness ( $\eta$ , eV)	2.411	1.795	2.008
Electrophilicity index ( $\omega$ , eV)	2.385	3,302	3.548

The difference between the HOMO-LUMO energies (gap) is important to indicate how stable the structure of the molecule is, so that the greater this difference is, the greater the stability of the molecule, and consequently, the lower its reactivity in chemical reactions. Based

on the gap values shown in Fig. 8, naphthalene has a greater gap (4,823 eV), which indicates greater stability and less reactivity, whereas anthracene has a smaller gap (3,591 eV), thus indicating less stability and greater reactivity than naphthalene and fluoranthene (Umadevi and Sastry, 2011). According to the study by Naghavi et al. (2011), the gap depends on the molecular size, so this difference decreases as the PAH size increases, decreasing their stability.

HOMO and LUMO energies can also be used to calculate the quantum chemical parameters, according to Equations 1-3.  $\mu$  measures the tendency of electrons to escape from the system (Parr and Pearson, 1983);  $\eta$  measures resistance to changes in electron density; in other words, it measures resistance to deformation, helping to determine the stability and reactivity of the molecule (Pearson, 1992);  $\omega$  is an indicator of the ability to accept electrons (Parr et al., 1999).

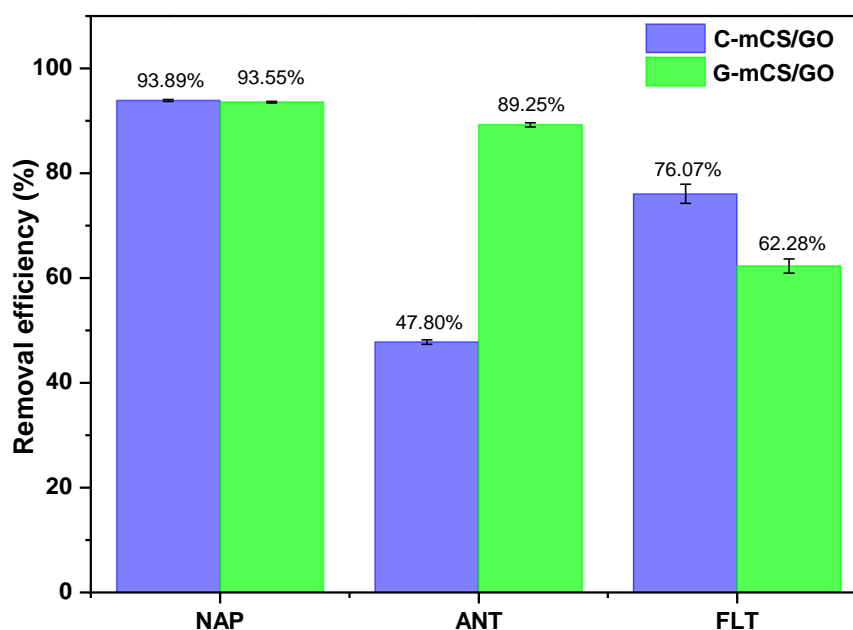
Comparing the values of  $\mu$ ,  $\eta$  and  $\omega$  for naphthalene, anthracene and fluoranthene, presented in Table 3.5, it is observed that FLT fluoranthene has a higher chemical potential, thus indicating a lower capacity to retain electrons; therefore, fluoranthene has less stability and greater reactivity than naphthalene and anthracene. Naphthalene is the hardest molecule, showing greater resistance to deformation in its electron density, while anthracene has less resistance to deformation. The value of the electrophilicity index indicates that fluoranthene is the strongest electrophile, with a greater tendency to accept electrons. Through the theoretical analysis of quantum chemical descriptors, it is concluded that anthracene and fluoranthene are the most reactive among the evaluated PAHs.

### 3.3.3. Adsorptive affinity assays

Through the adsorptive affinity assays, it was possible to evaluate the removal potential of PAHs (naphthalene, anthracene and fluoranthene) by the C-mCS/GO and G-mCS/GO adsorbents for a contact time of 30 min. The adsorption capacities ( $q(t)$ ) of the PAHs by the adsorbents are shown in Table 3.6, and the removal efficiencies of the PAHs is shown in Fig. 3.9.

**Table 3.6.** Adsorption capacity of PAHs by the adsorbents (C-mCS/GO and G-mCS/GO).

PAHs	Adsorption capacity (mmol.g <sup>-1</sup> )	
	C-mCS/GO	G-mCS/GO
Naphthalene	0.094	0.093
Anthracene	0.048	0.089
Fluoranthene	0.076	0.062

**Figure 3.9.** Removal efficiency (%Rem) of PAHs (naphthalene, anthracene and fluoranthene). Conditions: C<sub>0</sub>=0.01 mmol.L<sup>-1</sup>, dosage of adsorbent of 0.1 mg.mL<sup>-1</sup>, 25 °C for 30 min.

From the results presented in Fig. 3.9 and Table 3.6, it is observed that the best removal efficiency (%) and adsorption capacity (mmol.g<sup>-1</sup>) were obtained by naphthalene for both C-mCS/GO and G-mCS/GO. The results also showed that the G-mCS/GO adsorbent was highly efficient for the removal of anthracene compared to the conventional adsorbent. These results show that G-mCS/GO is a potential adsorbent for PAH removal from wastewater. Table 3.7 shows a comparison of the adsorption and removal capacity of C-mCS/GO and G-mCS/GO for PAH adsorption with other materials presented in the literature.

**Table 3.7.** Comparison of the adsorption capacity and removal efficiency of C-mCS/GO and G-mCS/GO with other adsorbents studied in the literature.

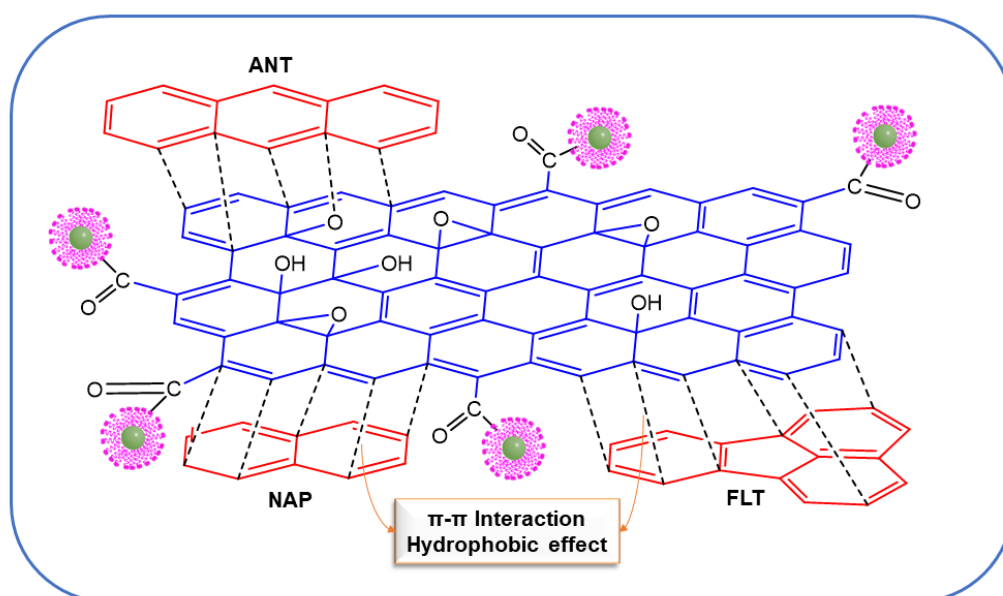
PAHs	Adsorbents	Experimental conditions	Adsorption capacity (mmol.g <sup>-1</sup> )	Removal efficiency (%)	References
Anthracene	Nitrogen-doped reduced graphene oxide (NRGO)	C <sub>0</sub> : 0.0056 mmol.L <sup>-1</sup> , 298 K, pH 7, 150 rpm, 48 h, D: 0.1 mg.mL <sup>-1</sup>	0.0324	58	[10]
Naphthalene	Thiourea-Magnetite-TiO <sub>2</sub> modified chitosan beads (Cs-T-M-Ti)	C <sub>0</sub> : 0.078 mmol.L <sup>-1</sup> , 298 K, pH 6.5, 200 rpm, 24 h, D: 0.5 mg.mL <sup>-1</sup>	0.067	-	[22]
Anthracene, Fluoranthene	Cetylpyridinium chloride (CPC)-MC; Didodecyldimethylammonium bromide (DDAB)-MC; Hexadecyltrimethylammonium bromide (HDTMA)-MC	C <sub>0</sub> : 2.8x10 <sup>-4</sup> mmol.L <sup>-1</sup> (ANT), C <sub>0</sub> : 4.9x10 <sup>-4</sup> mmol.L <sup>-1</sup> (FLT), 293 K, pH 6.5, 24 h, D: 1 mg.mL <sup>-1</sup>	ANT (4x10 <sup>-3</sup> , 4.1 x10 <sup>-3</sup> , 4.2 x10 <sup>-3</sup> ) FLT (6.7x10 <sup>-3</sup> , 7.8x10 <sup>-3</sup> , 6.4x10 <sup>-3</sup> )	Anthracene (61, 71, 65.6) Fluoranthene (52.5, 61.8, 44)	[50]
Fluoranthene	Lightweight expanded clay aggregate (LECA)	C <sub>0</sub> : 9.9x10 <sup>-5</sup> mmol.L <sup>-1</sup> , 298 K, pH 6.5, 300 rpm, 21 h, D: 2 mg.mL <sup>-1</sup>	3.5x10 <sup>-5</sup>	70.83	[51]
Naphthalene, Anthracene, Fluoranthene	C-mCS/GO	C <sub>0</sub> : 0.01 mmol.L <sup>-1</sup> , 298 K, pH 6.5, 200 rpm, 30 min, D: 0.1 mg.mL <sup>-1</sup>	0.094, 0.048, 0.076	93.89, 47.80, 76.07	This study
Naphthalene, Anthracene, Fluoranthene	G-mCS/GO	C <sub>0</sub> : 0.01 mmol.L <sup>-1</sup> , 298 K, pH 6.5, 200 rpm, 30 min, D: 0.1 mg.mL <sup>-1</sup>	0.093, 0.089, 0.062	93.55, 89.25, 62.28	This study

When compared with conventional materials, green synthesized adsorbents are an alternative methodology to decrease the toxic effects associated with the excessive application of chemical products in conventional synthesis. In addition, the use of natural agents can be of great advantage for green synthesis processes due to the presence of active compounds, such as polyphenols and flavones, which can act as stabilizing and crosslinking agents. Such compounds can improve the properties of these green materials, boosting their performance in pollutant adsorptive processes from wastewater (Shi et al., 2020; Zhang et al., 2021).

### 3.3.4. Mechanisms of PAH adsorption

The results obtained with the molecular simulation indicated that NAP molecules have greater stability than anthracene and fluoranthene molecules, which may contribute to increasing the  $\pi$ - $\pi$  interactions between naphthalene molecules and the adsorbent surface (Li et al., 2018). Furthermore, the presence of oxygenated functional groups such as C=O and O-H in the structure of the adsorbents, as indicated in the FT-IR analyses (Fig. 3.2b), may be one of the factors that contribute to the presence of strong  $\pi$ - $\pi$  interactions between the molecules of PAHs and the surface of the adsorbents (Song et al., 2021). Thus, the presence of these interactions can induce a greater adsorptive efficiency between PAHs and both C-mCS/GO and G-mCS/GO adsorbents. Fig. 3.10 illustrates the possible mechanisms involved in the naphthalene, anthracene and fluoranthene adsorption processes into G-mCS/GO.

**Figure 3.10.** Adsorption mechanisms of PAHs into the G-mCS/GO.



Another mechanism that can contribute to PAH adsorption on the adsorbent surface is the hydrophobic effect. This effect is very important for the adsorption of nonpolar compounds, which contributes to increasing their adsorption capacity into the adsorbents (Wang et al., 2014). The adsorption mechanism of PAHs can also be influenced by the effect of pH and zero charge point; thus, the zeta potentials (ZP) for C-mCS/GO and G-mCS/GO in the presence of naphthalene, anthracene and fluoranthene are shown in Fig. 3.6(d-f). Comparing these results with the ZP before (Fig. 3.6c) and after adsorption (Fig. 3.6(d-f)), it is observed that at pH 4, 6 and 8, there was a decrease in the surface charge of the composites after PAH adsorption, as they have very little negative charge. At pH 10, however, the difference between the ZP values before and after adsorption was very small, which indicates that these suspensions are more negatively charged, which makes them more stable, in accordance with the results presented in the literature (Zhang et al., 2013; Li et al., 2015). In solutions with  $\text{pH} \geq 10$ , it is possible that the decrease in the adsorption capacity is associated with the electrostatic repulsion of negative ions, which can reduce the formation of  $\pi$ - $\pi$  interactions, thus generating a decrease in the adsorptive performance at basic pH (Tang et al., 2021).

### 3.4. Challenges, limitations and future prospects

The results and discussions addressed in this study have as the main objective to fill gaps in the literature regarding the development of eco-friendly and low-cost materials based on the principles of green chemistry, aiming at their application for the adsorption of contaminants from wastewater. The results obtained indicated that G-mCS/GO is a potential green adsorbent for the removal of PAHs, presenting competitive adsorption capacities when compared to those of conventional adsorbents. However, it is important to highlight some challenges and limitations that still need to be overcome by green synthesis processes with regard to the application of different natural agents, such as stabilizing, crosslinking or capping agents. In this context, some perspectives for future studies can be proposed to overcome these limitations, such as (i) studies aimed at optimizing the synthesis processes of new green adsorbents, aiming at the application of different natural agents replacing toxic chemical reagents; (ii) application of green materials in dynamic fixed-bed systems, aiming at industrial scale application and treatment of real effluents; and (iii) studies involving the regeneration of these materials in different adsorption cycles.

### 3.5. Conclusions

In this study, the synthesis of adsorbents by conventional and green routes (C-mCS/GO and G-mCS/GO, respectively) was performed and then applied to PAH adsorption to investigate their efficiency in naphthalene, anthracene and fluoranthene removal from wastewater. The characterization analyses confirmed the obtainment of magnetic composites with high adsorptive capacities. The results indicate that the application of PAS as a crosslinking agent in the synthesis of G-mCS/GO contributed to improving its thermal and magnetic properties when compared to C-mCS/GO. The adsorption assays showed a better adsorptive capacity of PAHs on G-mCS/GO, for a contact time of 30 min and dosage of adsorbent of  $0.1 \text{ mg.mL}^{-1}$ , mainly for naphthalene and anthracene when compared to the conventional one, with 93.55% and 89.25% removal efficiency, respectively. The affinity assays along with the results of the molecular simulations indicated that the adsorption processes are possibly governed by  $\pi$ - $\pi$  interactions and hydrophobic effects. In addition, the zeta potential analyses indicated a better adsorption performance at neutral pH. The results obtained in this study point to G-mCS/GO as a novel green composite, which can be applied as an up-and-coming material for the removal of PAHs from wastewater when compared to conventional adsorbents.

#### Declaration of Interest

No conflicts of interest were declared by the authors of this study.

#### CRedit authorship contribution statement

**Ruth Nóbrega Queiroz:** Methodology and validation method, Investigation, Analysis, Data evaluation, Writing - original sketch, review and editing. **Tauany de Figueiredo Neves:** Investigation, Methodology. **Meuris Gurgel Carlos da Silva:** Oversight, Acquisition funding. **Valmor Roberto Mastelaro:** Analysis, Investigation. **Patrícia Prediger:** Project administration, Analysis, Investigation, Resources, Data evaluation, Writing - review and editing, Acquisition funding. **Melissa Gurgel Adeodato Vieira:** Project administration, Resources, Investigation, Data evaluation, Writing - review and editing, Acquisition funding.

## Acknowledgment

This research was supported by FAPESP (n. 2019/07822-2, 2019/25228-0 and 2013/07296-2), CNPq (Grant #308046/2019-6 and Grant #141469/2018-8), CAPES (Finance Code 001) and PRH-ANP (n. 29, 5485). The authors are grateful to the CENAPAD SP for making available the molecular simulation software licenses, LNBR (CNPEM/MCTIC) for the support provided in the characterization of the materials by Zeta potential analysis and Dr. Josiane Vendemiatti for the SEM analyses carried out at the Faculty of Technology at UNICAMP-Limeira.

## References

- Abdel-Shafy, H.I., Mansour, M.S.M., 2016. A review on polycyclic aromatic hydrocarbons: source, environmental impact, effect on human health and remediation. *Egypt. J. Pet.* 25, 107-123. doi: 10.1016/j.ejpe.2015.03.011.
- Adeola, A., Forbes, P. B. C., 2022. Assessment of reusable graphene wool adsorbent for the simultaneous removal of selected 2–6 ringed polycyclic aromatic hydrocarbons from aqueous solution. *Environmental Technology.* 43 (8), 1255-1268. doi: 10.1080/09593330.2020.1824024.
- Brião, G. V., Jahn, S. L., Foletto, E. L., Dotto, G. L., 2018. Highly efficient and reusable mesoporous zeolite synthesized from a biopolymer for cationic dyes adsorption. *Colloids and Surfaces A: Physicochemical and Engineering Aspects.* 556, 43-50. doi: 10.1016/j.colsurfa.2018.08.019.
- Francisco, W., Ferreira, F.V., Ferreira, E.V., Cividanes, L.S., Coutinho, A.R., Thim, G.P., 2015. Functionalization of Multi-Walled Carbon Nanotube and Mechanical Property of Epoxy-Based Nanocomposite. *Journal of Aerospace Technology and Management.* 7, 289-293. doi: 10.5028/jatm.v7i3.485.
- Ganguly, A., Sharma, S., Papakonstantinou, P., Hamilton, J., 2011. Probing the Thermal Deoxygenation of Graphene Oxide Using High-Resolution In Situ X-ray-Based Spectroscopies. *The Journal of Physical Chemistry C.* 115, 17009-17019. doi: 10.1021/jp203741y.
- Gul, K., Sohni, S., Waqar, M., Ahmada, F., Norulaini, N.A.N., Mohd. Omar A.K., 2016. Functionalization of magnetic chitosan with graphene oxide for removal of cationic and anionic dyes from aqueous solution. *Carbohydrate Polymers.* 152, 520-531. doi: 10.1016/j.carbpol.2016.06.045.
- Guo, Y., Sun, X., Liu, Y., Wang, W., Qiu, H., Gao, J., 2012. One pot preparation of reduced graphene oxide (RGO) or Au (Ag) nanoparticle-RGO hybrids using chitosan as a reducing and stabilizing agent and their use in methanol electrooxidation. *Carbon.* 50, 2513-2523. doi: 10.1016/j.carbon.2012.01.074.

Gurunathan, S., Han, J. W., Kim, E., Kwon, D.N., Park, J.K., Kim, J.H., 2014. Enhanced green fluorescent protein-mediated synthesis of biocompatible graphene. *Journal of Nanobiotechnology*. 12, 41-57. doi: 10.1186/s12951-014-0041-9.

Han, Q., Wang, Z., Xia, J., Chen, S., Zhang, X., Ding, M., 2012. Facile and tunable fabrication of Fe<sub>3</sub>O<sub>4</sub>/graphene oxide nanocomposites and their application in the magnetic solid-phase extraction of polycyclic aromatic hydrocarbons from environmental water samples. *Talanta*. 101, 388-395. doi: 10.1016/j.talanta.2012.09.046.

Haneef, T., Mustafa, M. R. U., Rasool, K., Ho, Y. C., Kutty, S. R. M., 2020. Removal of Polycyclic Aromatic Hydrocarbons in a Heterogeneous Fenton Like Oxidation System Using Nanoscale Zero-Valent Iron as a Catalyst. *Water*. 12 (9), 2430. doi: <https://doi.org/10.3390/w12092430>.

Hedayati, M.S., Abida, O., Li, L.Y., 2021. Adsorption of polycyclic aromatic hydrocarbons by surfactant-modified clinoptilolites for landfill leachate treatment. *Waste Management*. 131, 503-512. doi: 10.1016/j.wasman.2021.06.033.

Hsu, H., Kuo, C., Jehng, J., Wei, C., Wen, C., Chen, J., Chen, L., 2019. Application of Graphene Oxide Aerogel to the Adsorption of Polycyclic Aromatic Hydrocarbons Emitted from the Diesel Vehicular Exhaust. *Journal of Environmental Chemical Engineering*. 7 (6), 103414. doi: 10.1016/j.jece.2019.103414.

Huang, D., Xu, B., Wu, J., Brookes, P.C., Xu, J., 2019. Adsorption and desorption of phenanthrene by magnetic graphene nanomaterials from water: Roles of pH, heavy metal ions and natural organic matter. *Chemical Engineering Journal*. 368, 390-399. doi: 10.1016/j.cej.2019.02.152.

Hummers, W. S., Offeman, R. E., 1958. Preparation of Graphitic Oxide. *Journal of the American Chemical Society*. 80, 1339. doi: 10.1021/ja01539a017.

Jiang, Y., Gong, J.L., Zeng, G.M., Ou, X.M., Chang, Y.N., Deng, C.H., Zhang, J., Liu, H.Y., Huang, S.Y., 2016. Magnetic chitosan-graphene oxide composite for antimicrobial and dye removal applications. *International Journal of Biological Macromolecules*. 82, 702-710. doi: 10.1016/j.ijbiomac.2015.11.0210.

Kalliola, S., Repo, E., Srivastava, V., Heiskanen, J.P., Sirvio, J.A., Liimatainen, H., Mika Sillanpää, M., 2017. The pH sensitive properties of carboxymethyl chitosan nanoparticles cross-linked with calcium ions. *Colloids and Surfaces B: Biointerfaces*. 153, 229-236. doi: 10.1016/j.colsurfb.2017.02.025.

Li, B., Ou, P., Wei, Y., Zhang, X., Song, J., 2018. Polycyclic Aromatic Hydrocarbons Adsorption onto Graphene: A DFT and AIMD Study. *Materials*. 11, 726. doi: 10.3390/ma11050726.

Li, M.F., Liu, Y.G., Zeng, G.M., Liu, S.B., Hu, X.J., Shu, D., Jiang, L.H., Tan, X.F., Cai, X.X., Yan, Z.L., 2017. Tetracycline adsorbed onto nitrilotriacetic acid-functionalized magnetic graphene oxide: Influencing factors and uptake mechanism. *Journal of Colloid and Interface Science*. 485, 269-279. doi: 10.1016/j.jcis.2016.09.037.

Li, S., Luo, J., Hang, X., Zhao, S., Wan, Y., 2019. Removal of polycyclic aromatic hydrocarbons by nanofiltration membranes: Rejection and fouling mechanisms. *Journal of Membrane Science*. 582, 264-273. doi: 10.1016/j.memsci.2019.04.008.

Li, Z., Sellaoui, L., Franco, D., Netto, M. S., Georgin, J., Dotto, G. L., Bajahzar, A., Belmabrouk, H., Petriciolet, A. B., Li, Q., 2020. Adsorption of hazardous dyes on functionalized multiwalled carbon nanotubes in single and binary systems: Experimental study and physicochemical interpretation of the adsorption mechanism. *Chemical Engineering Journal*. 389, 124467. doi: 10.1016/j.cej.2020.124467.

Maleki, A., Paydar, R., 2015. Graphene oxide–chitosan bionanocomposite: a highly efficient nanocatalyst for the one-pot three-component synthesis of trisubstituted imidazoles under solvent-free conditions. *The Royal Society of Chemistry*. 5, 33177-33184. doi: 10.1039/c5ra03355a.

Maswanganyi, S., Gusain, R., Kumar, N., Kankeu, E. F., Waanders, F. B., Ray, S. S., 2021. Bismuth Molybdate Nanoplates Supported on Reduced Graphene Oxide: An Effective Nanocomposite for the Removal of Naphthalene via Adsorption–Photodegradation. *ACS Omega*. 6, 16783-16794. doi: 10.1021/acsomega.1c01296.

Mishra, P.C., Yadav, A., 2012. Polycyclic aromatic hydrocarbons as finite size models of graphene and graphene nanoribbons: Enhanced electron density edge effect. *Chemical Physics*. 402, 56-68. doi: 10.1016/j.chemphys.2012.04.005.

Naghavi, S. S., Gruhn, T., Alijani, V., Fecher, G. H., Felser, C., Medjanik, K., Kutnyakhov, D., Nepijko, S. A., Schönhense, G., Rieger, R., Baumgarten, M., Müllen, K., 2011. Theoretical study of new acceptor and donor molecules based on polycyclic aromatic hydrocarbons. *Journal of Molecular Spectroscopy*. 265, 95-101. doi: 10.1016/j.jms.2010.12.004.

Neves, T. F., Dalarme, N. B., Silva, P. M. M., Landers, R., Piconec, C. S. F., Prediger, P., 2020. Novel magnetic chitosan/quaternary ammonium salt graphene oxide composite applied to dye removal. *Journal of Environmental Chemical Engineering*. 8, 103820. doi: 10.1016/j.jece.2020.103820.

Nkansah, M.A., Christy, A.A., Barth, T., George William Francis, G.W., 2012. The use of lightweight expanded clay aggregate (LECA) as sorbent for PAHs removal from water. *Journal of Hazardous Materials*. 217-218, 360-365. doi: 10.1016/j.jhazmat.2012.03.038.

Pal, P., Pal, A., Nakashima, K., Yadav, B. K. 2020. Applications of Chitosan in Environmental Remediation: A Review. *Chemosphere*. 266, 128934. <https://doi.org/10.1016/j.chemosphere.2020.128934>.

Parr, R.G., Pearson, R.G., 1983. Absolute Hardness: Companion Parameter to Absolute Electronegativity. *J. Am. Chem. Soc.* 105, 7512-7516. doi: 10.1021/ja00364a005.

Parr, R.G., Szentpály, L. V., Liu, S., 1999. Electrophilicity Index. *J. Am. Chem. Soc.* 121,1922-1924. doi: 10.1021/ja983494x.

Pearson, R.G., 1992. Chemical hardness and the electronic chemical potential. *Inorganica Chim. Acta*. 198-200, 781-786. doi:10.1016/S0020-1693(00)92423-X.

Prediger, P., Cheminski, T., Neves, T. F., Nunes, W. B., Sabino, L., Picone, C. S. F., Oliveira, R. L., Correia, C. R. D., 2018. Graphene oxide nanomaterials for the removal of nonionic surfactant from water. *Journal of Environmental Chemical Engineering*. 6, 1536-1545. doi: 10.1016/j.jece.2018.01.072.

Queiroz, R. N., Prediger, P., Vieira, M.G. A., 2022. Adsorption of polycyclic aromatic hydrocarbons from wastewater using graphene-based nanomaterials synthesized by conventional chemistry and green synthesis: a critical review. *Journal of Hazardous Materials*, 422, 126904. doi: 10.1016/j.jhazmat.2021.126904.

Salter, C., Foresman, J. B., 1998. Naphthalene and Azulene I: Semimicro Bomb Calorimetry and Quantum Mechanical Calculations. *Journal of Chemical Education*. 75, 1341-1345. doi: 10.1021/ed075p1341.

Santos, C. B. R., Lobato, C. C., Sousa, M. A. C., Macêdo, W. J. C., Carvalho, J. C. T., 2014. Molecular Modeling: Origin, Fundamental Concepts and Applications Using Structure-Activity Relationship and Quantitative Structure-Activity Relationship. *Reviews in Theoretical Science*. 2, 91-115. doi:10.1166/rits.2014.1016.

Santos, N. T. G., Moraes, L. F., Silva, M. G. C., Vieira, M. G. A., 2020. Recovery of gold through adsorption onto sericin and alginate particles chemically crosslinked by proanthocyanidins. *Journal of Cleaner Production*. 253, 119925. doi: 10.1016/j.jclepro.2019.119925.

Silva, V. A. J., Andrade, P. L., Silva, M. P. C., Dominguez, A. B., Valladares, L. D. L. S., Aguiar, J. A., 2013. Synthesis and characterization of Fe<sub>3</sub>O<sub>4</sub> nanoparticles coated with fucan polysaccharides. *J. Magn. Magn. Mater.* 343, 138-143. doi: 10.1016/j.jmmm.2013.04.062.

Shahraki, S., Delarami, H. S., Khosravi, F., Nejat, R., 2020. Improving the adsorption potential of chitosan for heavy metal ions using aromatic ring-rich derivatives. *Journal of Colloid and Interface Science*. 576, 79-89. doi: 10.1016/j.jcis.2020.05.006.

Sheshmani, S., Ashori, A., Hasanzadeh, S., 2014. Removal of Acid Orange 7 from aqueous solution using magnetic graphene/chitosan: A promising nano-adsorbent. *International Journal of Biological Macromolecules*. 68, 218-224. doi: 10.1016/j.ijbiomac.2014.04.0570.

Shi, Y., Xing, Y., Deng, S., Zhao, B., Fu, Y., Liu, Z., 2020. Synthesis of proanthocyanidins-functionalized Fe<sub>3</sub>O<sub>4</sub> magnetic nanoparticles with high solubility for removal of heavy-metal ions. *Chemical Physics Letters*. 753, 137600. doi: 10.1016/j.cplett.2020.137600.

Solano, R. A., León, L. D. D., Ávila, G. D., Herrera, A. P., 2021. Polycyclic aromatic hydrocarbons (PAHs) adsorption from aqueous solution using chitosan beads modified with thiourea, TiO<sub>2</sub> and Fe<sub>3</sub>O<sub>4</sub> nanoparticles. *Environmental Technology & Innovation*. 21, 101378. doi: 10.1016/j.eti.2021.101378.

Song, L., Niu, X., Zhang, N., Li, T., 2021. Effect of biochar-immobilized *Sphingomonas* sp. PJ2 on bioremediation of PAHs and bacterial community composition in saline soil. *Chemosphere*. 279, 130427. doi: 10.1016/j.chemosphere.2021.130427.

Song, T., Weijun Tian, W., Qiao, K., Zhao, J., Chu, M., Du, Z., Wang, L., Xie, W., 2021. Adsorption Behaviors of Polycyclic Aromatic Hydrocarbons and Oxygen Derivatives in Wastewater on N-Doped Reduced Graphene Oxide. *Separation and Purification Technology*. 254, 117565. doi: 10.1016/j.seppur.2020.117565.

Stankovich, S., Dikin, D.A., Piner, R.D., Kohlhaas, K.A., Kleinhammes, A., Jia, Y., Wu, Y., Nguyen, S. T., Ruoff, R.S., 2007. Synthesis of graphene-based nanosheets via chemical reduction of exfoliated graphite oxide. *Carbon*. 45, 1558-1565. doi: 10.1016/j.carbon.2007.02.034.

Subedi, N., Lähde, A., Danso, E.A., Iqbal, J., Bhatnagar, A., 2019. A comparative study of magnetic chitosan (Chi@Fe<sub>3</sub>O<sub>4</sub>) and graphene oxide modified magnetic chitosan (Chi@Fe<sub>3</sub>O<sub>4</sub>GO) nanocomposites for efficient removal of Cr(VI) from water. *International Journal of Biological Macromolecules*. 137, 948-959. doi: 10.1016/j.ijbiomac.2019.06.151.

Tang, T., Cao, S., Xi, C., Chen, Z., 2021. Multifunctional magnetic chitosan-graphene oxide-ionic liquid ternary nanohybrid: An efficient adsorbent of alkaloids. *Carbohydrate Polymers*. 255, 117338. doi: 10.1016/j.carbpol.2020.117338.

Travlou, N.A., Kyzas, G.Z., Lazaridis, N.K., Deliyanni, E.A., 2013. Functionalization of Graphite Oxide with Magnetic Chitosan for the Preparation of a Nanocomposite Dye Adsorbent. *Langmuir*. 2013, 29, 1657-1668. doi: 10.1021/la304696y.

Umadevi, D., Sastry, G. N., 2011. Molecular and Ionic Interaction with Graphene Nanoflakes: A Computational Investigation of CO<sub>2</sub>, H<sub>2</sub>O, Li, Mg, Li<sup>+</sup>, and Mg<sup>2+</sup> Interaction with Polycyclic Aromatic Hydrocarbons. *The Journal of Physical Chemistry C*. 115, 9656-9667. doi: 10.1021/jp201578p.

Wang, D., Liu, L., Jiang, X., Yu, J., Chen, X., Chen, X., 2015. Adsorbent for p-phenylenediamine adsorption and removal based on graphene oxide functionalized with magnetic cyclodextrin. *Applied Surface Science*. 329, 197-205. doi: 10.1016/j.apsusc.2014.12.161.

Wang, S., Li, E., Li, J., Du, Z., Cheng, F., 2020. Preparation and coagulation-flocculation performance of covalently bound organic hybrid coagulant with excellent stability. *Colloids and Surfaces A*. 600, 124966. doi: 10.1016/j.colsurfa.2020.124966.

Wang, Y., Li, L., Luo, C., Wang, X., Duan, H., 2016. Removal of Pb<sup>2+</sup> from water environment using a novel magnetic chitosan/graphene oxide imprinted Pb<sup>2+</sup>. *International Journal of Biological Macromolecules*. 86, 505-511. doi: 10.1016/j.ijbiomac.2016.01.035.

Yang, F., Liu, Y., Gao, L., Sun, J., 2010. pH-Sensitive Highly Dispersed Reduced Graphene Oxide Solution Using Lysozyme via an in Situ Reduction Method. *J. Phys. Chem.* 114, 22085-22091. doi: 10.1021/jp1079636.

Zhang, H.P., Yang, B., Wang, Z.M., Xie, C., Tang, P., Bian, L., Dong, F., Tang, Y., 2019. Porous graphene oxide/chitosan nanocomposites based on interfacial chemical interactions. *European Polymer Journal*. 119, 114-119. doi: 10.1016/j.eurpolymj.2019.07.032.

Zhang, Q., Zhang, Y., Li, Y., Ding, P., Xu, S., Cao, J., 2021. Green synthesis of magnetite nanoparticle and its regulatory effect on fermentative hydrogen production from lignocellulosic hydrolysate by *Klebsiella* sp. *International Journal of Hydrogen Energy*. 46, 20413-20424. doi: 10.1016/j.ijhydene.2021.03.142.

Zuo, P.P., Feng, H.F., Xu, Z.Z., Zhang, L.F., Zhang, Y.L., Xia, W., Zhang, W.Q., 2013. Fabrication of biocompatible and mechanically reinforced graphene oxide-chitosan nanocomposite films. *Chemistry Central Journal*. 7, 39. doi: 10.1186/1752-153X-7-39.

## Capítulo 4. Estudo de adsorção do naftaleno em green mCS/GO

### Adsorption of naphthalene polycyclic aromatic hydrocarbon from wastewater by a green magnetic composite based on chitosan and graphene oxide<sup>5</sup>

Ruth Nóbrega Queiroz<sup>a</sup>, Meuris Gurgel Carlos da Silva<sup>a</sup>, Valmor Roberto Mastelaro<sup>c</sup>, Patrícia Prediger<sup>b</sup> and Melissa Gurgel Adeodato Vieira<sup>a\*</sup>

<sup>a</sup>Process and Product Development Department, School of Chemical Engineering, University of Campinas – UNICAMP, Albert Einstein Avenue, 500, 13083-852 Campinas, São Paulo, Brazil.

<sup>b</sup>School of Technology, University of Campinas – UNICAMP, 13484-332 Limeira, São Paulo, Brazil.

<sup>c</sup>São Carlos Institute of Physics, University of São Paulo, Av. Trabalhador São Carlense, 400, São Carlos, SP, 13566-590, Brazil.

\*melissag@unicamp.br

#### Abstract

A green magnetic composite mCS/GO was synthesized using water hyacinth extract, as a reducing agent, and proanthocyanidin, as a crosslinking agent, for the adsorption of naphthalene from effluents. The green composite was evaluated using different characterization techniques to determine its thermal (TG/DTG), structural (BET, XPS and FTIR), crystallographic (XRD) and textural (SEM) properties in natura and post-adsorption. The results obtained through a central composite design (CCD) experiment indicated that the initial concentration of NAP and the adsorbent dosage are significant for the adsorption capacity. The adsorption assays indicated that physisorption, through  $\pi$ - $\pi$  and hydrophobic interactions, were the main mechanism involved in the NAP adsorption. However, the adjustment to the PSO and Freundlich models, obtained through kinetic and equilibrium studies, indicated that chemisorption also influences the adsorptive process. The thermodynamic study indicated physisorption as the mechanism responsible for the NAP adsorption. Also, the adsorbent has high affinity for the adsorbate and the process is spontaneous and endothermic. The maximum adsorption capacity ( $q_{\max}$ ) of the green mCS/GO was 334.37 mg.g<sup>-1</sup> at 20 °C. Furthermore, the green mCS/GO was effectively

---

<sup>5</sup> Article submitted to the Environmental Science and Pollution Research on August 22<sup>th</sup>, 2022.

regenerated with methanol and reused for five consecutive cycles, the percentage of NAP recovery went from approximately 91% to 75% after the fifth cycle. The green composite was also applied in the adsorption of NAP from river water samples, aiming to evaluate the feasibility of the method in real applications. The adsorption efficiency was approximately 70%. From what we know, this is the first time that a green adsorbent was recycled after the polycyclic aromatic hydrocarbon (PAHs) adsorption process.

**Keywords:** Green nanomaterials; Graphene Oxide; Adsorption; Naphthalene; Regeneration; River water.

#### 4.1. Introduction

The pollutants, polycyclic aromatic hydrocarbons (PAHs), are generated through pyrogenic and petrogenic processes, mainly from the oil and gas industry. The presence of PAHs in industrial effluents, even in low concentrations, has a high toxic and contaminating potential, which can be harmful to the ecosystems, especially to the aquatic nature (Queiroz et al. 2022a).

Published studies seek to optimize wastewater treatment processes, including bioremediation (Shahsavari et al. 2019), membrane technology purification (Goswami et al. 2019), AOP's (Mokhtaria et al. 2021) and adsorptive processes (Song et al. 2021). Among those different treatment techniques, adsorption processes have stood out due to their low investment cost, can be used for low concentrations, applied in non-continuous and continuous processes and allows the regeneration of the adsorbent (Manousi et al. 2021). Graphene-based materials have stood out for presenting characteristics, such as thermal and mechanical resistance, high surface area and availability for the formation of  $\pi$ - $\pi$  stacking interactions, in addition to having an abundance of oxygenated functional groups, which contributes to improve the adsorption capacity of organic compounds, such as PAHs (Peng et al. 2022; Tong et al. 2022). Besides that, chitosan can be obtained mainly from chitin present in crustacean shells, presenting high biocompatibility and biodegradability, which makes it biologically and chemically acceptable for various applications (Li et al. 2021).

The association between graphene oxide (GO) and chitosan can modify the characteristics of GO, enhancing its thermal stability, surface area, as well as its performance in the adsorption of hydrophobic substances, such as aromatic pollutants, thus increasing the efficiency of the process (Neves et al. 2020). Furthermore, to improve the adsorption efficiency,

$\text{Fe}_3\text{O}_4$  nanoparticles can be incorporated into the composite to make it magnetic, facilitating its separation and post-process recovery (Manousi et al. 2021).

In the recent years, the application of green agents, such as botanical extracts and biopolymers, for the preparation of novel adsorbent composites has gained prominence, due to the relevance of the topic to the current context. Therefore, these agents have been applied to reduce the toxicity produced by the use of harmful chemical reagents in the conventional methodologies, in addition to make those processes more sustainable and efficient (Zhang et al. 2021). Although some recent studies report the application of green adsorbents to remove PAHs (Ruiz et al. 2020; Queiroz et al. 2022b), there are still gaps in the literature, especially with regard to the application of these materials to remediate petrochemical contaminants, such as PAHs. In addition, most of the methodologies currently published present complex, expensive synthesis steps that demand high energy consumption. Based on this, we believe that this paper can bring valuable contributions to the research area, since, as far as we are aware, none of these reports carried out a study on the regeneration of these green materials after the adsorption process of PAHs and application in real river water samples.

In this study, a green adsorbent composite (mCS/GO) was employed in the naphthalene (NAP) removal from residual water, aiming to optimize the adsorption process and evaluate the mechanisms involved. Different characterization methods evaluated the structural, textural, thermal and magnetic properties of the green composite before and post-adsorption process. The CCD experiment was carried out to optimize the adsorption operating conditions, thus determining the factors that directly influence the NAP adsorption process. Kinetic, isothermal and thermodynamic studies were performed to determine the mechanisms that govern the adsorption process. A regeneration study was carried out to assess the regeneration capacity of green mCS/GO over several adsorption cycles. In addition, the green composite was applied in the removal of NAP from river water, aiming to investigate the feasibility of its application in real effluents. From what we know, it is the first time that a green adsorbent was recycled after the NAP adsorption process.

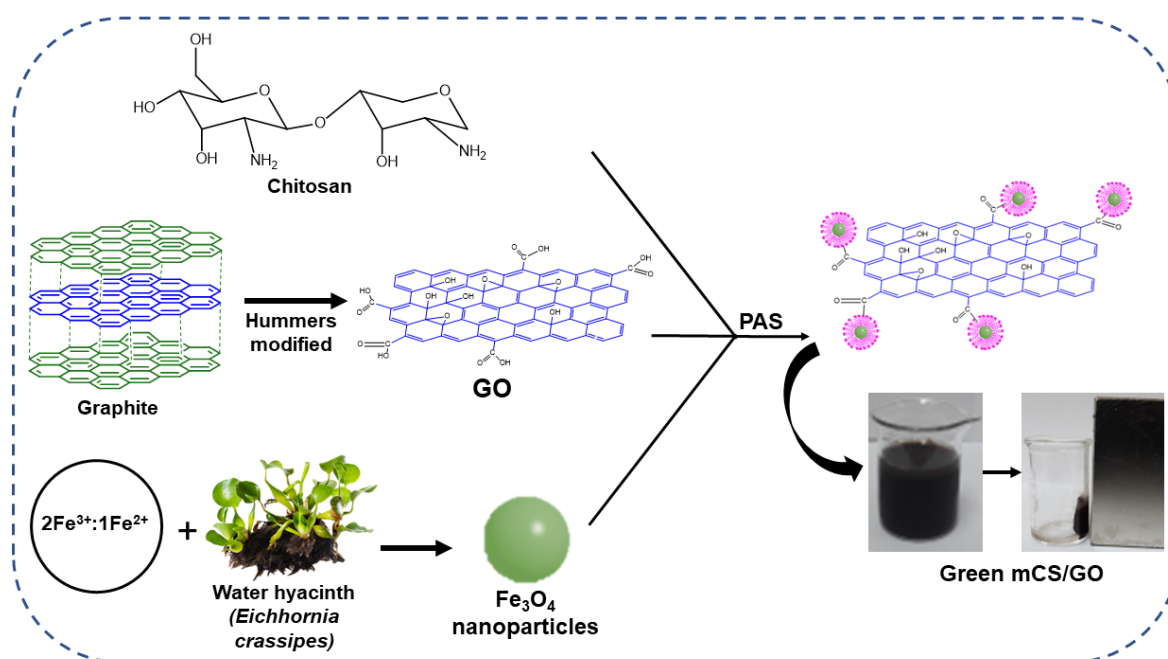
## **4.2. Methodology**

The reagents, materials and methodologies applied for the synthesis of the green composite mCS/GO are detailed in the Supplementary Material.

#### 4.2.1. Green mCS/GO synthesis

The synthesis of the green composite mCS/GO was performed in steps as shown in Fig. 4.1, according to the procedures reported by Queiroz et al. (2022b). The GO was produced following the methodology proposed by Hummers and Offeman (1958), using pre-oxidized graphite. Then, the synthesis of iron nanoparticles ( $\text{Fe}_3\text{O}_4$ ) was accomplished by using *Eichhornia crassipes* extract (water hyacinth) as a reducing/stabilizing agent, following the methodology by Zhang et al. (2021). The green composite mCS/GO was synthesized as reported by Queiroz et al. (2022b). In which, chitosan (CS), GO and green  $\text{Fe}_3\text{O}_4$  particles were synthesized using proanthocyanidin as a crosslinking agent, under mechanical agitation at 25 °C for 2 h. The material obtained was washed with ultrapure water and stored in the refrigerator.

**Figure 4.1.** Methodological representation of the preparation steps for the green mCS/GO.



#### 4.2.2. Characterization analysis

The green mCS/GO particles were characterized before and after the adsorption process of NAP, aiming to evaluate the physicochemical properties, as well as the mechanisms that govern the adsorption processes. The magnetic composites were also characterized after the regeneration process by FTIR and SEM techniques. The characterization techniques, as well as the operating conditions are described in Table 4.1.

**Table 4.1.** Green mCS/GO characterization techniques before and after the adsorptive process.

Technique	Equipment	Procedure
X-ray diffraction (XRD)	-	.
X-ray photoelectron spectroscopy (XPS)	XPS spectrometer (ScientaOmicron ESCA+) with a high-performance hemispheric analyzer (EAC2000), using the CASA XPS software.	Al K $\alpha$ ( $h\nu = 1486.6$ eV) radiation as the excitation source, $10^{-9}$ Pa. The XPS high-resolution spectra were recorded at constant pass energy of 20 eV with a 0.05 eV per step.
Fourier transform infrared spectroscopy (FTIR)	Thermo Scientific equipment (Nicolet 6700, Madison/USA).	KBr method, range 4000–400 $\text{cm}^{-1}$ , resolution 4 $\text{cm}^{-1}$ , and scan 32.
Raman spectroscopy	Witec (Ulm, Germany) equipped with Nikon lens (100xNA = 0.9)	The material was excited with an ion argon laser (514 nm; 10 mW) and the signal measured with a back-illuminated Peltier-cooled CCD with 600 grooves/mm.
Brunauer, Emmett and Teller method (BET)	ASAP 2010, Micromeritics (Austin, EUA)	Vacuum pre-treatment for 12h at 105°C and relative pressure ranging from 0.1 to 0.99.
Scanning Electron Microscopy (SEM)	Jeol model J6360 LV	A drop of the suspension containing the composites was placed on a silicon wafer and vacuum dried.
Thermogravimetric analysis (TG/DTG)	DTG-60, Shimadzu, Japan	N <sub>2</sub> atmosphere and flow of 50 mL.min <sup>-1</sup> , from 25 °C to 1000 °C with heating rate of 10 °C.min <sup>-1</sup> .

#### 4.2.3. CCD experiment

The central composite design (CCD) experiment was performed to investigate the operational parameters that influence the adsorption process of PAH (naphthalene) from wastewater. The adsorbent dosage (green mCS/GO), pH and initial concentration of adsorbate in the solution had their effect evaluated in the removal process of naphthalene (NAP) from a synthetic effluent. The experimental conditions evaluated in the CCD experiment are described

in Table 4.2. For the central points, 3 repetitions were performed with central level (0). Finally, the axial points were individually varied between  $-\alpha$  to  $+\alpha$ .

**Table 4.2.** Experimental conditions investigated in the central composite design.

Factor	Units	Levels				
		$-\alpha$	Low (-1)	Central (0)	High (+1)	$+\alpha$
A	mmol.L <sup>-1</sup>	0.0103	0.0156	0.0234	0.0312	0.0365
B	mg.mL <sup>-1</sup>	0.132	0.2	0.3	0.4	0.468
C	-	4.64	6	8	10	11.36

A: initial concentration of adsorbate (NAP);

B: adsorbent dosage (green mCS/GO);

C: pH.

Experimental conditions: 30 min, 200 rpm and 25 °C.

According to the CCD matrix, 17 assays were performed at 25 °C, under constant agitation at 200 rpm for 30 min, as presented in Table 3. The effect of experimental factors on the response variable (adsorption capacity - mmol.g<sup>-1</sup>) was analyzed by a statistical study carried out in Minitab® 17 software, applying a 95% confidence level and taking into account residual errors. The empirical mathematical models, as well as the analysis of variance (ANOVA), were evaluated considering only the influence of significant terms ( $p < 0.05$ ).

**Table 4.3.** Central composite design (CCD) matrix of experiments.

Assays	Factors			Response variable	
	A	B	C	Adsorption capacity (mmol.g <sup>-1</sup> )	Removal efficiency (%)
1	0.0156	0.2000	6.0000	0.0744	95.3223
2	0.0312	0.2000	6.0000	0.1514	97.0063
3	0.0156	0.4000	6.0000	0.0378	96.8767
4	0.0312	0.4000	6.0000	0.0757	97.0551
5	0.0156	0.2000	10.0000	0.0748	95.8642
6	0.0312	0.2000	10.0000	0.1505	96.4722
7	0.0156	0.4000	10.0000	0.0375	96.1942
8	0.0312	0.4000	10.0000	0.0755	96.7130
9	0.0234	0.3000	4.6400	0.0755	96.8019
10	0.0234	0.3000	11.3600	0.0750	96.1222
11	0.0234	0.1320	8.0000	0.1694	95.5496
12	0.0234	0.4680	8.0000	0.0485	97.0712
13	0.0103	0.3000	8.0000	0.0325	94.5988
14	0.0365	0.3000	8.0000	0.1186	97.4053
15	0.0234	0.3000	8.0000	0.0751	96.2019
16	0.0234	0.3000	8.0000	0.0751	96.2221
17	0.0234	0.3000	8.0000	0.0751	96.2437

A: initial concentration of adsorbate (NAP) – mmol.L<sup>-1</sup>;

B: adsorbent dosage (green mCS/GO) – mg.mL<sup>-1</sup>;

C: pH.

#### 4.2.4. Adsorption assays

The adsorptive assays of the NAP onto the green adsorbent were conducted, in a shaker (SI-600R - Jeio Tech), according to the optimized operating conditions obtained through the CCD experiment. The NAP working solution was prepared by diluting the stock solution (10 mg.L<sup>-1</sup>). The stock solution was prepared using methanol as a solvent, with a ratio of 4% CH<sub>3</sub>OH: 96% H<sub>2</sub>O. The working solution was prepared daily before the adsorptive experiments.

The removal percentage of NAP (%R) and the  $q_t$  were estimated by the Equations (1) and (2), respectively:

$$\%R = \frac{(C_0 - C_t)}{C_0} \cdot 100 \quad (1)$$

$$qt = \frac{(C_0 - C_t)}{m} \cdot V \quad (2)$$

Where,  $qt$  is the adsorption capacity ( $\text{mmol.g}^{-1}$ ),  $V$  is the volume (L),  $C_0$  is the initial NAP concentration ( $\text{mmol.L}^{-1}$ ),  $C_t$  is the NAP concentration at a given time ( $\text{mmol.L}^{-1}$ ) and  $m$  is the green adsorbent mass (g).

#### 4.2.4.1. Kinetic study

The adsorptive kinetics assays of NAP onto mCS/GO were conducted in a batch system at 25 °C, under agitation at 200 rpm, mCS/GO dosage of  $0.15 \text{ mg.mL}^{-1}$  and pH 6.5. The assays were performed in three different initial concentrations of NAP (2.5, 4.5 and  $5.5 \text{ mg.L}^{-1}$  or 0.0195, 0.0351 and  $0.0429 \text{ mmol.L}^{-1}$ ). Samples were taken at time intervals from 0 to 100 min. Following this step, the material was isolated from the solution by using a magnet and the supernatant was agitated at 6000 rpm for 15 min. The samples were filtered with a  $0.45 \mu\text{m}$  PTFE syringe filter and their final NAP concentration was quantified. The obtained data were adjusted to the kinetic models, PFO, PSO, IP and EMTR (Table 4).

Mathematical adjustments to the kinetic curves were performed by using the OriginPro8® and Maple17® software, from which it is possible to assess the mechanisms involved in the NAP adsorption.

**Table 4.4.** Kinetics and equilibrium models.

Models	Equation	Parameters
Pseudo-First Order - PFO (Lagergren, 1898)	$q(t) = q_e(1 - e^{-k_1 t})$	$k_1$ is the PFO rate constant ( $\text{min}^{-1}$ ).
Pseudo-Second Order - PSO (Ho and McKay, 1999)	$q(t) = \frac{k_2 q_e^2 t}{1 + k_2 q_e t}$	$k_2$ is the PSO rate constant ( $\text{g.mg}^{-1}.\text{min}^{-1}$ ).
Intraparticle diffusion - IP (Weber and Morris, 1963)	$q(t) = k_i t^{0.5} + I$	$k_i$ is the intraparticle diffusion rate constant ( $\text{g.mmol}^{-1}.\text{min}^{-0.5}$ ); $I$ is the linear coefficient of the model ( $\text{mmol.g}^{-1}$ ).
External Mass Transfer Resistance - EMTR (Puranik et al., 1999)	$\frac{dC}{dt} = -k_{TM}(C_t - C_p(t))$	$k_{TM}$ is the external mass transfer resistance ( $\text{min}^{-1}$ ); $C_p$ is the adsorbate concentration at the interface between the liquid and the adsorbent as a function of time ( $\text{mmol.L}^{-1}$ ).
Langmuir (1918)	$q_e = \frac{q_{max} k_L C_e}{1 + k_L C_e}$	$k_L$ is the Langmuir equilibrium constant associated with the affinity of the sites ( $\text{L.mmol}^{-1}$ ).
Freundlich (1906)	$q_e = k_F C_e^{\frac{1}{n}}$	$k_F$ is the Freundlich constant [( $\text{mmol.g}^{-1}$ ).( $\text{L.mmol}^{-1}$ ) $^{1/n}$ ]; $n$ is the empirical constant associated with the adsorption intensity (dimensionless).
Dubinin-Radushkevich (1947)	$q_e = q_m e^{-k_{DR} \varepsilon^2}$	$k_{RD}$ is the constant associated with the adsorption energy ( $E$ ) ( $\text{mol}^2.\text{J}^{-2}$ ); $\varepsilon$ is the Polanyi potential ( $\text{J.mol}^{-1}$ ).

$q_e$ : adsorbate concentration in equilibrium on the adsorbent surface ( $\text{mmol.g}^{-1}$ );

$q_{max}$ : maximum adsorption capacity ( $\text{mmol.g}^{-1}$ );

$C_e$ : equilibrium concentration of the adsorbate ( $\text{mmol.L}^{-1}$ );

$q_m$ : adsorption capacity related to the micropore volume ( $\text{mmol.g}^{-1}$ );

#### 4.2.4.2. Equilibrium study

The equilibrium assays was performed in a shaker with different NAP concentrations (0.5, 1, 2, 3, 4, 5 and 6  $\text{mg.L}^{-1}$ ), under agitation at 200 rpm, mCS/GO dosage of 0.15  $\text{mg.mL}^{-1}$

and pH 6.5. The assays were carried at 20 °C, 30 °C and 40 °C and the samples were kept under constant agitation for 1 h until reaching equilibrium. The green material was recovered by using a magnet and the supernatant was centrifuged at 6000 rpm for 15 min. Then, the samples were filtered with a 0.45 µm PTFE syringe filter and their final NAP concentration was quantified. The data were adjusted to the isotherm models, as presented in Table 4.

Mathematical adjustments to the isotherm models were carried out by using the OriginPro8® software, from which it is possible to determine the nature of the adsorptive processes.

#### 4.2.4.3. Regeneration study

The desorption experiments, followed by adsorbent regeneration, were performed following the methodology by Chen et al. 2018, Zhou et al. 2019 and Song et al. 2021. Initially, 30 mg of the magnetic adsorbent were added to 25 mL of NAP solution (8 mg.L<sup>-1</sup>) and the sample was agitated in the shaker at 25 °C until it reached equilibrium (approximately 1h). Then, magnetic separation of the adsorbent was performed and the supernatant was agitated at 6000 rpm for 15 min and then its concentration was quantified by HPLC analysis. Then, the material was subjected to a desorption process with 3 mL of different organic solvents (methanol, acetonitrile, acetone and ethanol) in an ultrasound bath for 5 min. Then, the material washing step with deionized water was performed in an ultrasound bath for 1 min. The regenerated adsorbent was reused for five subsequent adsorption cycles. The supernatant of the desorption process was collected, centrifuged at 6000 rpm for 15 min, filtered with a PTFE (0.45 µm) syringe filter and its concentration was quantified by HPLC analysis. The percentage of NAP recovery in each regeneration cycle was quantified through Equation (3):

$$\%recovery = \frac{C_f}{C_i} \cdot 100\% \quad (3)$$

Where,  $C_f$  is the post-desorption NAP concentration and  $C_i$  is the initial NAP concentration, both in (mmol.L<sup>-1</sup>).

#### 4.2.5. HPLC quantification analysis

PAH was quantified by using a HPLC system (Shimadzu), at 25 °C, equipped with SPD-10AV UV-Vis detector. Separations were performed by a C18 column (5 µm, 150 mm x 4.6 mm) (Phenomenex). The samples were manually injected with a volume of 25 µL. A mobile

phase of 15% deionized water and 85% methanol (15% H<sub>2</sub>O: 85% CH<sub>3</sub>OH) was applied, with a 1 mL.min<sup>-1</sup> and 254 nm wavelength. Chromatographic signals were analyzed using the LC Solution® software. The validation of the analytical method was carried out according to the criteria established by the Institute of Metrology, Standardization and Industrial Quality (INMETRO), according to DOQ-CGCRE-008/2020. The following parameters were evaluated: Selectivity (Fig. S1), LOD, LOQ, linearity, repeatability and accuracy. More information on the validation parameters evaluated in this work can be found in the Supplementary Material.

### **4.3. Results and discussion**

#### **4.3.1. Adsorbent characterizations before and after NAP adsorption**

The BET isotherms, as well as the pore size distribution of the green mCS/GO, pure and post-adsorption are displayed in Fig. 4.2. According to the results presented in Fig. 4.2a, the isotherms obtained can be classified as type II, which can be observed in macroporous and mesoporous materials, that show strong interaction between the adsorbent and NAP (Aranovich and Donohue, 1998). In this type of isotherms is observed the formation of monolayers followed by the formation of multilayers on the surface of the material. The results also indicated the presence of an H3 hysteresis loop, which is characteristic of plate-like particle aggregation. In addition, a greater opening of the hysteresis loop is observed in regions with relative pressure close to 1.0, which indicates the presence of mesopores (Zhou et al., 2012; Cychosz et al., 2017). The superficial area and pore volume of the green composite before and post-adsorptive process are shown in Table 4.5.

**Figure 4.2.** BET isotherms (a) and pore size distribution (b) of green mCS/GO and green mCS/GO+NAP.

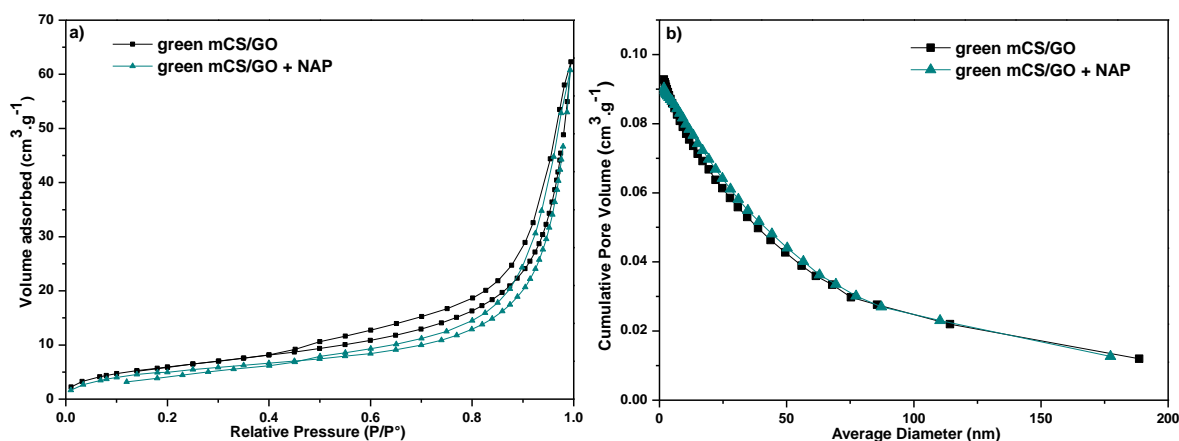


**Table 4.5.**  $SSA_{BET}$ , pore volume and diameter of green mCS/GO before and after NAP adsorption.

Samples	$SSA_{BET}^a$ ( $m^2.g^{-1}$ )	$V_{micro}^b$ ( $cm^3.g^{-1}$ )	$V_{meso}^c$ ( $cm^3.g^{-1}$ )	$V_{macro}^c$ ( $cm^3.g^{-1}$ )	Average pore diameter (nm)
green mCS/GO	22.8358	0.0030	0.0827	0.0137	14.4964
green mCS/GO + NAP	19.4064	0.0022	0.0692	0.0239	14.2685

<sup>a</sup>Brunauer-Emmet-Teller method;

<sup>b</sup>t-plot method;

<sup>c</sup>Barrett-Joyner-Halenda method.

In the isotherms obtained (Fig. 4.2a), the presence of three distinct regions can also be observed. The first region, at low relative pressures, ( $P/P_0 < 0.2$ ), corresponds to the adsorption of  $N_2$  in the monolayer, indicating the occupation of the micropore volume by the NAP molecules. The second region, in which, ( $P/P_0 = 0.4 - 0.8$ ), occurs the formation of multilayers and capillary condensation characteristic of mesoporous materials. In this region, a slow linear growth is observed, which suggests that the presence of mesopores is predominant on the surface of the material. Finally, in the third region ( $P/P_0 > 0.8$ ), adsorption occurs in the multilayers on the external surface of the material, which suggests the presence of macropores (Soboleva et al., 2010).

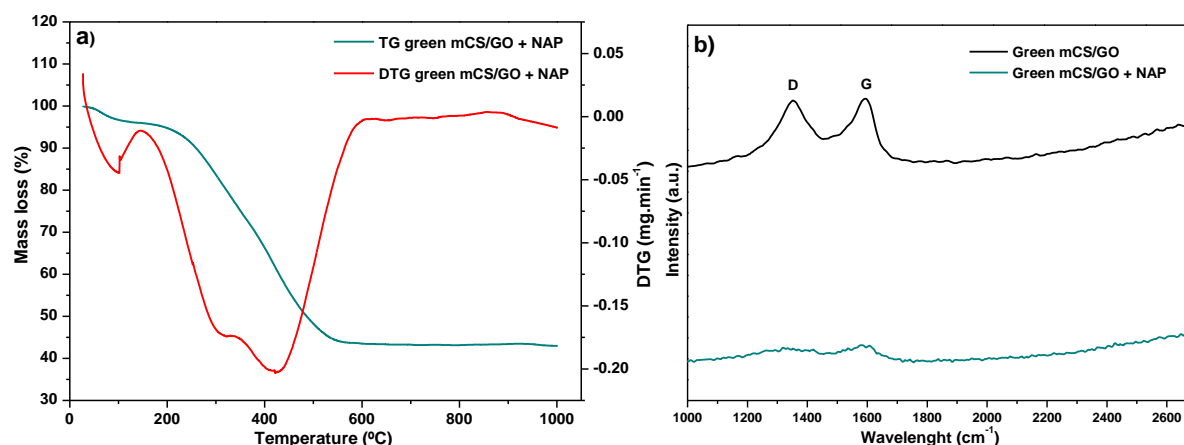
Based on the results presented in Table 4.5, a  $SSA_{BET}$  of 22.8358 and 19.4064  $m^2.g^{-1}$  was obtained through the BET method for green mCS/GO and green mCS/GO+NAP, respectively. The decrease in the  $SSA_{BET}$  observed for the green mCS/GO+NAP is associated with the occupation of the material surface by the NAP after the adsorptive process (Cui et al, 2015). It was also observed a decrease in the volume of mesopores from 0.0827 to 0.0692  $cm^3.g^{-1}$  after naphthalene adsorption. The pore size distribution (Fig. 4.2b) showed that the composite

consists predominantly of mesopores and macropores, moreover, the presence of micropores (< 2 nm) was also observed (Yang et al., 2018).

The thermal stability of the green mCS/GO were assessed by analyzing the thermogravimetric curve shown in Fig. 4.3a. The mass loss percentage (%) occurred through two distinct stages. For temperature region from 28 °C to 146 °C, an initial mass loss of 3.96% is observed, which is associated with the evaporation of surface water present on the material. In the second region (146 °C – 672 °C), a greater material loss of 52.53% was observed, which is related to the oxygenated functional groups decomposition, organic matter associated with NAP molecules, nitrogen compounds of chitosan, as well as the degradation of iron particles stabilized with biomolecules from plant extract (Bai et al., 2021; Inbaraj et al., 2021). For temperatures above 700 °C, there was a mass loss of less than 2%. Through the analysis of the thermogravimetric results, the material showed high thermal stability even after the NAP adsorption process.

Through the Raman spectra, it is possible to determine the structural changes of the green mCS/GO composite before and after the adsorptive process, as shown in Fig. 4.3b. The results of the spectral measurements indicate the presence of the characteristic bands D and G at approximately 1350 and 1589  $\text{cm}^{-1}$  for the green mCS/GO, respectively. These bands are commonly associated with carbonaceous materials, such as graphene-based materials, to investigate the ordered and disordered structures of carbon (Yang et al., 2018). The D band refers to the structural disorder associated with  $\text{sp}^3$  hybridized carbon bonds, while the G band refers to the  $\text{sp}^2$  hybridized carbon network (Rebekah et al., 2021). The presence of the characteristic bands corresponds to the degree of disorder of the GO structure, the higher this ratio, the greater the degree of disorder in the material structure (Zhang et al., 2018). The  $I_D/I_G$  values for the green mCS/GO and green mCS/GO + NAP are 0.9960 and 0.9993, respectively. After the NAP adsorption process, there was a slight increase in the  $I_D/I_G$  ratio, which is associated with the increase in  $\text{sp}^3$  hybridized carbon bonds, which can generate defects in the aromatic structure of the post-process material (Prediger et al., 2018).

**Figure 4.3.** Thermogravimetric curves (a) and Raman spectrum (b) of green mCS/GO and green mCS/GO + NAP.

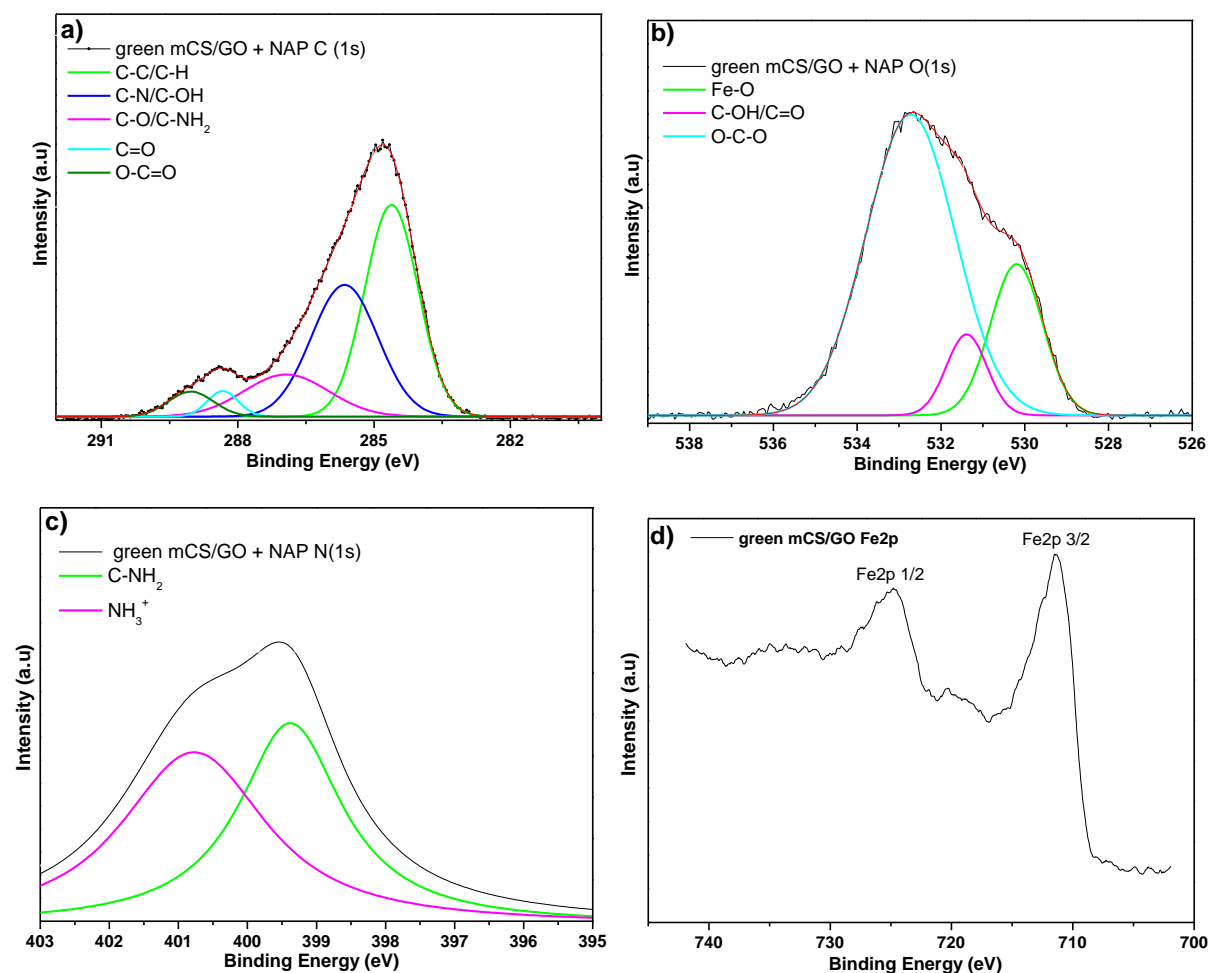


XPS analysis can specify the chemical composition and the functional groups present in the green mCS/GO samples after the NAP adsorption process. The survey of the mCS/GO + NAP is displayed in Fig. S2, through which the characteristic peaks of GO can be observed and also the indicative of the presence of NAP in the material's structure, such as C(1s) at 286.4 eV and O(1s) at 530.8 eV. The survey also showed the peaks of N(1s) at 401.6 eV and Fe(2p) at 711.1 and 725.1 eV, related with the chitosan and iron particles, respectively, in the composite structure (Almeida et al., 2022). Through this analysis, the elemental composition of the evaluated elements C, O, N and Fe was also determined. The results indicated an elemental composition of C (70.4%) and O (25.6%), comparing these values with the results reported by Queiroz et al. (2022b), there was an increase in the composition of C and a decrease in the composition of O, which is associated with GO and the presence of NAP on the material after the adsorption process. Furthermore, the decrease in O composition can be attributed to the NAP present on the surface of the material, through the formation of bonds with the oxygenated groups in  $sp^3$  regions (Yao et al., 2020). The results also indicated the presence, in smaller amounts, of N (1.5%) and Fe (2.5%), associated with the presence of CS and  $Fe_3O_4$ .

The XPS C(1s) high-resolution of green mCS/GO + NAP (Fig. 4.4a) showed characteristic peaks at 284.6, 285.7, 286.7, 288.3 and 289.3 eV, related with carbon functional groups C-C/C-H (50.7%), C-N/C-OH (25.9%), C-O/C-NH<sub>2</sub> (11.5%), C=O (9.1%) and O-C=O (2.7%), respectively (Almeida et al., 2022). The O(1s) high-resolution (Fig. 4.4b) showed peaks at 530.3, 531.9 and 533.3 eV, which are related to the groups Fe-O (26.8%), C=O (35.9%) and O-C-O (37.3%), respectively (Liu et al., 2022). The N(1s) high-resolution (Fig. 4.4c) showed peaks at 399.7 and 401.2 eV, which correspond to C-NH<sub>2</sub> (69.9%) and NH<sub>3</sub><sup>+</sup> (30.1%), which are attributed to the CS present in the material's structure (Li et al., 2021). The Fe (2p) high-

resolution (Fig. 4.4d), showed peaks at 711.4 and 724.8 eV, related with Fe 2p<sup>3/2</sup> and Fe 2p<sup>1/2</sup>, respectively, indicating that the material remained magnetized after the adsorptive process (Tang et al., 2021).

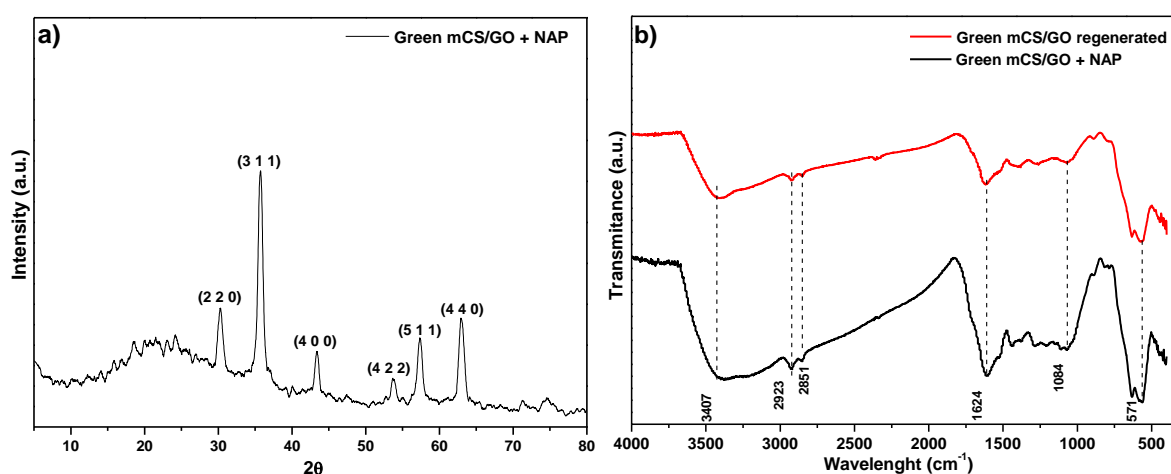
**Figure 4.4.** High-resolution of C(1s) (a); O(1s) (b); N(1s) (c) and Fe(2p) (d).



The XRD green mCS/GO diffractograms after the NAP adsorption is shown in Fig. 4.5a. The XRD pattern analysis indicated the presence of diffraction peaks at  $2\Theta = 30.2^\circ$ ,  $35.7^\circ$ ,  $43.3^\circ$ ,  $53.6^\circ$ ,  $57.3^\circ$  and  $62.9^\circ$ , which are attributed to the characteristic crystalline planes of the cubic structure of Fe<sub>3</sub>O<sub>4</sub> in (2 2 0), (3 1 1), (4 0 0), (4 2 2), (5 1 1) and (4 4 0), respectively (Abbasabadi and Azarifar, 2019; Manousi et al., 2021). This result indicates that even after the adsorption process, Fe<sub>3</sub>O<sub>4</sub> particles preserved their crystalline structure, thus maintaining their magnetic properties, which facilitates their recovery from the green material after the NAP adsorption (Majd and Nojavan, 2021). Comparing the results obtained in this study with those reported by Queiroz et al. (2022b), it is observed that the NAP adsorption did not generate changes in the crystalline structure and properties of the material after the treatment process.

Fig. 4.5b shows the green mCS/GO FT-IR after NAP adsorption and after the fifth regeneration cycle. The spectra showed a peak up to  $3407\text{ cm}^{-1}$ , which represents the bonding of the amine groups NH associated with the chitosan present in the structure of the material and OH associated with GO (Naing et al., 2016). The spectra also showed peaks at 2923, 2851 and  $571\text{ cm}^{-1}$ , which corresponds with the C-H bonds related with the groups present in oleic acid and *Eichhornia crassipes* extract that act as reducing agents in the synthesis of  $\text{Fe}_3\text{O}_4$  magnetic particles, thus indicating that the adsorptive process did not change the magnetic properties of the material (Manousi et al., 2021). The peaks at 1624 and  $1084\text{ cm}^{-1}$  are related with C=O and C-O, confirming the presence of -COOH and C-O-C, which confirms the abundance of oxygenated functional groups on the material's surface after the adsorption process (Bulin et al., 2020; Song et al., 2021). Comparing the results obtained in this study with those reported by Queiroz et al. (2022b), a slight change in the position and intensity of the peaks is observed after the adsorption, which can be attributed to the NAP on the composite surface. Furthermore, it is observed that after the 5<sup>th</sup> cycle of regeneration the intensity of the bands decreased, which may be associated with the reduction of the intensity of the oxygenated functional groups, which may have been caused by wear on the surface of the material due to the regeneration cycles to which the same was submitted.

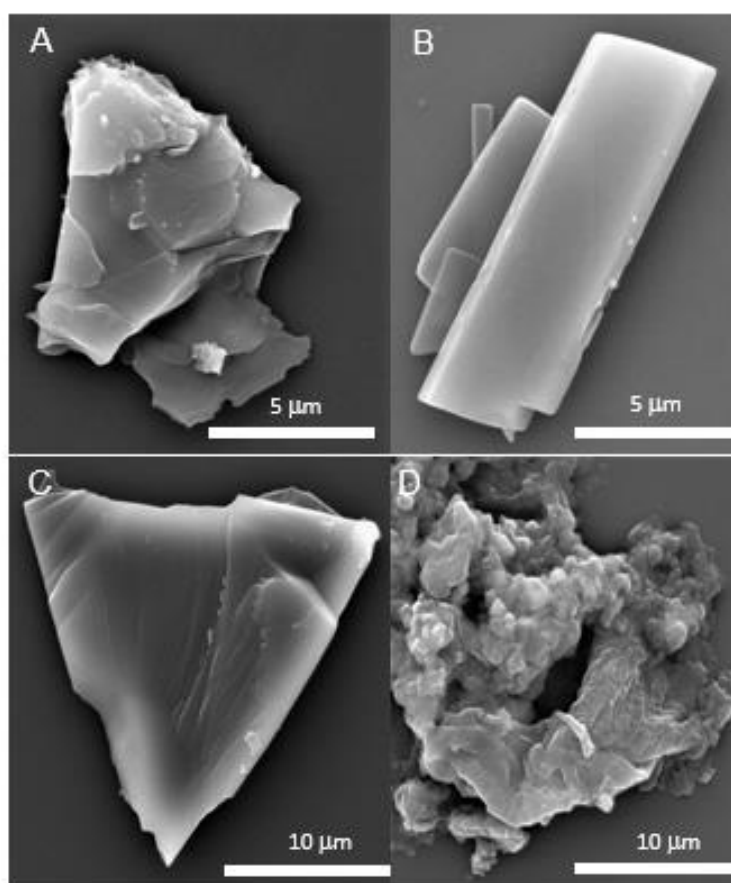
**Figure 4.5.** XRD patterns of green mCS/GO + NAP (a) and FT-IR spectra of green mCS/GO + NAP (black line) and regenerated green mCS/GO + NAP (red line).



The micrographs of the green mCS/GO after NAP adsorption and after the regeneration cycles are shown in Fig. 4.6. The micrographs of the green mCS/GO + NAP (Fig. 4.6a-b) show the form of a planar nanosheet-shaped layers with a wrinkled surface. Comparing the micrographs before adsorption (Queiroz et al., 2022b) and with NAP-loaded, it can be observed

a decrease in wrinkles on the surface of the material, such a change may be associated with the adsorption process of NAP, which may have resulted in a decrease in adsorption sites. Furthermore, the honeycomb-shaped molecular structure of NAP, which is also similar to the structure of graphene, may have been responsible for this change in the material's surface structure. A comparable result was obtained in the studies by Song et al. (2021), after anthracene adsorption onto nitrogen-doped reduced graphene oxide materials. Fig. 4.6c-d show the micrographs of the green mCS/GO regenerated after the fifth adsorption cycle, through which an increase in roughness on the composite surface is observed. Besides, no significant abrasion was verified, which indicates that the material has the potential for regeneration, and can be used for different adsorption cycles.

**Figure 4.6.** SEM images of green mCS/GO + NAP (a-b) and green mCS/GO + NAP regenerated (c-d).



### 4.3.2. Statistical analysis

Through the ANOVA analysis it is possible to evaluate the effects of experimental parameters on the response variable (Y - adsorption capacity). Through the statistical parameters, F-value and P-value, the significance of the terms and the model fitting are determined (Table 4.6). The higher F-value provides a higher precision of the data, whereas for  $P\text{-value} \leq 0.05$ , the terms are significant (Yaqubzadeh et al., 2016).

**Table 4.6.** Results of ANOVA for quadratic model.

Factor	df	Sum of Squares	Mean Square	F-value	P-value	
Model	10	0.026139	0.002614	66.85	0.000	Significant
A	1	0.010208	0.010208	261.04	0.000	Significant
B	1	0.013407	0.013407	342.86	0.000	Significant
C	1	0.000000	0.000000	0.01	0.937	Not Significant
AB	1	0.000737	0.000737	18.85	0.005	Significant
AC	1	0.000000	0.000000	0.00	0.948	Not Significant
BC	1	0.000000	0.000000	0.00	1.000	Not Significant
A <sup>2</sup>	1	0.000135	0.000005	0.14	0.723	Not Significant
B <sup>2</sup>	1	0.001566	0.001338	34.21	0.001	Significant
C <sup>2</sup>	1	0.000007	0.000007	0.17	0.690	Not Significant
Residual	6	0.000235	0.000039			
Lack of fit	4	0.000235	0.000059			
Total	16	0.026374				

A: initial concentration of adsorbate (NAP);

B: adsorbent dosage (green mCS/GO);

C: pH;

df: degrees of freedom;

$R^2 = 0.9911$

$\text{Adj-}R^2 = 0.9763$

The F value of 66.85 indicates that the model is significant, in addition the significant terms, with  $P\text{-value} \leq 0.05$ , indicate that the model is quadratic. The coefficient of determination ( $R^2=0.9911$ ) indicates a high fit to the data. The coded regression model, considering only the significant terms, is described by Equation (4):

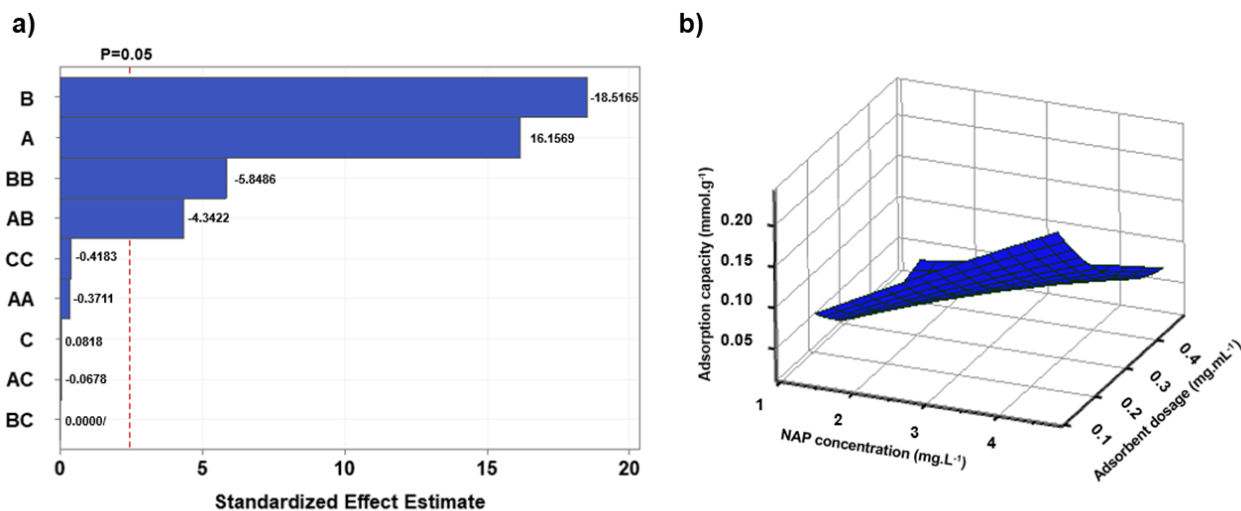
$$Y = 8.17 \times 10^{-2} + 6.1 \times 10^{-2}A - 6.93 \times 10^{-1}B - 9.6 \times 10^{-2}AB + 1.113B^2 \quad (4)$$

Where,  $Y$  in  $\text{mmol.g}^{-1}$ ,  $A$  is the NAP concentration ( $\text{mg.L}^{-1}$ ) and  $B$  is the green mCS/GO dosage ( $\text{mg.mL}^{-1}$ ).

The significance, as well, the intensity of the effect of the factors on the response variable were analyzed according to the Pareto chart (Fig. 4.7a). The factors CC, AA, C, AC and BC are below the reference line, thus indicating the minimal contribution and the non-significant effect of these factors on adsorption capacity. The factors B, A, BB and AB had a significant effect on the response variable, for the 95% confidence interval. Positive coefficients for the model terms indicate that the effect is favorable or synergistic for the NAP adsorption. Besides that, negative coefficients indicate that the effect is unfavorable or antagonistic to the process (Ghaedi et al., 2016). Thus, the linear term B has a greater negative influence on the process, that is, the lower the adsorbent dosage, the greater is the adsorption capacity. The quadratic term ( $B^2$ ) and the AB term also had a negative influence on the process. The linear term (A) has a positive influence on the process, thus indicating that the increase of the NAP concentration contributes to increase  $Y$ .

The Normal Probability and the Internally Studentized Residuals charts, shown in Fig. S2 (a-b), suggest an acceptable adequacy between the data and the model. The response surface for  $Y$  ( $\text{mmol.g}^{-1}$ ) as a function of NAP concentration ( $\text{mmol.L}^{-1}$ ) and adsorbent dosage ( $\text{mg.mL}^{-1}$ ), is displayed in Fig. 4.7(b). It is observed that a higher adsorption capacity is obtained as the adsorbent dosage decreases and the NAP concentration increases, which suggests that the available adsorption sites on the surface of the material were not completely saturated. These results indicate that the material has a high superficial area and a greater number of adsorption sites available for capturing PAHs (Tang et al., 2021). In addition, the ideal experimental conditions obtained through simulation in the Minitab® 17 software are: NAP concentration of  $4.5 \text{ mg.L}^{-1}$ , mCS/GO dosage of  $0.15 \text{ mg.mL}^{-1}$  and neutral pH (approximately 7.0).

**Figure 4.7.** Pareto Chart (a) and Response surface for Y ( $\text{mmol.g}^{-1}$ ) as a function of NAP concentration ( $\text{mmol.L}^{-1}$ ) and mCS/GO dosage ( $\text{mg.mL}^{-1}$ ).



#### 4.3.3. Adsorption kinetics

The kinetic study was conducted to examine the mechanisms that govern the adsorptive process. The study was performed for different NAP concentrations 0.0195, 0.0351 and 0.0429  $\text{mmol.L}^{-1}$ , as shown in Fig. 4.8(a). The kinetic curves indicate that the adsorption capacity ( $q_t$ ) increases rapidly in the first 10 min until the equilibrium at approximately 40 min, indicating a fast NAP adsorption. The fast adsorption rate is attributed to the structure and molecular size of NAP, giving it a greater affinity with the adsorbent, thus contributing to the adsorption process. This kinetic behavior was also studied by Haro et al. (2011) and Eeshwarasinghe et al. (2018), who attribute this behavior to the molar volume and molecular structure of NAP, when compared to other PAHs. The adsorbent equilibrium adsorption capacity ( $q_e$ ) was 0.1165, 0.2074, 0.2580  $\text{mmol.g}^{-1}$  for each concentration, respectively. The adjustment parameters for the PFO, PSO, EMTR and IP kinetic models are presented in Table 4.7.

**Table 4.7.** Fit parameters of kinetic models PFO, PSO, EMTR and IP.

Model	Parameter	C <sub>0</sub> = <b>0.0195</b> mmol.L <sup>-1</sup>	C <sub>0</sub> = <b>0.0351</b> mmol.L <sup>-1</sup>	C <sub>0</sub> = <b>0.0429</b> mmol.L <sup>-1</sup>
PFO	q <sub>e</sub> calc (mmol.g <sup>-1</sup> )	0.1136	0.2060	0.2472
	q <sub>e</sub> exp (mmol.g <sup>-1</sup> )	0.1165	0.2074	0.2580
	k <sub>1</sub> (min <sup>-1</sup> )	1.0111	1.4507	2.3078
	R <sup>2</sup>	0.9553	0.9678	0.7465
	AICc	-107.45	-119.11	-86.42
PSO	<b>q<sub>e</sub> calc (mmol.g<sup>-1</sup>)</b>	<b>0.1174</b>	<b>0.2090</b>	<b>0.2490</b>
	<b>q<sub>e</sub> exp (mmol.g<sup>-1</sup>)</b>	<b>0.1165</b>	<b>0.2074</b>	<b>0.2513</b>
	<b>k<sub>2</sub> (g.mmol<sup>-1</sup>.min<sup>-1</sup>)</b>	<b>1.6799</b>	<b>3.1630</b>	<b>7.8730</b>
	<b>R<sup>2</sup></b>	<b>0.9914</b>	<b>0.9566</b>	<b>0.8826</b>
	AICc	-126.18	-116.97	-111.17
EMTR	q <sub>e</sub> calc (mmol.g <sup>-1</sup> )	0.1151	0.2076	0.2488
	q <sub>e</sub> exp (mmol.g <sup>-1</sup> )	0.1165	0.2074	0.258
	k <sub>TM</sub> (min <sup>-1</sup> )	0.5188	0.6860	0.7906
	R <sup>2</sup>	0.9704	0.9618	0.9354
	AICc	-115.96	-146.51	-85.25
IP	k <sub>i</sub> (g.mmol <sup>-1</sup> .min <sup>-0.5</sup> )	0.0187	0.0240	0.0046
	I (mmol.g <sup>-1</sup> )	0.0573	0.1377	0.2212
	R <sup>2</sup>	0.9505	0.9566	0.892

$$AICc \text{ is the Akaike information criteria: } AICc = N \cdot \ln \left[ \frac{\sum_{i=1}^N (q_{exp} - q_{calc})^2}{N} \right] + 2p + \frac{2p(p+1)}{N-p-1}$$

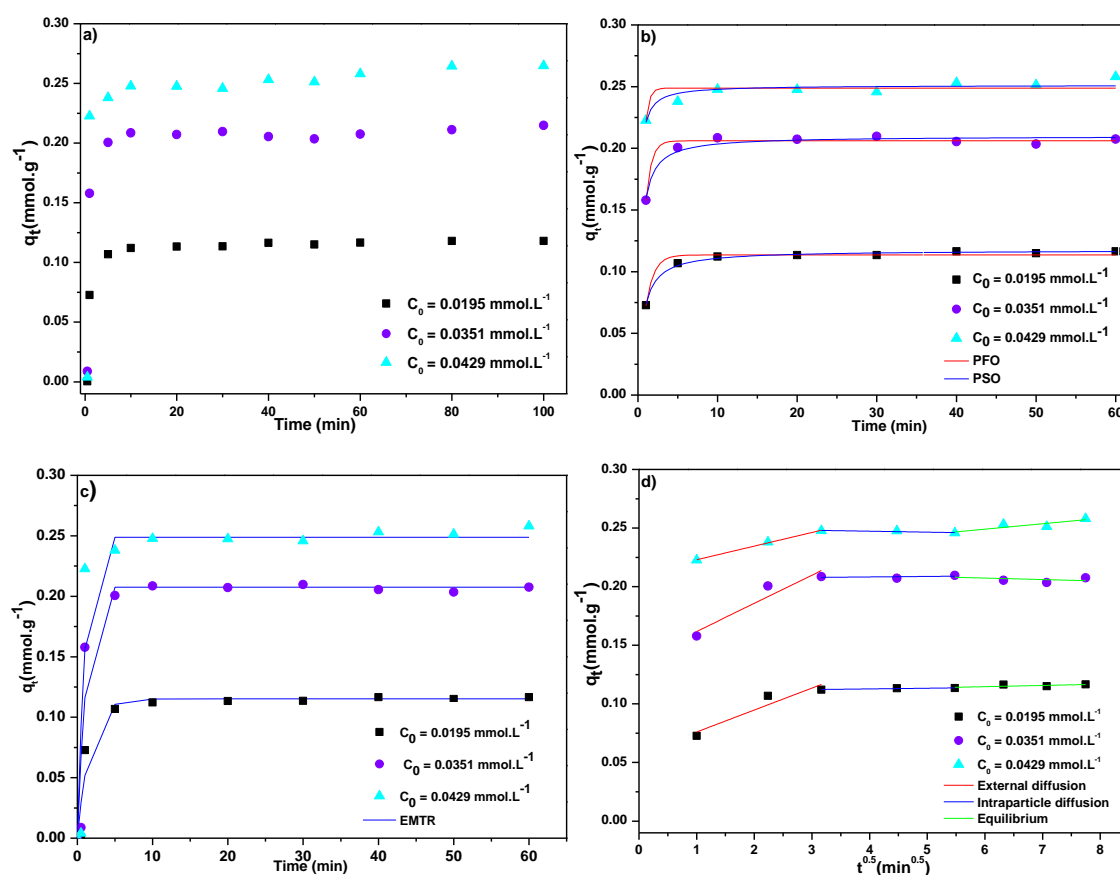
Where: N is the number of experimental data points; q<sub>exp</sub> is the experimental adsorption capacity (mmol.g<sup>-1</sup>); q<sub>calc</sub> is the adsorption capacity calculated by the model (mmol.g<sup>-1</sup>) and p is the number of parameters of the model.

The results presented in Fig. 4.8(b) and Table 4.7 showed a good data adjustment to the PFO and PSO. However, according to the value of R<sup>2</sup>, the PSO model showed a better experimental data adjustment, thus indicating that chemisorption is the limiting mechanism in the adsorptive process. Nonetheless, the value of R<sup>2</sup> for the PFO model indicates that physisorption also influences the process. Therefore, this finding suggests that the NAP adsorption process can be governed by both chemisorption, due to electrostatic interactions between the cationic surface of the adsorbent and the NAP molecules, as well as physisorption, due to π-π and hydrophobic interactions (Ruiz et al., 2020; Song et al., 2021; Tang et al., 2021).

From the experimental data adjustment to the IP model, it is possible to observe that the intraparticle diffusion curve (Fig. 4.8d) does not pass through the origin, which suggests that the diffusion process is govern by more than one limiting step. As shown in Fig. 4.8d, three linear regions are observed, thus indicating that the NAP adsorption is govern by three steps. Initially, the PAH molecules are transported between the solution and the mCS/GO surface,

which occurs quickly due to the rigorous agitation of the suspension. This result is evidenced by the good fit to the EMTR model, as shown in Fig. 4.8c. In the second step, the PAH molecules diffuse onto the adsorbent pores. Finally, in the third step, the adsorption reaches equilibrium. Thus, the results indicate that the NAP adsorption onto the mCS/GO involved more than one step. Comparable results were acquired in the studies by Ruiz et al. (2020), who reported the adsorption of PAHs in chitosan modified with iron oxide and titanium dioxide, and by Song et al. (2021), who reported the PAHs adsorption on nitrogen-doped reduced graphene oxide.

**Figure 4.8.** Adsorption kinetics curves of NAP onto the green adsorbent (a); Fitting of the experimental data to the PFO and PSO (b); EMTR (c) and IP models (d).



#### 4.3.4. Adsorption isotherms

The isotherm models evaluate the interactions between the adsorbate and the adsorbent surface until the equilibrium. Equilibrium experimental data for the NAP adsorption were adjusted to the Langmuir, Freundlich and Dubinin-Radushkevich models as displayed in Fig. 4.9(a-d). The adjustment parameters, as well as the  $R^2$  calculated according to the models are presented in Table 4.8.

**Figure 4.9.** Adsorption isotherms at 20 °C, 30 °C and 40 °C (a); Langmuir, Freundlich and Dubinin-Radushkevich adsorption isotherm models at 20 °C (b); 30 °C (c) and 40 °C.

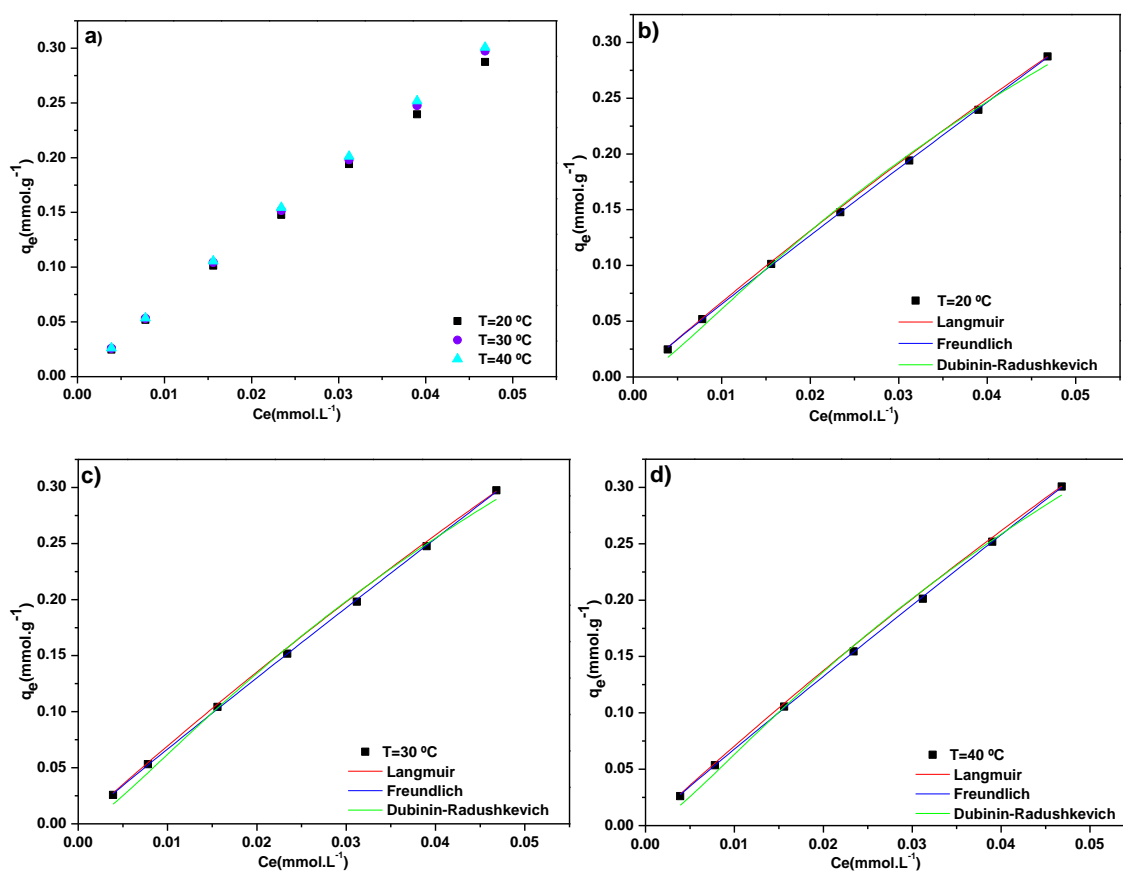


**Table 4.8.** Fit parameters of equilibrium isotherm models Langmuir, Freundlich and Dubinin-Radushkevich.

Model	Parameter	T=20 °C	T=30 °C	T=40 °C
Langmuir	$q_{\max}$ (mmol.g <sup>-1</sup> )	2.6088	2.6554	2.6764
	$k_L$ (L.mmol <sup>-1</sup> )	2.6439	2.6862	2.7077
	$R^2$	0.9985	0.9977	0.9979
	AICc	-60.2464	-57.2541	-57.5334
Freundlich	$k_F$ (mmol.g <sup>-1</sup> ).(L.mmol <sup>-1</sup> ) <sup>1/n</sup>	<b>5.3774</b>	<b>5.7097</b>	<b>5.7229</b>
	<b>n</b>	<b>1.0442</b>	<b>1.0346</b>	<b>1.0381</b>
	<b>R<sup>2</sup></b>	<b>0.9998</b>	<b>0.9997</b>	<b>0.9998</b>
	<b>AICc</b>	<b>-89.5125</b>	<b>-86.4541</b>	<b>-88.9576</b>
Dubinin-Radushkevich	$q_m$ (mmol.g <sup>-1</sup> )	0.9918	1.0389	1.04818
	$K_{DR}$ (mol <sup>2</sup> .J <sup>-2</sup> )	2.2048e <sup>-8</sup>	2.0837e <sup>-8</sup>	1.9528e <sup>-8</sup>
	E (kJ.mol <sup>-1</sup> )	4.7621	4.8984	5.0600
	$R^2$	0.9954	0.9944	0.9905
	AICc	-65.6340	-63.8492	-64.5250

The results of the correlation coefficients and the parameters of the isotherm models indicated a good adjustment for both the Langmuir and Freundlich models, which suggests that the adsorption process occurs through the formation of monolayers as well as multilayers. Regardless, the Freundlich isotherm exhibited a slightly better data fit, which suggests that the formation of multilayers on the heterogeneous surface is predominant over the process. According to Fig. 4.9a, a linear behavior and a continuous increase in the adsorption capacity are observed, which can also be observed through the values of  $q_{\max}$  and  $q_m$  calculated using the Langmuir and Dubinin-Radushkevich models. Such behavior is associated with the high availability of adsorption sites, thus allowing a greater adsorption capacity to be obtained even when the adsorbate concentration is very low. In addition, it is observed that the variation in temperature not have a great influence on the adsorption capacity (Ruiz et al., 2020).

As stated in Fig. 4.9(b-d), a better adjustment of the data to the Freundlich model is observed, besides, the higher value of  $k_F$  suggests that the adsorbate has a high affinity for the green adsorbent. The value of  $n$ , above 1.0, indicates that the NAP adsorption is favorable, moreover, it indicates the presence of strong bonds between NAP and the adsorbent (Eeshwarasinghe et al., 2018). The D-R model indicates if the adsorption process is whether physical or chemical. Thus, the free energy adsorption (E) was calculated as the inverse of the square root of  $2k_{DR}$ . For E values between 8 and 16 kJ.mol<sup>-1</sup>, the adsorptive process is chemical, if  $E < 8$  KJ.mol<sup>-1</sup>, the physical adsorption occurs (Tripathy and Raichur, 2008). According to

the E values calculated for the model (Table 4.8), it is observed that they are smaller than 8 KJ.mol<sup>-1</sup>, which suggests that the NAP adsorption occurs mainly by physisorption, through van der Waals forces, which includes  $\pi$ - $\pi$  and hydrophobic interactions. However, the high fit to the Freundlich model indicates that chemisorption also influences the process, pointing out the presence of electrostatic interactions. Comparable results were published by Eeshwarasinghe et al. (2018) and Song et al. (2021).

#### 4.3.5. Thermodynamic study

The thermodynamic study evaluates the nature of the NAP adsorption, through the determination of the thermodynamic parameters,  $\Delta G^\circ$ ,  $\Delta H^\circ$ ,  $\Delta S^\circ$  and  $\Delta H_{st}$ . Which were calculated from the thermodynamics fundamental Equations (5) and (6):

$$\Delta G^\circ = -R T \ln K_C \quad (5)$$

$$\Delta G^\circ = \Delta H^\circ - T\Delta S^\circ \quad (6)$$

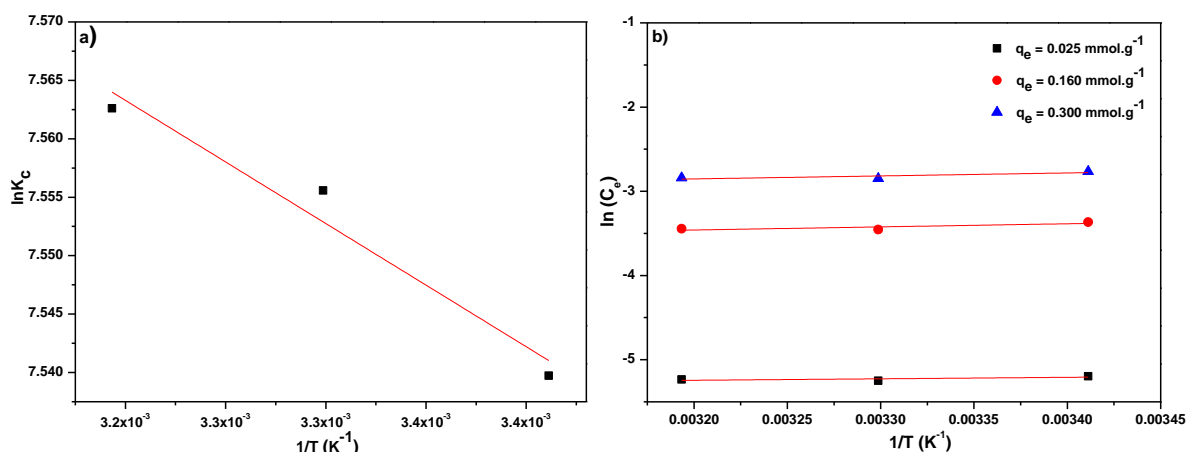
Where,  $K_C$  is the constant of chemical equilibrium, R is the ideal gas constant (mol<sup>-1</sup>.K<sup>-1</sup>) and T is the temperature (K).  $K_C$  is calculated through the intercept of  $\ln(q_e/C_e)$  versus  $q_e$ , for each temperature (20 °C, 30 °C and 40 °C), where,  $C_e$  is the NAP equilibrium concentration (mmol.L<sup>-1</sup>) and  $q_e$  is the equilibrium adsorption capacity (mmol.g<sup>-1</sup>). To obtain dimensionless constant  $K_C$ , Milonjić (2007), suggests that it can be multiplied by 1000. Enthalpy and entropy were calculated through the slope and intercept of  $\ln K_C$  versus  $1/T$ , respectively, investigating the influence of temperature on the process (Fig. 4.10a) The thermodynamic results obtained through the adsorption of NAP onto mCS/GO are shown in Table 4.9.

**Table 4.9.** Thermodynamic parameters for NAP adsorption at 20 °C, 30 °C and 40 °C.

T (°C)	$\Delta H^\circ$ (J.mol <sup>-1</sup> )	$\Delta S^\circ$ (J.mol <sup>-1</sup> .K <sup>-1</sup> )	$\Delta G^\circ$ (J.mol <sup>-1</sup> )	$E_a$ (J.mol <sup>-1</sup> )
20			-18379.3510	3313.5553
30	876.3062	65.6853	-19036.2044	3396.6953
40			-19693.0577	3479.8353

Where:  $E_a$  is the Activation Energy (J.mol<sup>-1</sup>), calculated by:  $E_a = \Delta H^\circ + RT$ .

**Figure 4.10.** Plot of  $\ln K_c$  versus  $1/T$  (a); Plot of  $\ln C_e$  versus  $1/T$  obtained for the adsorption of NAP onto green mCS/GO (b).



From the results presented in Table 4.9, it is possible to observe the endothermic nature of the adsorptive process of NAP onto the green mCS/GO ( $\Delta H^\circ > 0$ ). Through the magnitude of the value of  $\Delta H^\circ$  it can be identified if the adsorption process is governed by physisorption ( $\Delta H^\circ < 25$  kJ.mol $^{-1}$ ) or chemisorption ( $\Delta H^\circ > 40$  kJ.mol $^{-1}$ ). The value of  $\Delta H^\circ$  obtained indicates that the main mechanism involved in the NAP adsorption is physisorption. Furthermore, the positive entropy value ( $\Delta S^\circ > 0$ ) suggests high affinity for the green adsorbent. The values of change in Gibbs energy were negative ( $\Delta G^\circ < 0$ ) for all temperatures evaluated, which indicates the spontaneous nature of the adsorptive process (Yang et al., 2013). It was also observed that  $\Delta G^\circ$  values were more negative with the temperature increasing, which suggests that the adsorption of PAHs is favored by increasing the process temperature (Sharma et al., 2017).

The isosteric heat ( $\Delta H_{st}$ ) was calculated using the Clausius-Clapeyron Equation (7) (Young and Crowell, 1963). So, the value of ( $\Delta H_{st}$ ) (kJ.mol $^{-1}$ ) was obtained from the slope of  $\ln C_e$  versus  $1/T$ , keeping  $q_e$  constant. The equilibrium concentration ( $C_e$ ) was obtained from the Freundlich isotherm model for each temperature.

$$\Delta H_{st} = R \frac{d \ln C_e}{d \left( \frac{1}{T} \right)} \quad (7)$$

The isosteres obtained by adsorption of NAP onto the green adsorbent at different values of  $q_e$  (0.025, 0.160 and 0.300 mmol.g $^{-1}$ ) are displayed in Fig. 4.10b and the  $\Delta H_{st}$  values obtained are shown in Table 4.10. Therefore, a variation in  $\Delta H_{st}$  values was observed through the increase of the surface charge, which suggests that the green material is energetically heterogeneous. The  $\Delta H_{st}$  values obtained ( $< 80$  kJ.mol $^{-1}$ ) also indicate that the adsorption mechanism is control by physical processes, in accordance with the results obtained from the

adjustment of the equilibrium data to the Freundlich and Dubinin- Radushkevich models (Almeida et al., 2022).

**Table 4.10.** Isothermic heat values ( $\Delta H_{st}$ ) obtained through the adsorption of NAP onto green mCS/GO.

$q_e$ (mmol.g <sup>-1</sup> )	$\Delta H_{st}$ (kJ.mol <sup>-1</sup> )	$R^2$
0.025	1.4573	0.7051
0.160	3.0843	0.8260
0.300	2.9459	0.8351

#### 4.3.6. Adsorption Mechanisms

The results obtained in this study indicated that both  $\pi$ - $\pi$  interactions and the hydrophobic effect influence the NAP adsorption process. Some studies have pointed out that in the PAHs adsorption processes onto carbon-based materials, the  $\pi$ - $\pi$  and hydrophobic interactions are the mechanisms that most influence the adsorption of these compounds (Wang and Chen, 2015). Comparable results were published by Zhao et al. (2014), targeting the removal of phenanthrene onto multilayer graphene, and Song et al. (2021) for the adsorption of anthracene and 2-methylanthraquinone onto nitrogen-doped reduced graphene oxide materials.

The results of isotherms and thermodynamics adsorption showed that physisorption is the mechanism that control the process. However, the Freundlich model adjustment indicated that chemisorption also influences the adsorption process. This behavior suggests that the NAP adsorption is related with the functional groups present in the green composite structure, as indicated by the XPS and FTIR analyses, allowing the formation of clusters with the NAP molecules, through electrostatic interactions, thus indicating the influence of chemisorption. Comparable results were reported by Ruiz et al. (2020) for the NAP adsorption onto chitosan beads modified with nanoparticles of iron oxide and titanium dioxide. Table 4.11 shows a comparison of the  $q_{max}$  of Langmuir obtained in this study and other studies for PAHs adsorption onto different carbon adsorbents.

Based on the data presented in Table 4.11, the green mCS/GO showed high  $q_{max}$  compared with others adsorbent materials published. These results point to the green composite as a promising and ecologically-clean material for the PAHs removal. Comparing the methodology of synthesis of the composite presented in this work with the different materials

discussed in Table 11, it is observed that the protocols of preparation of the green mCS/GO were optimized, aiming to make the process of synthesis of a material more efficient and cost-effective. In addition, the use of botanical extracts and biopolymers, contribute to minimizing the excessive use of toxic chemical reagents, making it more sustainable, and contributing to improve its performance in the adsorption of pollutants from the oil and gas industry.

### **3.7. Adsorbent regeneration cycles**

The recovery and reuse of an adsorbent after the adsorption of pollutants is a crucial step to ensure the economic efficiency of the process, especially when it comes to the development of new adsorbent materials. During the desorption and regeneration process of graphene-based materials, the elution solvent election, as well as the nature of the adsorbate, are very important factors to ensure the process efficiency (Hossain et al., 2020).

In the green mCS/GO regeneration study, the recovery efficiency of the elution solvents was evaluated as shown in Fig. 4.11a. Among the solvents evaluated, methanol exhibited the highest desorption efficiency. The desorption and regeneration steps were repeated for five consecutive cycles using methanol as the elution solvent (Fig. 4.11b). After the fifth cycle, the percentage of NAP recovery went from approximately 91% to 75%, thus indicating a 16% reduction in process efficiency. This decrease is associated with loss of active sites due to adsorbate accumulation throughout the desorption cycles (Sharma et al., 2017). On the fifth treatment cycle, a mass loss of 6.8% (2.04 mg) was observed in comparison to the initial adsorbent mass (30 mg). Thus, the achieved results indicated the green mCS/GO as a stable and promising material for the PAHs removal, which can be easily recovered and reprocess efficiently during several regeneration cycles.

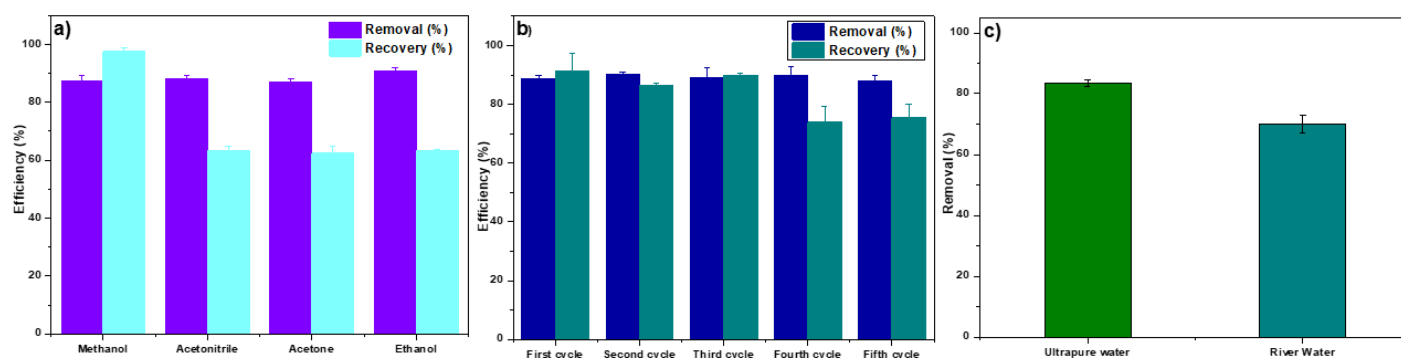
**Table 4.11.** Comparison of the  $q_{\max}$  for the green mCS/GO with other adsorbents.

PAHs	Adsorbents	$q_{\max}$ (mg.g <sup>-1</sup> )	Experimental conditions*	References
NAP	Bismuth molybdate/reduced graphene oxide (Bi <sub>2</sub> MoO <sub>6</sub> /rGO)	173.611	25 °C, 60 min, D: 0.3 mg.mL <sup>-1</sup>	Maswanganyi et al. (2021)
NAP	Activated Graphene Nanosheets (AGN)	180.7	C <sub>0</sub> = 0.2-20 ppm, 25 °C, 24 h, D: 0,045 mg.mL <sup>-1</sup>	Wang et al. (2016)
NAP	β-cyclodextrin grafted onto activated carbon (CDAC)	476.19 (20 °C) 588.24 (35 °C) 555.56 (40 °C)	C <sub>0</sub> = 10-50 ppm, 150 rpm, 60 min, D: 0.15 mg.mL <sup>-1</sup>	He et al. (2018)
NAP	Reduced graphene oxide/iron oxide (GO/FeO•Fe <sub>2</sub> O <sub>3</sub> )	337.088 (10 °C) 635.726 (30 °C) 733.135 (50 °C)	pH 7, 48h, D: 0.1 g.L <sup>-1</sup>	Yang et al. (2013)
NAP ANT PYR	Reduced graphene oxides (rGOs)	NAP: 766.59 ANT: 80.92 PYR: 198.003	25 °C, pH: 6.5	Sun et al. (2013)
NAP	Chitosan beads modified with iron oxide (FeO) and titanium dioxide (TiO <sub>2</sub> ) (Ch-FeO/ TiO <sub>2</sub> )	149.3	25 °C, pH: 8, 175 rpm, 48 h, D: 3 g.L <sup>-1</sup>	Ruiz et al. (2020)
NAP FLU	Double-functionalized GO with functional biopolymers	NAP: 116.7 FLU: 102.04	C <sub>0</sub> = 35-50 ppm, 25 °C, 12 h, D: 2,5 g	Arshad et al. (2020)
NAP	ZnO/Ag/GO nanocomposite	500	25 °C, 20 min, D: 0.25 g.L <sup>-1</sup>	Mukwevho et al. (2020)
NAP	<b>green mCS/GO</b>	<b>334.3712 (20 °C) 340.3439 (30 °C) 343.0355 (40 °C)</b>	<b>D: 0.15 mg.mL<sup>-1</sup>, pH 6.5, 200 rpm, 60 min</b>	<b>This study</b>

\*Where: D is the adsorbent dosage

Some reported studies, evaluated the regeneration of different graphene-based materials through several adsorption cycles. Song et al. (2021) published in their study the synthesis of NRGO aiming the adsorption of anthracene and its oxygenated derivative (2-MAQ). The material was regenerated and reused for 3 consecutive cycles, maintaining its removal efficiency up to 94% and 77% for anthracene and 2-MAQ, respectively. Tong et al. (2022) reported the adsorption of different PAHs onto magnetic polyamidoamine nanoparticles modified with graphene oxide, the material was regenerated and reused for 10 consecutive cycles and the results indicated a mass loss of less than 5%.

**Figure 4.11.** Efficiency of different elution solvents in NAP recovery (a); Regeneration cycles of NAP onto green mCS/GO using methanol as eluent (b); NAP removal (%) in ultrapure water and river water (c).



#### 4.3.8. Adsorption of PAHs from river water samples

The application of an adsorbent material in river water samples is very important to evaluate the viability of the method, allowing its application in large-scale and for real cases and. The samples were collected from Anhumas River (Campinas, SP – Brazil) and doped with NAP to evaluate its adsorption in a real medium. The organic matter present in the natural water effluents can influence the PAHs removal process, thus generating a competition for the adsorption sites in the adsorbent material between the organic matter present in the sample matrix and the PAHs (Antonelli et al., 2022). Assays were performed for an NAP concentration of  $2.5 \text{ mg.L}^{-1}$ ,  $0.15 \text{ mg.mL}^{-1}$  of adsorbent dosage, pH 6.5 for 1h at  $25 \text{ }^\circ\text{C}$ . The data showed that the adsorption efficiency was high (70%) either in real medium. This decrease is associated with the presence of different organic and inorganic complexes in the real matrix (such as humic acid,  $\text{Na}^+$ ,  $\text{Ca}^{2+}$  and others), which can interfere in the adsorption process of PAHs (Fig. 4.11c). Similar results have been reported for PAHs adsorption in real river water samples through

carbon nanotubes (Guo and Lee, 2011) and magnetic activated carbon nanocomposites (Inbaraj et al., 2021). The results showed the green mCS/GO as a promising material for the removal of PAHs in real samples, since in the presence of a complex organic matrix a significant reduction of NAP was obtained.

#### 4.4. Conclusions

In this study, the green mCS/GO composite was employed for the removal of naphthalene from synthetic effluent, aiming to demonstrate its efficiency in the adsorption process. The characterization analyses indicated that the material maintained its structural, thermal, textural and magnetic properties after the adsorption process, which suggests that the material remained stable, facilitating its recovery and post-process regeneration. Through FTIR and XPS analysis, it was concluded that the functional groups contributed for the NAP adsorption. The results obtained through the central composite design experiment indicated that the model is quadratic, with a high fit to the data ( $R^2=0.9911$ ), and that the factors NAP concentration and adsorbent dosage significantly influences the process. The results of the adsorption kinetics, isotherms and thermodynamics tests showed that physisorption, through the  $\pi$ - $\pi$  and hydrophobic interactions, was the main mechanism involved in the adsorption process of NAP. However, the good fit to the PSO model, provided through the kinetic study, and Freundlich model, provided through the equilibrium study, indicated the influence of chemisorption, through multilayer adsorption, which is associated with the functional groups in the adsorbent structure. The results obtained through the thermodynamic study, by calculating the  $\Delta H^\circ$ ,  $\Delta S^\circ$ ,  $\Delta G^\circ$  and isosteric heat ( $\Delta H_{st}$ ), indicated physisorption as the main NAP adsorption mechanism, in addition, the adsorbent has high affinity for the adsorbate and that the nature of the process is spontaneous and endothermic. Comparing the maximum adsorption capacity of Langmuir results from the green mCS/GO with other materials dated in the literature, it is achieved that the green adsorbent is a promising and eco-friendly material for the PAHs removal. The regeneration study showed that green mCS/GO remained efficient after the fifth consecutive adsorption-desorption cycle, with a mass loss of approximately 6.8%. The application study in real water samples showed the composite green as a promising material for applications in river water sample. Therefore, the achieved results in this study pointed to the green mCS/GO as an efficient, economical and sustainable material for the organic pollutants removal, such as NAP from industrial effluents.

### Declaration of Interest

No conflicts of interest were declared by the authors of this study.

### CRedit authorship contribution statement

**Conceptualization:** Melissa Gurgel Adeodato Vieira and Patrícia Prediger

**Methodology and data analysis:** Ruth Nóbrega Queiroz

**Writing - original sketch, review and editing:** Ruth Nóbrega Queiroz

**Analysis:** Valmor Roberto Mastelaro

**Writing - review and editing:** Melissa Gurgel Adeodato Vieira and Patrícia Prediger

**Acquisition funding:** Melissa Gurgel Adeodato Vieira, Meuris Gurgel Carlos da Silva and Patrícia Prediger

**Project administration:** Melissa Gurgel Adeodato Vieira

### Acknowledgment

This research was supported by PRH-ANP (n. 29, 5485), FAPESP (n. 2019/07822-2 and 2013/07296-2), CNPq (#308046/2019-6 and #141469/2018-8) and CAPES (001). The authors are grateful to Dr. Josiane Vendemiatti for the SEM analyses carried out at the Faculty of Technology at UNICAMP-Limeira.

### References

Abbasabadi, M. K., Azarifar, D. (2019). Magnetic Fe<sub>3</sub>O<sub>4</sub>-supported sulfonic acid-functionalized graphene oxide (Fe<sub>3</sub>O<sub>4</sub>@GO-naphthalene-SO<sub>3</sub>H): a novel and recyclable nanocatalyst for green one-pot synthesis of 5-oxo-dihydropyrano[3,2-c]chromenes and 2-amino-3-cyano-1,4,5,6-tetrahydropyrano[3,2-c]qui. *Research on Chemical Intermediates*, 45, pp. 2095–2118. doi:10.1007/s11164-018-03722-y

Almeida, A.S.V., Mastelaro, V.R., Silva, M.G.C., Prediger, P., Vieira, M.G.A. (2022). Adsorption of 17 $\alpha$ -ethinylestradiol onto a novel nanocomposite based on graphene oxide, magnetic chitosan and organoclay (GO/mCS/OC): Kinetics, equilibrium, thermodynamics and selectivity studies. *Journal of Water Process Engineering*, 47(102729). doi:10.1016/j.jwpe.2022.102729

Antonelli, R., Malpass, G.R.P., Silva, M.G.C., Vieira, M.G.A. (2022). Ofloxacin degradation in chloride-containing medium by photo-assisted sonoelectrochemical process using a mixed metal oxide anode. *Journal of Environmental Chemical Engineering*, 10(2), p. 107174. doi:10.1016/j.jece.2022.107174

Aranovich, G., Donohue, M. (1998). Analysis of Adsorption Isotherms: Lattice Theory Predictions, Classification of Isotherms for Gas–Solid Equilibria, and Similarities in Gas and Liquid Adsorption Behavior. *200*(2), pp. 273-290. doi:10.1006/jcis.1997.5398

Bai, L., Tajikfar, A., Tamjidi, S., Foroutan, R., Esmaili, H. (2021). Synthesis of MnFe<sub>2</sub>O<sub>4</sub>@graphene oxide catalyst for biodiesel production from waste edible oil. *Renewable Energy*, *170*, pp. 426-437. doi:10.1016/j.renene.2021.01.139

Bulin, C., Zhang, Y., Li, B., Zhang, B. (2020). Removal performance of aqueous Co(II) by magnetic graphene oxide and adsorption mechanism. *Journal of Physics and Chemistry of Solids*, *144*, p. 109483. doi:10.1016/j.jpcs.2020.109483

Chen, K., Jin, R., Luo, C., Song, G., Hu, Y., Cheng, H. (2018). Synthesis of polydopamine-functionalized magnetic graphene and carbon nanotubes hybrid nanocomposites as an adsorbent for the fast determination of 16 priority polycyclic aromatic hydrocarbons in aqueous samples. *Journal of Separation Science*, *41*(8), pp. 1847-1855. doi:10.1002/jssc.201700888

Cui, L., Guo, X., Wei, Q., Wang, Y., Gao, L., Yan, L., Yan, T., Du, B. (2015). Removal of mercury and methylene blue from aqueous solution by xanthate functionalized magnetic graphene oxide: Sorption kinetic and uptake mechanism. *Journal of Colloid and Interface Science*, *439*, pp. 112-120. doi:10.1016/j.jcis.2014.10.019

Cychosz, K. A., Nicolas, R. G., Martínez, J.G., Thommes, M. (2017). Recent advances in the textural characterization of hierarchically structured nanoporous materials. *Chemical Society Reviews*, *46*(2), pp. 389-414. doi:10.1039/C6CS0039

Dubinin, M.M., Radushkevich, L.V. (1947). Equation of the Characteristic Curve of Activated Charcoal Proceedings of the Academy of Sciences. *Physical Chemistry Section USSR*, *55*, pp. 331-333.

Eeshwarasinghe, D. L. (2018). Removing polycyclic aromatic hydrocarbons from water using granular activated carbon: kinetics and equilibrium adsorption studies. *Environmental Science and Pollution Research*, *25*, pp. 13511–13524. doi:10.1007/s11356-018-1518-0

Freundlich, H. (1906). Over the adsorption in solution. *The Journal of Physical Chemistry*, *57*, pp. 385 – 471.

Ghaedi, M., Daneshyar, A., Asfaram, A., Purkait, M.K., (2016). Adsorption of naphthalene onto high-surface-area nanoparticle loaded activated carbon by high performance liquid chromatography: response surface methodology, isotherm and kinetic study. *RSC Advances*, *6*(54322), pp. 54322–54330. doi:10.1039/C6RA09500C

Goswami, L., Kumar, R. V., Pakshirajan, K., Pugazhenti, G.,. (2019). A novel integrated biodegradation—microfiltration system for sustainable wastewater treatment and energy recovery. *Journal of Hazardous Materials*, 707-715. doi:10.1016/j.jhazmat.2018.11.029

Guo, L., Lee, H.K.,. (2011). Development of multiwalled carbon nanotubes based micro-solid-phase extraction for the determination of trace levels of sixteen polycyclic aromatic hydrocarbons in environmental water samples. *Journal of Chromatography A*, 1218(52), pp. 9321-9327. doi:10.1016/j.chroma.2011.10.066

Haro, M., Cabal, B., Parra, J. B., Ania, C. O. (2011). On the Adsorption Kinetics and Equilibrium of Polyaromatic Hydrocarbons from Aqueous Solution. *Adsorption Science & Technology*, 29, pp. 467–478. doi:10.1260/0263-6174.29.5.467

Ho, Y.S., Mckay, G. (1999). Pseudo-second order model for sorption processes. *Process Biochemistry*, 34, pp. 451- 465. doi:10.1016/S0032-9592(98)00112-5

Hossain, M.D.F., Akther, N., Zhou, Y. (2020). Recent advancements in graphene adsorbents for wastewater treatment: Current status and challenges. *Chinese Chemical Letters*, 31(10), pp. 2525-2538. doi:10.1016/j.ccl.2020.05.011

Hummers, W.S., Offeman, R.E. (1958). Preparation of Graphitic Oxide. *Journal of the American Chemical Society*, 80, p. 1339. doi:10.1021/ja01539a017

Inbaraj, B. S., Sridhar, K., Chen, B. H. (2021). Removal of polycyclic aromatic hydrocarbons from water by magnetic activated carbon nanocomposite from green tea waste. *Journal of Hazardous Materials*, 415, p. 125701. doi:10.1016/j.jhazmat.2021.125701

INMETRO - NATIONAL INSTITUTE OF METROLOGY. (June 09<sup>th</sup>, 2020). Guidance on validation of chemical testing methods. Rio de Janeiro.

Lagergren, S. (1898). About the theory of so-called adsorption of soluble substances. *Kunliga Svenska Vetenskapsakademiens. Handlingar.*, 24, pp. 1-39.

Langmuir, I. (1918). The adsorption of gases on plane surfaces of glass, mica and platinum. *Journal of the American Chemical Society*, 40, p. 1361.

Li, Y., Dong, X., Zhao, L. (2021). Application of magnetic chitosan nanocomposites modified by graphene oxide and polyethyleneimine for removal of toxic heavy metals and dyes from water. *International Journal of Biological Macromolecules*, 192, pp. 118-125. doi:10.1016/j.ijbiomac.2021.09.202

Liu, M., Liu, Q., Zang, Z., Han, R. (2022). Adsorptive removal of sulfosalicylic acid from aqueous medium by iron(III)-loaded magnetic chitosan/graphene oxide. *Journal of Colloid and Interface Science*, 606, pp. 1249-1260. doi:10.1016/j.jcis.2021.08.097

Majd, M., Nojavan, S., (2021). Determination of polycyclic aromatic hydrocarbons in soil, tree leaves, and water samples by magnetic dispersive solid-phase extraction based on  $\beta$ -cyclodextrin functionalized graphene oxide followed by GC-FID. *Microchemical Journal*, 171, p. 106852. doi:10.1016/j.microc.2021.106852

Manousi, N., Deliyanni, E.A., Rosenberg, E., Zachariadis, G.A. (2021). Ultrasound-assisted magnetic solid-phase extraction of polycyclic aromatic hydrocarbons and nitrated polycyclic aromatic hydrocarbons from water samples with a magnetic polyaniline modified graphene oxide nanocomposite. *Journal of Chromatography A*, 1645, p. 462104. doi:10.1016/j.chroma.2021.462104

Milonjić, S. (2007). A consideration of the correct calculation of thermodynamic parameters of adsorption. *Journal of the Serbian Chemical Society*, 72(12), pp. 1363–1367. doi:10.2298/JSC0712363M

Mokhtaria, S. A., Gholami, M., Dargahi, A., Vosoughi, M. (2021). Removal of polycyclic aromatic hydrocarbons (PAHs) from contaminated sewage sludge using advanced oxidation process (hydrogen peroxide and sodium persulfate). *Desalination and Water Treatment*, 213, pp. 311–318. doi:10.5004/dwt.2021.26716

Naing, N. N., Li, S. F. Y., Lee, H. K. (2016). Magnetic micro-solid-phase-extraction of polycyclic aromatic hydrocarbons in water. *Journal of Chromatography A*, 1440, pp. 23-30. doi:10.1016/j.chroma.2016.02.046

Neves, T. F., Dalarme, N. B., Silva, P. M. M., Landers, R., Picone, C. S. F., Prediger, P. (2020). Novel magnetic chitosan/quaternary ammonium salt graphene oxide composite applied to dye removal. *Journal of Environmental Chemical Engineering*, 8(4), p. 103820. doi:10.1016/j.jece.2020.103820

Peng, S., Huang, Y., Ouyang, S., Huang, J., Shi, Y., Tong, Y.J., Zhao, X., Li, N., Zheng, J., Zheng, J., Gong, X., Xu, J., Zhu, F., Ouyang, G., (2022). Efficient solid phase microextraction of organic pollutants based on graphene oxide/chitosan aerogel. *Analytica Chimica Acta*, 1195(339462). doi:10.1016/j.aca.2022.339462

Prediger, P., Cheminski, T., Neves, T. F., Nunes, W. B., Sabino, L., Picone, C. S. F., Oliveira, R. L., Correia, C. R. D. (2018). Graphene oxide nanomaterials for the removal of non-ionic surfactant from water. *Journal of Environmental Chemical Engineering*, 6, pp. 1536-1545. doi:10.1016/j.jece.2018.01.072

Puranik, P.R., Modak, J.M., Paknikar, K.M. (1999). A comparative study of the mass transfer kinetics of metal biosorption by microbial biomass. *Hydrometallurgy*, 52 (2), pp. 189–197. doi:10.1016/S0304-386X(99)00017-1

Queiroz, R. N., Prediger, P., Vieira, M. G. A., (2022a). Adsorption of polycyclic aromatic hydrocarbons from wastewater using graphene-based nanomaterials synthesized by conventional chemistry and green synthesis: A critical review. *Journal of Hazardous Materials*, 422(126904). doi:10.1016/j.jhazmat.2021.126904

Queiroz, R.N., Neves, T.F., Silva, M.G.C., Mastelaro, V. R., Vieira, M.G.A., Prediger, P. (2022b). Comparative efficiency of polycyclic aromatic hydrocarbon removal by novel graphene oxide composites prepared from conventional and green synthesis. *Journal of Cleaner Production*, 361(132244). doi:10.1016/j.jclepro.2022.132244

Rebekah, A., Sivaselvam, S., Viswanathan, C., Prabhu, D., Gautam, R., Ponpandian, N. (2021). Magnetic nanoparticle-decorated graphene oxide-chitosan composite as an efficient nanocarrier for protein delivery. *Colloids and Surfaces A: Physicochemical and Engineering Aspects*, 610(125913). doi:10.1016/j.colsurfa.2020.125913

Ruiz, D.A.P., Ávila, G., Suesca, C.A., Delgado, A.D.G., Herrera, A. (2020). Ionic Cross-Linking Fabrication of Chitosan-Based Beads Modified with FeO and TiO<sub>2</sub> Nanoparticles: Adsorption Mechanism toward Naphthalene Removal in Seawater from Cartagena Bay Area. *ACS Omega*, 5, pp. 26463–26475. doi:10.1021/acsomega.0c02984

Santos, N. T. G., Moraes, L. F., Silva, M. G. C., Vieira, M. G. A. (2020). Recovery of gold through adsorption onto sericin and alginate particles chemically crosslinked by proanthocyanidins. *Journal of Cleaner Production*, 253(119925). doi:10.1016/j.jclepro.2019.119925

Shahsavari, E., Schwarz, A., Medina, A. A., Ball, A. S. (2019). Biological Degradation of Polycyclic Aromatic Compounds (PAHs) in Soil: a Current Perspective. *Current Pollution Reports volume*, 5, pp. 84–92. doi:10.1007/s40726-019-00113-8

Sharma, A., Siddiqi, Z.M., Pathania, D. (2017). Adsorption of polyaromatic pollutants from water system using carbon/ZnFe<sub>2</sub>O<sub>4</sub> nanocomposite: Equilibrium, kinetic and thermodynamic mechanism. *Journal of Molecular Liquids*, 240, pp. 361-371. doi:10.1016/j.molliq.2017.05.083

Soboleva, T. Z., Xie, Z., Navessin, T., & Holdcroft, S. (2010). On the Micro-, Meso-, and Macroporous Structures of Polymer Electrolyte Membrane Fuel Cell Catalyst Layers. *Applied Materials & Interfaces*, 2(2), pp. 375–384. doi:10.1021/am900600y

Song, T., Weijun Tian, W., Qiao, K., Zhao, J., Chu, M., Du, Z., Wang, L., Xie, W. (2021). Adsorption Behaviors of Polycyclic Aromatic Hydrocarbons and Oxygen Derivatives in Wastewater on N-Doped Reduced Graphene Oxide. *Separation and Purification Technology*, 254(117565). doi:10.1016/j.seppur.2020.117565

Tang, T., Cao, S., Xi, C., Z. Chen., (2021). Multifunctional magnetic chitosan-graphene oxide-ionic liquid ternary nanohybrid: An efficient adsorbent of alkaloids. *Carbohydrate Polymers*, 255. doi:10.1016/j.carbpol.2020.117338

Tong, Y., Li, S., Wu, Y., Guo, J., Zhou, B., Zhou, Q., Jiang, L., Niu, J., Zhang, Y., Liu, H., Yuan, S., Huang, S., Zhan, Y.,. (2022). Graphene oxide modified magnetic polyamidoamide dendrimers based magnetic solid phase extraction for sensitive measurement of polycyclic aromatic hydrocarbons. *Chemosphere*, 296(134009). doi:10.1016/j.chemosphere.2022.134009

Tripathy, S.S., Raichur, A.M. (2008). Abatement of fluoride from water using manganese dioxide-coated activated alumina. *Journal of Hazardous Materials*, 153, pp. 1043-1051. doi:10.1016/j.jhazmat.2007.09.100

Wang, J., Chen, B. (2015). Adsorption and coadsorption of organic pollutants and a heavy metal by graphene oxide and reduced graphene materials. *Chemical Engineering Journal*, 281, pp. 379-388. doi:10.1016/j.cej.2015.06.102

Weber, W.J., Morris, J.C. (1963). Kinetics of adsorption on carbon from solution. *Journal of the Sanitary Engineering Division*, 89 , pp. 31-60.

Yang, H., Zhang, K., Wang, Y., Yan, C., Lin, S. (2018). CoFe<sub>2</sub>O<sub>4</sub> derived-from bi-metal organic frameworks wrapped with graphene nanosheets as advanced anode for high-performance lithium ion batteries. *Journal of Physics and Chemistry of Solids*, 115, pp. 317-321. doi:10.1016/j.jpcs.2017.12.042

Yang, X., Li, J., Wen, T., Ren, X., Huang, Y., Wang, X. (2013). Adsorption of naphthalene and its derivatives on magnetic graphene composites and the mechanism investigation. *Colloids and Surfaces A: Physicochemical and Engineering Aspects*, 422, pp. 118 - 125. doi:10.1016/j.colsurfa.2012.11.063

Yao, N., Li, C., Yu, J., Xu, Q., Wei, S., Tian, Z., Yang, Z., Yang, W., Shen, J. (2020). Insight into adsorption of combined antibiotic-heavy metal contaminants on graphene oxide in water. *Separation and Purification Technology*, 236(116278). doi:10.1016/j.seppur.2019.116278

Yaqubzadeh, A.R., Ahmadpour, A., Bastami, T.R., Hataminia, M.R. (2016). Low-cost preparation of silica aerogel for optimized adsorptive removal of naphthalene from aqueous

solution with central composite (CCD). *Journal of Non-Crystalline Solids*, 447, pp. 307-314. doi:10.1016/j.jnoncrysol.2016.06.022

Young, D. M., Crowell, A. D. (1963). Physical Adsorption of Gases. *Physics Today*, 16, p. 80. doi:10.1063/1.3050674

Zhang, K., Yang, H., Lü, M., Yan, C., Wu, H., Yuan, A., Lin, S. (2018). Porous MoO<sub>2</sub>-Cu/C/Graphene nano-octahedrons quadruple nanocomposites as an advanced anode for lithium ion batteries with enhanced rate capability. *Journal of Alloys and Compounds*, 731, pp. 646-654. doi:10.1016/j.jallcom.2017.10.091

Zhang, Q., Zhang, Y., Li, Y., Ding, P., Xu, S., Cao, J. (2021). Green synthesis of magnetite nanoparticle and its regulatory effect on fermentative hydrogen production from lignocellulosic hydrolysate by *Klebsiella* sp. *International Journal of Hydrogen Energy*, 46, pp. 20413-20424. doi:10.1016/j.ijhydene.2021.03.142

Zhao, J., Wang, Z., Zhao, Q., Xing, B. (2014). Adsorption of Phenanthrene on Multilayer Graphene as Affected by Surfactant and Exfoliation. *Environmental Science & Technology*, 48, pp. 331–339. doi:10.1021/es403873r

Zhou, J., Tang, C., Cheng, B., Yu, J., Jaroniec, M. (2012). Rattle-type Carbon–Alumina Core–Shell Spheres: Synthesis and Application for Adsorption of Organic Dyes. *Applied Materials & Interfaces*, 4(4), pp. 2174–2179. doi:10.1021/am300176k

Zhou, Q., Wang, Y., Xiao, J., Fan, H., Chen, C.,. (2019). Preparation and characterization of magnetic nanomaterial and its application for removal of polycyclic aromatic hydrocarbons. *Journal of Hazardous Materials*, 371, pp. 323-331. doi:10.1016/j.jhazmat.2019.03.027

## Capítulo 5. Discussão Geral

A presença de contaminantes orgânicos, em especial os Hidrocarbonetos Policíclicos Aromáticos (PAHs), nos efluentes provenientes dos processos de exploração e produção de petróleo e gás representa uma fonte de preocupação para o setor, devido aos efeitos tóxicos e nocivos para os seres humanos e ecossistemas, principalmente ao meio aquático. Os PAHs são poluentes orgânicos formados principalmente via combustão incompleta da matéria orgânica, como petróleo, carvão e madeira, podendo ser de origem natural (biológica) e antropogênica (pirogênica e petrogênica) (Queiroz et al., 2022a). Diante disto, diferentes tecnologias têm sido desenvolvidas visando à remoção desses poluentes dos efluentes industriais, tais como biorremediação (Sun et al., 2019), separação por membranas (Qiao et al., 2019), coagulação-floculação (Wang et al., 2020), processos oxidativos avançados (POAs) (Haneef et al., 2020) e adsorção (Queiroz et al., 2022b). Dentre as metodologias de remediação de poluentes, os processos adsorptivos têm se destacado por serem um método simples, eficiente e rápido para a remoção de PAHs de águas residuais. Neste contexto, o presente trabalho de mestrado foi desenvolvido com vistas a avaliar o processo adsorção de diferentes PAHs (naftaleno, antraceno e fluoranteno) em materiais a base de grafeno e quitosana magnética, sintetizados via rotas convencional e química verde.

Nos últimos anos, a aplicação dos princípios da química verde para o desenvolvimento de materiais adsorventes vem ganhando destaque, devido à grande importância do tema para o cenário atual. Assim, a síntese de materiais verdes, produzidos através do uso de agentes naturais, como extratos de plantas, microorganismos e resíduos agrícolas, tem sido, cada vez mais estudada, visando minimizar os impactos ambientais causado pelo uso excessivo de reagentes químicos tóxicos nos processos convencionais de síntese. No Capítulo 2, deste presente trabalho, foi realizada uma revisão bibliográfica dos principais estudos publicados nos últimos cinco anos, visando assim, comparar as diferentes metodologias de remediação de PAHs com os processos adsorptivos. Dentre os tópicos abordados no *Review*, a adsorção de PAHs em nanomateriais à base de grafeno teve um foco principal, devido às propriedades físico-químicas singulares do grafeno, como elevada área específica, estabilidade térmica, e resistência mecânica, o que o tornam um material ideal para aplicações em processos de remediação de PAHs em efluentes industriais.

Outro tópico abordado no decorrer do Capítulo 2 diz respeito ao desenvolvimento e aplicação de nanomateriais verdes para a remoção de poluentes orgânicos aromáticos de efluentes provenientes dos processos de produção e exploração de petróleo. A síntese de

materiais adsorventes verdes oriundos de agentes naturais, biodegradáveis e não-tóxicos vem ganhando cada vez mais destaque, por se apresentarem como uma metodologia sustentável, eficiente e de baixo custo para a remediação de contaminantes. Comparou-se o desempenho entre os adsorventes produzidos via rota convencional e rota verde para a remoção de diferentes contaminantes petrogênicos. Alguns estudos publicados sobre a aplicação de adsorventes verdes para remoção de PAHs, como Ruiz et al. (2020) e Inbaraj et al. (2021) apontaram, em seus resultados um bom desempenho desses adsorventes para a remoção de PAHs quando comparados aos materiais convencionais.

No que se refere aos processos de síntese verde de adsorventes, muitos desafios ainda precisam ser superados, principalmente quanto à otimização dos processos de síntese, pois ainda existem muitas lacunas na literatura no tocante à metodologia de preparação e suas aplicações nos processos adsorptivos. A síntese do mCS/GO via rota convencional e verde (C-mCS/GO e G-mCS/GO, respectivamente) foi abordada no decorrer do Capítulo 3. Em seguida, realizou-se um estudo de afinidade adsorptiva para comparar a *performace* de ambos os materiais na adsorção de diferentes PAHs (naftaleno, antraceno e fluoranteno) em efluentes sintéticos. O óxido de grafeno (GO) foi sintetizado segundo o método de Hummers modificado (1958), utilizando grafite pré-oxidado de acordo com a metodologia descrita por Prediger et al. (2018). A síntese do adsorvente convencional (C-mCS/GO) foi realizada em três etapas, na qual, inicialmente, as partículas de ferro (C-Fe<sub>3</sub>O<sub>4</sub>) foram preparadas através da metodologia descrita por Silva et al. (2013). Na segunda etapa, foi sintetizada a quitosana magnética (mCS) utilizando-se o glutaraldeído como agente reticulante de acordo com a metodologia relatada por Wang et al. (2016). Por fim, na terceira etapa foi realizada a preparação do compósito C-mCS/GO utilizando o DCC (N,N-dicyclohexylcarbodiimide) e DMAP (4-dimethylaminopyridine) como agente reticulante, conforme reportado por Maleki e Paydar (2015).

O desenvolvimento do adsorvente verde (G-mCS/GO) visou otimizar o processo de síntese, tornando o processo mais simples e com melhor custo-benefício, conforme a metodologia adaptada de Santos et al. (2020). A síntese do compósito verde foi desenvolvida em duas etapas, na qual, inicialmente, as partículas de ferro (G-Fe<sub>3</sub>O<sub>4</sub>) foram preparadas segundo a metodologia descrita por Zhang et al. (2021), usando extrato de folhas de aguapé, como agente redutor/estabilizante. Na segunda etapa, sintetizou-se o G-mCS/GO usando a proantocianidina como agente reticulante.

As análises de caracterizações indicaram a obtenção dos compósitos magnéticos por meio das técnicas de DRX, XPS, FTIR, curva de magnetização, MEV/EDS, TG/DTG e

potencial zeta, conforme os resultados apresentados no Capítulo 3. Os resultados obtidos através das análises de DRX indicaram a presença dos picos de difração característicos das partículas de ferro em ambos os compósitos. As análises das curvas de magnetização confirmaram a obtenção de compósitos magnéticos, no entanto, os resultados indicaram que o compósito verde apresentou maior magnetização de saturação do que o compósito convencional. As análises de FTIR indicaram a presença de grupos funcionais associados ao óxido de grafeno, quitosana e as partículas de ferro. Comparando-se os resultados das caracterizações do compósito verde e convencional, observou-se que a aplicação da proantocianidina, como agente reticulando na síntese do G-mCS/GO, contribuiu para melhorar as propriedades térmicas, estruturais, magnéticas e texturais do compósito verde.

Os materiais adsorventes foram aplicados na remoção de diferentes PAHs (naftaleno, antraceno e fluoranteno) para comparar o desempenho adsorptivo dos materiais, através de ensaios de afinidade adsorptiva por meio de um sistema batelada, para um tempo de contato de 30 minutos. A Tabela 5.1 apresenta os percentuais de eficiência de remoção (%) dos PAHs para o C-mCS/GO e G-mCS/GO.

**Tabela 5.1.** Resultados de eficiência de remoção (%) dos PAHs para os materiais adsorventes.

PAHs	Eficiência de remoção (%)	
	C-mCS/GO	G-mCS/GO
Naftaleno	93,89	93,55
Antraceno	47,80	89,25
Fluoranteno	76,07	62,28

Os resultados obtidos nos ensaios de adsorção indicaram que maiores eficiência de remoção (%) e capacidade de adsorção ( $\text{mmol.g}^{-1}$ ) foram obtidas pelo naftaleno tanto para C-mCS/GO quanto para G-mCS/GO. Os resultados também mostraram que o adsorvente verde apresentou alta eficiência para a remoção do antraceno comparado ao adsorvente convencional. A simulação molecular revelou que as moléculas de naftaleno apresentam maior estabilidade do que as moléculas de antraceno e fluoranteno, o que pode contribuir para aumentar as interações  $\pi$ - $\pi$  entre as moléculas de naftaleno e a superfície do adsorvente. Esses resultados corroboram com os resultados dos ensaios de adsorção, indicando assim, que os processos de adsorção são possivelmente governados por interações  $\pi$ - $\pi$  e efeitos hidrofóbicos. Além disso, as análises do potencial zeta, antes e após a adsorção, indicaram que o melhor desempenho adsorptivo foi obtido em pH neutro.

Os ensaios de afinidade no Capítulo 3 apontaram o compósito verde G-mCS/GO como um material promissor e eficiente para a remoção de PAHs de efluentes industriais quando comparado ao adsorvente convencional. Assim, com base nesses resultados, o melhor sistema adsorvente/adsorbato (G-mCS/GO/naftaleno) foi definido para as próximas etapas da pesquisa. No Capítulo 4 foram realizados um planejamento composto central rotacional (DCCR) e um estudo adsorptivo cinético, de equilíbrio e termodinâmico para avaliar o potencial de remoção do naftaleno pelo adsorvente verde G-mCS/GO, seguido de um estudo de regeneração do adsorvente por cinco ciclos de adsorção/dessorção através da aplicação do metanol como solvente de eluição. Por fim, realizou-se a adsorção do naftaleno em um efluente real coletado do rio Anhumas (Campinas, SP – Brazil), visando avaliar o processo de adsorção do contaminante em uma matriz real.

O material verde foi caracterizado por meio das técnicas TG/DTG, BET, XPS, FTIR, DRX e MEV, a fim de avaliar as propriedades térmicas, estruturais, texturais e morfológicas do adsorvente antes e pós-processo de adsorção. As análises de caracterização indicaram que o material manteve suas propriedades magnéticas e estruturais estáveis após o processo de adsorção do naftaleno. As análises de FTIR e XPS revelaram a presença de grupos funcionais oxigenados que contribuíram para a adsorção do naftaleno.

O planejamento DCCR foi aplicado para otimizar as condições operacionais do processo, bem como determinar os fatores que influenciam o processo de adsorção do naftaleno. Os resultados apontaram que o modelo preditivo teve um excelente ajuste aos dados experimentais, por meio do ajuste do  $R^2 = 0,9911$ . Além disso, os fatores concentração de naftaleno ( $\text{mmol.L}^{-1}$ ) e dosagem de adsorvente ( $\text{mg.mL}^{-1}$ ) apresentam influência significativa sobre a variável resposta, capacidade adsorptiva ( $\text{mmol.g}^{-1}$ ). Assim, observou-se que uma maior capacidade de adsorção é obtida à medida que a dosagem do adsorvente diminui e a concentração de NAP aumenta, o que sugere que os sítios de adsorção disponíveis na superfície do material não são completamente saturados durante o processo de adsorção.

Os resultados dos testes cinéticos, de equilíbrio e termodinâmicos mostraram que a fisissorção é o principal mecanismo envolvido no processo de adsorção do naftaleno, por meio das interações  $\pi$ - $\pi$  e hidrofóbicas. No entanto, o bom ajuste ao modelo de pseudo-segunda ordem (PSO), fornecido pelo estudo cinético, e ao modelo Freundlich, fornecido pelo estudo de equilíbrio, indicaram a influência da quimissorção, por meio da adsorção multicamada, que está associada à presença dos grupos funcionais na estrutura do material adsorvente. A determinação das grandezas termodinâmicas forneceu informações sobre a natureza do processo adsorptivo. O valor de  $\Delta H^\circ$  obtido indicou que o principal mecanismos envolvido no processo é a fisissorção.

Já o valor positivo de  $\Delta S^\circ$  sugere que o adsorvente verde possui alta afinidade com o naftaleno e o valor negativo de  $\Delta G^\circ$  sugere que o processo é espontâneo e está associado diretamente ao aumento da temperatura. A variação nos valores de  $\Delta H_{st}$  foi observada através do aumento da carga superficial, o que indica que o adsorvente verde é energeticamente heterogêneo. A Tabela 5.2. apresenta os resultados dos parâmetros dos modelos cinéticos, de equilíbrio e termodinâmicos que tiveram o melhor ajuste conforme os dados obtidos em ensaios adsorptivos.

**Tabela 5.2.** Parâmetros de ajuste dos modelos cinéticos, de equilíbrio e termodinâmicos.

Modelos	Parâmetros	Condições experimentais		
		$C_0=0.0195$ mmol.L <sup>-1</sup>	$C_0=0.0351$ mmol.L <sup>-1</sup>	$C_0=0.0429$ mmol.L <sup>-1</sup>
PSO	<b>Modelo cinético:</b>			
	q <sub>e</sub> calc (mmol.g <sup>-1</sup> )	0,1174	0,2090	0,2490
	q <sub>e</sub> exp (mmol.g <sup>-1</sup> )	0,1165	0,2074	0,2513
	k <sub>2</sub> (g.mmol <sup>-1</sup> .min <sup>-1</sup> )	1,6799	3,1630	7,8730
	R <sup>2</sup>	0,9914	0,9566	0,8826
Freundlich	<b>Modelo de equilíbrio:</b>	<b>T=20 °C</b>	<b>T=30 °C</b>	<b>T=40 °C</b>
	k <sub>F</sub> (mmol.g <sup>-1</sup> ).(L.mmol <sup>-1</sup> ) <sup>1/n</sup>	5,3774	5,7097	5,7229
	n	1,0442	1,0346	1,0381
	R <sup>2</sup>	0,9998	0,9997	0,9998
	AICc	-89,5125	-86,4541	-88,9576
<b>Grandezas termodinâmicas:</b>		<b>T=20 °C</b>	<b>T=30 °C</b>	<b>T=40 °C</b>
$\Delta H^\circ$ (J.mol <sup>-1</sup> )			876,3062	
$\Delta S^\circ$ (J.mol <sup>-1</sup> .K <sup>-1</sup> )			65,6853	
$\Delta G^\circ$ (J.mol <sup>-1</sup> )		-18379,3510	-19036,2044	-19693,0577
E <sub>a</sub> (J.mol <sup>-1</sup> )		3313,5553	3396,6953	3479,8353

A regeneração do material após o processo de adsorção é muito importante para assegurar a viabilidade econômica do processo. Assim, foi realizado um estudo de regeneração do material verde usando diferentes solventes de eluição, como metanol, acetonitrila, acetona e etanol. Os resultados apontaram que o metanol apresentou o melhor desempenho no processo de dessorção do naftaleno. Com base nesses resultados, o metanol foi selecionado como solventes de eluição para a regeneração do material verde por cinco ciclos consecutivos. Após o quinto ciclo, o percentual de recuperação de naftaleno passou de aproximadamente 91% para 75%, indicando uma redução de 16% na eficiência do processo. Observou-se uma perda de

massa total de aproximadamente 6,8% (2,04 mg), em relação à massa inicial de adsorvente (30 mg). Os resultados apontaram o adsorvente verde mCS/GO como um material estável e promissor para a remoção de PAHs, podendo ser facilmente recuperado e reprocessado de forma eficiente durante vários ciclos de regeneração. Além disso, as propriedades magnéticas do compósito contribuíram para sua recuperação pós-processo adsortivo, evitando perdas de massa significativas após o processo.

Um estudo da adsorção em amostras de efluentes reais, as quais foram dopadas com naftaleno com uma concentração inicial de  $2,5 \text{ mg.L}^{-1}$ , foi realizado a fim de se avaliar a viabilidade do material adsorvente em uma matriz real, pois a presença de matéria orgânica e outros contaminantes, como ácido húmico,  $\text{Na}^+$  e  $\text{Ca}^{2+}$ , pode exercer influência sobre o processo de adsorção do naftaleno. Os resultados indicaram uma remoção de aproximadamente 70% para a amostra real, enquanto que para amostra sintética em água ultrapura obteve-se uma remoção em torno de 80%. Assim, o adsorvente verde se mostrou promissor para a remoção de PAHs em efluentes reais, uma vez que, a presença de uma matriz orgânica complexa pode influenciar significativamente sobre o processo de adsorção de contaminantes.

Em suma, os resultados obtidos durante o desenvolvimento desta dissertação de mestrado demonstraram o potencial do material verde mCS/GO como um adsorvente sustentável e eficiente para a remoção de PAHs em efluentes da indústria de óleo e gás. Além disso, o material se mostrou eficiente nos processos de regeneração e aplicação em amostras reais, indicando assim, que as metodologias de síntese e de aplicação propostas nesta dissertação são promissores para os propósitos as quais se destinam.

## Capítulo 6. Conclusão Geral e Sugestões

A presente dissertação de mestrado mostrou o desenvolvimento e aplicação de adsorventes verdes como uma metodologia alternativa, eficiente e de baixo custo para a remediação de poluentes orgânicos como os PAHs em efluentes da indústria petrolífera. A síntese de adsorventes pelas rotas convencional e verde (C-mCS/GO e G-mCS/GO, respectivamente) foi realizada e então aplicada à adsorção de PAH para investigar sua eficiência na remoção de naftaleno, antraceno e fluoranteno de efluentes. Também foi aplicado um planejamento experimental do tipo DCCR visando otimizar as condições operacionais, bem como um estudo de regeneração do adsorvente e um estudo de aplicação em efluente real. Com base nos resultados e discussões desenvolvidas neste estudo, obteve-se as seguintes conclusões:

- As análises de caracterização confirmaram a obtenção de compósitos magnéticos com altas capacidades adsorptivas;
- Os resultados indicam que a aplicação da proantocianidina como agente reticulante na síntese do G-mCS/GO contribuiu para melhorar suas propriedades térmicas e magnéticas quando comparado ao C-mCS/GO;
- Os ensaios de adsorção mostraram que a melhor capacidade adsorptiva foi obtida pelo G-mCS/GO para o naftaleno e o antraceno, para um tempo de contato de 30 min e dosagem de adsorvente de  $0,1 \text{ mg.mL}^{-1}$ , com 93,55% e 89,25% de eficiência de remoção, respectivamente;
- Os ensaios de afinidade, juntamente com os resultados das simulações moleculares, indicaram que os processos de adsorção são possivelmente governados por interações  $\pi$ - $\pi$  e efeitos hidrofóbicos;
- As análises de potencial zeta indicaram um melhor desempenho de adsorção em pH neutro;
- O novo compósito verde G-mCS/GO é um material promissor para a remoção de PAHs de efluentes industriais, quando comparado aos adsorventes convencionais;
- O compósito mCS/GO adsorvente verde foi empregado com êxito na remoção de naftaleno de efluente sintético;
- As análises de caracterização indicaram que o material manteve suas propriedades estruturais, térmicas, texturais e magnéticas após o processo de adsorção, confirmando a estabilidade do material, o que facilita sua recuperação e regeneração pós-processo;

- A partir das análises de FTIR e XPS, concluiu-se que a presença de grupos funcionais oxigenados contribuiu para a adsorção de naftaleno, permitindo a formação de *clusters* com as moléculas do adsorbato;
- Os resultados obtidos nos experimentos de delineamento composto central indicaram que o modelo é quadrático, com um bom ajuste aos dados experimentais ( $R^2=0,9911$ ), e que os fatores concentração inicial de naftaleno tem influencia positiva e dosagem de adsorvente tem influência negativa sobre o processo adsorptivo;
- Os ensaios de cinética, equilíbrio e termodinâmica de adsorção mostraram que a fisissorção, como mecanismo adsorptivo principal, devido às interações  $\pi$ - $\pi$  e hidrofóbicas;
- Observou-se também a influência da quimissorção como mecanismo adsorptivo secundário, devido às interações eletrostáticas, as quais estão associadas a presença dos grupos funcionais oxigenados, confirmados através das análises de FTIR e XPS;
- As grandezas  $\Delta H^\circ$ ,  $\Delta S^\circ$  e  $\Delta G^\circ$  determinadas pelo estudo termodinâmico indicaram que o processo de adsorção do naftaleno tem como mecanismo principal a fisissorção, além disso, observou-se que o adsorvente possui alta afinidade pelo adsorbato e a natureza do processo é espontânea e endotérmica, associada diretamente ao aumento da temperatura;
- A variação nos valores de  $\Delta H_{st}$  sugere que o principal mecanismo de adsorção é físico, além disso, o aumento da carga superficial observado indica que o adsorvente verde é energeticamente heterogêneo;
- O estudo de regeneração mostrou que o mCS/GO verde permaneceu eficiente após o quinto ciclo consecutivo de adsorção-dessorção para o naftaleno, com perda de massa de aproximadamente 6,8%;
- O estudo de aplicação em amostras reais de água mostrou o compósito verde como um material promissor para aplicações em amostras de água de rios, chegando a 70% de remoção;
- Os resultados obtidos neste estudo apontaram o mCS/GO verde como um material eficiente, econômico e sustentável para a remoção de poluentes orgânicos de efluentes industriais.

Nesse contexto, algumas perspectivas para estudos futuros podem ser abordadas, tais como:

- (i) Estudo das propriedades adsorptivas do rGO verde para a remediação de PAHs de efluentes, uma vez que a modificação na sua estrutura pode contribuir para melhorar as interações  $\pi$ - $\pi$  e hidrofóbicas, conferindo alta afinidade com os PAHs;
- (ii) Estudos de reutilização/regeneração de nanoadsorventes verdes, visando, assim, otimizar as condições operacionais desse processo;
- (iii) Aplicação de adsorventes verdes em sistemas dinâmicos de leito fixo;
- (iv) Análise econômica de custos para aplicação em sistemas adsorptivos de grande porte com vistas à aplicação em escala industrial;
- (v) Análise do ciclo de vida dos adsorventes verdes, desde a síntese até sua aplicação, visando assim, para avaliar o impacto ambiental causado durante este processo.

## REFERÊNCIAS

- ABDEL-SHAFY, H. I., MANSOUR, M. S. M., 2016. A review on polycyclic aromatic hydrocarbons: Source, environmental impact, effect on human health and remediation. *Egyptian Journal of Petroleum*. 25, 107-123. <http://dx.doi.org/10.1016/j.ejpe.2015.03.011>.
- BEYER, J., GOKSØYR, A., HJERMANN, D. O., KLUNGSØYR, J., 2020. Environmental effects of offshore produced water discharges: A review focused on the Norwegian continental shelf. *Marine Environmental Research*. 162, 105-155. <https://doi.org/10.1016/j.marenvres.2020.105155>.
- BOLADE, O. P., WILLIAMS, A. B., BENSON, N. U., 2020. Green synthesis of iron-based nanomaterials for environmental remediation: A review. *Environmental Nanotechnology, Monitoring & Management*. 13, 100279. <https://doi.org/10.1016/j.enmm.2019.100279>.
- CHEN, W. H., HUANG, J. R., 2020. Adsorption of organic including pharmaceutical and inorganic contaminants in water toward graphene-based materials, in: Maldonado, A. J. H., Blaney, L. (Eds.), *Contaminants of Emerging Concern in Water and Wastewater*. Elsevier Inc., pp. 93-113.
- HANEEF, T., MUSTAFA, M. R. U., RASOOL, K., HO, Y. C., KUTTY, S. R. M., 2020. Removal of Polycyclic Aromatic Hydrocarbons in a Heterogeneous Fenton Like Oxidation System Using Nanoscale Zero-Valent Iron as a Catalyst. *Water*. 12 (9), 2430. <https://doi.org/10.3390/w12092430>.
- HUMMERS, W. S.; OFFEMAN, R. E., 1958. Preparation of Graphitic Oxide. *Journal of the American Chemical Society*. 80, 1339. <https://doi.org/10.1021/ja01539a017>.
- INBARAJ, B. S., SRIDHAR, K., CHEN, B. H., 2021. Removal of polycyclic aromatic hydrocarbons from water by magnetic activated carbon nanocomposite from green tea waste. *Journal of Hazardous Materials*. 415, 125701. <https://doi.org/10.1016/j.jhazmat.2021.125701>.
- LI, S., LUO, J., HANG, X., ZHAO, S., WAN, Y., 2019. Removal of polycyclic aromatic hydrocarbons by nanofiltration membranes: Rejection and fouling mechanisms. *Journal of Membrane Science*. 582, 264-273. <https://doi.org/10.1016/j.memsci.2019.04.008>.
- MALEKI, A., PAYDAR, R., 2015. Graphene oxide–chitosan bionanocomposite: a highly efficient nanocatalyst for the one-pot three-component synthesis of trisubstituted imidazoles under solvent-free conditions. *The Royal Society of Chemistry*. 5, 33177-33184. <https://doi.org/10.1039/c5ra03355a>.
- NASUHOGLU, D.; RODAYAN, A.; BERK, D.; YARGEAU, V., 2012. Removal of the antibiotic levofloxacin (LEVO) in water by ozonation and TiO<sub>2</sub> photocatalysis. *Chemical Engineering Journal*. 189-190, 41-48. <https://doi.org/10.1016/j.cej.2012.02.016>.
- NEVES, T. F., DALARME, N. B., SILVA, P. M. M., LANDERS, R., PICONE, C. S. F.; PREDIGER, P., 2020. Novel magnetic chitosan/quaternary ammonium salt graphene oxide composite applied to dye removal. *Journal of Environmental Chemical Engineering*. 8, 103820. <https://doi.org/10.1016/j.jece.2020.103820>.

PAL, P., PAL, A., NAKASHIMA, K., YADAV, B. K. 2020. Applications of Chitosan in Environmental Remediation: A Review. *Chemosphere*. 266, 128934. <https://doi.org/10.1016/j.chemosphere.2020.128934>.

PREDIGER, P., CHEMINSKI, T., NEVES, T. F., NUNES, W. B., SABINO, L., PICONE, C. S. F., OLIVEIRA, R. L., CORREIA, C. R. D., 2018. Graphene oxide nanomaterials for the removal of non-ionic surfactant from water. *Journal of Environmental Chemical Engineering*. 6, 1536-1545. <https://doi.org/10.1016/j.jece.2018.01.072>.

QI, Y.; WANG, C.; LV, C.; LUN, Z.; ZHENG, C., 2017. Removal Capacities of Polycyclic Aromatic Hydrocarbons (PHAs) by a Newly Isolated Strain from Oilfield Produced Water. *International Journal of Environmental Research and Public Health*. 14, 215. <https://doi.org/10.3390/ijerph14020215>.

QIAO, M., FU, L., CAO, W., BAI, Y., HUANG, Q., ZHAO, X., 2019. Occurrence and removal of polycyclic aromatic hydrocarbons and their derivatives in an ecological wastewater treatment plant in South China and effluent impact to the receiving river. *Environmental Science and Pollution Research*. 26, 5638-5644. <https://doi.org/10.1007/s11356-018-3839-4>.

QUEIROZ, R. N., PREDIGER, P., VIEIRA, M. G. A., 2022a. Adsorption of polycyclic aromatic hydrocarbons from wastewater using graphene-based nanomaterials synthesized by conventional chemistry and green synthesis: A critical review. *Journal of Hazardous Materials*, 422, 126904. <https://doi.org/10.1016/j.jhazmat.2021.126904>.

QUEIROZ, R.N., NEVES, T.F., SILVA, M.G.C., MASTELARO, V. R., VIEIRA, M.G.A., PREDIGER, P., 2022b. Comparative efficiency of polycyclic aromatic hydrocarbon removal by novel graphene oxide composites prepared from conventional and green synthesis. *Journal of Cleaner Production*, 361, 132244. <https://doi.org/10.1016/j.jclepro.2022.132244>.

RUIZ, D. A. P., ÁVILA, G. D., SUESCA, C. A., DELGADO, A. D. G., HERRERA, A., 2020. Ionic Cross-Linking Fabrication of Chitosan-Based Beads Modified with FeO and TiO<sub>2</sub> Nanoparticles: Adsorption Mechanism toward Naphthalene Removal in Seawater from Cartagena Bay Area. *ACS Omega*. 5, 26463–26475. <https://dx.doi.org/10.1021/acsomega.0c02984>.

SANTOS, N. T. G., MORAES, L. F., SILVA, M. G. C., VIEIRA, M. G. A., 2020. Recovery of gold through adsorption onto sericin and alginate particles chemically crosslinked by proanthocyanidins. *Journal of Cleaner Production*. 253, 119925. <https://doi.org/10.1016/j.jclepro.2019.119925>.

SILVA, V. A. J., ANDRADE, P. L., SILVA, M. P. C., DOMINGUEZ, A. B., VALLADARES, L. D. L. S., AGUIAR, J. A., 2013. Synthesis and characterization of Fe<sub>3</sub>O<sub>4</sub> nanoparticles coated with fucan polysaccharides. *J. Magn. Mater.* 343, 138-143. <https://doi.org/10.1016/j.jmmm.2013.04.062>.

SHI, Y., XING, Y., DENG, S., ZHAO, B., FU, Y., LIU, Z., 2020. Synthesis of proanthocyanidins-functionalized Fe<sub>3</sub>O<sub>4</sub> magnetic nanoparticles with high solubility for removal of heavy-metal ions. *Chemical Physics Letters*. 753, 137600. <https://doi.org/10.1016/j.cplett.2020.137600>.

SONG, T., TIAN, W., QIAO, K., ZHAO, J., CHU, M., DU, Z., WANG, L., XIE, W., 2021. Adsorption Behaviors of Polycyclic Aromatic Hydrocarbons and Oxygen Derivatives in Wastewater on N-Doped Reduced Graphene Oxide. *Separation and Purification Technology*. 254, 117565. <https://doi.org/10.1016/j.seppur.2020.117565>.

SUN, S., WANG, Y., ZANG, T., WEIB, J., WUA, H., WEIB, C., QIU, G., LIB, F., 2019. A biosurfactant-producing *Pseudomonas aeruginos* S5 isolated from coking wastewater and its application for bioremediation of polycyclic aromatic hydrocarbons. *Bioresource Technology*. 281, 421-428. <https://doi.org/10.1016/j.biortech.2019.02.087>.

WANG, Y., LI, L., LUO, C., WANG, X., DUAN, H., 2016. Removal of  $Pb^{2+}$  from water environment using a novel magnetic chitosan/graphene oxide imprinted  $Pb^{2+}$ . *International Journal of Biological Macromolecules*. 86, 505-511. doi: 10.1016/j.ijbiomac.2016.01.035.

WANG, S., LI, E., LI, J., DU, Z., CHENG, F., 2020. Preparation and coagulation-flocculation performance of covalently bound organic hybrid coagulant with excellent stability. *Colloids and Surfaces A*. 600, 124966. <https://doi.org/10.1016/j.colsurfa.2020.124966>.

ZHANG, Q., ZHANG, Y., LI, Y., DING, P., XU, S., CAO, J., 2021. Green synthesis of magnetite nanoparticle and its regulatory effect on fermentative hydrogen production from lignocellulosic hydrolysate by *Klebsiella* sp. *International Journal of Hydrogen Energy*. 46, 20413-20424. <https://doi.org/10.1016/j.ijhydene.2021.03.142>.

## ANEXO I. Licenças de publicação de artigos na dissertação

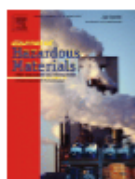
Autorizações da *Elsevier* para a inclusão do artigo publicado em *Journal of Hazardous Materials* no Capítulo 2 desta dissertação.

03/06/2022 09:48

Rightslink® by Copyright Clearance Center



Home | Help | Live Chat | Ruth Queiroz



### Adsorption of polycyclic aromatic hydrocarbons from wastewater using graphene-based nanomaterials synthesized by conventional chemistry and green synthesis: A critical review

Author: Ruth Nóbrega Queiroz, Patrícia Prediger, Melissa Gurgel Adeodato Vieira

Publication: Journal of Hazardous Materials

Publisher: Elsevier

Date: 15 January 2022

© 2021 Elsevier B.V. All rights reserved.

#### Journal Author Rights

Please note that, as the author of this Elsevier article, you retain the right to include it in a thesis or dissertation, provided it is not published commercially. Permission is not required, but please ensure that you reference the journal as the original source. For more information on this and on your other retained rights, please visit: <https://www.elsevier.com/about/our-business/policies/copyright#Author-rights>

BACK

CLOSE WINDOW

Autorizações da *Elsevier* para a inclusão do artigo publicado em *Journal of Cleaner Production* no Capítulo 3 desta dissertação.

03/08/2022 09:41

Rightslink® by Copyright Clearance Center



Home | Help | Live Chat | Ruth Queiroz



### Comparative efficiency of polycyclic aromatic hydrocarbon removal by novel graphene oxide composites prepared from conventional and green synthesis

**Author:**

Ruth Nóbrega Queiroz, Tauany de Figueiredo Neves, Meuris Gurgel Carlos da Silva, Valmor Roberto Mastelaro, Melissa Gurgel Adeodato Vieira, Patrícia Prediger

**Publication:** Journal of Cleaner Production

**Publisher:** Elsevier

**Date:** 10 August 2022

© 2022 Elsevier Ltd. All rights reserved.

#### Journal Author Rights

Please note that, as the author of this Elsevier article, you retain the right to include it in a thesis or dissertation, provided it is not published commercially. Permission is not required, but please ensure that you reference the journal as the original source. For more information on this and on your other retained rights, please visit: <https://www.elsevier.com/about/our-business/policies/copyright#Author-rights>

[BACK](#)[CLOSE WINDOW](#)

Comprovante de submissão do artigo ao *Environmental Science and Pollution Research* apresentado no Capítulo 4 desta dissertação

Environmental Science and Pollution Research - Submission Notification to co-author -    
[EMID:abfd5809366c8897]  Caixa de entrada x



**Environmental Science and Pollution Research** <em@editorialmanager.com>  
para mim ▾

seg., 22 de ago. 07:12   

 inglês ▾ > português ▾ [Traduzir mensagem](#)

[Desativar para: inglês](#) x

Re: "Adsorption of naphthalene polycyclic aromatic hydrocarbon from wastewater by a green magnetic composite based on chitosan and graphene oxide"  
Full author list: Ruth Nóbrega Queiroz; Meuris Gurgel Carlos da Silva; Valmor Roberto Mastelaro; Patricia Prediger; Melissa Gurgel Adeodato Vieira

Dear Ms Ruth Queiroz,

We have received the submission entitled: "Adsorption of naphthalene polycyclic aromatic hydrocarbon from wastewater by a green magnetic composite based on chitosan and graphene oxide" for possible publication in *Environmental Science and Pollution Research*, and you are listed as one of the co-authors.

The manuscript has been submitted to the journal by Dr. Prof Melissa Gurgel Adeodato Vieira who will be able to track the status of the paper through his/her login.

If you have any objections, please contact the editorial office as soon as possible. If we do not hear back from you, we will assume you agree with your co-authorship.

Thank you very much.

## **ANEXO II. Materiais Suplementares**

Adsorption of Polycyclic Aromatic Hydrocarbons from wastewater using graphene-based nanomaterials synthesized by conventional chemistry and green synthesis: A critical review<sup>6</sup>

Ruth Nóbrega Queiroz<sup>a</sup>, Patrícia Prediger<sup>b</sup>, Melissa Gurgel Adeodato Vieira<sup>a\*</sup>

<sup>a</sup>Process and Product Development Department, School of Chemical Engineering, University of Campinas – UNICAMP, Albert Einstein Avenue, 500, 13083-852 Campinas, São Paulo, Brazil.

<sup>b</sup>School of Technology, University of Campinas – UNICAMP, 13484-332 Limeira, São Paulo, Brazil.

\*melissag@unicamp.br

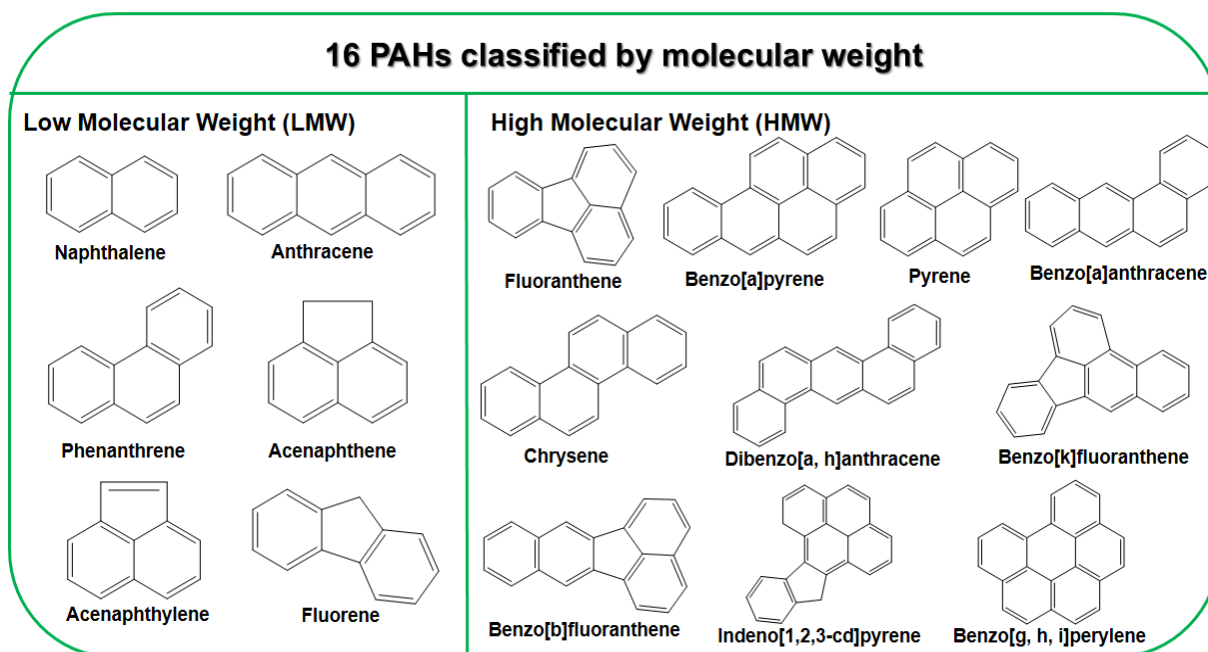
## **SUPPLEMENTARY MATERIALS**

---

<sup>6</sup> Supplementary Materials published in Journal of Hazardous Materials 422 (2022) 126904. DOI: 10.1016/j.jhazmat.2021.126904. Reprinted with permission from Journal of Hazardous Materials. Copyright 2021 Elsevier (Capítulo 2).

The 16 PAHs, listed by the United States Environmental Protection Agency (US EPA) as priority contaminants, are illustrated in Figure S1. Table S1 shows the physical and chemical properties of the 16 PAHs listed by the US EPA.

**Fig. S1** 16 PAHs listed as priority pollutants by the US EPA and classified according to their molecular weight.



1 **Table S1** Physicochemical properties of 16 PAHs (Adapted from Mackay et al. 1992).

PAHs	Symbol	Number of rings	Molecular weight	Aqueous solubility (mg.L <sup>-1</sup> )	Vapor pressure (Pa)	Partition coefficient log K <sub>ow</sub>
Naphthalene	NAP	2	128	31	1.0x10 <sup>2</sup>	3.37
Acenaphthylene	ACN	3	152	16	9.0x10 <sup>-1</sup>	4.00
Acenaphthene	ACE	3	154	3.8	3.0x10 <sup>-1</sup>	3.92
Fluorene	FLU	3	166	1.9	9.0x10 <sup>-2</sup>	4.18
Phenanthrene	PHEN	3	178	1.1	2.0x10 <sup>-2</sup>	4.57
Anthracene	ANT	3	178	0.045	1.0x10 <sup>-3</sup>	4.54
Pyrene	PYR	4	202	0.13	6.0x10 <sup>-4</sup>	5.18
Fluoranthene	FLT	4	202	0.26	1.2x10 <sup>-3</sup>	5.22
Benzo[a]anthracene	BaA	4	228	0.011	2.8x10 <sup>-5</sup>	5.91
Chrysene	CHR	4	228	0.006	5.7x10 <sup>-7</sup>	5.91
Benzo[b]fluoranthene	BbF	5	252	0.0015	-	5.80
Benzo[k]fluoranthene	BkF	5	252	0.0008	5.8x10 <sup>-8</sup>	6.00
Benzo[a]pyrene	BaP	5	252	0.0038	7.0x10 <sup>-7</sup>	5.91
Dibenzo[a, h]anthracene	DahA	6	278	0.0006	3.7x10 <sup>-10</sup>	6.75
Indeno[1, 2, 3-cd]pyrene	IP	6	276	0.00019	-	6.50
Benzo[g, h, i]perylene	BPer	6	276	0.00026	1.4x10 <sup>-8</sup>	6.50

2

3

The sources of natural (biological) or anthropogenic (pyrogenic and petrogenic) PAHs are represented schematically by Figure S2.

**Fig. S2** Schematic representation of the sources of Polycyclic Aromatic hydrocarbons (PAHs).

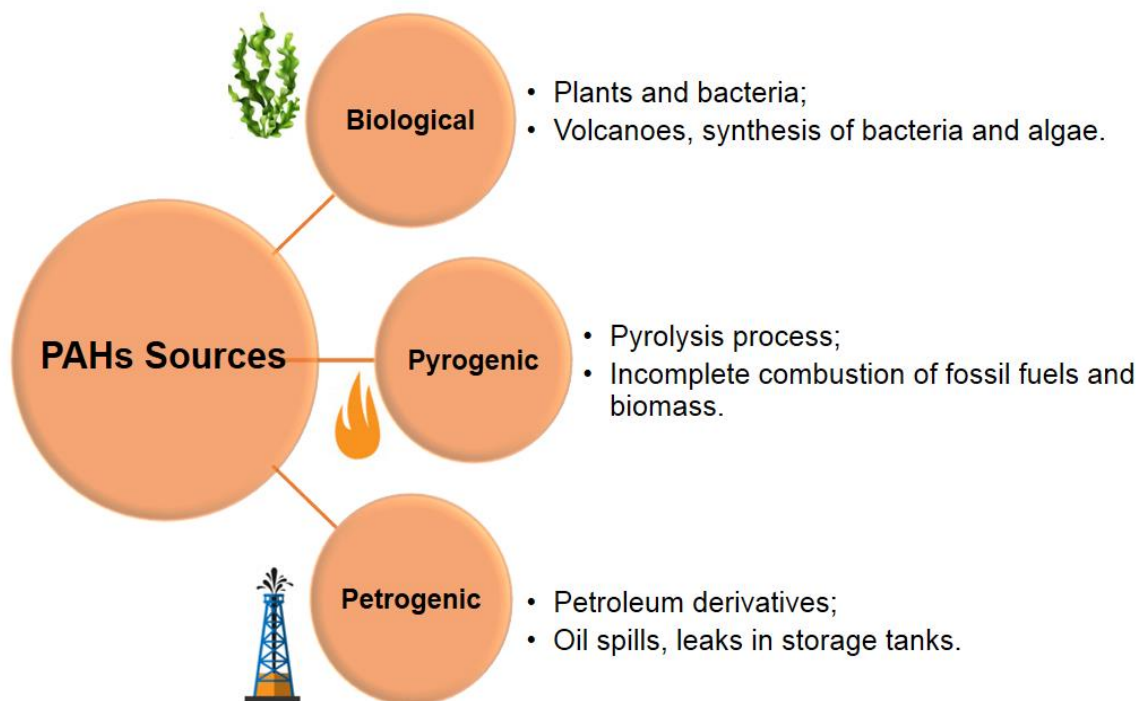
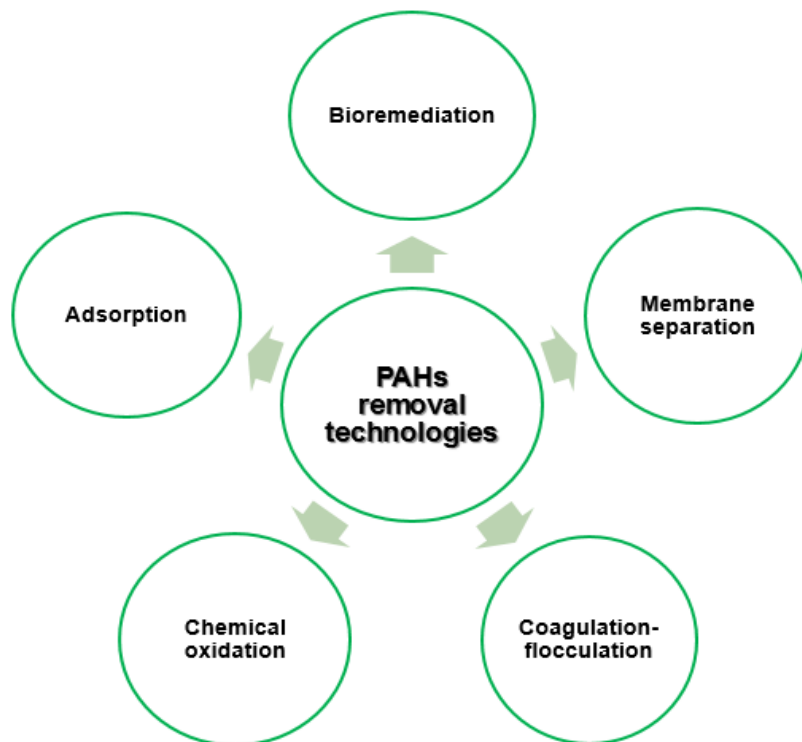


Figure S3 presents a schematic diagram of the main PAHs removal technologies from wastewater.

**Fig. S3** Schematic diagram of the main PAHs removal technologies.



## References

Mackay, D., Shiu, W. Y., Ma, K. C., 1992. Illustrated handbook of physical-chemical properties and environmental fate for organic chemicals: Polynuclear aromatic hydrocarbons, polychlorinated dioxins and dibenzofurans. Lewis Publishers, Chelsea, Michigan, USA.

Comparative efficiency of polycyclic aromatic hydrocarbon removal by novel graphene oxide composites prepared from conventional and green synthesis<sup>7</sup>

Ruth Nóbrega Queiroz<sup>a</sup>, Tauany de Figueiredo Neves,<sup>b</sup> Meuris Gurgel Carlos da Silva<sup>a</sup>, Valmor Roberto Mastelaro<sup>c</sup>, Patrícia Prediger<sup>b</sup> and Melissa Gurgel Adeodato Vieira<sup>a\*</sup>

<sup>a</sup>Process and Product Development Department, School of Chemical Engineering, University of Campinas – UNICAMP, Albert Einstein Avenue, 500, 13083-852 Campinas, São Paulo, Brazil.

<sup>b</sup>School of Technology, University of Campinas – UNICAMP, 13484-332 Limeira, São Paulo, Brazil.

<sup>c</sup>São Carlos Institute of Physics, University of São Paulo, Av. Trabalhador São-carlense, 400, São Carlos, SP, 13566-590, Brazil.

\*melissag@unicamp.br

## **SUPPLEMENTARY MATERIALS**

---

<sup>7</sup> Supplementary Materials published in Journal of Cleaner Production 361 (2022) 132244. DOI: 10.1016/j.jclepro.2022.132244. Reprinted with permission from Journal of Cleaner Production. Copyright 2022 Elsevier (Capítulo 3).

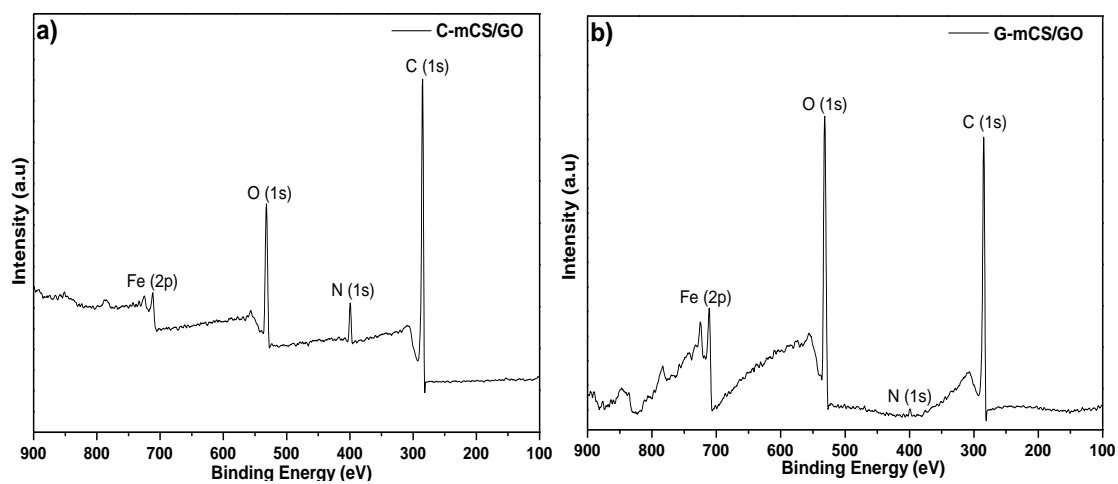


**Fig. S1** Survey XPS spectra of C-mCS/GO (a) and G-mCS/GO (b)

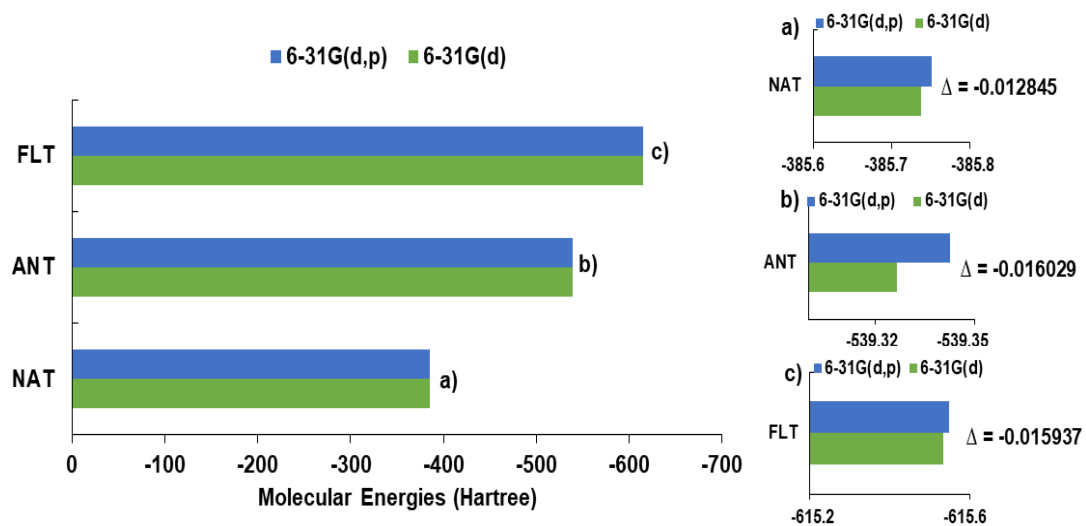


**Fig. S2** Molecular energies of NAT, ANT and FLT obtained from geometry optimization of the molecules by the B3LYP method, using the basis sets 6-31G (d) and 6-31G (d,p).

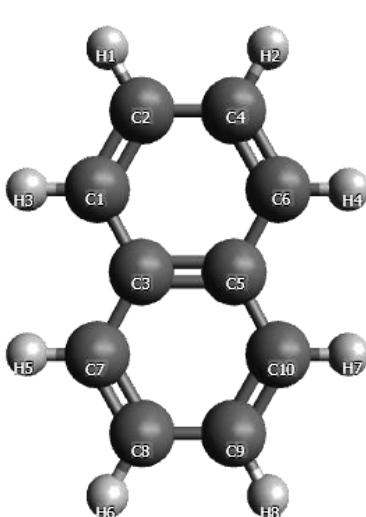
**Table S1.** Calibration curves of PAHs, linearity ranges, correlation coefficients, LODs and LOQs.

PAHs	Regression equation	Linearity (mg.L <sup>-1</sup> )	R <sup>2</sup>	LODs (mg.L <sup>-1</sup> )	LOQs (mg.L <sup>-1</sup> )
NAP	$y = 22922x - 822.33$	0.1 - 6	0.9993	0.012	0.035
ANT	$y = 0.1876x + 0.1194$	0.1 - 4	0.9932	0.010	0.031
FLT	$y = 0.2067x + 0.0783$	0.1 - 4	0.9988	0.055	0.168

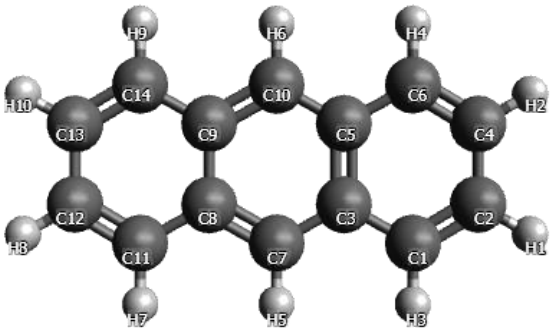
\*Where: y represents the peak area for HPLC or absorbance for UV-Vis; x represents the concentration of PAHs; LODs is the limit of detection; LOQs is the limit of quantification.

\*\*The parameters were validated according to the guidelines of the Institute of Metrology, Standardization and Industrial Quality (INMETRO), DOQ-CGCRE-008 (2020).

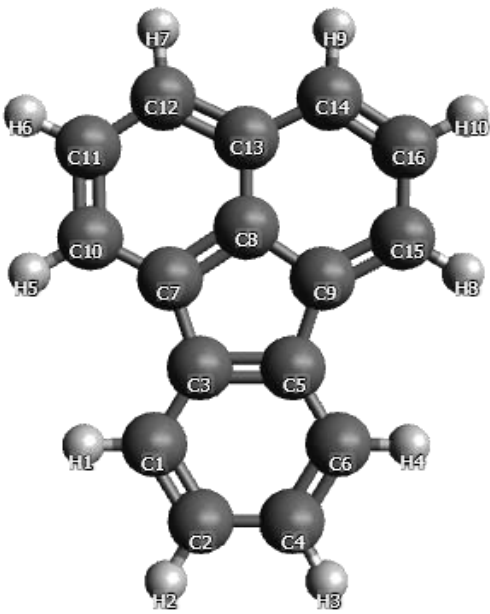
**Table S2.** Bond lengths (Å) of Naphthalene (NAT) with optimized geometry obtained with the B3LYP/6-31G(d,p) model.

Molecule with labels	Bond	Length (Å)
	C1-C2	1.3763
	C1-C3	1.4209
	C1-H3	1.0871
	C2-C4	1.4166
	C2-H1	1.0861
	C3-C5	1.4344
	C3-C7	1.4209
	C4-C6	1.3763
	C4-H2	1.0861
	C5-C6	1.4209
	C5-C10	1.4209
	C6-H4	1.0871
	C7-C8	1.3763
	C7-H5	1.0871
	C8-C9	1.4166
	C8-H6	1.0861
	C9-C10	1.3763
C9-H8	1.0861	
C10-H7	1.0871	

**Table S3.** Bond lengths (Å) of Anthracene (ANT) with optimized geometry obtained with the B3LYP/6-31G(d,p) model.

Molecule with labels	Bond	Length (Å)
	C1-C2	1.3696
	C1-C3	1.4299
	C1-H3	1.0869
	C2-C4	1.4260
	C2-H1	1.086
	C3-C5	1.4453
	C3-C7	1.4003
	C4-C6	1.3696
	C4-H2	1.086
	C5-C6	1.4299
	C5-C10	1.4003
	C6-H4	1.0869
	C7-C8	1.4003
	C7-H5	1.0877
	C8-C9	1.4453
	C8-H11	1.4299
	C9-C10	1.4003
	C9-H14	1.4299
	C10-H6	1.0877
	C11-C12	1.3696
C11-H7	1.0869	
C12-C13	1.4260	
C12-H8	1.086	
C13-C14	1.3696	
C13-H10	1.086	
C14-H9	1.0869	

**Table S4.** Bond lengths (Å) of Fluoranthene (FLT) with optimized geometry obtained with the B3LYP/6-31G(d,p) model.

Molecule with labels	Bond	Length (Å)
	C1-C2	1.4001
	C1-C3	1.3911
	C1-H1	1.0865
	C2-C4	1.3976
	C2-H2	1.0860
	C3-C5	1.4276
	C3-C7	1.4760
	C4-C6	1.4001
	C4-H3	1.0860
	C5-C6	1.3911
	C5-C9	1.4760
	C6-H4	1.0865
	C7-C8	1.4181
	C7-C10	1.3802
	C8-C9	1.4181
	C8-C13	1.4034
	C9-C15	1.3801
	C10-C11	1.4232
	C10-H5	1.0865
	C11-C12	1.3844
	C11-H6	1.0862
	C12-C13	1.4243
	C12-H7	1.0867
	C13-C14	1.4243
	C14-C16	1.3844
	C14-H9	1.0867
C15-C16	1.4232	
C15-H8	1.0865	
C16-H10	1.0863	

**References**

INMETRO - NATIONAL INSTITUTE OF METROLOGY. Guidance on validation of chemical testing methods. Rio de Janeiro. DOQ-CGCRE-008. Review 09. Jun. 2020.

Adsorption of naphthalene polycyclic aromatic hydrocarbon from wastewater by a green magnetic composite based on chitosan and graphene oxide<sup>8</sup>

Ruth Nóbrega Queiroz<sup>a</sup>, Meuris Gurgel Carlos da Silva<sup>a</sup>, Valmor Roberto Mastelaro<sup>c</sup>, Patrícia Prediger<sup>b</sup> and Melissa Gurgel Adeodato Vieira<sup>a\*</sup>

<sup>a</sup>Process and Product Development Department, School of Chemical Engineering, University of Campinas – UNICAMP, Albert Einstein Avenue, 500, 13083-852 Campinas, São Paulo, Brazil.

<sup>b</sup>School of Technology, University of Campinas – UNICAMP, 13484-332 Limeira, São Paulo, Brazil.

<sup>c</sup>São Carlos Institute of Physics, University of São Paulo, Av. Trabalhador São Carlense, 400, São Carlos, SP, 13566-590, Brazil.

\*melissag@unicamp.br

## **SUPPLEMENTARY MATERIALS**

---

<sup>8</sup> Supplementary Materials submitted with the manuscript to the Journal of Cleaner Production on June 2nd, 2022 (Capítulo 4)

### Materials and chemical reagents

Mineral graphite micrograf 99507 UJ - (Nacional Grafite Ltda., Limeira, SP, Brasil); Concentrated sulfuric acid ( $\text{H}_2\text{SO}_4$ ) - (ACS); Potassium persulfate ( $\text{K}_2\text{SO}_4$ ) - (ACS); Phosphorus pentoxide ( $\text{P}_2\text{O}_5$ ) (high purity, 99%) - (Sigma Aldrich); Sodium nitrate ( $\text{NaNO}_3$ ) - (ACS); Potassium permanganate ( $\text{KMnO}_4$ ) (high purity, 99%) - (CRQ Eireli Chemical Products); Hydrogen peroxide ( $\text{H}_2\text{O}_2$ ) (Grade II, 30% w/w) - (Sigma Aldrich); Hydrochloric acid (HCl) (37%) - (ACS); Iron (II) chloride ( $\text{FeCl}_2 \cdot 4\text{H}_2\text{O}$ ) - (Dynamics); Iron (III) chloride ( $\text{FeCl}_3 \cdot 6\text{H}_2\text{O}$ ) - (Sigma Aldrich); Ammonium hydroxide ( $\text{NH}_4\text{OH}$ ) (28%) - (CRQ Eireli Chemical Products); Chitosan (CS) - (Sigma Aldrich); Liquid Vaseline (mineral oil) - (Dynamics); Oleic acid - (Synth); Acetic acid ( $\text{CH}_3\text{COOH}$ ) (60%) - (Synth); Glutaraldehyde (Grade II, 25% w/w) - (Sigma Aldrich); Pure petroleum ether (30 -60 °C) - (Sigma Aldrich); Sodium hydroxide (NaOH) (high purity, 99.99%) - (Synth); Dry N,N-dimethylformamide (DMF) (anhydrous, 99.8%) - (Sigma Aldrich); N,N-dicyclohexylcarbodiimide (DCC) (high purity, 99%) - (Sigma Aldrich); 4-dimethylaminopyridine (DMAP) (high purity, 99%) - (Sigma Aldrich); Methanol ( $\text{CH}_3\text{OH}$ ) (P.A.) - (ACS); Ethanol ( $\text{C}_2\text{H}_5\text{OH}$ ) (technical grade, 99%) - (Sigma Aldrich); Acetone ( $\text{C}_3\text{H}_6\text{O}$ ) (P.A.) - (ACS); Water hyacinth extract (*Eichhornia crassipes*) - (UNICAMP, Limeira, SP, Brazil); Proanthocyanidin (PAS) - (Galena); Naphthalene (purity, 99%) - (Sigma Aldrich); Anthracene (purity, 99%) - (Sigma Aldrich); Fluoranthene (purity, 99%) - (Sigma Aldrich); Methanol ( $\text{CH}_3\text{OH}$ ) (HPLC Grade) - (ACS); Acetonitrile ( $\text{C}_2\text{H}_3\text{N}$ ) (HPLC Grade) - (ACS); Ultrapure water (OS20LXE, Gehaka).

### Analytical method validation

- **Selectivity:** Selectivity is the ability of a method to determine the analyte in the presence of other substances. In the study, the selectivity of naphthalene (NAP) over fluoranthene (FLT) was evaluated (Fig. S1).

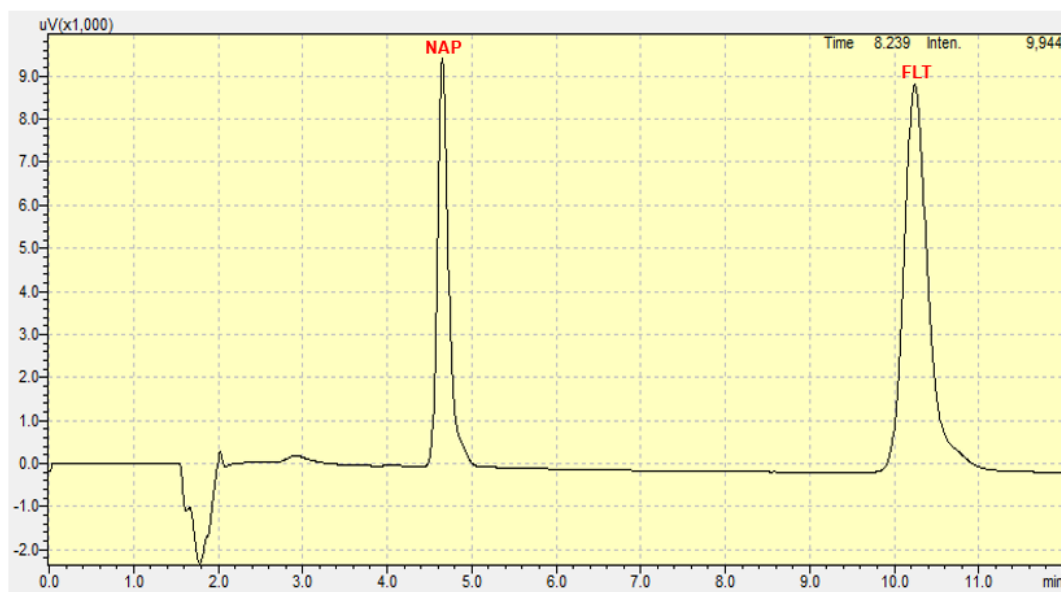


**Fig. S1** Chromatogram with the compounds injected in a binary solution, with a concentration of  $4 \text{ mg.L}^{-1}$  for NAP and  $2 \text{ mg.L}^{-1}$  for the FLT. Analytical conditions: Mobile phase of 85% methanol and 15% deionized water; flow rate:  $1 \text{ mL.min}^{-1}$ , injection volume:  $25 \text{ }\mu\text{L}$ ; wavelength: 254 nm.

- **Limit of detection (LOD):** The smallest amount of analyte that can be detected by the method. The LOD can be estimated by Equation (S1):

$$LOD = \frac{3.3 \cdot \delta}{b} \quad (\text{S1})$$

Where,  $\delta$  is the standard deviation of the blank response and  $b$  is the slope of the analytical curve.

- **Limit of quantification (LOQ):** The smallest amount of the analyte in the sample that can be quantitatively determined with acceptable precision and accuracy. The LOQ can be estimated by Equation (S2):

$$LOQ = \frac{10 \cdot \delta}{b} \quad (\text{S2})$$

Where,  $\delta$  is the standard deviation of the blank response and  $b$  is the slope of the analytical curve.

- **Precision (repeatability):** Repeatability was determined by performing independent injections at three concentration levels (0.1, 1 and 6 mg.L<sup>-1</sup>) in triplicate. The percentage relative standard deviation (RSD%) can be determined through Equation (S3):

$$RSD\% = \left( \frac{\delta}{\bar{x}} \right) * 100\% \quad (S3)$$

Where,  $\delta$  is the standard deviation for the three injections and  $\bar{x}$  average concentration for the three injections. The repeatability values obtained for each concentration level injected are presented in Table S2, it appears that the RSD% values comply with the criteria established in DOQ-CGCRE-008/2020.

**Table S2.** Repeatability values obtained for each concentration level for naphthalene.

Concentration (mg.L <sup>-1</sup> )	$\delta$	RSD (%)	Criteria (%)*
0.1	0.008357	4.503598	11.0
1.0	0.008099	0.887391	7.3
6.0	0.09894	2.021019	7.3

\*According with DOQ-CGCRE-008/2020.

- **Accuracy (recovery):** Recovery was determined by injections at three levels concentration in triplicate (0.4, 2, 4 mg.L<sup>-1</sup>). The recovery (%) was calculated by Equation (S4):

$$Recovery\% = \left( \frac{\text{experimental concentration}}{\text{theoretical concentration}} \right) * 100\% \quad (S4)$$

The recovery (%) values obtained for each concentration level injected are presented in Table S3, it appears that the recovery (%) values comply with the criteria established in DOQ-CGCRE-008/2020.

**Table S3.** Recovery values obtained for each concentration level for naphthalene.

Theoretical (mg.L <sup>-1</sup> )	Experimental (mg.L <sup>-1</sup> )	Recovery (%)	Criteria (%)*
0.4	0.447693	109.1935338	80 - 110
2.0	1.898872	94.94358748	80 - 110
4.0	4.030377	100.7594132	80 - 110

\*According with DOQ-CGCRE-008/2020.

- **Linearity:** To obtain the calibration curve of the NAP, a series of injections were performed at five concentration levels in triplicate (0.1, 0.5, 1, 3 and 6 mg.L<sup>-1</sup>). Linearity was determined by the linear regression coefficient. Table S4 presents the parameters obtained through the validation method for the NAP.

**Table S4.** Calibration curves of NAP, linearity ranges, correlation coefficients, LODs and LOQs.

PAHs	Ret. Time (min)	Regression equation	Range (mg.L <sup>-1</sup> )	Linearity (R <sup>2</sup> )	LODs (mg.L <sup>-1</sup> )	LOQs (mg.L <sup>-1</sup> )
NAP	4.66	$y = 22922x - 822.33$	0.1 - 6	0.9993	0.012	0.035

\*The parameters were validated according to the guidelines of the Institute of Metrology, Standardization and Industrial Quality (INMETRO), DOQ-CGCRE-008 (2020).

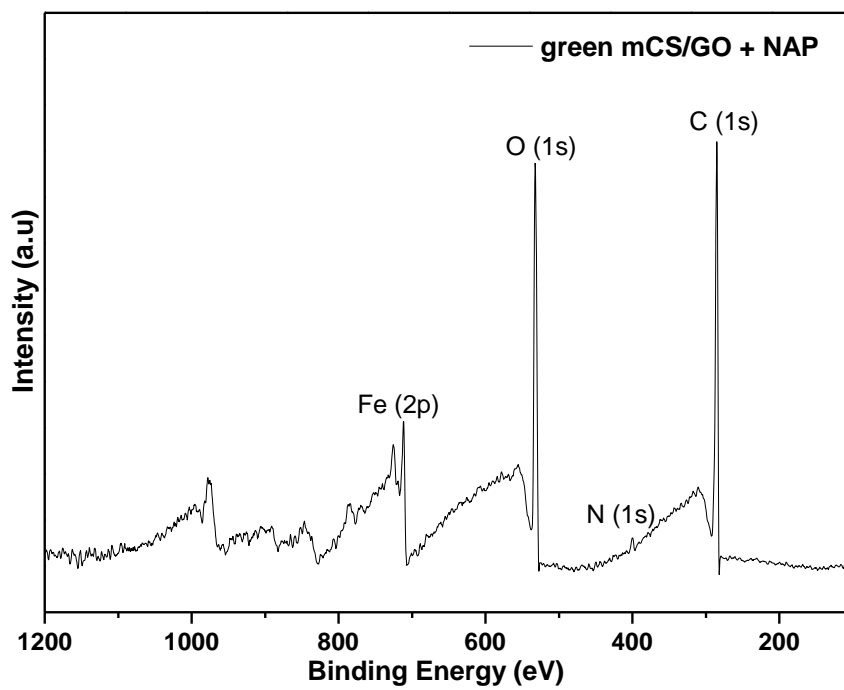


**Fig. S2** XPS survey spectra of green mCS/GO after the NAP adsorption.

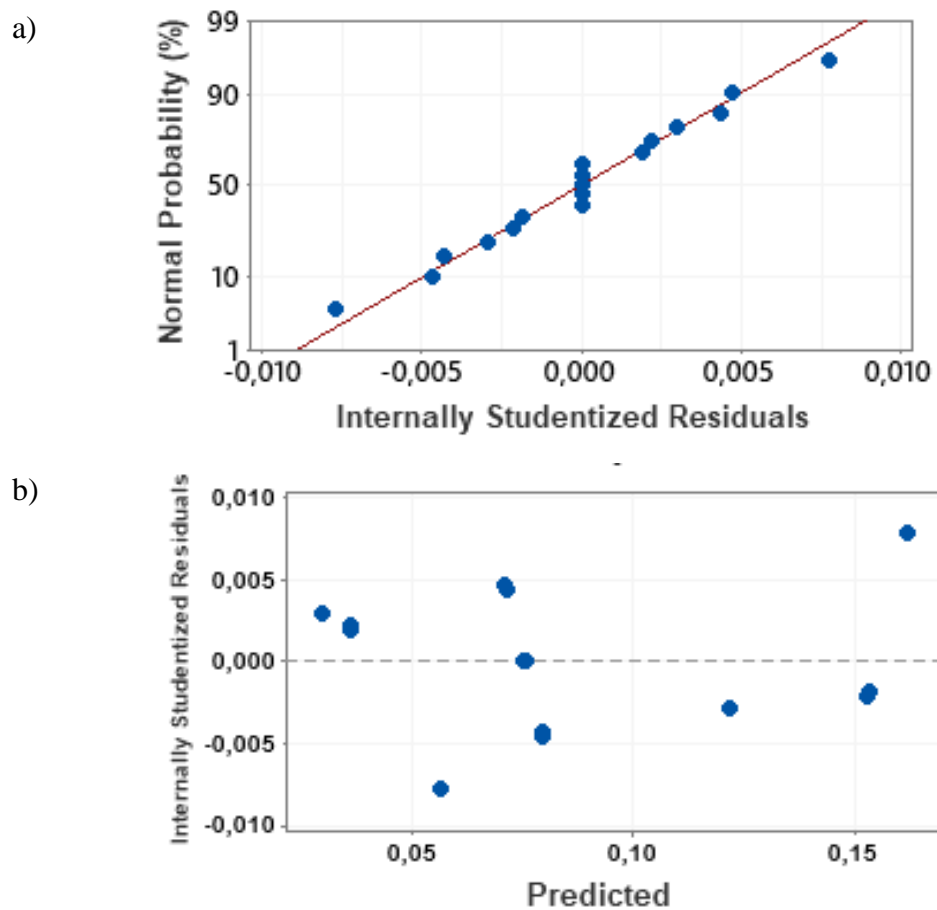


**Fig. S3** Normal probability (%) versus Internally Studentized Residuals (a); Predicted value versus Internally Studentized Residuals (b).

**References**

INMETRO - NATIONAL INSTITUTE OF METROLOGY. (June 09<sup>th</sup>, 2020). Guidance on validation of chemical testing methods. Rio de Janeiro.